Carbon dioxide treatments of wood

Trevor G. Jones

A thesis presented for the degree of
Doctor of Philosophy in Forestry
at the University of Canterbury, Christchurch, New Zealand.

March 1993

Abstract

The application of carbon dioxide to wood drying processes and chemical extraction of bark was investigated. Dissolved carbon dioxide gas supersaturation in the water of green wood was utilised in decompression drying of *Pinus radiata* sapwood chips and in the kiln drying of collapse-susceptible *Eucalyptus delegatensis* heartwood. The transport properties and solubilities of dissolved carbon dioxide gas in green wood that form the basis of such treatments were studied in *Nothofagus fusca* heartwood. Supercritical carbon dioxide and carbon dioxide/methanol were utilised to extract resin acid, fatty acids, and sterols from *Pinus radiata* bark.

Non-steady state desorption of dissolved carbon dioxide gas from wood samples saturated with carbon dioxide gas under pressure was used to measure transverse diffusion coefficients of dissolved carbon dioxide gas in green *Nothofagus fusca* heartwood. The activation energy of dissolved carbon dioxide gas diffusion in green *N. fusca* heartwood was higher than the activation energy of dissolved carbon dioxide gas diffusion in water, suggesting the presence of a reaction mechanism between the dissolved carbon dioxide gas molecules and the cell wall constituents. Initial carbon dioxide gas loss after decompression is both rapid and substantial. This is due to mass flow of carbon dioxide gas bubbles from surface vessels and longitudinal diffusion, principally from the end grain. In long wood samples the majority of carbon dioxide gas is lost by transverse diffusion. A bimodal diffusion equation is proposed for modelling carbon dioxide gas absorption and desorption by longitudinal and transverse diffusion. Carbon dioxide gas solubilities in the water of green wood were similar to published values of solubilities in pure water.

Carbon dioxide gas bubble nucleation in supersaturated aqueous solutions on decompression in *Pinus radiata* sapwood chips, partially saturated with carbon dioxide gas under pressure, was effective in removing a significant

proportion of the water. The volume of gas bubbles formed was found to be an important criterion for water loss at high carbon dioxide gas solubilities. Water loss increased with gas pressure and absorption time. Large variations in water loss occurred with temperature at low gas pressure. Water loss was found to be more effective with repeated cycles of decompression drying. At low gas solubilities in water the volume of air in the wood became an important criterion for water loss. Compression and expansion of air bubbles was thought to be the main mode of water loss at low gas solubilities along with expansion of compressed gas that had moved behind the wet line through adjacent dry tracheids. The energy efficiency of decompression drying was far lower than that of compression drying with hydraulically driven platens.

Drying collapse in *Eucalyptus delegatensis* heartwood was unaffected by carbon dioxide gas supersaturation in the sap of green wood, saturated under pressure at a range of gas solubilities and dried at different temperatures. It appears that carbon dioxide gas bubble nucleation does not occur within the water-saturated cells of impermeable heartwood. Drying temperature did have a significant effect on drying collapse, however, the response varied greatly with the wood source. Significant drying collapse and basic density variation occurred among the regions Nelson and Southland, among trees within the regions, and among height classes within the trees. The differences in drying collapse between the two regions was attributed to regional differences in the pattern of inter- and intra-incremental basic density variation, caused by strong environmental control of these wood properties. The significant variation of drying collapse among trees within regions suggests some genetic control of drying collapse.

Pinus radiata bark was extracted using a once-through flow of supercritical carbon dioxide at a temperature of 50 ° C and pressures from 10 to 30 MPa. Extraction was also performed with supercritical carbon dioxide containing 4.3 % methanol as a co-solvent at 30 MPa. Extract yields increased with pressure. HPLC analysis using ultraviolet absorption identified the resin acid abietic acid, the fatty acids linoleic, linolenic, and palmitoleic acid, and the sterols β-sitosterol and campesterol as present in the extracts. The amount of each compound extracted increased with increasing pressure, with the proportion of abietic acid and β-sitosterol in the extract increasing

as the pressure increased. The flavonoid dihydroquercetin was not found in the extracts, even with the addition of the co-solvent methanol.

Acknowledgements

A large number of people provided guidance, assistance, ideas and encouragement during the course of this work.

My supervisor, John Walker, gave me a very free hand in pursuing the work of this thesis. I am grateful for his patience and understanding, his encouragement and the ideas he brought to this work. His prompt and thorough reviews of written drafts made a very real improvement to the final form of the thesis.

Hillary Langer provided invaluable guidance on statistical design and analysis.

Wayne Miller provided encouragement and some useful ideas, particularly with regard to image processing. I am grateful for his support in making available staff and equipment at the Forest Research Institute, Rotorua, and for the efforts he took to make my visits so worthwhile.

Phil Bones kindly allowed me to make extensive use of the Electrical and Electronic Engineering Department's Vax image processing system.

Nick Ward from the Forest Research Institute kindly made his Vax image processing program for collapse measurement available for use.

Peter Kho from the Department of Chemical and Process Engineering provided encouragement and assistance, particularly with regard to kiln drying.

New Zealand Timberlands Limited, made available trees of *Eucalyptus delegatensis* from their stands in Nelson and Southland for the project on drying collapse. In particular, I would like to thank Mark Bendall (Nelson

District) and Dennis Guild (Southland District) for the time and effort they put in to ensure things ran smoothly during my time in both places.

Tim Langrish from the Department of Chemical and Process Engineering, provided encouragement and many ideas on a wide range of topics.

Pat Jordan from the Department of Chemical and Process Engineering kindly allowed me to use his supercritical fluid and HPLC equipment, providing technical advice and training, particularly in the use of HPLC equipment.

Richard Vannoort from the Department of Scientific and Industrial Research provided indispensible training on the use of the supercritical fluid equipment.

Terry Lomax of the Forest Research Institute provided many useful ideas on the design of the supercritical fluid extraction project.

Financial support was provided by a studentship funded by the Forest Research Institute, Ministry of Forestry.

Finally, I would like to thank my parents for their support during my years as a postgraduate student.

Contents

Chapter 1

Dissolved carbon dioxide gas diffusion in green *Nothofagus fusca* heartwood

1.1 Introduction

Dissolved carbon dioxide gas transport properties and solubilities in green wood were utilised in many of the carbon dioxide gas treatments studied in this thesis. Basic data on dissolved carbon dioxide gas diffusivities and solubilities in green wood were therefore required for effective carbon dioxide gas treatments to be formulated. Given the absence of such data in the literature, dissolved carbon dioxide gas diffusivities and solubilities were therefore measured in green *Nothofagus fusca* heartwood. The procedures used and the results obtained are outlined in this chapter.

1.2 Diffusion theory

1.2.1 Flux

The rate of migration of matter is measured by its flux J - the quantity passing through unit area per unit time. The flux of matter (the rate of diffusion) parallel to an axis x (denoted J_x) is proportional to the concentration gradient along that axis, $J_x \propto dC/dx$ (figure 1.1). Matter flows down a concentration gradient - in this case

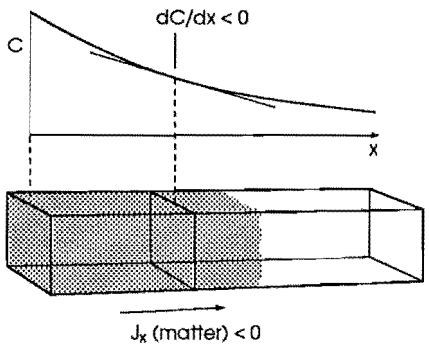

Figure 1.1 The flux of particles down a concentration gradient. Fick's Law states that the flux of matter (the number of particles per unit area per unit time) is proportional to the density gradient at that point (from Atkins 1986).

towards increasing x. The flux of matter is therefore positive in the direction of a negative concentration gradient, dC/dx. The coefficient of proportionality in the matter flux expression must therefore be negative, and we denote it -D, where D is called the diffusion coefficient. This leads to Fick's First Law of diffusion:

$$J_x = -D\left(\frac{dC}{dx}\right)$$

1.2.2 Diffusion

The flux of matter from the region of high concentration to low concentration along the x axis, causes an increase over time of the concentration at any point along the x axis. If we consider two adjacent points such as x and x + Δx (figure 1.2), the rate of flow of matter across x will be greater than that across x + Δx because a portion of the matter moving across x will be retained in the thin slab (of cross-sectional area A) between x and x + Δx, increasing the concentration of matter in the slab with only the remainder flowing across x + Δx.

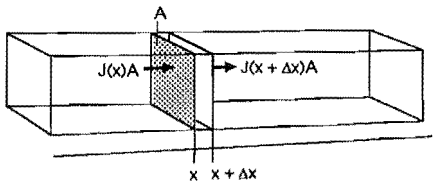

Figure 1.2 The net flux in a region is the difference between the flux entering the region of high concentration (on the left) and the flux leaving to the region of low concentration (on the right) (from Atkins 1986).

The quantity of matter that enters the slab per unit time is $J_{(x)}A$, and results in an increase in concentration within the slab, given by

$$\frac{\partial C}{\partial t} = \frac{J_{(x)}A}{A\Delta x} = \frac{J_{(x)}}{\Delta x}$$

The outflow at x + Δx is $J_{(x + \Delta x)}$, and the change of concentration due to this efflux is

$$\frac{\partial C}{\partial t} = \frac{-J_{(x + \Delta x)}A}{A\Delta x} = \frac{-J_{(x + \Delta x)}}{\Delta x}$$

The net change of concentration is therefore

$$\frac{\partial C}{\partial t} = \frac{\{J(x) - J(x + \Delta x)\}}{\Delta x}$$

The fluxes are proportional to the concentration gradients at x and x + Δx. Using Fick's First Law of diffusion we can write the above expression as

$$J(x) - J(x + \Delta x) = -D\left(\frac{\partial C_{(x)}}{\partial x}\right) + D\left(\frac{\partial C_{(x + \Delta x)}}{\partial x}\right)$$

$$= -D\left(\frac{\partial C}{\partial x}\right) + D\frac{\partial}{\partial x}\left\{C + \left(\frac{\partial C}{\partial x}\right)\Delta x\right\}$$

$$= D\left(\frac{\partial^2 C}{\partial x^2}\right)\Delta x$$

Substituting this relation into the expression for the rate of change of concentration in the slab, leads to Fick's Second Law of diffusion:

$$\frac{\partial C}{\partial t} = D\left(\frac{\partial^2 C}{\partial x^2}\right)$$

The equation applies to one-dimensional diffusion. For diffusion in three dimensions along axes x, y and z, the equation takes the form:

$$\frac{\partial C}{\partial t} = D\left(\frac{\partial^2 C}{\partial x^2} + \frac{\partial^2 C}{\partial y^2} + \frac{\partial^2 C}{\partial z^2}\right)$$

1.3 Dissolved gas diffusion in green wood

A study by Huang et al. (1977) on dissolved oxygen gas diffusion in water-saturated Douglas fir sapwood provides the only published data on dissolved gas diffusivities in wood. Diffusion coefficients were calculated from measurements of one-dimensional steady state diffusion flow in wood chips of tangential, radial and longitudinal orientation (thickness 1.1 - 4.0 mm). Tangential and radial diffusivities were 1.4 - 2.3 × 10^{-10} m^2 s^{-1} at 25 ° C, which is about 6 - 10 % of the dissolved oxygen diffusivity in water. The radial diffusivity in latewood was about one half that of the earlywood. The tangential and radial diffusivities varied with the proportion of earlywood and latewood in the growth rings. Longitudinal

diffusivities were about 5.5 times those of transverse diffusivities. The high longitudinal diffusivities result from the anisotropic structure of the woods anatomy.

1.4 Experiment design

Dissolved carbon dioxide gas diffusivities in green *Nothofagus fusca* heartwood, at temperatures of 1, 20 and 30 ° C, were measured using non-steady state desorption from wood samples saturated with carbon dioxide gas at a pressure of 1.5 MPa. The wood samples were cut in the form of a rectangular parallelepiped, with diffusion occuring in three dimensions.

Nothofagus fusca heartwood was used because of its very high impermeability. The pit membranes and cell lumina are occluded with heavy deposits of polyphenolic extractives (Kininmonth 1972) which minimise the mass flow of carbon dioxide gas and water at the commencement of desorption when gas decompression occurs.

Wood samples of large longitudinal length were used to minimise the contribution of longitudinal diffusion to total carbon dioxide gas loss. This enabled transverse dissolved carbon dioxide gas diffusivity to be measured. The effect of sample length on measured diffusivities was studied using a sample of half and quarter length boards in addition to full length boards for diffusion at 20 ° C. The similar diffusivities of tangential and radial dissolved oxygen gas diffusion in Douglas fir sapwood obtained by Huang et al. (1977) suggested that the dissolved gas diffusion in wood could be treated as isotropic, provided the wood samples were long. This assumption of isotropic diffusion was applied in the following solution of Fick's Second Law of diffusion.

1.5 Solution of Fick's Second Law of diffusion

A solution of Fick's Second Law of diffusion for non-steady state desorption from a rectangular parallelpiped (length, width and thickness 2a, 2b and 2c respectively) with boundary conditions:

(i) uniform initial concentration

$C = C_o$ when $t = 0$

(ii) surface concentration is equal to the equilibrium concentration when time $t > 0$

$C = C_e$ at $x = -a, a$; $y = -b, b$; $z = -c, c$ when $t > 0$

was derived by Jason (1959).

$$\frac{C - C_e}{C_o - C_e} = \frac{8}{\pi^2} \sum_{l=0}^{\infty} \sum_{m=0}^{\infty} \sum_{n=0}^{\infty} \frac{1}{(2l+1)^2(2m+1)^2(2n+1)^2} \exp\left\{ -\frac{\pi^2}{4} D \left(\frac{(2l+1)^2}{a^2} + \frac{(2m+1)^2}{b^2} + \frac{(2n+1)^2}{c^2} \right) t \right\}$$

The series in the equation converges rapidly so that

$$\frac{C - C_e}{C_o - C_e} \approx \frac{8}{\pi^2} \exp\left\{ -\frac{\pi^2}{4} D (a^{-2} + b^{-2} + c^{-2}) t \right\}$$

Now $W_t - W_e = 8abc (C - C_e)$
and $W_o - W_e = 8abc (C_o - C_e)$

so the equation becomes

$$\frac{W_t - W_e}{W_o - W_e} \approx \frac{8}{\pi^2} \exp\left\{ -\frac{\pi^2}{4} D (a^{-2} + b^{-2} + c^{-2}) t \right\}$$

where W_t = weight at any time t;
W_o = weight at time $t = 0$;
W_e = weight attained when in equilibrium with surroundings.

If the logarithm of the weight of carbon dioxide in a sample of wood of dimensions 2a, 2b and 2c is plotted against time, the curve will ultimately become a straight line of slope

$$S = -\frac{\pi^2}{4} D (a^{-2} + b^{-2} + c^{-2})$$

rearrangement of which provides an estimate of the diffusion coefficient D.

1.6 Wood - Source, preparation and storage

The *Nothofagus fusca* heartwood used was obtained from the butt logs of two trees milled at McInroe's sawmill, Ikamatua, Westland. The boards were sealed in plastic during transit to Christchurch, dressed and cut to dimensions 500 mm × 100 mm × 25 mm, and stored in water. A small amount of formalin was added to the water to prevent decay.

1.7 Experimental procedures

The boards were cut to final dimensions 490 mm × 100 mm × 25 mm, and the green board length, width, thickness and weight were measured. The half and quarter length boards were of length 240 mm and 116 mm respectively. The boards were than sealed in polythene sleeving with a small slit cut at one end to permit entry and exit of carbon dioxide gas. The effect of the polythene was to minimise water loss from the boards during the period of carbon dioxide gas desorption. The weight of the board plus polythene sleeving was measured and the boards placed in the pressure cylinders. The cylinders were pressurised with carbon dioxide gas to a total pressure of 1.5 MPa, and the temperature maintained at 1, 20 or 30 ° C. Carbon dioxide gas absorption was for a period of 10 weeks to ensure a close approximation to saturation.

A second experimental procedure was used to check on the validity of using polythene sleeving to minimise water loss and to observe whether the sleeve might have an effect on the rate of carbon dioxide gas loss. This alternative procedure involved placing the boards in a controlled relative humidity cabinet, maintained at 93 % relative humidity and 30 ° C, during the period of carbon dioxide gas desorption. The boards were of smaller cross-sectional dimensions, 25 mm × 25 mm, with lengths of 489.5, 244.5 and 122.5 mm. Carbon dioxide gas absorption was for a period of 10 weeks.

Carbon dioxide gas desorption was initiated by rapid gas decompression to atmospheric pressure. The boards were removed from the pressure cylinders and the rate of carbon dioxide gas desorption measured by weighing the boards over time. The boards in the controlled relative humidity cabinet were hung from wires through plugged holes in the top of the cabinet. The boards were weighed by connecting the wires with the hook attachment on the underside of a Sartorius electronic balance placed directly above the holes.

Water loss also occurred from the boards during the period of carbon dioxide gas desorption. This was measured over time by weighing a separate groups of control boards that were not subject to carbon dioxide gas saturation.

When carbon dioxide gas desorption was complete, the boards were oven dried at 105 ° C and re-weighed.

1.8 Equipment

The dissolved carbon dioxide gas diffusivities at 20 and 30 ° C were measured in an air-conditioned room with the temperature thermostatically controlled to ± 0.5 ° C. Two pressure cylinders of internal volume 18 000 cm^3 were housed in this room. The gas pressure in each cylinder was measured with Ashcroft type 2279 Duratran pressure transmitters, pressure range 0 - 1000 psi (Dresser Industries Inc., Stratford, Connecticut, USA) and relayed to a Shinaden digital display. The temperature inside each cylinder was measured with inserted thermocouples linked to the Shinaden digital display.

A smaller pressure cylinder of internal volume 4000 cm^3 was used with the boards placed in the controlled relative humidity cabinet. The cylinder and the humidity cabinet were both housed in a laboratory in the Chemical and Process Engineering Department. The gas pressure in the cylinder was measured by a pressure gauge (Applied Instruments Ltd), with the temperature maintained at 30 ° C by a water bath heated by thermostatically controlled electrical heating coils and a motor-driven stirrer.

The controlled relative humidity cabinet was constructed of thick polystyrene sheets. The relative humidity was maintained at 93 % by trays of water placed in the bottom. The temperature was maintained at 30 ° C by a thermostatically controlled light bulb and a circulation fan.

The dissolved carbon dioxide gas diffusivity at 1 ° C was measured in a refrigerated storage room. A small pulp digester was used to saturate the boards with carbon dioxide gas. The gas pressure was measured using a pressure transducer (Action Instruments).

The board weights were measured using a Sartorius electronic balance.

1.9 Analysis procedures

1.9.1 Dissolved carbon dioxide gas diffusion coefficients

Corrections were required for the contribution of water loss to the total weight loss data of carbon dioxide gas desorption boards before dissolved gas diffusion coefficients could be calculated.

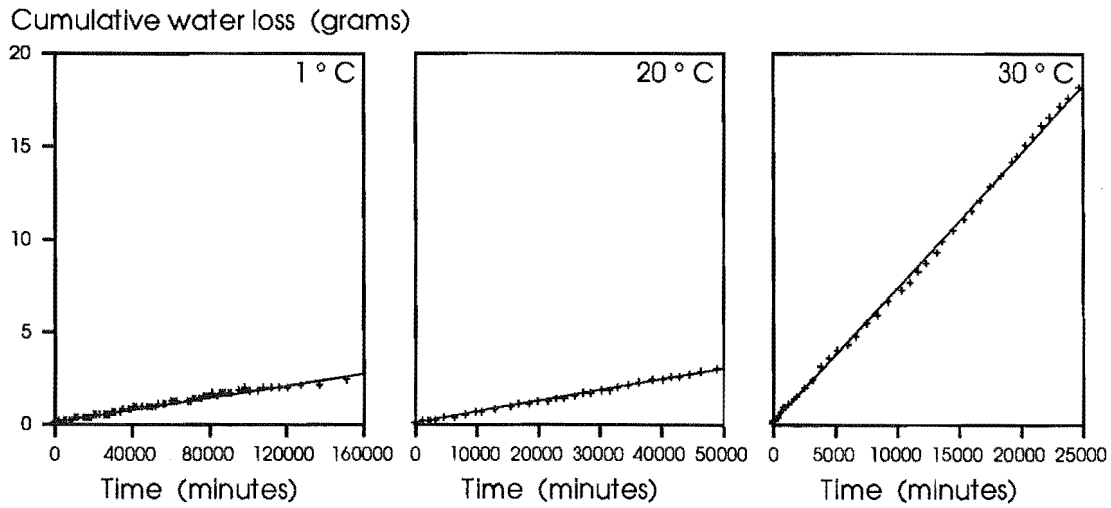

Figure 1.3 Cumulative water loss from full length green *Nothofagus fusca* heartwood boards in polythene sleeving at 1, 20 and 30 ° C. Note the different time scales of the plots.

Water loss from the boards with polythene sleeving was a linear function of time, and could be modelled using linear regression equations (figure 1.3). A range of regression coefficients were obtained from the water loss measurements of control boards. These were used as a guide in selecting a regression coefficient, for each carbon dioxide desorption board, that equilibrated with the water loss or rather weight loss beyond the period of carbon dioxide gas desorption. The regression coefficients were used to correct the weight loss data of each board for water loss during the period of carbon dioxide gas desorption, giving the rate of carbon dioxide gas loss.

Water loss from control boards in the controlled relative humidity cabinet showed a pattern of decreasing water loss with time (figure 1.4). The water loss values of the control boards of each length were therefore used to correct for the contribution of water loss to the total weight loss of carbon dioxide desorption boards. The small differences in water loss between the control boards and some carbon dioxide gas desorption boards, as shown by weight loss or gain after the period of carbon dioxide gas desorption, was further corrected by the addition or subtraction of a small quantity of water as a linear function of time, using linear regression equations, to give the rate of carbon dioxide gas loss.

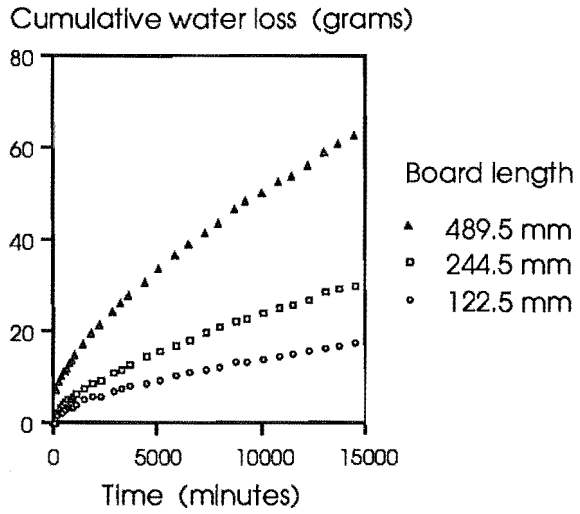

Figure 1.4 Cumulative water loss from green *Nothofagus fusca* heartwood boards of different lengths placed in the controlled relative humidity cabinet at 30 ° C.

When the logarithm of carbon dioxide gas loss $(W_t - W_e)/(W_o - W_e)$ was plotted against time, the curve became a straight line after a certain period of time had elapsed (figure 1.5). The linear portion of the curve represents transverse dissolved carbon dioxide gas diffusion, the slope of which

$$s = -\frac{\pi^2}{4} D (a^{-2} + b^{-2} + c^{-2})$$

is used to calculate the diffusion coefficient

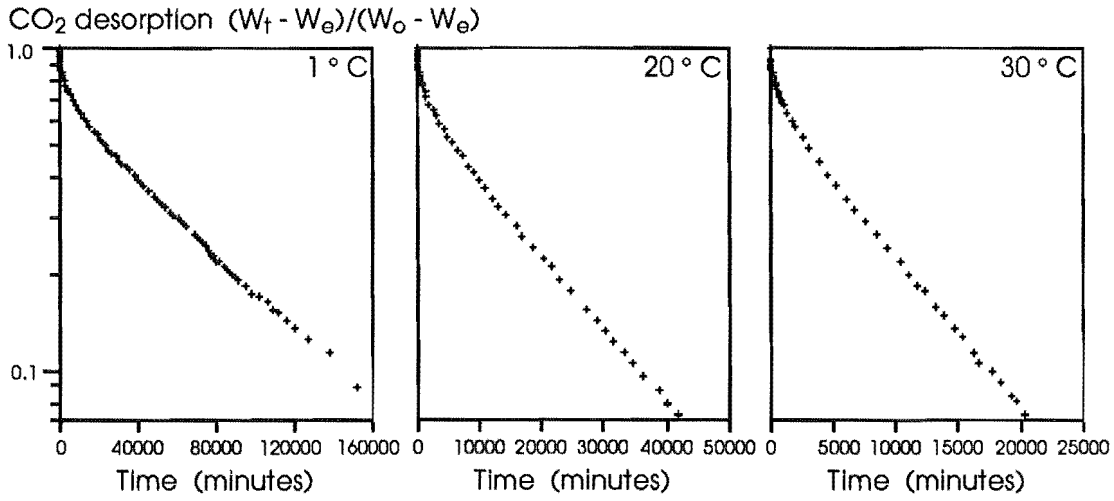

Figure 1.5 Carbon dioxide gas desorption from full length boards of green *Nothofagus fusca* heartwood at 1, 20 and 30 ° C. Note the different time scales of the plots.

$$D = \frac{4}{\pi^2} \frac{s}{(a^{-2} + b^{-2} + c^{-2})}$$

where a, b and c are half board length, width and thickness.

1.9.2 Carbon dioxide gas solubility

The amount of carbon dioxide gas absorbed in the wood was determined by extrapolating the initial board weight loss measurements back to time zero, the time at which the carbon dioxide gas decompression took place, and subtracting the weight of the board prior to placement in the pressure cylinder. From measurements of green and oven dry board weight, the amount of water in each board was calculated. The volume fraction occupied by the wood tissue, water and air within the wood were calculated using their respective densities. Following Weatherwax and Tarkow (1968) these were taken to be 1545.7 and 1000 kg/m^3 for wood tissue and water respectively.

The green wood contained a small but significant volume of air, the values for the percent saturation ranged from 79 - 99 % (percent saturation is defined as the proportion of the total volume other than wood tissue that is occupied by water, thus 90 % saturation implies that 90 % of this space is occupied by water and 10 % by air/carbon dioxide gas). Dissolved carbon dioxide gas will be absorbed in the air bubbles during the process of

saturation. To correct for this, the amount of carbon dioxide absorbed in the air bubbles was calculated and subtracted from the weight of carbon dioxide absorbed in the wood. This involved calculating the volume occupied by carbon dioxide gas in the air bubbles at a pressure of 1.5 MPa, and multiplying with density values obtained from Huang et al.'s (1985) equation of state for carbon dioxide.

Carbon dioxide gas solubility in water is also affected by the reaction of dissolved carbon dioxide molecules with water forming carbonic acid.

$$CO_2 + H_2O \rightleftharpoons H_2CO_3$$

The effect is very small, however, with only one out of very 400 molecules forming carbonic acid in solution.

Carbon dioxide gas solubilities were calculated as grams of carbon dioxide gas absorbed in the water per 100 grams of water in the wood.

1.10 Results

1.10.1 Dissolved carbon dioxide gas diffusion coefficients

Transverse diffusion coefficients of dissolved carbon dioxide gas in green *Nothofagus fusca* heartwood boards at 1, 20 and 30 ° C are presented in tables 1.1 - 1.3. Mean transverse diffusion coefficients in full length boards (490 mm) were 0.6×10^{-11} m^2 s^{-1} at 1 ° C, 4.2×10^{-11} m^2 s^{-1} at 20 ° C and 8.40×10^{-11} m^2 s^{-1} at 30 ° C. Individual transverse diffusion coefficients are plotted in figure 1.6.

The contribution of longitudinal diffusion was checked using boards of different length. Longitudinal diffusivities were observed by Huang et al. (1977) to be 5.5 times that of transverse diffusivity for dissolved oxygen diffusion in Douglas fir sapwood. Any increase in the contribution of longitudinal diffusion should therefore be marked by increase in the diffusion coefficient. Mean diffusivities of dissolved carbon dioxide gas in

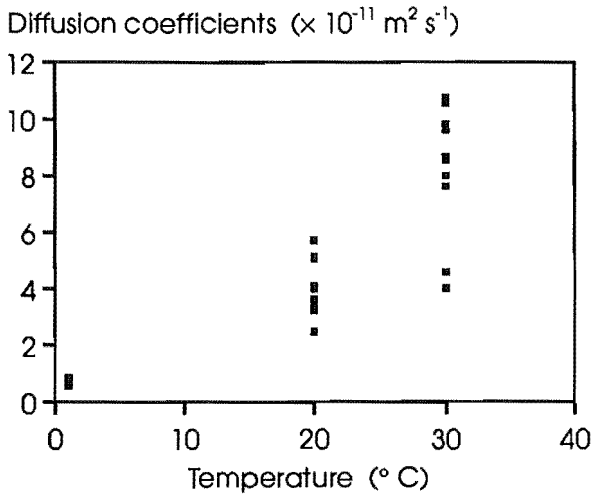

Figure 1.6 Transverse diffusion coefficients of dissolved carbon dioxide gas in green *Nothofagus fusca* heartwood boards at 1, 20 and 30 ° C.

green *N. fusca* heartwood at 20 ° C were essentially the same at 4.22 × 10^{-11} m^2 s^{-1} and 4.46 × 10^{-11} m^2 s^{-1} for boards of length 490 and 240 mm but increased to 8.77 × 10^{-11} m^2 s^{-1} at a length of 116 mm (figure 1.7). The results confirm that provided the boards are of sufficient length, the contribution of longitudinal diffusion can be considered negligible with dissolved carbon dioxide gas desorption occuring principally by transverse diffusion.

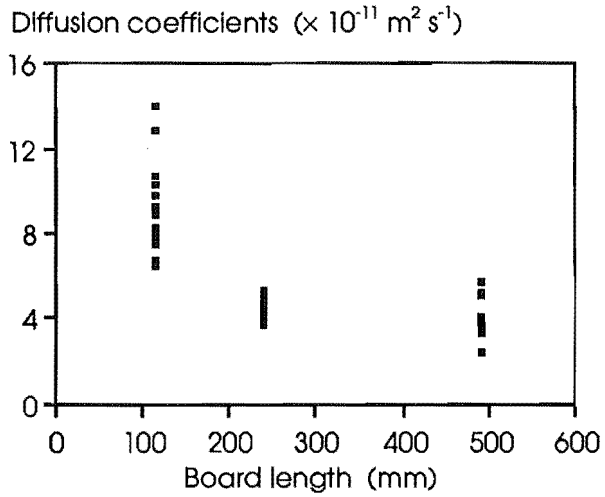

Figure 1.7 Effect of board length on dissolved carbon dioxide gas diffusion coefficients in green *Nothofagus fusca* heartwood.

Table 1.1 Transverse diffusion coefficients of dissolved carbon dioxide gas in full length green *Nothofagus fusca* heartwood boards at 1 ° C (× 10^{-11} m^2 s^{-1}).

Code	Run 1
B2	0.66
C2	0.62
D3	0.63
M1	0.61
W 1	0.83

Table 1.2 Transverse diffusion coefficients of dissolved carbon dioxide gas in green *Nothofagus fusca* heartwood boards at 20 ° C ($\times 10^{-11}$ m^2 s^{-1}).

Code	Run1	Code	Run2
Full length boards			
3A	5.03	B3	4.04
3B	3.34	C1	5.71
3C	5.17	H2	3.60
5B	2.46	J2	4.08
5D	3.64	Q1	3.27
9A	5.17	Q2	5.08
Half length boards			
B11	5.38	B12	5.25
J11	4.44	J12	4.30
L11	4.52	K11	3.83
P21	3.76	K12	4.16
X21	4.86	L12	4.35
X22	5.07	P22	3.64
Quarter length boards			
E122	9.79	E111	10.63
G111	8.14	E112	10.72
I211	7.67	E121	14.00
I222	7.70	G112	7.48
K221	9.30	G121	8.95
K222	8.27	G122	7.96
P111	6.58	I221	6.52
P112	7.83	K211	9.00
P121	6.51	K212	7.67
X112	8.13	P122	6.79
X121	9.00	X111	10.28
		X122	12.79

Table 1.3 Transverse diffusion coefficients of dissolved carbon dioxide gas in full length green *Nothofagus fusca* heartwood boards at 30 ° C ($\times 10^{-11}$ m^2 s^{-1}).

Code	Run1	Code	Run2
AE1	9.65	AA1	9.65
AU1	9.82	AO2	10.59
AW2	7.63	AU2	8.57
BA1	4.40	AX2	8.04
BB1	4.59	BC1	8.71
		BC2	10.72

The transverse diffusion coefficients of dissolved carbon dioxide gas in green N. fusca heartwood boards placed in the controlled relative humidity cabinet at 30 ° C were used as a check on the effect polythene sleeving had on the rate of carbon dioxide gas loss. The mean transverse diffusion coefficient for the full length boards in the controlled relative humidity cabinet was 7.98×10^{-11} m^2 s^{-1} (table 1.4). This is very similar to the mean value of 8.40×10^{-11} m^2 s^{-1} obtained at 30 ° C for boards wrapped in polythene sleeving. The polythene sleeving appears to have no effect on the rate of carbon dioxide gas loss, confirming the validity of the previous results.

The transverse diffusion coefficients for the board lengths 489.5 and 244.5 mm were similar with means of 7.98×10^{-11} m^2 s^{-1} and 9.12×10^{-11} m^2 s^{-1} respectively. At the board length 122.5 mm, however, there is the suggestion that one of the boards (AN32) may have been affected by longitudinal diffusion giving a diffusion coefficient double that of other boards. This ties in well with the previous results on the effect of board length at 20 ° C where the diffusion coefficients of boards of length 116 mm were double those of boards of lengths 490 and 240 mm.

The activation energy (E_a) for the diffusion of dissolved carbon dioxide gas in green *Nothofagus fusca* heartwood was obtained using the Arrhenius equation

$$D = Ae^{-E_a/RT}$$

Table 1.4 Transverse diffusion coefficients of dissolved carbon dioxide gas in green *Nothofagus fusca* heartwood boards placed in the controlled relative humidity cabinet at 30 ° C ($\times 10^{-11}$ m^2 s^{-1}).

Code	Run1
Board length 489.5 mm	
AN1	6.13
BF2	8.63
AJ2	9.17
Board length 244.5 mm	
AN31	8.51
AJ11	10.05
BF31	8.84
BF11	9.07
Board length 122.5 mm	
AN32	20.51
BF12	8.49
AJ12	6.89
BF32	6.98

where A is a constant called the pre-exponential factor, R the gas constant, and T the temperature. The equation can also be written as

$$\ln D = \ln A - E_a/RT$$

A plot of ln D against $1/T$ gives a straight line the slope of which is $-E_a/R$ and the intercept at $1/T = 0$ is ln A.

Plotting the transverse diffusion coefficients of dissolved carbon dioxide gas in green *N. fusca* heartwood at 1, 20 and 30 ° C (tables 1.1 - 1.3) gives a slope of -7.15×10^3 (figure 1.8) and an activation energy of 59.4 kJ mol^{-1}.

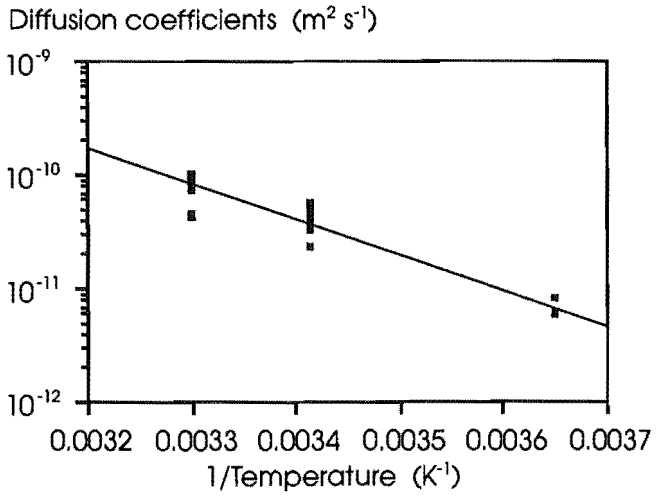

Figure 1.8 The Arrhenius plot of ln D against 1/T for the diffusion of dissolved carbon dioxide gas in green *Nothofagus fusca* heartwood.

1.10.2 Carbon dioxide gas solubility

The carbon dioxide gas solubilities obtained for the water in green *Nothofagus fusca* heartwood at 1, 20 and 30 ° C and 1.5 MPa are presented in tables 1.5 - 1.7 and figure 1.9.

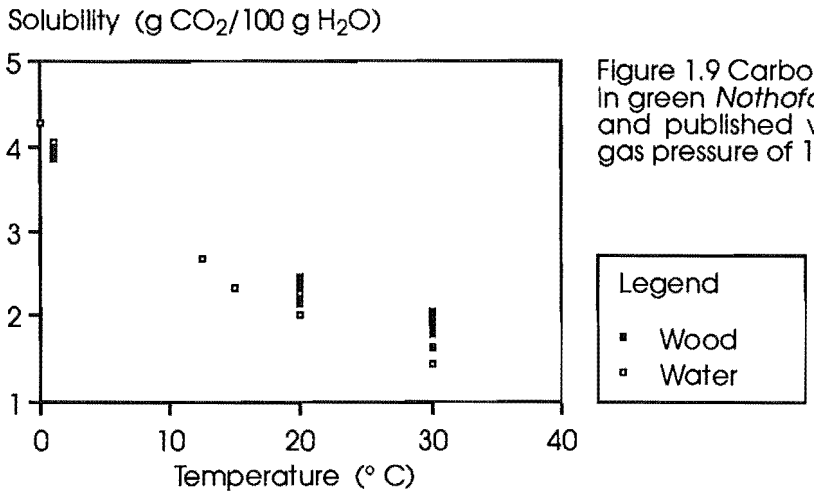

Figure 1.9 Carbon dioxide gas solubility in green *Nothofagus fusca* heartwood and published values for water at a gas pressure of 1.5 MPa.

The solubilities at 1 ° C correspond well with the literature value for pure water of 4.05 g CO_2/100 g H_2O obtained from Dodds et al.'s (1956) smoothed solubility curves (figure 1.9). The solubilities at 20 ° C correspond well with the experimental value for pure water of 2.283 g CO_2/100 g H_2O obtained by Bartholome and Fritz (1956), but appear a little high compared with the solubility value of 2.0 g CO_2/100 g H_2O obtained from Dodds et al.'s smoothed solubility curves. Bartholome and Fritz's solubility value may be a little high in view of the fact that over a range of

pressure and temperature their experimental values are higher than those of other workers. The solubility of carbon dioxide gas in the water of *N. fusca* heartwood at 30 ° C also appears a little high when compared with the solubility value for pure water of 1.43 g CO_2/100 g H_2O obtained from Dodds et al.'s smoothed solubility curves. It is questionable whether any conclusions can be drawn regarding an interaction of dissolved carbon dioxide gas and wood constituents at higher temperatures, due to a lack of experimental values for carbon dioxide gas solubilities in pure water at 1.5 MPa and the relatively small deviations of *N. fusca* values from published solubility curves.

Table 1.5 Carbon dioxide gas solubility in the water of full length green *Nothofagus fusca* heartwood boards at 1 ° C and 1.5 MPa (g CO_2/100 g H_2O).

Code	Run1
B2	3.91
C2	4.00
D3	4.02
M1	4.01
V1	3.85
W1	4.06

Table 1.6 Carbon dioxide gas solubility in the water of green *Nothofagus fusca* heartwood boards at 20 ° C and 1.5 MPa (g CO_2/100 g H_2O).

Code	Run1	Code	Run2
Full length boards			
3A	2.36	B3	2.38
3B	2.34	C1	2.36
3C	2.31	H2	2.41
5B	2.14	J2	2.47
5D	2.41	Q1	2.32
9A	2.34	Q2	2.34

Half length boards

B11	2.29	B12	2.35
J11	2.38	J12	2.25
L11	2.34	K11	2.21
P21	2.37	K12	2.29
X21	2.30	L12	2.21
X22	2.37	P22	2.25

Quarter length boards

E122	2.33	E111	2.27
G111	2.40	E112	2.19
I211	2.36	E121	2.16
I212	2.25	G112	2.29
I222	2.30	G121	2.22
K221	2.32	G122	2.22
K222	2.38	I221	2.29
P111	2.26	K211	2.26
P112	2.24	K212	2.21
P121	2.28	P122	2.26
X112	2.31	X111	2.15
X121	2.26	X122	2.17

Table 1.7 Carbon dioxide gas solubility in the water of full length green *Nothofagus fusca* heartwood boards at 30 ° C and 1.5 MPa (g CO_2/100 g H_2O).

Code	Run1	Code	Run2
AE1	1.62	AA1	1.93
AH1	1.85	AO2	1.98
AU1	2.06	AU2	1.96
AW2	1.78	AX2	1.94
BA1	2.04	BC1	1.93
BB1	1.81	BC2	1.95

1.11 Discussion

Transverse diffusion coefficients of dissolved carbon dioxide gas in green *Nothofagus fusca* heartwood were slightly lower than those obtained by Huang et al. (1977) for dissolved oxygen diffusion in Douglas fir sapwood. The differences can probably be attributed to the molecular sizes of the solutes and the wood anatomy of the two species.

The transverse diffusion coefficients in *N. fusca* wood are much smaller than the published values of dissolved carbon dioxide diffusivity in water at 0, 20 and 30 ° C (table 1.8). Transverse dissolved carbon dioxide diffusivity in *N. fusca* at 1 ° C is about 0.6 % of the dissolved carbon dioxide diffusivity in water (using Tammann and Jessen's value at 0 ° C). At 20 ° C this increases to about 2.5 % and at 30 ° C the transverse diffusivity in *N. fusca* is about 3.8 % of the dissolved carbon dioxide diffusivity in water. The diffusion of dissolved carbon dioxide gas in *N. fusca* increases at a greater rate with increasing temperature than the diffusion of dissolved carbon dioxide gas in water. The diffusion coefficient of dissolved carbon dioxide gas in *N. fusca* approximately doubles with each 10 ° C increase in temperature (figure 1.6).

Table 1.8 Carbon dioxide diffusion coefficients in water

Temperature °C	Diffusion coefficient $\times 10^{-9}$ m^2 s^{-1}	Source
0	0.96	Tammann and Jessen (1929)
20	1.77	Onda, Okamato and Yamaji (1960)
	1.60	Tang and Himmelblau (1963)
	1.63	Davidson and Cullen (1957)
	1.69	Nijsing, Hendriksz and Kramers (1959)
30	2.06	Ringbom (1938)
	2.29	Peaceman (1951)
	2.25	Davidson and Cullen (1957)
	2.15	Tang and Himmelblau (1963)

From Himmelblau (1964).

This temperature dependence of the diffusion coefficient follows the Arrhenius equation (figure 1.8) giving an activation energy value of 59.4 kJ mol^{-1} for the diffusion of dissolved carbon dioxide gas in *N. fusca*, three times the activation energy value of 18.8 kJ mol^{-1} for the diffusion of dissolved carbon dioxide gas in water (Maharajh and Walkley 1973). The higher activation energy explains the steeper temperature dependence of the dissolved carbon dioxide gas diffusion coefficients in *N. fusca* and suggests that there is some form of reaction mechanism between the dissolved carbon dioxide gas molecules and the cell wall constituents. It was not previously known that such a reaction mechanism occurred.

The variation of transverse diffusion coefficients among boards (figure 1.6) probably results from differences in wood anatomy such as the proportion of earlywood and latewood within growth rings, differences in the amount of air present in the wood and from errors in the water loss correction. The percent saturation of boards varied from 79 - 99 % and while this could be expected to affect the diffusion coefficients of dissolved carbon dioxide gas in wood, no consistent pattern was observed due presumably to the interaction of other factors. Changes in the linear coefficients of water loss were observed over time in some control boards and there can be little doubt this also occured in some carbon dioxide gas desorption boards. The correction for water loss, based on the rate of water loss after the period of carbon dioxide gas desorption, could therefore introduce an error into the diffusion coefficient if the rate of water loss during the period of carbon dioxide gas desorption had been greater or smaller than the subsequent water loss. The contribution of this error is unknown, but boards that failed to produce a convincing straight line when the logarithm of carbon dioxide gas loss was plotted against time were excluded from the analysis. Only two were noted, one quarter length board at 20 ° C and one full length board at 30 ° C.

Substantial carbon dioxide gas loss occurs during the initial stages of desorption before the plot of the logarithm of carbon dioxide gas loss against time becomes a straight line (figure 1.5). This is believed to be the result of mass flow of carbon dioxide gas and the longitudinal diffusion of dissolved carbon dioxide gas from the board end faces. Microscopic observations of initial carbon dioxide gas loss showed mass flow of carbon dioxide gas bubbles occuring from vessels, principally those cut on the

board end faces. The occlusion of pit membranes in *N. fusca* heartwood and the absence of any substantial mass flow of water would suggest that mass flow of carbon dioxide gas is confined to surface vessels. In *Nothofagus* the vessel lengths are very short. The majority of vessels in *N. fusca* are less than 2 cm long, with 97 % of the vessels shorter than 8 cm (Middleton and Butterfield 1990). In addition, vessels in the heartwood of *N. fusca* are generally sealed by tyloses that grow into the vessel lumen from neighbouring parenchyma cells. The mass flow of carbon dioxide gas in *N. fusca*, although occuring for a period of at least several hours, appears very restricted. The suggestion therefore is that much of the initial carbon dioxide gas loss occurs by longitudinal diffusion from the board ends.

Longitudinal and transverse dissolved carbon dioxide gas diffusion could be modelled using an bimodal diffusion equation (Jason and Peters 1973) that is the sum of two exponential terms, each containing a diffusion coefficient

$$\frac{W_t - W_e}{W_o - W_e} = \beta_1\Sigma_1 + \beta_2\Sigma_2$$

where W_t = weight at any time t;
W_o = weight at time t = 0;
W_e = weight attained when in equilibrium with surroundings;

$$\Sigma_1 = \sum_{n=0}^{\infty} \frac{1}{(2n+1)^2} \exp(-(2n+1)^2\alpha_1 t)$$

Σ_2 is as for Σ_1 with an appropriate value of α substituted;

$$\alpha = \frac{\pi^2}{4} \frac{D}{(a^2 + b^2 + c^2)}$$

D = diffusion coefficient;
a, b and c are half length, width and thickness;

$$\beta_1 = \frac{8}{\pi^2} \frac{M_{1o} - M_{1e}}{M_o - M_e}$$

β_2 is as for β_1 with values of M_{2o} and M_{2e} substituted;

M_{1o} and M_{2o} are the masses of carbon dioxide in each diffusion component at t = 0;

Mo = mass of carbon dioxide at t = 0;
Me = mass of carbon dioxide when in equilibrium with surroundings.

Measurements of the longitudinal and transverse diffusion coefficients of dissolved carbon dioxide gas in wood are required along with the corresponding components of carbon dioxide gas $(M_{1o} - M_{1e})/(M_o - M_e)$ and $(M_{2o} - M_{2e})/(M_o - M_e)$ that are attributed to longitudinal and transverse diffusion.

The contribution of the mass flow of carbon dioxide gas will depend on the internal volume of the cut surface vessels and the board shape. If mass flow can be expressed as a function of time, then a mathematical model of carbon dioxide gas desorption from green wood could be developed.

1.12 Summary

Non-steady state carbon dioxide gas desorption from green *Nothofagus fusca* heartwood boards saturated with carbon dioxide gas at a pressure of 1.5 MPa was used to determine transverse dissolved carbon dioxide gas diffusivities in wood at 1, 20 and 30 ° C. Mean transverse diffusion coefficients of dissolved carbon dioxide gas in *N. fusca* heartwood were 0.6 $\times 10^{-11}$ $m^2 s^{-1}$ at 1 ° C, 4.2 $\times 10^{-11}$ $m^2 s^{-1}$ at 20 ° C and 8.40 $\times 10^{-11}$ $m^2 s^{-1}$ at 30 ° C. These are 0.6, 2.5 and 3.8 % of the dissolved carbon dioxide gas diffusivities in water at 1, 20 and 30 ° C respectively.

The activation energy of dissolved carbon dioxide gas diffusion in *N. fusca* heartwood is 59.4 kJ mol^{-1}, three times the activation energy value of 18.8 kJ mol^{-1} for the dissolved carbon dioxide gas diffusion in water. The higher activation energy explains the steeper temperature dependence of the dissolved carbon dioxide gas diffusion coefficients in *N. fusca* heartwood, and suggests some form of reaction mechanism between the dissolved carbon dioxide gas molecules and the cell wall constituents.

Initial carbon dioxide gas loss from *N. fusca* heartwood after decompression is both rapid and substantial. This is derived from mass flow and longitudinal diffusion from board ends. Mass flow of carbon dioxide gas is confined to surface vessels due to the occluded nature of heartwood pits. It occurs for a period of at least several hours. The contribution it makes to the total carbon dioxide gas loss depends on the internal volume of the cut surface vessels and the board shape. Longitudinal diffusion from board ends occurs for a period of several days to a few weeks depending on temperature and is thought to be responsible for much of the initial carbon dioxide gas loss. The contribution of longitudinal diffusion to the total carbon dioxide gas loss becomes increasingly important in boards of short length. Measurements of transverse dissolved carbon dioxide gas diffusivities were unaffected by longitudinal diffusion provided boards were of length 240 mm or greater.

The solubilities of carbon dioxide gas in the water of *N. fusca* heartwood at a pressure of 1.5 MPa and temperatures 1, 20 and 30 ° C were similar to those published for carbon dioxide gas in pure water.

Further work is required before a model of dissolved carbon dioxide gas absorption and desorption in green wood can be developed. Measurement of longitudinal dissolved carbon dioxide gas diffusivities in green wood are needed, as well as their contribution to the total mass of carbon dioxide gas absorbed or desorbed. Account also needs to be taken of the contribution of mass flow and the way in which board shape affects each component of carbon dioxide gas absorption and desorption.

References

Atkins, P. W., 1986, Physical chemistry, Third edition, Oxford University Press, Oxford, 857 pp.

Bartholome, E. and Fritz, H., 1956, Solubility of carbon dioxide in water at high pressures, *Chemie Ingenieur Technik*, 11, 706 - 708.

Davidson, J. F. and Cullen, E. J., 1957, The determination of diffusion coefficients of sparingly soluble gases in liquids, *Transactions of the Institution of Chemical Engineers (London)*, 35, 51 - 60.

Dodds, W. S., Stutzman, L. F. and Sollami, B. J., 1956, Carbon dioxide solubility in water, *Industrial and Engineering Chemistry, Chemical and Engineering Data Series*, 1(1), 92 - 95.

Himmelblau, D. M., 1964, Diffusion of dissolved gases in liquids, *Chemical Reviews*, 64(5), 527 - 550.

Huang, F., Li, M., Lee, L. L., Starling, K. E. and Chung, F. T. H., 1985, An accurate equation of state for carbon dioxide, *Journal of Chemical Engineering of Japan*, 18(6), 490 - 496.

Huang, H. I., Sarkanen, K. V. and Johanson, L. N., 1977, Diffusion of dissolved oxygen in liquid-saturated Douglas fir sapwood, *Wood Science and Technology*, 11(3), 225 - 236.

Jason, A. C., 1959, A study of evaporation and diffusion processes in the drying of fish muscle, Fundamental aspects of the dehydration of food stuffs, *London: Society of Chemical Industry*, 103 - 134.

Jason, A. C. and Peters, G. R., 1973, Analysis of bimodal diffusion of water in fish muscle, *Journal of Physics D: Applied Physics*, 6(4), 512 - 521.

Kininmonth, J. A., 1972, Permeability and fine structure of certain hardwoods and effects on drying. II. Differences in fine

structure of *Nothofagus fusca* sapwood and heartwood, *Holzforschung*, 26(1), 32 - 38.

Maharajh, D. M. and Walkley, J., 1973, The temperature dependence of the diffusion coefficients of Ar, CO_2, CH_4, CH_3Cl, CH_3Br, and $CHCl_2F$ in water, *Canadian Journal of Chemistry*, 51, 944 - 952.

Middleton, T. M. and Butterfield, B. G., 1990, Vessel length distribution in the stems of three New Zealand species of *Nothofagus*, *Wood Science and Technology*, 24(1), 17 - 22.

Nijsing, R. A. T. O., Hendriksz, R. H. and Kramers, H., 1959, Absorption of CO_2 in jets and falling films of electrolyte solutions, with and without chemical reaction, *Chemical Engineering Science Genie Chimique*, 10(1/2), 88 - 104.

Onda, K., Okamato, T. and Yamaji, Y., 1960, *Chemical Engineering, Japan (Tokyo)*, 24, 918.

Peaceman, O. W., 1951, Sc.D. Thesis, Massachusetts Institute of Technology, USA.

Ringbom, A., 1938, *Zeitschrift fuer Anorganische und Allgemeine Chemie*, 238, 94.

Tammann, G. and Jessen, V., 1929, Diffusion coefficients in water and their temperature dependence, *Zeitschrift fuer Anorganische und Allgemeine Chemie*, 179, 125.

Tang, Y. P. and Himmelblau, D. M., 1963, Interphase mass transfer for laminar concurrent flow of carbon dioxide and water between parallel plates, *American Institute of Chemical Engineers Journal*, 9(5), 630 - 635.

Weatherwax, R. C. and Tarkow, H, 1968, Density of wood substance: the importance of penetration and adsorption compression of the displacement fluid, *Forest Products Journal*, 18(7), 44 - 46.

Chapter 2

Decompression drying of *Pinus radiata* sapwood chips

2.1 Introduction

The nucleation of bubbles of a solute gas in supersaturated aqueous solutions, provides a rapid means of drying sapwood chips. The supersaturated state is achieved by lowering the applied gas pressure, usually by some tens or hundreds of atmospheres, to atmospheric pressure. The bubbles that form consist almost entirely of molecules of the solute gas, with only negligible fractions of molecules of the solvent water. Within the wood structure, they effectively force the free water from the cell lumens.

The rate of bubble nucleation, J, is a very sensitive function of the supersaturation, σ. The supersaturation, σ, is given by α - 1, where α the saturation ratio is C_2/C_{2s}, where C_2 and C_{2s} are the concentrations of dissolved gas and the corresponding equilibrium concentration over a flat surface. Lubetkin and Blackwell (1988) showed quite clearly for carbon dioxide gas dissolved in water, that the number of bubbles and their rate of production increase with increasing supersaturation (figure 2.1).

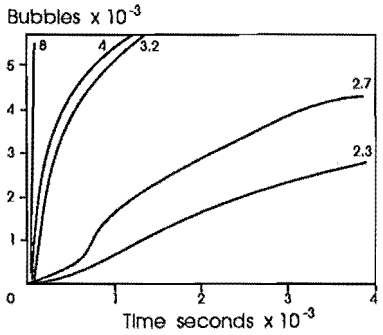

Figure 2.1 The number of bubbles released as a function of time at various supersaturations, σ, shown by the numbers associated with each curve, at 22 ° C.

The rate of dissolution of the gas under applied pressure into the water is determined by the rate of diffusion of the gas through the liquid-gas

interface. Subsequent diffusion within the water will be affected by the permeability of the woods structure. Gas absorption in wood chips will be expected to occur largely by longitudinal diffusion.

The permeability will also determine the ease with which the water is removed, under the influence of the pressure gradient generated by the expanding gas bubbles. The permeability is defined by Darcy's Law:

$$K = \frac{QL\eta}{A\Delta P}$$

where: K = permeability,
Q = flow rate,
L = length of the specimen,
η = viscosity,
A = cross-sectional area of flow,
ΔP = pressure difference across the specimen.

The permeability varies with the structural orientation of the wood. The ratio of longitudinal to tangential permeability varies from 520 - 81600, and the longitudinal to radial from 15 - 547000 depending on species (Comstock 1970). For *Pinus radiata* sapwood, tangential and radial permeabilities are only 0.01 % of the longitudinal permeability (table 2.1). Decompression drying would therefore, be expected to occur principally through the end-grain of sapwood chips.

Table 2.1 The permeability of green *Pinus radiata* sapwood

Identification number	Permeabilities Longitudinal ($\times 10^{-15}$ m^2)	Radial ($\times 10^{-18}$ m^2)	Tangential ($\times 10^{-18}$ m^2)
32	3600 ± 900	85 ± 50	263 ± 33
38	4100 ± 1900	65 ± 33	410 ± 200

from Booker 1990

Factors that affect longitudinal permeability of *Pinus radiata* sapwood include: sample length, the proportion of latewood/earlywood, compression wood, and the sampling of wood within and between trees. Longitudinal permeability is relatively constant with length, down to approximately 20 mm. Below this, longitudinal permeability increases

sharply with diminishing length. The longitudinal permeability of latewood and compression wood is very low compared with that of earlywood. Within trees, the longitudinal permeability increases with height from the butt to the crown. Three-quarters of this increase with height could be attributed to an increase in earlywood permeability. The remaining quarter is due to an increase in the proportion of earlywood. Significant longitudinal permeability differences were also found between trees (Booker and Kininmonth 1978).

2.2 Experiment design

The experiment involved an assessment of the relative effects of process variables on decompression drying. The variables included temperature, pressure and time. Temperature affects the rate of gas diffusion into the water, pressure the concentration of dissolved gas in the water, and time the amount of gas dissolved for a given temperature and pressure.

Table 2.2 Carbon dioxide and nitrogen gas diffusion coefficients and solubilities in water

Gas	Diffusion coefficients[1] ($\times 10^{-9}$ $m^2 s^{-1}$)	Solubilities[2] (cm^3 of gas at STP / g of H_2O) 25 ° C	50 ° C
Carbon dioxide	1.99	27.23	17.25
Nitrogen	2.19	0.67	0.53

1 measured at 25 ° C and 0.1013 MPa, from Ng and Walkley 1969,
2 measured at 5.065 MPa, from Wiebe 1941 and Wiebe et al. 1933.

The gases used were carbon dioxide and nitrogen. Both have similar diffusion coefficients in water, but carbon dioxide gas has a much greater solubility in water than nitrogen gas (table 2.2). High gas solubilities in water can be expected to improve the effectiveness of decompression drying by increasing the supersaturation, σ, of the gas in the water at decompression, increasing the number and the rate of gas bubble formation in the wood (figure 2.1). The way in which the process variables affect the solubility of the gas in the water and the total amount of gas absorbed, will, it is believed, determine how they affect the decompression drying of wood chips.

Pressure and temperature both have a strong effect on the solubility of carbon dioxide gas in water (figure 2.2). Carbon dioxide solubility increases with pressure but declines with temperature. The rate of dissolved carbon dioxide gas diffusion, however, increases with temperature which may to some extent offset the reduced solubility. The amount of carbon dioxide gas absorbed will increase with the period of absorption time. The response of decompression drying to process variables will therefore depend on the way in which the process variables interact with each other.

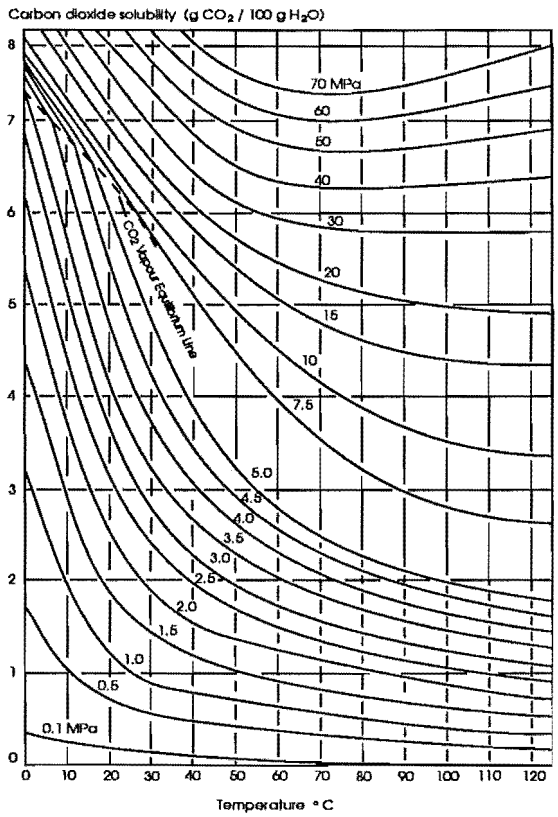

Figure 2.2 Effect of temperature and pressure on the solubility of carbon dioxide in water (from Dodds et al. 1956).

A three-way factorial analysis of variance (Anova) design was therefore used for the statistical analysis of carbon dioxide gas effects on decompression drying. A combination of five temperatures (15, 20, 25, 30, 35 and 40 ° C), three pressures (1.50, 4.89 and 6.89 MPa), and three absorption time periods (5, 15 and 45 minutes) were used in what amounted to two overlapping factorial analyses (table 2.3). The design was partially replicated.

Table 2.3 The combinations of temperature and pressure used for decompression drying with carbon dioxide gas

Temperature ° C	Pressure MPa		
15	1.50	4.89	
20	1.50	4.89	
25	1.50	4.89	
30	1.50	4.89	6.89
35	1.50	4.89	6.89
40	1.50	4.89	6.89

The very low solubility of nitrogen gas in water at a pressure of 5.065 MPa (table 2.2) suggests that the process variable pressure, which determines

the concentration of dissolved gas in the water, is of little importance in determining the decompression drying ability of nitrogen gas compared with temperature and absorption time, which determine the rate and amount of gas absorbed for a given solubility. The extent to which the water is saturated with nitrogen gas is probably of greatest importance given the low solubility.

A two-way factorial analysis of variance (Anova) design was therefore used for the statistical analysis of nitrogen gas effects on decompression drying. A combination of three temperatures (20, 30 and 40 ° C) and three absorption time periods (5, 15 and 45 minutes) were used with a nitrogen gas pressure of 4.89 MPa. The design was not replicated.

Decompression drying with carbon dioxide and nitrogen gas may also be affected by the extent to which the wood chips are saturated with water. The expansion of dissolved supersaturated carbon dioxide or nitrogen gas into pre-existing gas/water vapour bubbles within the wood chip could improve the process of decompression drying. Repeated cycles of decompression drying were used with a view to testing the idea. Two cyclic decompression drying time series were used, one involving nine repeated cycles of 5 minutes absorption time and the other three repeated cycles of 15 minutes absorption time, both giving a total gas absorption time of 45 minutes. The two cyclic decompression drying treatments were used with carbon dioxide and nitrogen gas for each combination of temperature and pressure. They were incorporated with the 5, 15 and 45 minute absorption times in the two- and three-way factorial analysis of variance. In addition, Scheffe's method was used to compare the effectiveness of cyclic versus non-cyclic decompression drying for a total gas absorption time of 45 minutes.

A separate three-way factorial analysis of variance was also performed to compare decompression drying with carbon dioxide and nitrogen gas at a pressure of 4.89 MPa and a combination of three temperatures (20, 30 and 40 ° C) and five absorption time periods (5, 15 and 45 minutes, 9 cycles of 5 minutes, and 3 cycles of 15 minutes). The variables in the analysis were temperature, time and carbon dioxide versus nitrogen (CO_2 vs N_2).

The process variables temperature, pressure and time were all fixed treatments, making the factorial analysis of variance a Model I Anova (Sokal and Rohlf 1981).

2.3 Decompression drying equipment

The equipment was housed in an air-conditioned room with the temperature thermostatically controlled to ± 0.5 ° C of the required operating temperature.

The pressure equipment consisted of two pressure cylinders connected in series to a carbon dioxide gas supply cylinder. The first served as a large reservoir cylinder (18 000 cm^3) to the second smaller cylinder (1800 cm^3), in which the decompression drying took place (figure 2.3). The cylinders were connected by Synflex hydraulic hosing (3130-06 SAE 100R71 3/8 ", working pressure 2250 psi, 155 bar) via ball valves (Klinger ball-o-top & NVC.DN15 PN140.SS types).

System pressure was measured with a Ashcroft type 2279 Duratran pressure transmitter, pressure range 0 - 1000 psi (Dresser Industries Inc., Stratford, Connecticut, USA) and relayed to a Shinaden digital display.

Temperature within the cylinders was measured using an inserted thermocouple linked to the Shinaden digital display.

A NVC.DN15 PN140.SS type ball valve, directly connected to the small decompression drying cylinder, was used to rapidly decompress the gas in the system at the end of the absorption period.

2.4 Wood chip preparation

Flat sawn boards (100 mm × 25 mm) of *Pinus radiata* sapwood were randomly selected from the grading table at McVicars sawmill, Christchurch, in September 1987. These were dressed, cross-cut to 0.5 m lengths, cut longitudinally into three strips (25 mm × 30 mm × 0.5 m), and

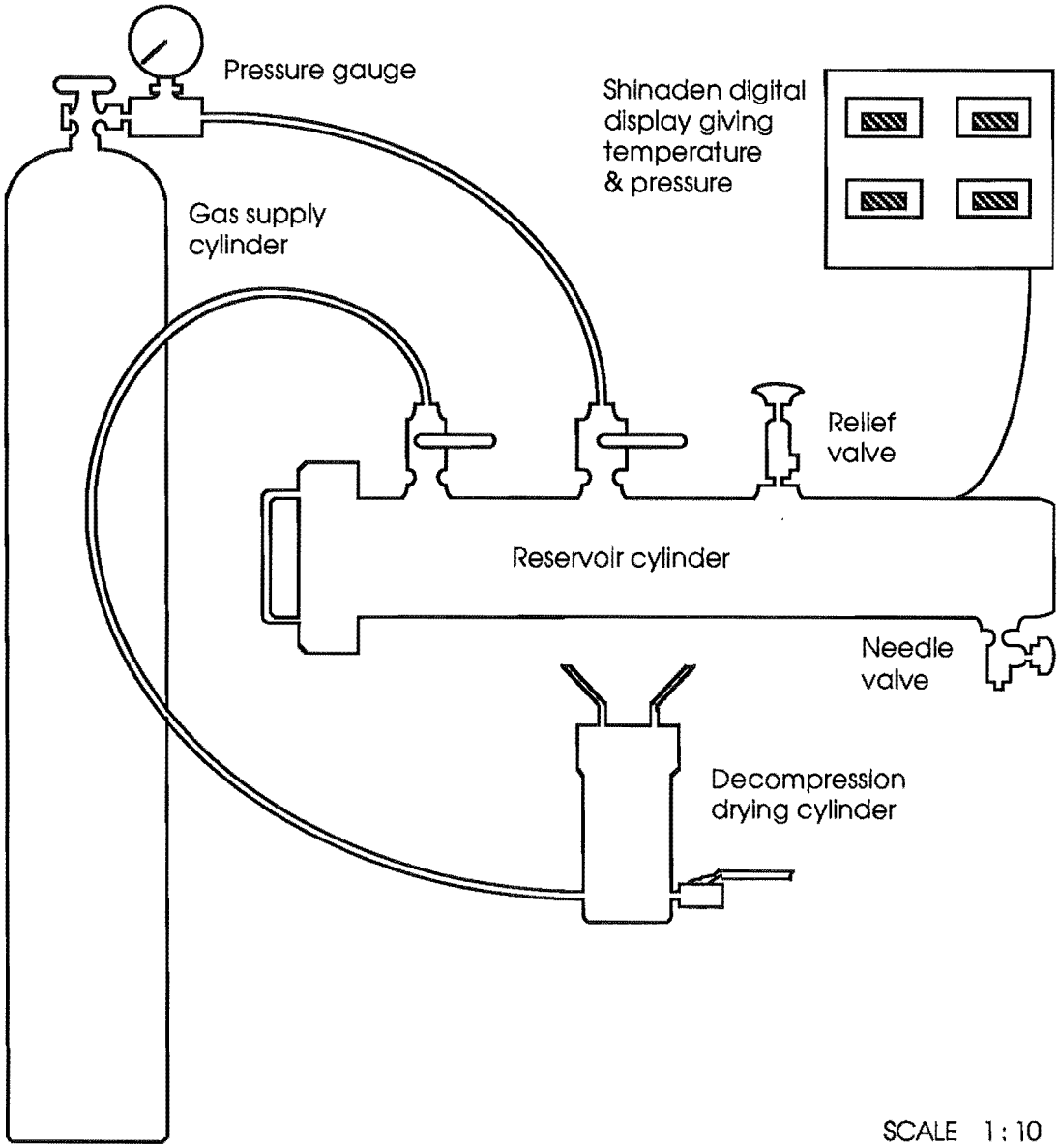

Figure 2.3 Decompression drying equipment

then ripped and cross-cut to give wood chips of dimensions 8 mm × 25 mm × 25 mm with a flat sawn orientation.

These were stored in water with the addition of a small amount of formalin to prevent decay.

Prior to decompression drying, the rough wood chip edges were trimmed with a razor blade, and the wood chips placed overnight in a water bath set to the operating temperature.

The wood chip moisture content ranged from 95 - 199 %, with percent saturations of 93 - 99 % and basic densities of 372 - 611 kg/m^3. The large range of values for moisture content and basic density reflect the large differences in the proportions of latewood and earlywood in the wood chips.

2.5 Decompression drying procedure

The reservoir cylinder was pressurised to the operating pressure, and its temperature allowed to re-equilibrate to the operating temperature.

One hundred wood chips were randomly selected for each run, fifty to measure decompression drying, and fifty as controls to correct for evaporative moisture loss, particularly at elevated operating temperatures. The wood chips were wiped dry, individually weighed, and placed in either the decompression drying cylinder or an enclosed metal container.

The decompression drying cylinder was pressurised from the reservoir cylinder by opening the ball valve separating the two, this remained open during the carbon dioxide absorption phase. The effect was very rapid pressurisation with only a small drop in pressure. This was quickly adjusted with the addition of gas from the carbon dioxide gas supply cylinder. The temperature increase associated with pressurisation was small, and quickly re-equilibrated to the operating temperature. Decompression was initiated by shutting off the ball valve between the reservoir and decompression drying cylinder, and opening the ball valve connected directly to the decompression drying cylinder. Decompression was rapid, taking just a few seconds, depending on the pressure.

The wood chips were quickly removed from the cylinder and wiped dry to prevent the re-absorption of water. Within the cylinder, the wood chips were placed on an aluminium mesh to allow the expelled water to drain

to the base of the cylinder. The wood chips were then individually weighed, and the procedure repeated for cyclic decompression drying .

2.6 Sequence of experimental runs

For practical reasons, the order in which the experimental runs were performed was determined randomly first on the basis of temperature, then pressure, and finally time. That is, the room and equipment were set to a particular temperature (in random order), each pressure was then performed for this temperature (in random order), and finally each time period performed for the set pressure. The rationale behind this was the time required for the room and equipment to reach thermal equilibrium at each temperature, and pressure. Pressurising the reservoir cylinder from 0.1013 MPa to 4.89 and 6.89 MPa, produced elevated gas temperatures that took some time to equilibrate. Complete randomization would also have required very large quantities of gas.

2.7 Energy efficiency calculations

Calculation of the energy efficiencies for water loss using carbon dioxide gas required the knowledge of how much energy was needed to compress the gas for each combination of temperature and pressure. The work required to compress carbon dioxide gas was calculated using the polytropic compression equation:

$$w = \frac{nRT_1}{n' - 1}\left(\left(\frac{P_2}{P_1}\right)^{\frac{n' - 1}{n'}} - 1\right)$$

where:
- w = work in joules,
- n = moles of carbon dioxide gas,
- R = universal gas constant, 8.314 J. mol^{-1}. K^{-1},
- T_1 = temperature, K,
- P_1 = initial gas pressure, MPa,
- P_2 = final gas pressure, MPa,
- n' = polytropic index, set to 1.4

The number of moles of carbon dioxide gas in the 1800 cm^3 decompression drying cylinder, was calculated using density values obtained from Huang et al.'s (1985) equation of state for carbon dioxide.

2.8 Data transformation

Transformations were made to the data prior to factorial analysis. Water loss from each wood chip was calculated as a percentage of the total water content of the chip. Because of the small size of the sample of wood chips in each batch (50 wood chips/batch) and the tendency for the distribution of wood chip water loss to be skewed toward zero, an arcsin transformation was used to improve the normality of the data. The percent water loss for each wood chip was transformed using

$$\arcsin\sqrt{\text{percent water loss}}$$

and the mean of the transformed values calculated for the 50 wood chips in each batch. The mean wood chip water loss appeared to be positively correlated with the variance of wood chip water loss among wood chips within batches (greater means are accompanied by greater variances). A logarithmic transformation was used to make the variance independent of the mean. The percent water loss for each wood chip was transformed using

$$\log(\text{percent water loss})$$

and the variance of the transformed values calculated for the 50 wood chips in each batch.

2.9 Results

2.9.1 Carbon dioxide

Decompression drying of *Pinus radiata* sapwood chips with carbon dioxide gas is strongly affected by pressure and to a lesser extent by time and temperature (Anova table 2.1). A significant interaction occurs between temperature and pressure (Anova table 2.1) that results from the variation of differences in water loss between pressures 1.50 and 4.89 MPa (table 2.4 and figure 2.4). The mean water loss for the five time periods (5, 15, 45, 9 × 5, and 3 × 15 minutes) when plotted against temperature in figure 2.4, show very low water loss values for 1.50 MPa at 20 and 35 ° C, and comparatively high values at 15, 25, 30, and 40 ° C. The pattern also occurs to a lesser extent at 4.89 and 6.89 MPa. The pattern of water loss at 1.50 MPa occurs consistently for each of the five time periods (5, 15, 45, 9 × 5, and 3 × 15 minutes) table 2.4 and figure 2.5. Temperature appears to have a strong effect on water loss with carbon dioxide gas at low pressure.

Anova table 2.1: Mean wood chip water loss with carbon dioxide gas.

Source of variation	*df*	*SS*	*MS*	*Fs*
Temperature	5	0.222	0.044	10.07**
Pressure	1	0.768	0.768	174.56**
Time	4	0.724	0.181	41.10**
Temperature × pressure	5	0.118	0.024	5.37**
Temperature × time	20	0.083	0.004	0.95 ns
Pressure × time	4	0.012	0.003	0.67 ns
Temperature × pressure × time	20	0.088	0.004	
Total	59	2.015		

** = P < 0.01 ns = not statistically significant

The variance of water loss among wood chips within batches with carbon dioxide gas is affected by pressure and temperature (Anova table 2.2). A significant interaction occurs between temperature and pressure, and another between pressure and time. The temperature × pressure interaction results from the very high level of water loss variation that occurs among wood chips decompression dried with carbon dioxide gas at

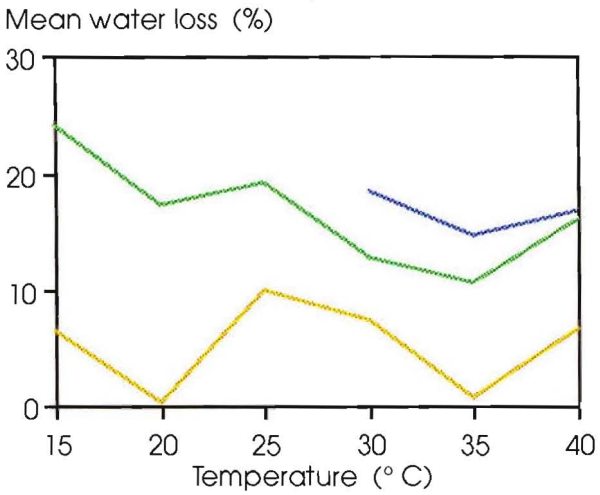

Figure 2.4 Temperature x pressure interaction for the mean water loss among wood chips within batches with carbon dioxide gas. The values plotted are the means for the five time periods (table 2.4).

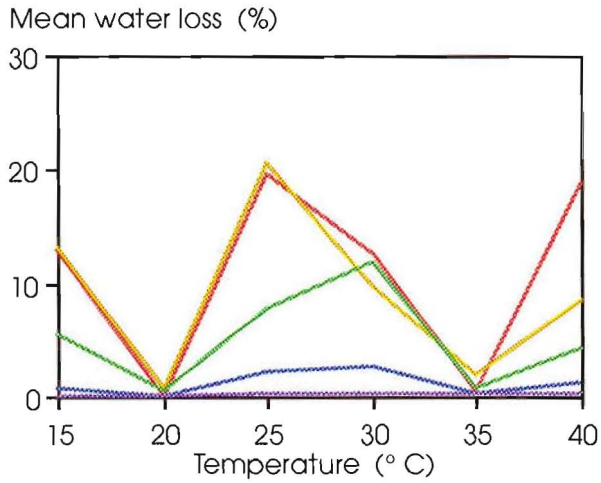

Figure 2.5 Mean water loss among wood chips within batches with carbon dioxide gas at 1.50 MPa (table 2.4).

Anova table 2.2: Variance of water loss with carbon dioxide gas among wood chips within batches.

Source of variation	*df*	*SS*	*MS*	*Fs*
Temperature	5	0.638	0.127	13.99**
Pressure	1	0.558	0.558	61.20**
Time	4	0.027	0.007	0.74 ns
Temperature x pressure	5	0.394	0.079	8.65**
Temperature x time	20	0.215	0.011	1.18 ns
Pressure x time	4	0.140	0.035	3.84*
Temperature x pressure x time	20	0.182	0.009	
Total	59	2.154		

** = P < 0.01 * = P < 0.05 ns = not statistically significant

Table 2.4 Mean water loss among wood chips within batches with carbon dioxide gas (as a percentage of the total water content in each wood chip).

Pressure (MPa)	Time (minutes)	Temperature (° C) 15	20	25	30	35	40	Mean
1.50	5	0.03	0.02	0.27	0.23	0.15	0.19	0.15
	15	0.75	0.03	2.23	2.51	0.19	1.08	1.13
	45	5.38	0.59	7.91	11.89	0.62	4.26	5.11
	9×5	13.01	0.69	20.59	9.66	2.00	8.62	9.09
	3×15	12.81	0.01	19.47	12.67	0.37	18.76	10.68
	Mean	6.39	0.27	10.09	7.39	0.67	6.58	5.23
4.89	5	7.80	3.75	3.17	4.31	2.86	6.51	4.73
	15	15.74	6.61	13.55	7.80	7.43	12.74	10.65
	45	22.48	18.14	20.83	14.45	11.82	18.45	17.70
	9×5	37.59	25.03	26.35	18.30	13.48	18.61	23.23
	3×15	37.01	33.95	31.97	19.87	18.45	24.69	27.66
	Mean	24.13	17.50	19.17	12.94	10.81	16.20	16.79
6.89	5				7.32	6.31	8.45	7.36
	15				8.68	9.07	15.17	10.97
	45				16.55	15.38	19.95	17.29
	9×5				29.03	18.61	16.11	21.25
	3×15				31.14	24.60	24.26	26.67
	Mean				18.54	14.80	16.79	17.95

1.50 MPa and 15 ° C (table 2.5 and figure 2.6). When the variance of water loss among wood chips within batches at 1.50 MPa is plotted for each of the five time periods (5, 15, 45, 9 × 5, and 3 × 15 minutes) figure 2.7, we see a consistent increase in the variance of water loss at 1.50 MPa and 15 ° C. The water loss appears to be more variable at low pressure and low temperature. The pressure × time interaction can be attributed to a reversal in the ranking of the variance of water loss among time periods (5, 15, 45, 9 × 5, and 3 × 15 minutes) at 1.50 and 4.89 MPa (table 2.5 and figure 2.8). Increased water loss among time periods at 4.89 MPa is accompanied by lower variance, while at 1.50 MPa increased water loss is accompanied by higher variance.

Scheffe's method was used to test whether repeated cycles of decompression drying (9 × 5 minutes and 3 × 15 minutes) conveys an advantage compared with non-cyclic decompression drying (45 minutes) for an equivalent carbon dioxide gas absorption period. Analysis of variance mean squares and F-values were recalculated for each of the three pressures (1.50, 4.89 and 6.89 MPa) using arcsin transformed means and log transformed variances. Only at the pressure 4.89 MPa was water loss consistently greater with repeated cycles of decompression drying (tables 2.4 and 2.6). The variance of water loss among wood chips within batches was lower with repeated cycles of decompression drying at 4.89 MPa (tables 2.5 and 2.6).

Table 2.6 Cyclic versus non-cyclic water loss

Pressure MPa	F - values Mean water loss	Variation of water loss among wood chips
1.50	0.88 ns	0.44 ns
4.89	4.31 *	5.03 **
6.89	1.24 ns	1.07 ns

** = P < 0.01 * = P < 0.05 ns = not statistically significant

2.9.2 Nitrogen

Decompression drying of *Pinus radiata* sapwood chips with nitrogen gas is affected only by time at the pressure 4.89 MPa (Anova table 2.3). Comparison of water loss for different gas absorption times (table 2.7 and figure 2.9) showed a large increase in the water loss with repeated cycles of

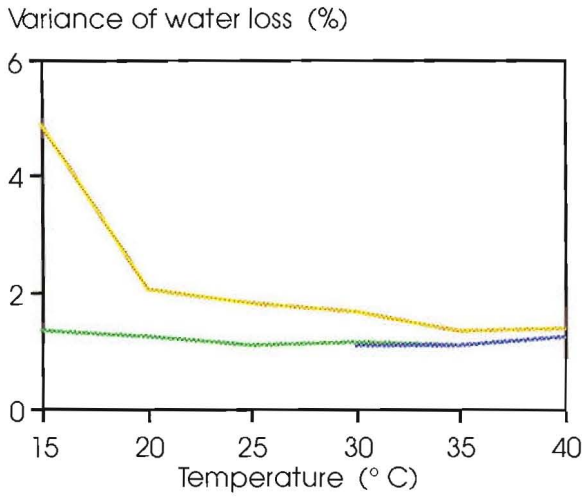

Figure 2.6 Temperature × pressure interaction for the variance of water loss among wood chips within batches. The values plotted are the means for the five time periods (table 2.5).

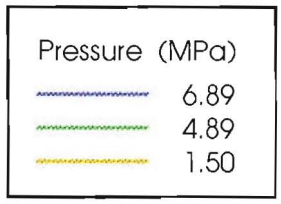

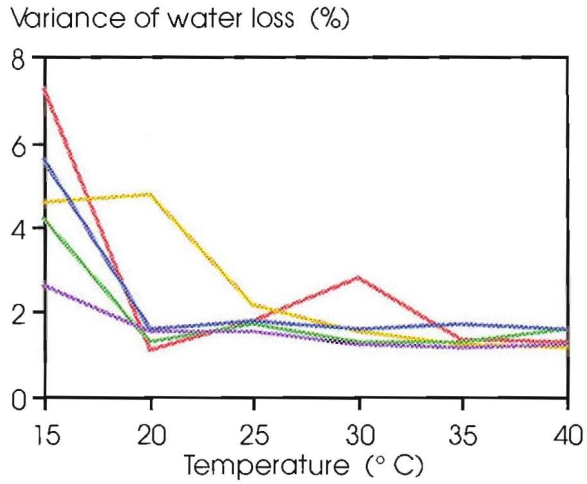

Figure 2.7 Variance of water loss among wood chips within batches with carbon dioxide gas at 1.50 MPa (table 2.5).

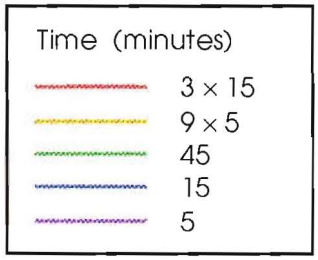

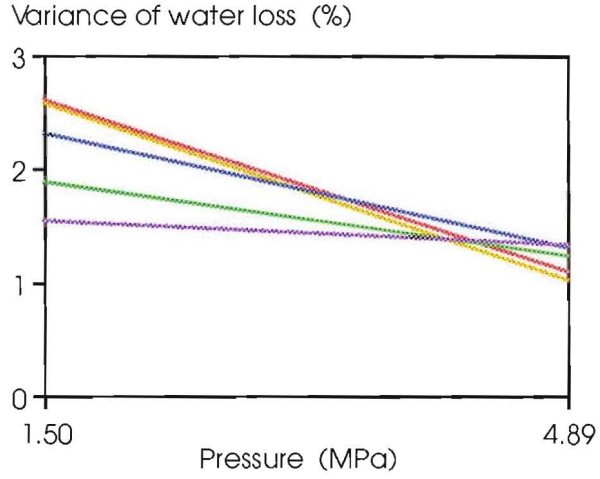

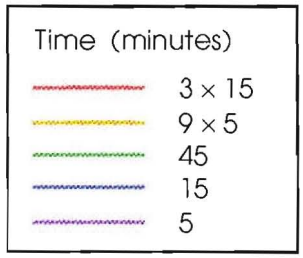

Figure 2.8 Pressure × time interaction for the variance of water loss among wood chips within batches with carbon dioxide gas. The values plotted are the means for the six temperatures (table 2.5).

Table 2.5 Variance of the water loss among wood chips within batches with carbon dioxide gas (as a percentage of the total water content in each wood chip).

Pressure (MPa)	Time (minutes)	Temperature (° C) 15	20	25	30	35	40	Mean
1.50	5	2.61	1.52	1.55	1.23	1.13	1.22	1.54
	15	5.57	1.60	1.75	1.61	1.69	1.61	2.31
	45	4.20	1.28	1.71	1.25	1.29	1.57	1.88
	9×5	4.60	4.73	2.19	1.52	1.21	1.13	2.57
	3×15	7.23	1.09	1.79	2.77	1.35	1.29	2.59
	Mean	4.84	2.05	1.80	1.68	1.33	1.36	2.18
4.89	5	1.61	1.43	1.24	1.19	1.13	1.44	1.34
	15	1.50	1.42	1.09	1.25	1.20	1.39	1.31
	45	1.38	1.25	1.13	1.13	1.13	1.36	1.23
	9×5	1.02	1.07	1.01	1.03	1.02	1.02	1.03
	3×15	1.27	1.04	1.05	1.08	1.05	1.04	1.09
	Mean	1.36	1.24	1.10	1.14	1.11	1.25	1.20
6.89	5				1.18	1.26	1.33	1.26
	15				1.18	1.15	1.50	1.27
	45				1.19	1.15	1.36	1.23
	9×5				1.01	1.01	1.01	1.01
	3×15				1.03	1.03	1.05	1.04
	Mean				1.12	1.12	1.25	1.16

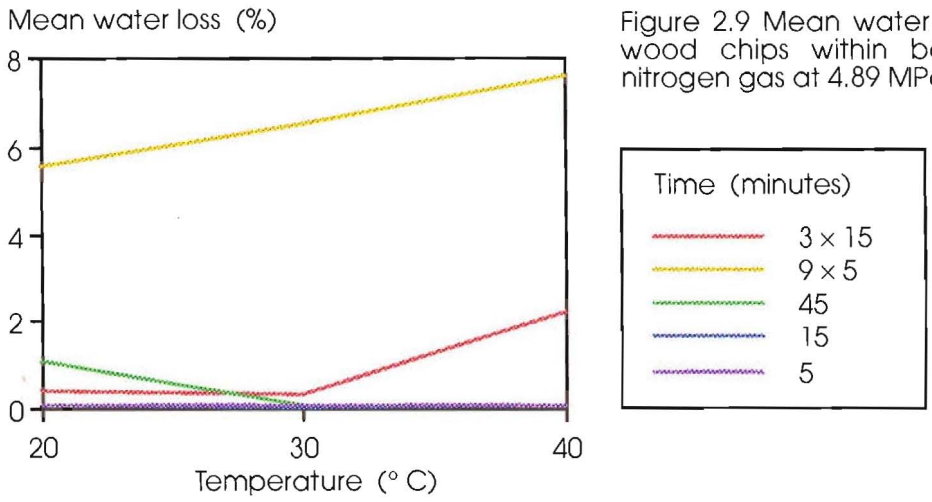

Figure 2.9 Mean water loss among wood chips within batches with nitrogen gas at 4.89 MPa (table 2.6).

decompression drying. It appears that the number of cycles of decompression drying rather than the length of gas absorption time is more important factor in determining water loss with nitrogen gas.

Anova table 2.3: Mean wood chip water loss with nitrogen gas.

Source of variation	*df*	*SS*	*MS*	*Fs*
Temperature	2	0.001	0.001	0.60 ns
Time	4	0.117	0.029	25.63**
Temperature × time	8	0.009	0.001	
Total	14	0.128		

** = P < 0.01 ns = not statistically significant

The variance of water loss with nitrogen gas among wood chips within batches is affected only by temperature (Anova table 2.4). This can be attributed to increases in the variance of water loss among wood chips at lower temperatures (table 2.8 and figure 2.10), particularly for the time periods 15 and 45 minutes at 20 ° C.

Anova table 2.4: Variance of water loss with nitrogen gas among wood chips within batches.

Source of variation	*df*	*SS*	*MS*	*Fs*
Temperature	2	0.046	0.023	6.30*
Time	4	0.018	0.004	1.22 ns
Temperature × time	8	0.029	0.004	
Total	14	0.093		

Table 2.7 Mean water loss among wood chips within batches with carbon dioxide versus nitrogen gas at 4.89 MPa (as a percentage of the total water content in each wood chip).

Gas	Temperature (°C)	Time (minutes) 5	15	45	9×5	3×15	Mean
CO_2	20	3.75	6.61	18.14	25.03	33.95	17.50
	30	4.30	7.80	14.45	18.30	19.87	12.94
	40	6.51	12.74	18.45	18.61	24.69	16.20
	Mean	4.86	9.05	17.02	20.65	26.17	15.55
N_2	20	0.04	0.05	1.06	5.51	0.36	1.40
	30	0.06	0.02	0.06	6.46	0.35	1.34
	40	0.05	0.05	0.05	7.53	2.23	1.98
	Mean	0.05	0.04	0.39	6.50	0.98	1.58

Table 2.8 Variance of the water loss among wood chips within batches with carbon dioxide versus nitrogen gas at 4.89 MPa (as a percentage of the total water content in each wood chip).

Gas	Temperature (°C)	Time (minutes) 5	15	45	9×5	3×15	Mean
CO_2	20	1.43	1.42	1.32	1.07	1.06	1.26
	30	1.19	1.25	1.13	1.03	1.08	1.14
	40	1.44	1.39	1.36	1.02	1.04	1.25
	Mean	1.35	1.35	1.27	1.04	1.06	1.21
N_2	20	1.41	1.71	2.01	1.32	1.13	1.52
	30	1.44	1.15	1.28	1.29	1.09	1.25
	40	1.13	1.10	1.08	1.04	1.11	1.09
	Mean	1.33	1.32	1.46	1.22	1.11	1.29

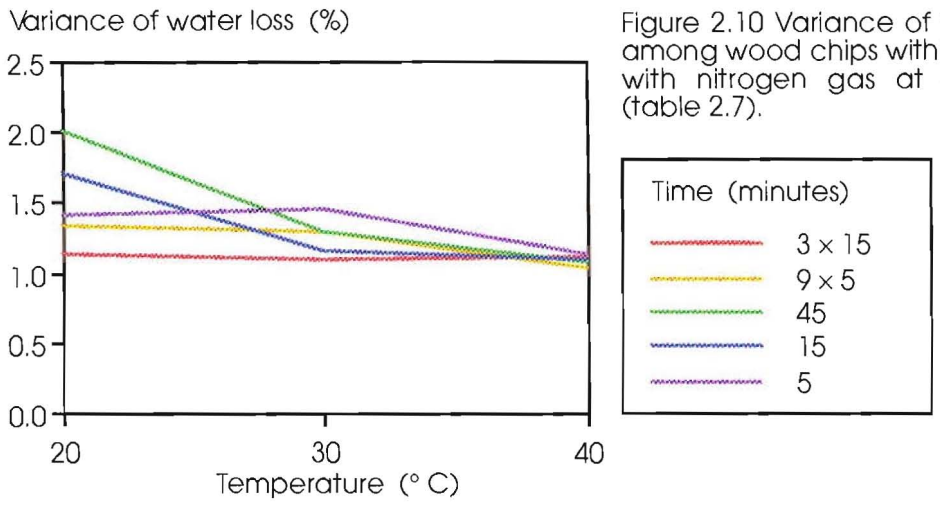

Figure 2.10 Variance of water loss among wood chips within batches with nitrogen gas at 4.89 MPa (table 2.7).

2.9.3 Carbon dioxide versus Nitrogen

Decompression drying of *Pinus radiata* sapwood chips is far more effective in terms of water loss with carbon dioxide gas than with nitrogen gas as shown by the very significant F-value for carbon dioxide versus nitrogen gas (CO_2 vs N_2) in Anova table 2.5.

Anova table 2.5: Comparison of water loss with carbon dioxide and nitrogen gas.

Source of variation	*df*	*SS*	*MS*	*Fs*
Temperature	2	0.008	0.004	1.69 ns
Time	4	0.245	0.061	26.36**
CO_2 vs N_2	1	0.688	0.688	295.82**
Temperature × time	8	0.010	0.001	0.52 ns
Temperature × CO_2 vs N_2	2	0.002	0.001	0.41 ns
Time × CO_2 vs N_2	4	0.067	0.017	7.20**
Temperature × time × CO_2 vs N_2	8	0.019	0.002	
Total	29	1.038		

** = $P < 0.01$ ns = not statistically significant

A significant interaction between time and CO_2 vs N_2 provides an insight into the differences in water loss of the two gases. The interaction results from differences in the rate of increase of water loss with increasing gas absorption time for carbon dioxide and nitrogen gas (table 2.7 and figure 2.11). This occurs, it is believed, because of differences in the solubility of the two gases in water. Carbon dioxide gas with a much higher solubility

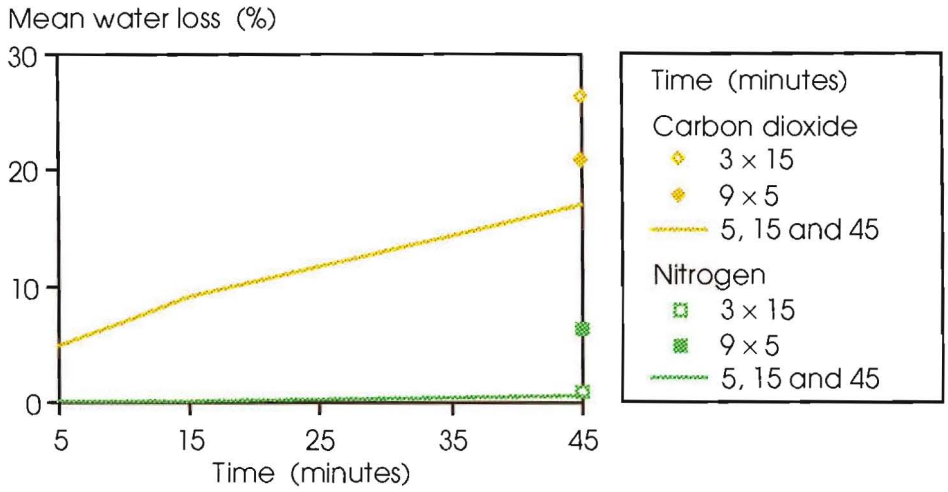

Figure 2.11 Time × carbon dioxide versus nitrogen gas interaction for the mean water loss among wood chips within batches at 4.89 MPa. The values plotted are the means for the three temperatures (table 2.6).

in water than nitrogen gas (table 2.2) should be absorbed in the water in larger quantities than nitrogen gas for an equivalent time period. The large water loss differences between carbon dioxide and nitrogen gas at 5, 15 and 45 minutes, in figure 2.11, would suggest that the quantities of carbon dioxide gas absorbed in the water for each time period are larger than those for nitrogen gas. The increase in water loss with carbon dioxide gas for time periods 15 to 45 minutes would also indicate that saturation is not achieved in 15 minutes of gas absorption.

The greater water loss with carbon dioxide gas and three cycles of 15 minutes compared with nine cycles of 5 minutes suggests that for carbon dioxide gas with its high solubility in water, the length of the period of gas absorption is more important than the number of decompression drying cycles for effective water loss. Nitrogen gas, in contrast, shows a far greater and surprisingly high water loss with nine cycles of 5 minutes compared with three cycles of 15 minutes gas absorption. The number of cycles of decompression drying rather than the length of gas absorption appears to be more important, which suggests that water loss with nitrogen gas is determined by factors other than the amount of gas absorbed. Water loss with repeated cycles of decompression drying with nitrogen gas and with carbon dioxide gas at low solubilities and short absorption times (1.50 MPa and 5 minutes) generally increases with each successive cycle of decompression drying. The amount of air present in the wood slowly increases with each cycle and it is this that appears to be the factor that determines water loss when only small amounts of gas are absorbed.

2.9.4 Cyclic decompression drying - sequential water loss variation among wood chips

A graphical assessment was made of the changes in the distribution of water loss among wood chips within batches for each successive drying cycle. The water loss for individual wood chips was plotted against their percent saturation at the commencement of each cycle. The illustrated examples are for repeated cycles of decompression drying with carbon dioxide gas at 1.50 and 4.89 MPa and 25 ° C with 9 cycles of 5 minutes and 3 cycles of 15 minutes (figures 2.12, 2.13, 2.14 and 2.15).

The pattern of water loss is similar for the pressures 1.50 and 4.89 MPa but the time scale of water loss at 1.50 MPa is greatly extended. The water loss achieved in 9 cycles of 5 minutes at 1.50 MPa can be attained in 5 cycles of 5 minutes at 4.89 MPa. The figures also show that water loss with repeated cycles of decompression drying with carbon dioxide gas at low solubilities and short absorption times is initially slow, but as the proportion of air to water increases to approximately 10 % the water loss increases substantially.

2.9.5 Energy efficiency of decompression drying

The energy efficiencies (grams of water removed per joule of compression energy) of decompression drying with carbon dioxide gas, for each combination of temperature, pressure and time are presented in figure 2.16. The values should only be compared with each other due to the fact that the pressure cylinder was not completely packed with wood chips.

A pattern of maximum energy efficiency occurs for the gas absorption time of 45 minutes for all temperatures except 40 ° C, where 3 cycles of 15 minutes is slightly more energy efficient. For most temperatures 3 cycles of 15 minutes is more energy efficient than a one-off 15 minute absorption absorption period. This is due to the very substantial increase in the amount of water removed during the second and third decompression drying cycles. The energy efficiency of repeated cycles of 5 minute decompression drying at 4.89 and 6.89 MPa would have been higher had the decompression drying cycles been discontinued once the majority of

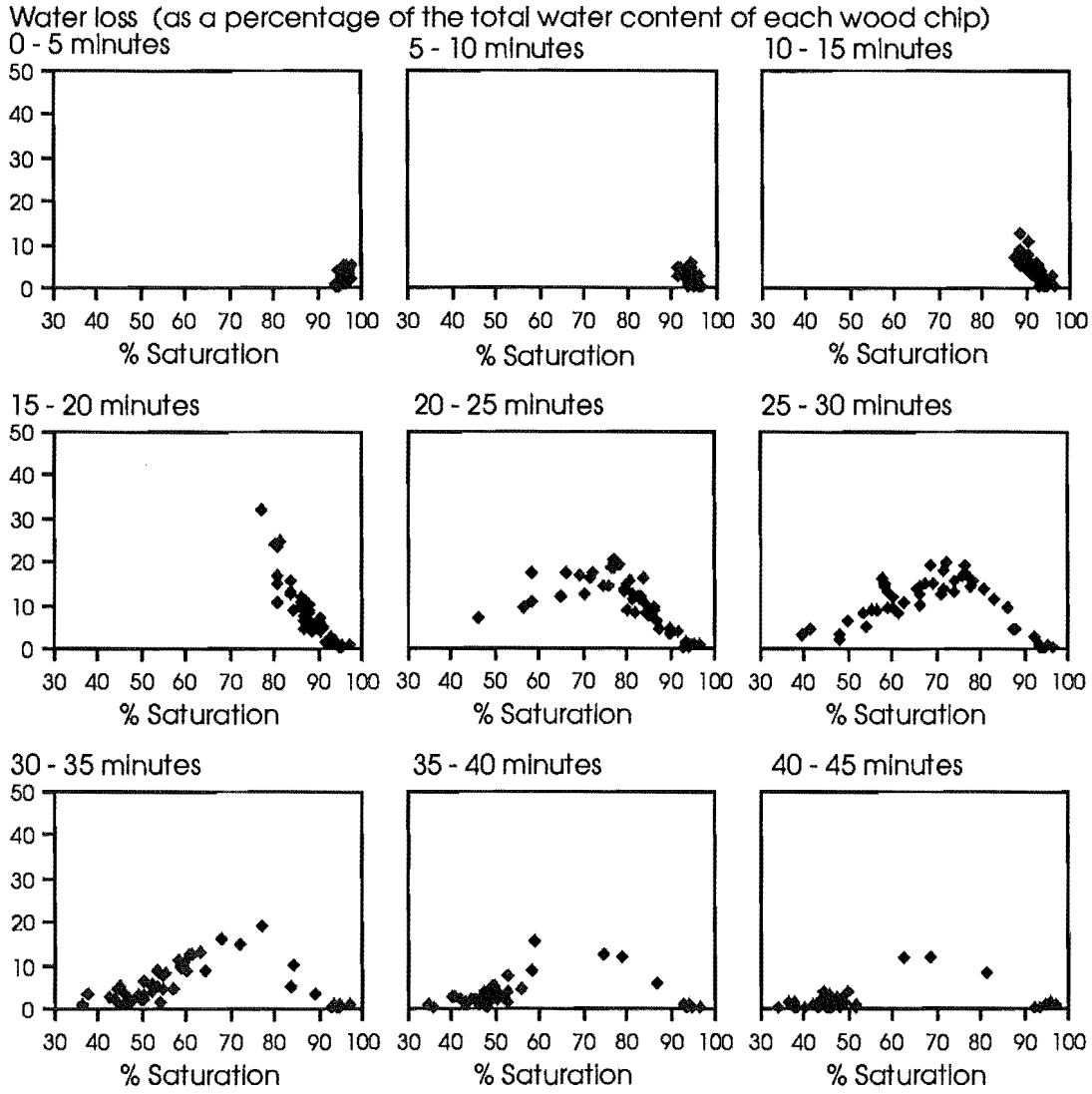

Figure 2.12 Sequential water loss among wood chips with carbon dioxide gas at 25 ° C and 1.50 MPa for nine decompression drying cycles of 5 minutes. The water loss for each wood chip is plotted against the percent saturation at which each cycle commenced.

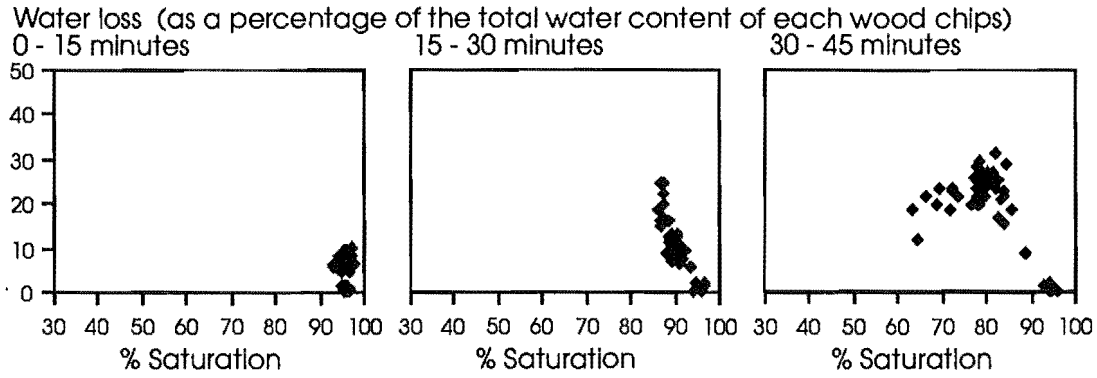

Figure 2.13 Sequential water loss among wood chips with carbon dioxide gas at 25 ° C and 1.50 MPa for three decompression drying cycles of 15 minutes. The water loss for each wood chip is plotted against the percent saturation at which each cycle commenced.

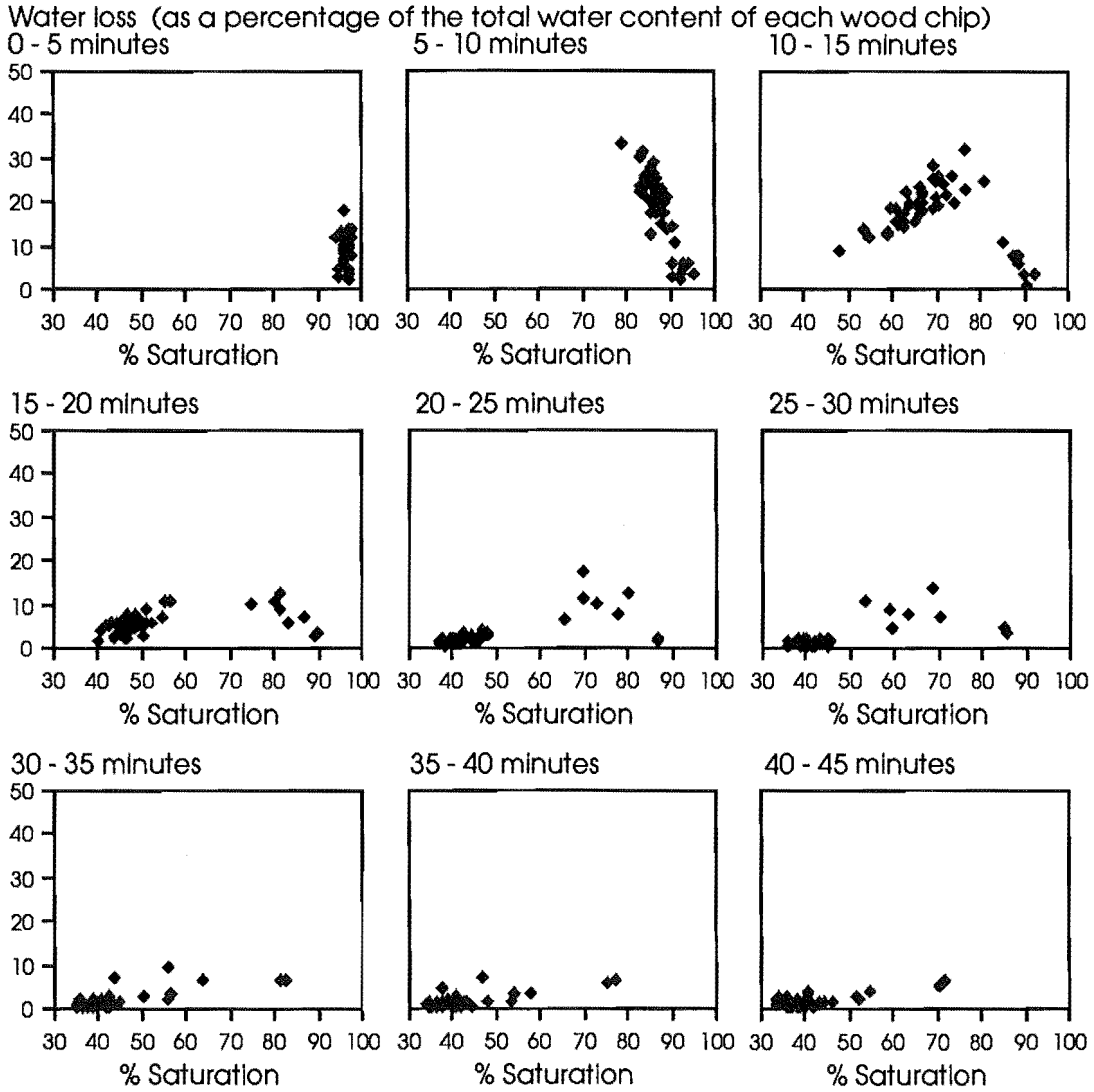

Figure 2.14 Sequential water loss among wood chips with carbon dioxide gas at 25 ° C and 4.89 MPa for nine decompression drying cycles of 5 minutes. The water loss for each wood chip is plotted against the percent saturation at which each cycle commenced.

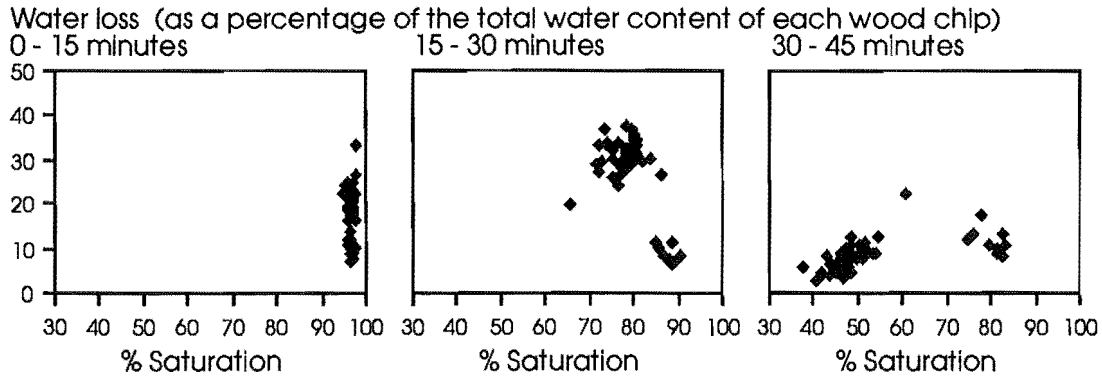

Figure 2.15 Sequential water loss among wood chips with carbon dioxide gas at 25 ° C and 4.89 MPa for three decompression drying cycles of 15 minutes. The water loss for each wood chip is plotted against the percent saturation at which each cycle commenced.

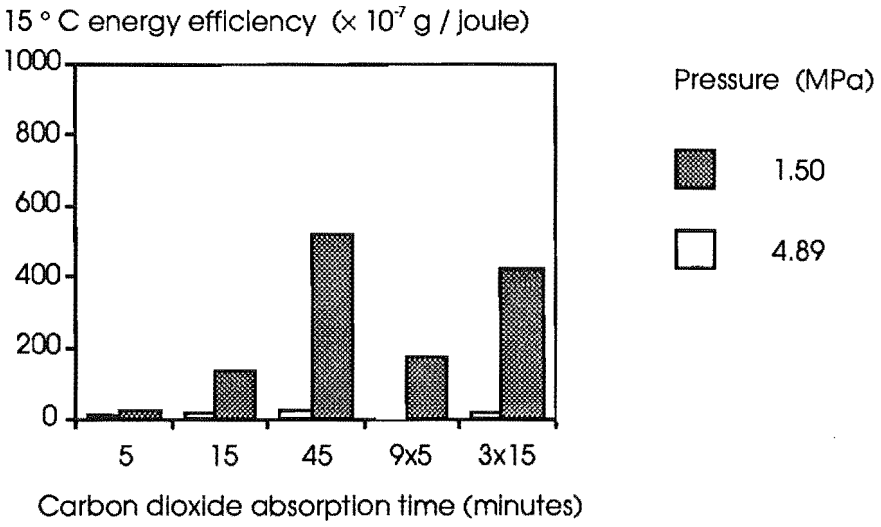
15 ° C energy efficiency (× 10⁻⁷ g / joule)
1000
800
600
400
200
0
5
15
45
9x5
3x15
Carbon dioxide absorption time (minutes)
Pressure (MPa)
1.50
4.89

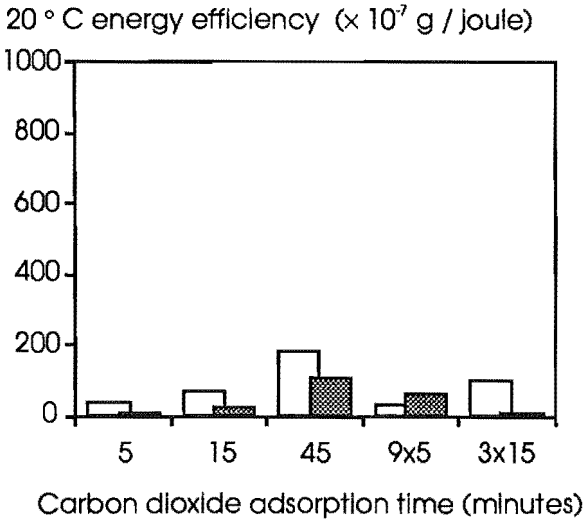
20 ° C energy efficiency (× 10⁻⁷ g / joule)
1000
800
600
400
200
0
5
15
45
9x5
3x15
Carbon dioxide adsorption time (minutes)

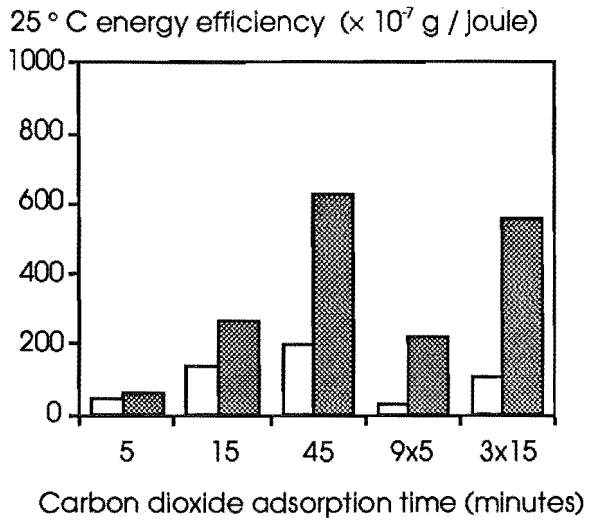
25 ° C energy efficiency (× 10⁻⁷ g / joule)
1000
800
600
400
200
0
5
15
45
9x5
3x15
Carbon dioxide adsorption time (minutes)

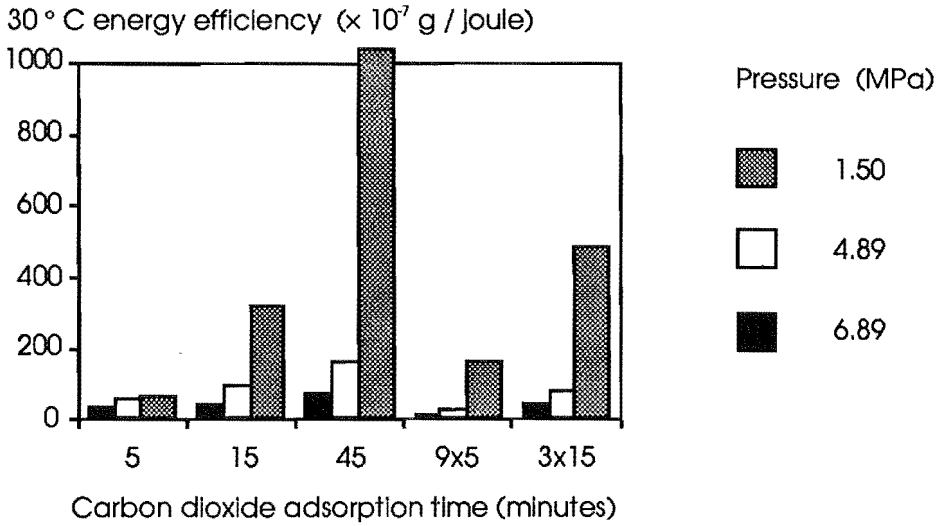

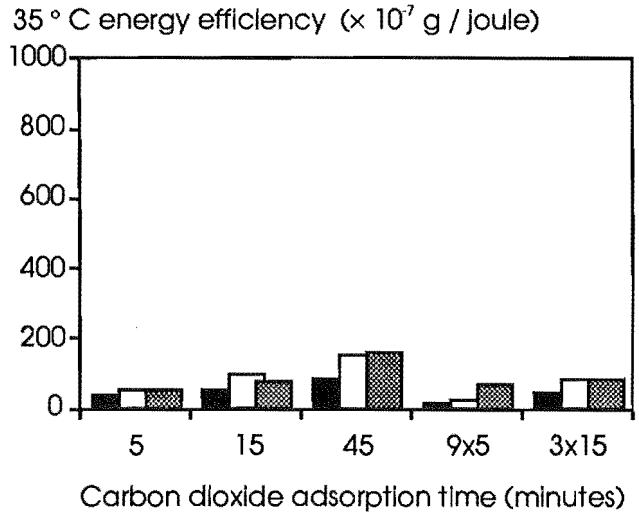

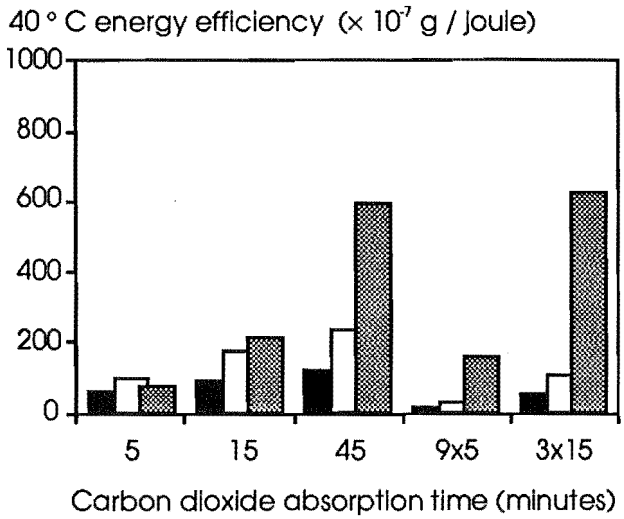

Figure 2.16 Energy efficiency of decompression drying with carbon dioxide gas at each combination of temperature, pressure and time.

the wood chips had reached a percent saturation of 30 - 50 %. From decompression drying at 4.89 MPa and 25 ° C (figure 2.14) it can be seen that water loss falls off rapidly after three 5 minute decompression drying cycles.

2.10 Discussion

The pattern of water loss that emerges is the result of the interaction of many variables - temperature, pressure, time, gas diffusivity and solubility, and wood permeability. The amount of gas absorbed by the lumen water appears to be important in determining the effectiveness of decompression drying with carbon dioxide gas at high solubilities, but at low solubilities and short absorption times and for nitrogen gas effective decompression drying depends on the proportion of air present in the wood.

For carbon dioxide gas, pressure has the most significant effect on water loss of the three variables (pressure, temperature and time) analysed. This can be explained in terms of the large solubility differences of carbon dioxide gas in water between 1.50 and 4.89 MPa (figure 2.2). The considerably smaller solubility differences between 4.89 and 6.89 MPa, help to explain the generally smaller increase in water loss at 6.89 MPa (figure 2.4).

The reduction in the solubility of carbon dioxide gas in water with temperature, might be expected to decrease the amount of water loss with temperature at constant pressure. The analysis showed however, that while the effects of temperature are significant on water loss, the pattern of change is not consistent with solubility changes. At 4.89 MPa, there is a general decrease in water loss from 15 ° C to 35 ° C, with modest increases at 25 and 40 ° C. At 1.50 MPa, the deviations from the trend observed at 4.89 MPa tend to be further accentuated (figure 2.4) with very little water loss at 20 and 35 ° C, and high levels of water loss at 15, 25, 30 and 40 ° C. The striking feature is that such large differences in water loss should occur over temperature intervals as small as 5 ° C, and that they should occur consistently for each of the five time periods (figure 2.5). Why this happens is not clear. In the analysis it gives rise to a significant

temperature × pressure interaction, but the inconsistent pattern of the interaction doesn't allow a useful interpretation to be made. It may be that the increased rate of gas absorption in water at higher temperatures plays a part, but other factors may also be responsible.

The effect of time is greater for gases of higher solubility in water. This was clearly demonstrated in the comparison of carbon dioxide and nitrogen gases (figure 2.11). The higher solubility of carbon dioxide gas in water produced a much greater increase of water loss with time than was obtained with nitrogen. It might be expected that at higher temperatures with lower solubilities and greater rates of gas absorption, the effects of increasing gas absorption time on water loss would diminish. The effect should show itself in a significant temperature × time interaction, but in the analysis of variance the interaction was not significant (Anova table 2.1).

The proportion of air present in the wood is important for effective water loss with carbon dioxide gas at low solubilities (1.50 MPa) and short absorption times (5 and 15 minutes) and for nitrogen gas. The volume of gas generated by bubble nucleation appears insufficient to expel the water. The loss of water is therefore thought to occur by the compression and expansion of pre-existing air bubbles at gas pressurisation and decompression, and the expansion of dissolved gas at decompression into pre-existing air bubbles. The very low solubility of nitrogen gas in water would suggest that water loss with nitrogen gas occurs by the process of air bubble compression and expansion. The quantity of carbon dioxide gas absorbed in the water, even at low solubilities, should be considerably greater. Expansion of dissolved carbon dioxide gas into pre-existing air bubbles could be expected to make some contribution to water loss, increasing the total water loss. Once some of the initial water has been lost, it may be possible that compressed gas will, through adjacent dry tracheids, get behind the wet line in the wood chip and force water from the chip when it expands during decompression. This process could contribute to the increased water loss as the percent saturation decreases.

Comparison can be made with the process of compression drying, where water is removed from the sapwood of permeable species by compression and distortion under the loading of a hydraulically driven platen. In *Pinus*

taeda, the water loss with compression drying is a linear function of compression strain (Haygreen 1981). Water loss occurs from the point at which the force/deformation curve of the wood reaches the limit of proportionality. As a result, the wood inevitably suffers structural damage during the process (Wingate-Hill and Cunningham 1986). In contrast, rapid decompression of carbon dioxide in wet and dry pine wood, even from pressures of 10 and 28 MPa at 40 and 100 ° C (the supercritical region) to atmospheric pressure, produces no structural damage to the wood (Ritter and Campbell 1986).

Energy requirements are however far lower for compression drying. Even at the most efficient combination of temperature, pressure and time (30 ° C, 1.50 MPa and 45 minutes), decompression drying with carbon dioxide gas (when allowance is made for cylinder packing) is approximately 200 times less energy efficient than compression drying. The comparison is based on the data of Wingate-Hill and Cunningham (1986).

2.11 Summary

Decompression drying of *Pinus radiata* sapwood chips with carbon dioxide gas, at temperatures of 15 - 40 °C, pressures of 1.50 - 6.89 MPa and absorption times of 5 - 45 minutes, is effective in removing a significant proportion of the free water present. Water loss increased with pressure and absorption time, and varied with temperature. The effect of pressure and time can be attributed to the high solubility of carbon dioxide gas in water at high pressures and the amount of carbon dioxide gas absorbed with time. The volume of the gas bubbles generated on decompression appears to be an important criterion for water loss. At low gas solubilities in water the volume of pre-existing gas bubbles in the wood becomes an important criterion for water loss. The volume of gas bubbles generated by the decompression of nitrogen gas and low pressure carbon dioxide gas is insufficient on its own to expel water from the wood. Water loss is thought to occur instead by the compression and expansion of pre-existing air bubbles with gas pressurisation and decompression. Water loss increases as the proportion of air increases. Expansion of compressed carbon dioxide and nitrogen gas that has moved behind the wet line in the wood through adjacent dry tracheids may contribute to this increase in

water loss with increasing air volume. At higher carbon dioxide gas pressures the presence of pre-existing gas bubbles appears to improve water loss. Repeated cycles of decompression drying was more effective than one cycle of equivalent gas absorption time with carbon dioxide gas at 4.89 MPa.

The variation of water loss with carbon dioxide gas among wood chips within batches increases at lower pressure, particularly at 15 ° C.

The energy efficiency of decompression drying is far lower than that of compression drying with hydraulically driven platens. Structural damage to the wood, however, is unlikely to occur with decompression drying.

Further work is needed to determine if the interaction between temperature and pressure of water loss with carbon dioxide gas can be reproduced and if so why the pattern is so inconsistent. Replication of the statistical design is also needed to determine whether the assumption of a non-significant second-order interaction between temperature, pressure and time is in fact correct. Of further interest would be an assessment of the effectiveness of decompression drying with carbon dioxide at gas pressures between 1.50 and 4.89 MPa given the large water loss differences between the two pressures.

References

Booker, R. E., 1990, Changes in transverse wood permeability during the drying of *Dacrydium cupressinum* and *Pinus radiata*, *New Zealand Journal of Forestry Science*, 20(2), 231 - 244.

Booker, R. E. and Kininmonth, J. A., 1978, Variation in Longitudinal permeability of green radiata pine wood, *New Zealand Journal of Forestry Science*, 8(2), 295 - 308.

Comstock, G. L., 1970, Directional permeability of softwoods, *Wood and Fiber*, 1(4), 283 - 289.

Dodds, W. S., Stutzman, L. F. and Sollami, B. J., 1956, Carbon dioxide solubility in water, *Industrial and Engineering Chemistry, Chemical and Engineering Data Series*, 1(1), 92 - 95.

Haygreen, J. G., 1981, Potential for compression drying of green wood chip fuel, *Forest Products Journal*, 31(8), 43 - 54.

Huang, F., Li, M., Lee, L. L., Starling, K. E. and Chung, F. T. H., 1985, An accurate equation of state for carbon dioxide, *Journal of Chemical Engineering of Japan*, 18(6), 490 - 496.

Lubetkin, S. and Blackwell, M., 1988, The nucleation of bubbles in supersaturated solutions, *Journal of Colloid and Interface Science*, 126(2), 610 - 615.

Ng, W. Y. and Walkley, J., 1969, Diffusion of gases in liquids: the constant size bubble method, *Canadian Journal of Chemistry*, 47(6), 1075 - 1077.

Ritter, D. C. and Campbell, A. G., 1986, The effects of supercritical carbon dioxide extraction on pine wood structure, *Biotechnology and Bioengineering Symposium*, No. 17, 179 - 182.

Sokal, R. R. and Rohlf, F. J., 1981, Biometry, Second edition, W. H. Freeman and Company, New York, 859 pp.

Wiebe, R., 1941, The binary system carbon dioxide - water under pressure, *Chemical Reviews*, 29(3), 475 - 481.

Wiebe, R., Gaddy, V. L. and Heins, C., 1933, The solubility of nitrogen in water at 50, 75 and 100 ° from 25 to 1000 atmospheres, *Journal of the American Chemical Society*, 55(3), 947 - 953.

Wingate-Hill, R. and Cunningham, R. B., 1986, Compression drying of sapwood, *Wood and Fiber Science*, 18(2), 315 - 326.

Chapter 3

Drying collapse in *Eucalyptus delegatensis* heartwood

3.1 A review of drying collapse in wood

The following is an explanation and discussion of the processes involved in the development of drying collapse in wood. It commences with a review of the underlying theory, and goes on to discuss some of the more recent ideas put forward to explain the observed patterns of collapse shown in the experimental data. It finishes with a discussion of the ways in which drying and wood variables affect drying collapse.

3.1.1 Surface tension

The surface of a liquid at a gas-liquid interface, is in a state of stress. The molecules experience an imbalance of intermolecular forces of attraction (van der Waal's, dipolar interaction, hydrogen bond) normal to the surface (figure 3.1). This is due to the greater attraction for surface molecules by bulk liquid molecules, compared with vapour molecules in the gas phase. A state of lateral tension develops in the surface, causing the surface to contract to minimise its area and energy. This it achieves by incorporating surface molecules into the bulk liquid. Surface molecules are in a higher free energy state than those of the bulk liquid, in part due to the fewer intermolecular interactions they experience compared with

Figure 3.1 Surface imbalance of intermolecular forces of attraction.

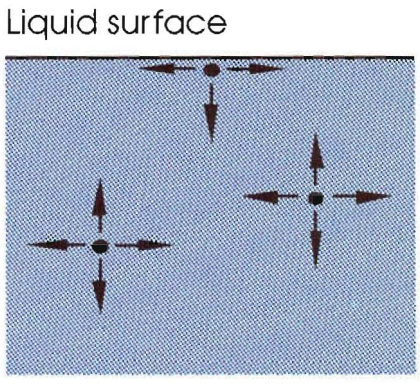

bulk liquid molecules. In much the same way, the surface tension of a liquid (pure substance) can be said to be independent of area. While energy is required to increase the surface area of a liquid, and therefore its energy state, the process does not stretch the surface of the liquid and increase its tension. Instead more surface is created by the movement of molecules from the bulk liquid to the surface. This process is reflected in the following definition of surface tension.

The surface tension (γ) of a liquid is the force (F) per unit length (l) on the surface that opposes the expansion of the surface area.

$$\gamma = \frac{F}{l}$$

The SI unit of surface tension is the Newton per metre (N m^{-1}).

The surface tension of a liquid surface in contact with its own vapour or with air, depends only on the nature of the liquid and its temperature. Surface tension usually decreases with increasing temperature, reaching zero at the liquid's critical temperature (figure 3.2).

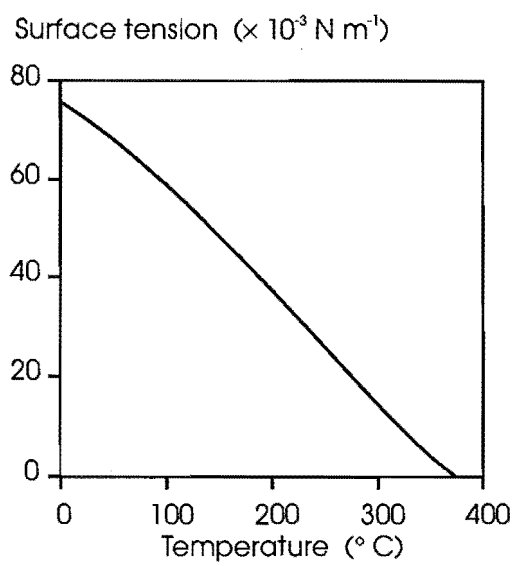

Figure 3.2 Decline with increasing temperature of the surface tension of water in contact with air.

Curvature of the surface at a gas-liquid interface, reflects the considerable changes in the physical properties of the gas and liquid phases. These result from the effects of surface tension, and are the subject of the next two sections. They provide a background to an understanding of the process of drying collapse.

3.1.2 Pressure difference across a curved surface

If we take a sufficiently large spherical bubble of vapour enclosed in liquid (a cavity really), a state of equilibrium is reached in which its tendency to

contract and reduce its surface area is balanced by an increase in the internal vapour pressure. If the pressure inside the bubble is p_{int} and its radius is r, the force inside the bubble is $4\pi r^2 p_{int}$. The opposing force is the sum of the external pressure p_{ext} multiplied by the bubble surface area $4\pi r^2 p_{ext}$ and the surface tension. The surface energy of the bubble is $4\pi r^2 \gamma$. If work is done on the bubble to increase its radius by dr, the surface area would increase by $8\pi r$ dr. Because work is force $\times$ distance, the force opposing expansion of the bubble through a distance dr when the radius is r is $8\pi\gamma r$. Balancing the forces gives:

$$4\pi r^2 p_{int} = 4\pi r^2 p_{ext} + 8\pi\gamma r$$

which rearranges to the Laplace equation:

$$p_{int} = p_{ext} + \frac{2\gamma}{r}$$

From this we can see that the pressure inside a curved surface is always greater than the pressure outside. The pressure difference decreases to zero when the radius of curvature becomes infinite; when the surface becomes flat (figure 3.3).

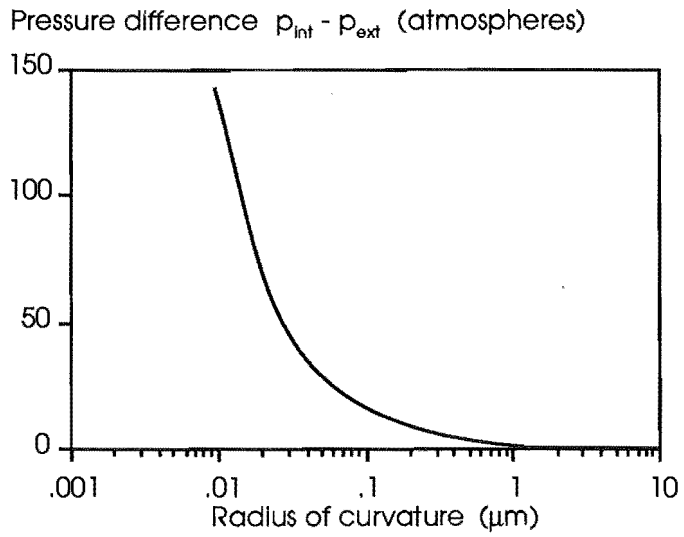

Figure 3.3 The pressure difference across a curved air-water interface, calculated using the Laplace equation.

This pressure difference across a curved liquid surface (or meniscus) in a cylindrical capillary tube is the phenomenon known as capillarity. The effect is illustrated by the elevation or depression of a column of liquid in a capillary tube placed in contact with a flat liquid surface (figure 3.4). The difference between this and the bubble in liquid, is the addition of a solid

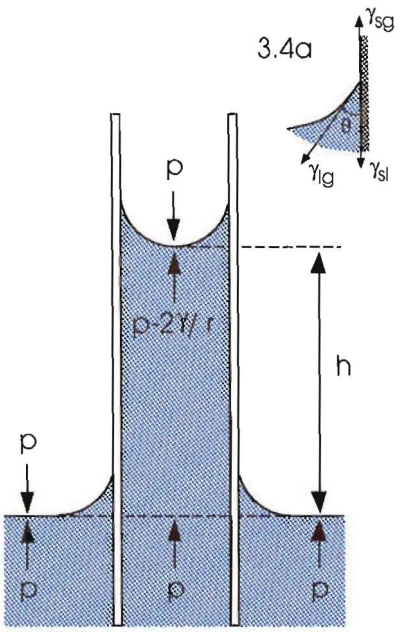

Figure 3.4 Effect of surface tension on the liquid in a capillary tube.

interface, in this case the glass capillary wall. Three interfaces are now present: liquid-gas or vapour (lg), solid-liquid (sl), and solid-gas(sg). This gives rise to a contact angle (θ) between the liquid and the solid surfaces from the point at which the three interfaces meet (figure 3.4a Cross-section of the solid-liquid line of contact). The contact angle depends on the relative surface tensions of the surface films between solid and liquid (γ_{sl}) and solid and gas (γ_{sg}). The surface films are only a few molecules thick. For water in contact with clean glass, γ_{sl} is less than γ_{sg}, which tells us that the energy is lowest when a thin film of water covers as much of the glass as possible. As the water creeps up the side of the glass capillary tube, it curves the surface of the water inside the tube, and from the Laplace equation we know the pressure below the surface curvature is less than that of the gas above by $p - 2\gamma/r$. The excess external pressure pushes the liquid up the tube until the hydrostatic pressure of the column of water in the tube equals the pressure difference caused by the liquids surface tension:

$$\text{Hydrostatic pressure} = \frac{\rho\pi r^2 hg}{\pi r^2} = \frac{2\gamma}{r}$$

($\rho\pi r^2 hg$ is the downward force exerted by the column of water, ρ is density, g is gravitational acceleration).

The equation is equivalent to the Laplace equation given earlier. With a capillary, however, a correction must be made for the contact angle (θ). The surface tension forces need to be balanced at the line of contact between liquid and solid, and this is given by the following relation:

$$\gamma_{sg} = \gamma_{sl} + \gamma_{lg} \cos\theta$$

which solves to

$$\cos\theta = \gamma_{sg} - \frac{\gamma_{sl}}{\gamma_{lg}}$$

the Laplace equation then becomes:

$$p_{int} = p_{ext} + \frac{2\gamma\cos\theta}{r}$$

The effect of the contact angle is to increase the radius of curvature of the liquid-gas interface, reducing the pressure difference between the gas and liquid phases.

3.1.3 Variation of vapour pressure with curvature

The Laplace equation shows that the pressure on the concave side of a curved liquid surface is lower than that for a plane (or flat) surface. The liquid surrounding a bubble or the liquid (of small contact angle) in a capillary tube is at reduced pressure. This reduced pressure has an effect on the vapour pressure at the gas-liquid interface, because as the pressure on a liquid decreases, its vapour pressure falls. The effect can be understood in this way: when a concave liquid surface is under lateral tension, the surface molecules are in closer proximity to one another, than for a plane surface, and so there is a greater tendency for molecules to be drawn into the bulk liquid. The potential energy of the surface molecules is therefore lower, reducing the proportion of molecules with sufficient energy to evaporate.

The change in vapour pressure with radius of curvature for a concave liquid surface is given by the following form of the Kelvin equation:

$$p = p_{sat}\, e^{-2\gamma Vm/rRT}$$

where p is the vapour pressure inside the cavity or bubble, p_{sat} is the saturated vapour pressure over a plane surface, and V_m the liquids molar volume.

Rearranging the equation gives the form:

$$\ln \frac{p}{p_{sat}} = \frac{-2\gamma V_m}{rRT}$$

The relative vapour pressure inside a bubble or capillary tube with liquid of small contact angle, decreases with an increase in surface curvature - as the bubble or capillary radius decreases. The relation is illustrated in figure 3.5. The Kelvin equation is only valid at relative vapour pressures close to saturation. Its derivation is based on the assumption that surface tension is independent of surface curvature. At a radius of curvature smaller than 0.01 μm, the thermodynamic properties of the equation no longer apply. At this size the radius of curvature is of molecular dimensions, and so no real bulk liquid is present.

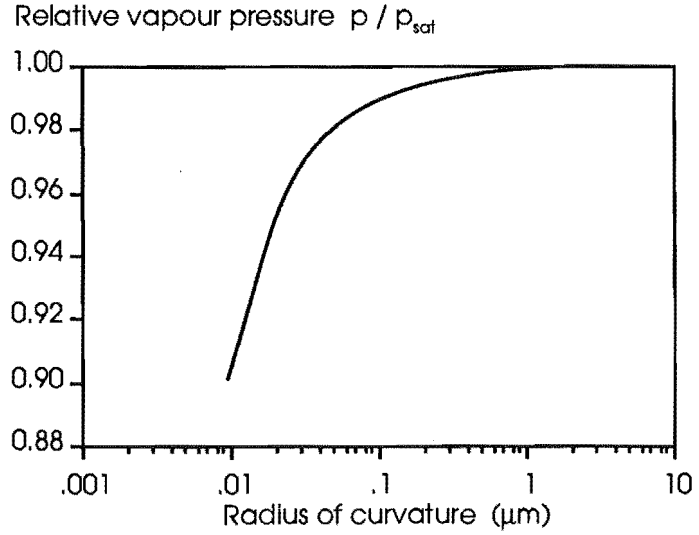

Figure 3.5 Effect of radius of curvature on the relative vapour pressure of a air-water interface, calculated using the Kelvin equation.

Applying the relations derived in the Laplace and Kelvin equations, gives us an explanation of the processes involved in the development of drying collapse in wood at high moisture contents.

3.1.4 Process of drying collapse

The pressure difference across a curved liquid-gas interface in a capillary, known as liquid-tension, is the process primarily responsible for drying collapse in wood. The superposition of drying stresses, caused by differential shrinkage of the wood structure, has the effect of influencing the severity with which drying collapse occurs.

3.1.4.1 Liquid-tension

As water evaporates from the surface cells (capillaries) of wood (figure 3.6), the evaporating liquid surfaces approach the pit openings that connect the cells with each other, reducing the evaporating surface radii. As the radii become smaller, the pressure difference across the gas-liquid interface (meniscus) increases. For the air-water interface in wood, this translates to a decrease in the pressure of the water phase, while the pressure of the air remains at 1.0 atmosphere. A few sample calculations illustrate the point further. For a capillary of radius 10 μm, the pressure difference across a water-air interface at 25 ° C is 0.14 atmospheres. With the air pressure at 1.0 atmosphere, the capillary water pressure is 0.86 atmospheres. If the capillary radius at the water-air interface decreases to 1 μm, the pressure difference increases to 1.4 atmospheres. With the air pressure again at 1.0 atmosphere, the capillary water pressure will now be -0.4 atmospheres. A negative pressure occurs, which indicates that the water is in a state of tension, better known as 'capillary tension'. The liquid is in effect trying to contract, and in doing so pulls on not only the gas-liquid interface, but on the capillary walls at the solid-liquid interface. Figure 3.7 illustrates the increase in negative pressure with decreasing capillary radius for a air-water interface at 25 ° C. The maximum negative pressure (tensile strength) that water can withstand before rupture, varies with temperature. Experimental measurements by Briggs (1950) show that between 0 and 6 ° C the maximum negative pressure of water increases sharply from 20 to 277 atmospheres, then decreases slowly with temperature to a value of 215 atmospheres at 50 ° C.

Figure 3.6 Evaporation of liquid from the surface cells. The surface menisci retreat to the pit membrane capillaries that connect the cells together.

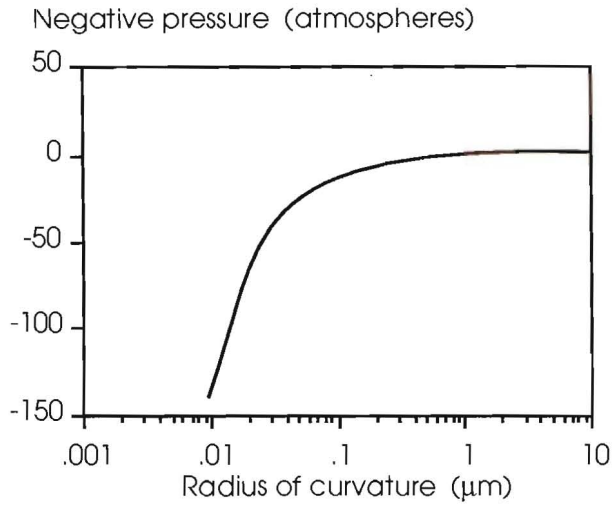

Figure 3.7 Increase in tensile stress of capillary water with decreasing radius of curvature of a air-water interface at 25 ° C.

The cell system of wood is interconnected by capillaries in the pit membranes and the cell walls (figure 3.6). The water held in these capillaries extends the negative pressure of water in the surface cells to cells throughout the system. This idea was first proposed by Hawley in 1931. The tensile stress is therefore exerted not only on surface menisci and cell walls, but also on the air-water interface of any air bubbles in the cell system. Should the radius of curvature of the retreating surface menisci reach a value less than the radius of curvature of a bubble in the system, the bubble will expand first before the meniscus retreats further, due to the lower tension of the water surrounding its surface. The bubble's expansion is achieved by the expansion of air within it, and the evaporation of water from its surface. The bubble will continue to expand until its surface reaches the pit openings of the cell wall (figure 3.8). The water migrates to adjoining cells, supplying the water of evaporation from the surface menisci. The cell is left with a slight positive pressure, equivalent to the vapour pressure of water (+0.03 atmospheres at 25 ° C), due to the very small volume of the initial air-water vapour bubble.

Figure 3.8 Expansion of air/vapour bubbles as surface menisci retreat into the pit membrane capillaries.

The tension of the water in the cell system continues to increase as the surface menisci retreat

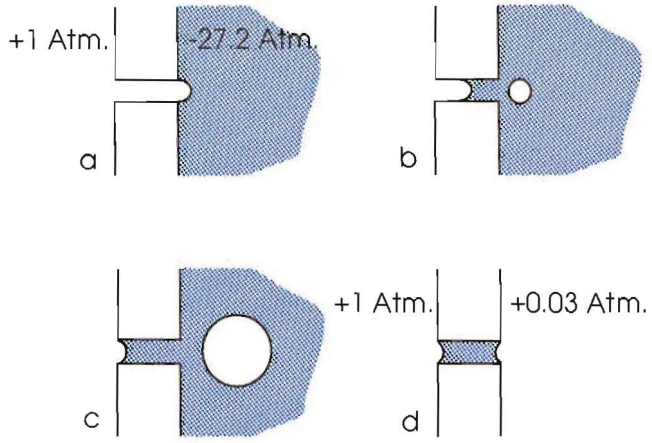

Figure 3.9 The sequence of steps that follow the movement of a meniscus through a pit membrane capillary (from Zimmermann 1983).

into the capillaries of the pit membranes and the cell wall. Interruptions to the process occur with the expansion of bubbles in response to the changing radius of curvature of surface menisci. However, because of the small diameter of the pit membrane and the cell wall capillaries, resistance to the flow of free water from cells with expanding bubbles is high. The flow of free water to surface mensici may not keep up with the rate of surface evaporation, leading to the continued retreat of surface menisci. The cell system experiences its maximum negative pressure or tension as the surface menisci are pulled through the pit membrane capillaries into adjoining cells. The process is illustrated in figure 3.9. As the meniscus reaches the water-filled cell (3.9a), water evaporates explosively into it. This causes expansion and an increase in its radius of curvature. The tension within the cell drops, reducing the pressure difference across the gas-water interface of the meniscus. This causes the pit membrane capillary to reseal, leaving a bubble of air and water vapour a fraction of a μm in diameter (3.9b). The bubble rapidly increases in size (3.9c), until its surface reaches the cell wall. The bubble may not detach from the cell wall as shown in 3.9b and c, in which case water will move in from within the cell wall to close it. The final cell pressure (3.9d) is equal to the vapour pressure of water (+0.03 atmospheres at 25 ° C), due to the very small size of the air bubble that enters the cell. The maximum tension the cell experiences, will depend on the size of the largest capillary in the pit membranes. In hardwoods, these capillaries have been measured (from electron micrographs) with diameters of 0.01-0.07 μm (Rudman 1966). At a diameter of 0.07 μm, the negative pressure experienced by the cells is -39.6 atmospheres at a temperature of 25 ° C if the surface tension of water is used (7.2×10^{-2} N m^{-1}). However, the water in wood contains extractives which act as wetting agents or surfactants,

reducing its surface tension to a value of approximately 5.0×10^{-2} N m^{-1} at 22 - 24 ° C (Stamm and Arganbright 1970). The negative pressure is therefore -27.2 atmospheres. This level of tensile stress may still be sufficient to cause cell walls to distort and collapse in some woods.

The absence of pre-existing bubbles of air/water vapour of a diameter larger than 0.07 μm, does not always predispose the cell to such large values of negative pressure. Cavitation - the rupture of a liquid under tension to form a bubble of vapour - can relieve the tension in a cell in the same way that a pre-existing bubble of air/water vapour does. It's a spontaneous process, that depends not on the surface tension of a liquid, but rather its cohesive strength or the strength of adhesion between the liquid and the cell wall. The maximum theoretical negative pressure of water has been calculated at -326 atmospheres (Sedgewick and Trevena 1976). Experimental measurements have reached values of -277 atmospheres (Briggs 1950). However it is uncertain whether experimental values such as those of Briggs, do in fact represent the true cohesive strength of water. Cavitation it is argued, occurred not by loss of cohesion in the liquid, but at the interface of solid and liquid. The inside surfaces of artifical containers always have many cracks and crevices that contain gas. Zimmermann (1983) suggests that what was measured was not the tensile strength of water, but the size of the gas nuclei (bubbles) extracted from the containers wall. The ability of the liquid to 'wet' (spread over) the solid surface is therefore important. This ability will depend on the relative strengths of the adhesive forces between the liquid and the solid, and the cohesive forces within the liquid. For surface wetting to occur, the adhesive forces between liquid and solid will need to be stronger than the cohesive forces within the liquid.

At a liquid-solid interface is a film of liquid molecules that are adsorbed (held) to the solids surface. The molecules will usually be positively adsorbed to the surface, that is, their concentration in the surface region (film) will be greater than in the bulk liquid. The thickness of this film will depend very much on the nature of the system; in water it can be several molecules thick. The forces between the adsorbed molecules and the surface may be weak van der Waals or hydrogen bonding type forces (physical adsorption), or involve the formation of chemical covalent bonds (chemical adsorption, or more usually chemisorption). The cell

wall of wood is made up of three main components: cellulose, hemicelluloses, and lignin. Adsorption of water to this surface involves physical adsorption - the formation of hydrogen bonds to the hydroxyl groups of primarily the cellulose and hemicelluloses, and to a lesser extent, the hydroxyl groups of lignin. If dry wood is wetted with water, heat is released by the process of bond formation during adsorption. The amount of heat released, suggests that for every water-water hydrogen bond broken, two bonds are formed between water molecules and cell wall hydroxyls (Rees 1960). This amount can be accounted for by assuming that two hydrogen bonds connect the oxygen in the water molecule with two oxygen atoms in the hydroxyl groups of the cell wall (Babbitt 1942). There is thus a greater binding energy between water molecules and the cell wall, than that between water molecules in the bulk liquid. The strength of adhesion between water and cell wall is greater than the strength of cohesion between water molecules. This however should not be taken to mean that rupture at the cell wall-water interface cannot occur. The surface of a solid is energetically non-uniform, due to the immobility of surface molecules. They are unable to take up their equilibrium positions, which means that localized differences will occur in the adsorption potential of the cell wall. Changes also occur in the surface properties of the cell wall as the cell ages within the living tree. This change becomes important with the advent of cell senescence and the development of heartwood.

The total heat released by cell wall adsorption of water, when dry wood is wetted, gives a measure of the hygroscopicity of the cell wall. That is, the number of sites at which water molecules can be adsorbed to the cell wall surface by the formation of hydrogen bonds. The total heat of adsorption for *Eucalyptus regnans* cell wall material is 18.6 calories/gram of wood. The components that make up this cell wall material gave the following heats of adsorption: cellulose 20.3 cal/g, hemicellulose 35.2 - 36.0 cal/g, and lignin 15.8 - 18.2 cal/g (Stamm 1964). The presence of extractives decreases the adsorption of water molecules by the cell wall. The effect of this is clearly demonstrated in the 30 % greater heat of adsorption for sapwood than heartwood. Alcohol-benzene extraction of heartwood can increase the heat of adsorption by as much as 38 % (Raczkowski 1963). The extraction removes heartwood extractives such as polyphenols which penetrate the cell wall after the cell has died, coating the cellulosic and

hemicellulosic materials (Bosshard 1968). The hygroscopicity of the cell wall declines as does the strength of adhesion between water and the cell wall, when cell senescence and heartwood formation occurs. It is the view of Bamber (1976) and Booker (1989) that this is not just a consequence of cell senescence, but that it occurs under the direct physiological control of the tree. The reduction in cell wall-water adhesion increases the chance of cavitation, and thereby embolism of the cell. The loss of water effectively seals the cell off from other cells, resulting in the cell's death. In Booker's view, this mechanism - of cavitation or rupture when the maximum sap to cell wall adhesion strength is exceeded - rather than the size of the pit membrane capillaries, is the main factor limiting cell collapse in wood during drying. If the maximum cell wall-sap adhesion strength is less than the tensile strength of the cell wall, cell collapse will not occur.

Booker's argument in favour of this approach to cell collapse takes a number of forms, and leads to a discussion of the various experimental procedures used in attempts to prevent liquid-tension collapse.

Evidence that pit membrane capillary size is not the limiting factor in the development of cell collapse comes in the absence of any clear correlation between the degree of collapse severity and wood permeability (figure 3.10).

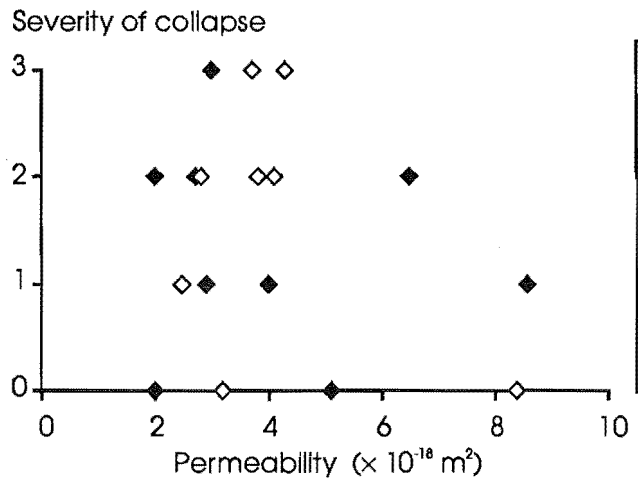

Figure 3.10 Effect of the permeability of *Eucalyptus delegatensis* wood on the severity of collapse. Data plotted from Booker 1989.

Surface tension has long been the focus of attempts at preventing collapse. Laplace's equation shows that a reduction in surface tension will reduce

$$p_{int} - p_{ext} = \frac{2\gamma \cos \theta}{r}$$

the pressure difference across a curved liquid-gas interface, and thereby the negative pressure experienced by a cell for a pit membrane capillary of a given size. The replacement of water in wood with miscible solvents of lower surface tension has produced substantial reductions in drying collapse. Replacement of water with methanol (figure 3.11) in *Eucalyptus delegatensis* reduced total shrinkage by 2/3's (CSIRO 1964). The amount of residual water was found, however, to influence the incidence of collapse. Ellwood et al. (1960) observed a reduction in collapse in *Quercus kelloggii* when the residual water associated with methanol replacement was reduced from 19.0 to 5.6 % of the oven dry weight. This reduction in collapse was supported by a further study using the solvent ethylene glycol monoethyl ether (cellosolve) and *Arbutus menziesii*. A curvilinear relationship was found for the reduction in total shrinkage with decreasing residual water content (figure 3.12). The rate of reduction of total shrinkage increases with decreasing residual water content, a trend contrary to the rate of decrease in surface tension. The suggestion was made by Ellwood et al. that some form of interaction between the replacement solvent and the cell wall could be responsible for cell collapse reduction, rather than just a decrease in liquid surface tension. Booker (1989) asserts that this reduction in collapse is due to the weaker strength of adhesion between the replacement solvent and the cell wall. This strength of adhesion will depend on the strength of hydrogen bond formation between the solvent and the cell wall hydroxyl groups.

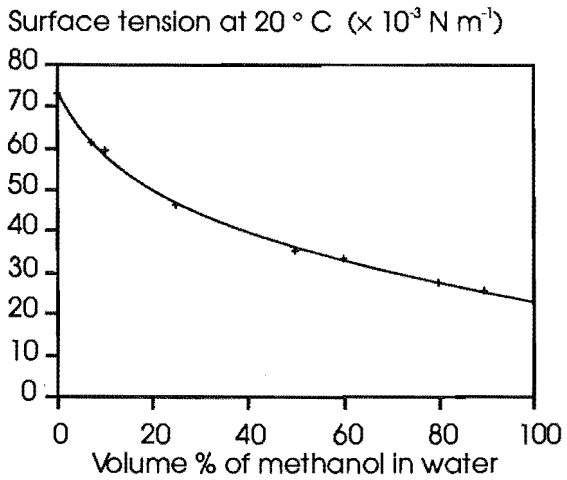

Figure 3.11 Reduction in surface tension with replacement of water with methanol.

The strength of hydrogen bonds can be measured using infrared spectroscopy. The infrared absorption band of the hydrogen-oxygen covalent bond of a free or unassociated hydroxyl group is shifted to a longer wavelength under the influence of hydrogen bonding. The hydrogen bond weakens the O-H covalent bond of the hydroxyl group - the stronger the hydrogen bond the weaker the O-H covalent bond -

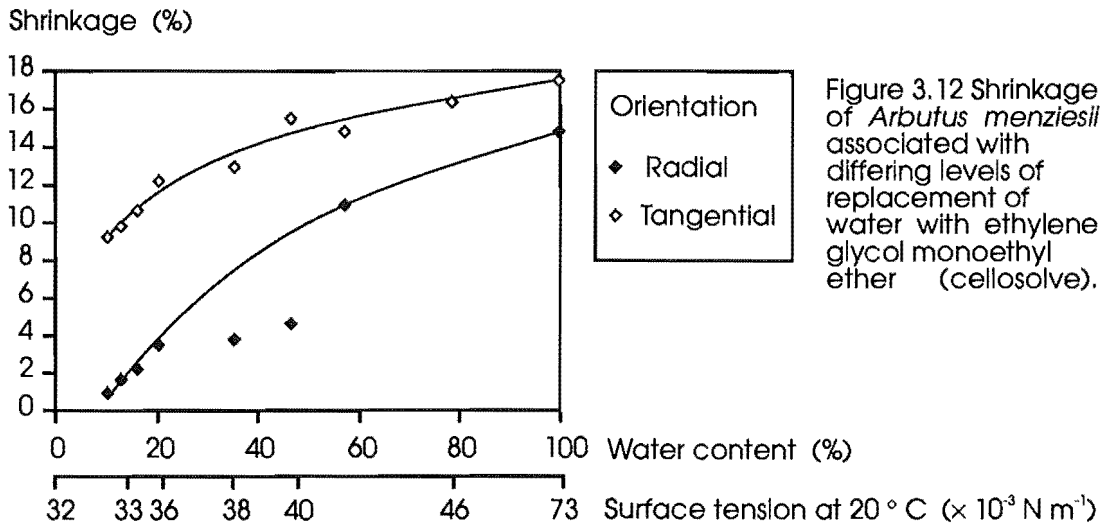

Figure 3.12 Shrinkage of *Arbutus menziesii* associated with differing levels of replacement of water with ethylene glycol monoethyl ether (cellosolve).

causing a shift in the wavelength at which it absorbs infrared light. Gordy (1939) used this technique to measure the strength of hydrogen bonds between hydroxyl groups and different solvents. The hydroxyl group of methanol was used, and the shift in wavelength of methanol at low concentration in benzene was used as a reference for other solvents. Methanol is unable to form hydrogen bonds with benzene, and at low concentration is unlikely to form hydrogen bonds with other methanol molecules, leaving the hydroxyl groups in a free or unassociated state. When Gordy's data is plotted against the solvent swelling of wood (figure 3.13), the correlation suggests the same pattern of solvent-methanol hydroxyl hydrogen bond strength also occurs with wood hydroxyl groups. However exceptions do occur, due to the effects of the differing structures to which the wood and methanol hydroxyl groups are attached. The solvents n-methyl and n-dimethylaniline, and di and tri-n-butylamine show a low level of swelling given their hydrogen bond strength with methanol hydroxyl groups. This suggests that steric hindrance, caused by differences in the size and shape of solvent molecules, and the rigid structure to which wood hydroxyl groups are attached, reduces the adsorption of solvent molecules to cell wall hydroxyl groups. The mobility of methanol molecules obviates this problem.

The reduction in the adsorption to cell wall hydroxyl groups, of a series of primary alcohols of increasing molecular volume (figure 3.14), was also attributed to steric hindrance (Kajita et al. 1979). Differences in molecular volume are due to alkyl chains of different length attached to the primary hydroxyl group. The heat of dissociation of members of the alcohol series

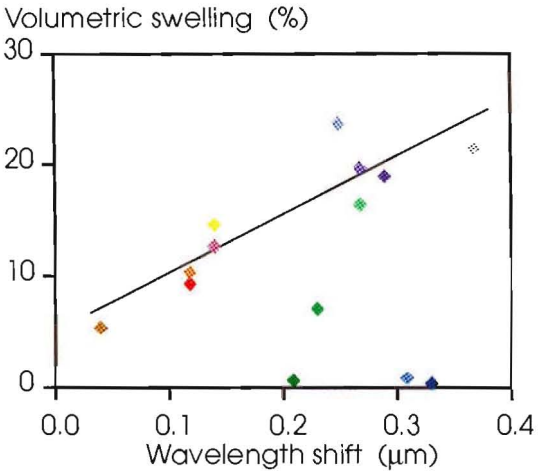

Figure 3.13 Correlation of the solvent swelling of oven dry *Acer saccharum* wood with solvent-hydroxyl hydrogen bond strength. Swelling data from Nayer & Hossfeld 1949.

is thought to vary little, which suggests that steric considerations limit bonding between solvent molecules and cell wall hyroxyl groups, accounting for the differences in heats of wetting.

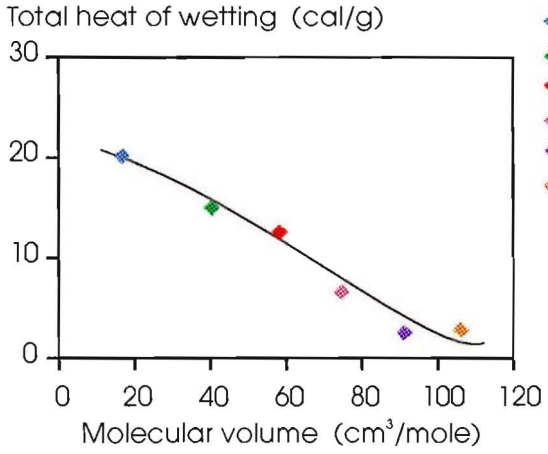

Figure 3.14 Adsorption of a series of primary alcohols of increasing molecular volume in the dry heartwood of *Chamaecyparis obtusa*.

Craver (1970) lends support to this idea with his measurements of the hydrogen bonding capability of solvents with cellulosic fibres (Whatman No. 2 chromatography paper). The velocity of sonic waves (10 kHz) in paper soaked with solvent, gives a measure of the extent of disruption of interfibre hydrogen bonds. The greater the disruption of these fibre-fibre hydrogen bonds, the slower the velocity. This results from the inability of fluids to effectively transmit the mode of sonic waves emitted. Solvents with a greater ability to form hydrogen bonds with hydroxyl groups, will therefore disrupt more of these fibre-fibre bonds, and give slower velocity measurements (table 3.1). Craver's data shows the same pattern observed by Kajita et al. (1979), of decreasing hydrogen bond capability of alcohols of increasing molecular volume with cellulose hydroxyl groups.

Table 3.1 Velocity of sound in paper saturated with alcohols of increasing molecular volume.

Alcohol	Velocity km/sec
Water	0.46
Methanol	0.64
Ethanol	1.21
1-Propanol	1.33
1-Butanol	1.41
1-Octanol	1.82

Booker's assertion of reduced strength of adhesion of solvent to cell wall appears to be borne out by experimental data. His argument that such hydrogen bonding considerations (under the influence of steric hindrance) prevail over those of the surface tension properties of the liquid, are further strengthened by the ineffectiveness of surfactants in preventing collapse. When surfactants are added to the water in wood cells, reducing the waters surface tension to that of organic solvents, the incidence of drying collapse is found to increase (Booker 1989 from Haslett and Booker unpublished data). The hydrogen bonding properties of water are believed to be the cause of the resulting collapse.

Table 3.2 The increase in collapse associated with air bubble removal in the wood of *Eucalyptus regnans*.

Orientation	Collapse %	
	Air-free	Air-saturated
Radial	3.5	0.9
Tangential	7.2	1.2

Collapse prevention through the introduction of gas bubbles of a critical size has also received attention. According to the Laplace equation, a bubble of radius larger than the surface air-water menisci will expand preventing cell collapse. When air bubbles normally present in green wood are eliminated prior to drying, the incidence of collapse increases. Kauman (1964) attributed the differences in drying collapse (table 3.2) of wood samples rehydrated in degased water and air-saturated water, to the presence/absence of air bubbles. Attempts at artifically inducing bubbles in cells, have however failed to prevent drying collapse.

The use of sodium bicarbonate - impregnation by diffusion - served only to increase collapse in *Eucalyptus regnans* (Kauman 1960a). Pressure impregnation with carbon dioxide gas at pressures of 50 and 250 atmospheres, for periods up to 17 hours, also failed to prevent collapse in *Eucalyptus regnans* (Kauman 1964). The release of pressure leaves the dissolved carbon dioxide in a supersaturated state, leading to the formation of gas bubbles within cells.

The application of ultrasonic energy to *Eucalyptus regnans* was also ineffective in preventing collapse (Kauman 1964). The high local stress concentrations generated by the ultrasonic vibrations, induce cavitation producing bubbles of water vapour within cells.

3.1.4.2 Drying stress

Moisture gradients develop as water evaporates from the wood surface, and air-water menisci retreat into the cell structure. The surface cells empty of water, and as the cell walls dry, shrinkage commences producing a stress distribution throughout the cell system. The pattern of changing stress distribution with time, can be determined by sectioning cross-sections of boards, at intervals, and measuring the recoverable strain produced by drying stress release (figure 3.15). Shrinkage of the surface layer is resisted by the wet internal layers (or core), producing severe surface tensile stress, balanced by milder internal compressive stress. When the stress exceeds the cell walls proportional limit of elastic deformation, inelastic deformation or creep occurs, permanently stretching or compressing the cell walls over a period of time, producing a condition known as set (figure 3.16).

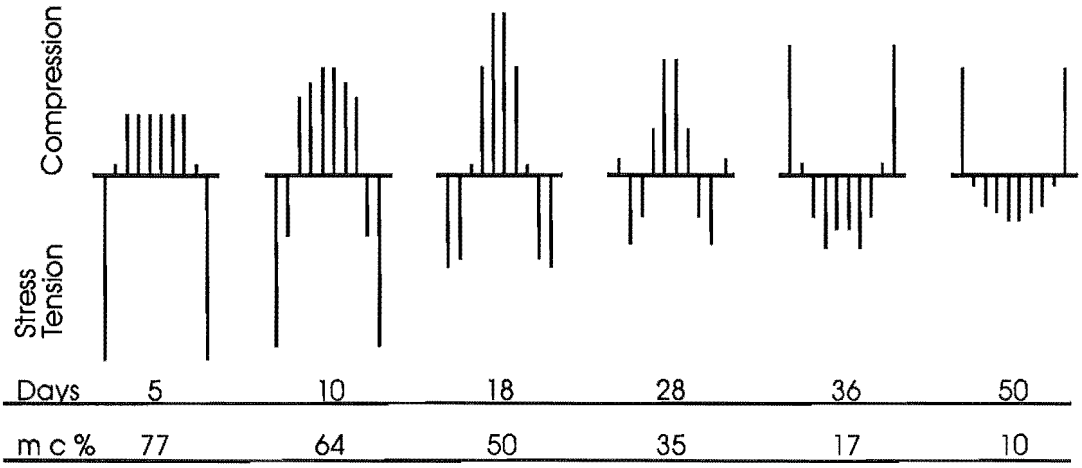

Figure 3.15 Distribution of drying stress at various stages of drying in boards of *Quercus rubra* (from McMillen 1955a).

As layers adjoining the surface layer also dry and shrink, they too develop tensile stress. The tensile stress of the surface layer declines, while the compressive stress of wet internal layers increases. The surface layer becomes set in tension, shrinking less than would be the case if it were

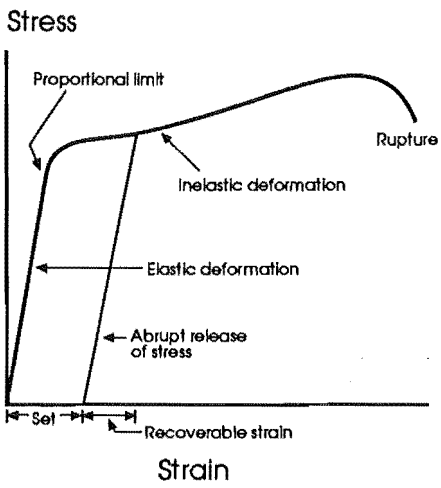

Figure 3.16 Stress - strain diagram.

free of tensile stress. As the internal layers dry, having been in compressive stress rather than tensile stress, they attempt to shrink more freely than the surface layer, but are restrained from doing so by tension set in the surface layer. They develop tensile stress and exert a compressive stress on the surface layer. The drying stress distribution is effectively reversed during the process of drying.

Compressive stress of the wet core during the initial stages of drying, tends to increase the severity of drying collapse. The compressive stress acts in conjunction with the liquid-tension inside the cell, increasing the stress to which the cell wall is subjected. The use of anti-shrink chemicals to reduce drying stress, while having an effect, is of limited use in preventing severe collapse (Ellwood et al. 1960).

Anti-shrink chemicals act in two ways to reduce drying stress. They lower the humidity over adsorbed water in the cell wall, reducing moisture gradients, and bulk the cell wall, reducing shrinkage. Water-soluble chemicals such as salts, sugars, and polyethylene glycol have been used. Saturated solutions of these chemicals in the cell wall lower the relative vapour pressure at which drying - and therefore shrinkage - occurs (figure 3.17a). Reduction in shrinkage is proportional to the volume of solute deposited in the cell wall. The higher the concentration of the solute at saturation - the more soluble the solute in water - the less the volume of water held in the cell wall, and the lower the shrinkage (figure 3.17b). Lithium chloride (LiCl) being more soluble than barium chloride ($BaCl_2$) in water, reduces shrinkage more. The plots in figure 3.17b, are linear and parallel because the loss of each increment of water from the cell wall is accompanied by the same amount of shrinkage

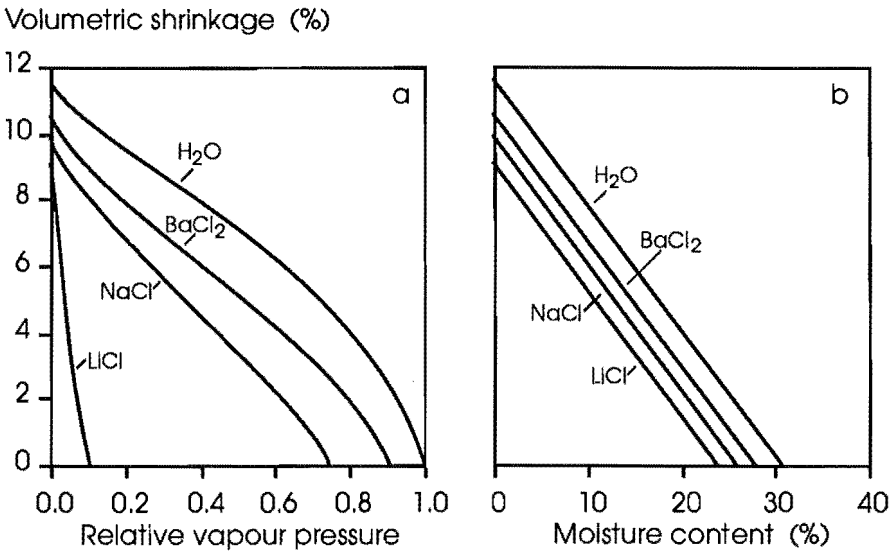

Figure 3.17 Effect of anti-shrink salts on the relative vapour pressure and shrinkage of cross-sections of *Picea sitchensis* (from Skaar 1988).

3.1.5 Drying variables

3.1.5.1 Temperature

The tendency to collapse increases with temperature. Over the temperature range 20 - 90 ° C, the increase in collapse is proportional to the wood temperature (figure 3.18), provided drying stress is low. High levels of compressive drying stress introduce deviations from the linear relation (Kauman 1960b).

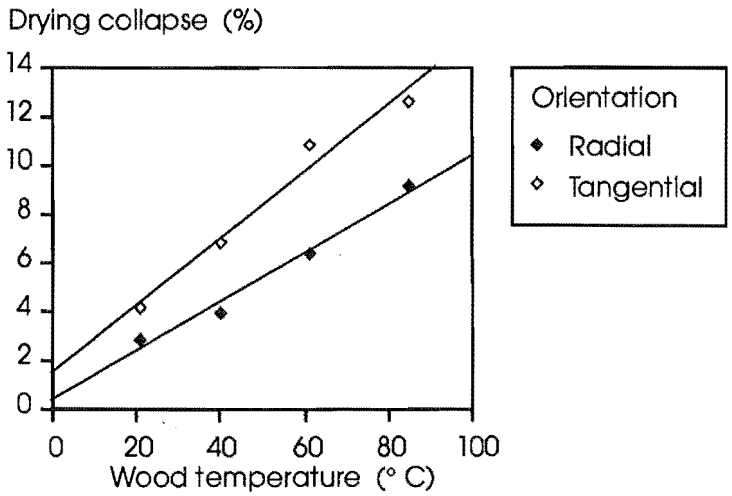

Figure 3.18 Linear increase of collapse with temperature. *Eucalyptus regnans* dried at high humidity (from Kauman 1960b).

Cell wall modulus of elasticity, modulus of rupture, and stress at the proportional limit decrease with increasing temperature. The surface tension of water also declines with increasing temperature (figure 3.2), however this effect is small, and falls far short of compensating for the loss of cell wall strength. The net effect is a reduction in the negative pressure required to cause collapse with increasing temperature (figure 3.19). Ellwood et al. (1960) derived the reduction in negative pressure required to cause collapse from the loss of cell wall strength of *Fagus grandifolia*, corrected for the decrease in surface tension of water.

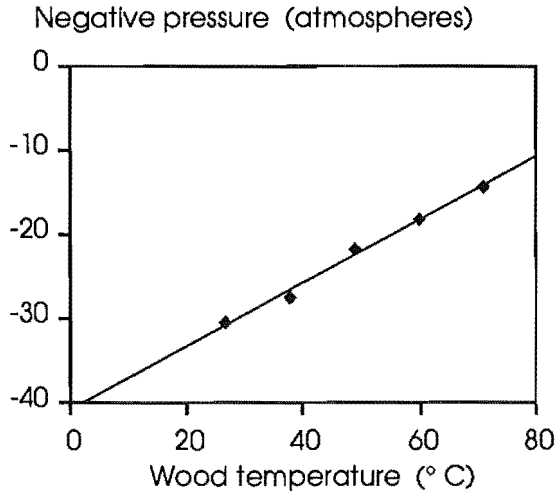

Figure 3.19 Reduction in negative pressure required to collapse cells of *Fagus grandifolia* with increasing temperature (from Ellwood et al. 1960).

Drying stresses also increase with increasing temperature. The drying stress distribution (figure 3.15) however remains the same over the temperature range 27 - 60 ° C (McMillen 1955b). Moisture gradients become steeper in response to increased temperature, increasing the maximum tensile stress in both the surface layer during initial drying, and the inner layers after stress reversal in the latter stages of drying. The increase in tensile stress actually corresponds to an increase in recoverable tensile strain: tension set is essentially unaffected by temperature over the above temperature range, showing only a slight increase at 60 ° C. The increase in tensile stress in conjunction with the decline in modulus of rupture of the cell wall, increases the incidence of surface and internal checks. The increase in internal checks is further exasperated if the maximum internal tensile stress is reached while some of the internal layers are above 30 % moisture content. The cell wall being much weaker in the water saturated state than the dry state.

The way in which internal compressive stress increases with temperature, differs from tensile stress. Internal compressive strain remains essentially constant over the temperature range 27 - 60 ° C, while internal compression set effectively doubles in magnitude. The increase in internal compressive set can be attributed to the reduction in the cell wall compressive strength at the proportional limit with increasing temperature. Inelastic deformation - in this case cell wall compression set - commences at lower stress levels with increasing temperature. The result is increased shrinkage. The increase in compressive stress exerted on the cell wall, in conjunction with decreased cell wall strength, increases the severity of collapse.

3.1.5.2 Humidity

Application of the Kelvin and Laplace equations, shows that very large negative pressures can develop within the cell system at relative humidities close to 100 %. The drop in vapour pressure associated with the reduced pressure of water surrounding a air-water meniscus, is given by the Kelvin equation. Using it we find the relative vapour pressures of menisci of radius 0.1, 0.05, and 0.02 μm are 99.0, 98.0, and 95.0 % respectively. The corresponding negative pressures, calculated from the Laplace equation using a surface tension of 5.0×10^{-2} N m^{-1} for sap at 22 - 24 ° C (Stamm and Arganbright 1970), are -8.9, -17.6, and -48.4 atmospheres respectively. This suggests that high humidities are unable to prevent collapse in collapse-susceptible wood when dried at elevated temperatures.

The reduction in drying stress at high humidities, increases cell wall shrinkage and collapse in *Eucalyptus regnans* dried at high humidity; the effects however are not large (Kauman 1960b). The reason for this lies in the restraining action of the tension set in the surface layers on internal shrinkage and collapse. At high humidities there is a reduction in the tension set in the surface layers. This maintains surface plasticity and permits freer shrinkage and collapse.

The rate at which relative humidity is reduced during drying affects the timing of maximum tensile and compressive stress. More rapid

reductions produce earlier maxima and steeper moisture gradients. Abrupt reductions of relative humidity during the kiln schedule can re-establish near maximum tensile and compressive stress.

3.1.5.3 Orientation and geometry

Differences in cell wall shrinkage and collapse of boards of different orientation (flat and quarter sawn) and cross-sectional geometry (square and rectangular), arise from the superposition of two effects:

- differences in tangential and radial shrinkage and collapse;

- the influence of cross-sectional geometry on the restraining action of surface tension set in the surface layers.

Collapse is usually 1.5 - 3.0 times greater tangentially than radially, provided drying stress is isotropic. This according to Kauman (1964) is probably due to radial reinforcement by the rays, and also possibly to preferential evacuation of cell water through fibre/ray pits. Drying stress may also contribute. The rate of deformation of wood under constant compressive stress perpendicular to the grain, is greater tangentially than radially. Tangential shrinkage is approximately double that of radial shrinkage. For *Eucalyptus delegatensis,* shrinkage to 12 % moisture content is 6.5 % tangentially and 3.2 % radially (Haslett 1988a).

Tension set in the surface layers of boards of rectangular cross-sectional geometry, restrains shrinkage and collapse in width, at the expense of increased shrinkage and collapse in thickness. The effect has been compared with the Poisson ratio in elasticity (Kauman 1958), where a primary strain in one direction sets up a secondary strain in another direction. Restraint or extension in one direction is accompanied by contraction in another direction. In wood, restraint in width is more effective than in thickness, producing what is akin to a Poisson ratio. The effect is small under conditions of low temperature and high humidity, but increases markedly at lower humidities and higher temperatures.

3.1.6 Wood variables

The collapse susceptibility of wood varies most between sites, then between trees and heights within trees at each site, and to a lesser extent in radius from pith to bark for trees at some sites. These were the conclusions of a study by Ilic and Hillis (1985) on regrowth stands of *Eucalyptus regnans* and *E. delegatensis* from five sites in Australia. The reasons for the pattern of variation were not given. However inferences about causes can be drawn from known patterns of collapse variation with wood and growth related variables.

3.1.6.1 Density

Collapse is negatively correlated with density (figure 3.20). The reason for this lies in increases in cell wall thickness with increasing density. It is the way in which this increase in cell wall thickness is distributed, however, that appears to determine collapse susceptibility. From image processing measurements of the cross-sectional fibre wall and lumen areas, Ilic and

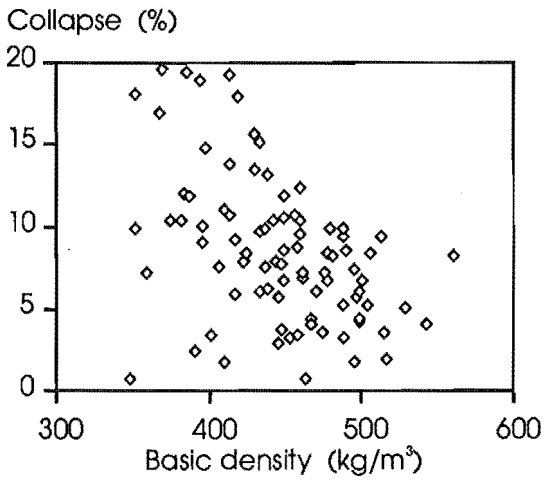

Figure 3.20 Decline in collapse with increasing density of *Eucalyptus regnans* heartwood (from Chafe 1985).

Hillis (1984) were able to calculate the Transverse Wall to Lumen Area Ratio of the Fibres (TWLARF). They found the upper 10 percentile value of the TWLARF distribution varied consistently with collapse. Mean TWLARF values were unable to predict collapse: the reason being that mean TWLARF is insensitive to differences in the TWLARF distribution. A wood sample with a small number of latewood fibres with very large TWLARF values will have the same mean as a sample with a larger

number of latewood fibres of lower TWLARF value. Mean basic density measurements of wood samples also suffer from this problem, which probably explains the large spread of values in figure 3.20. The conclusion drawn by Ilic and Hillis was that an increase in the proportion of latewood fibres provides greater resistance to drying collapse than just an increase in the density of the latewood band due to higher TWLARF values (figure 3.21).

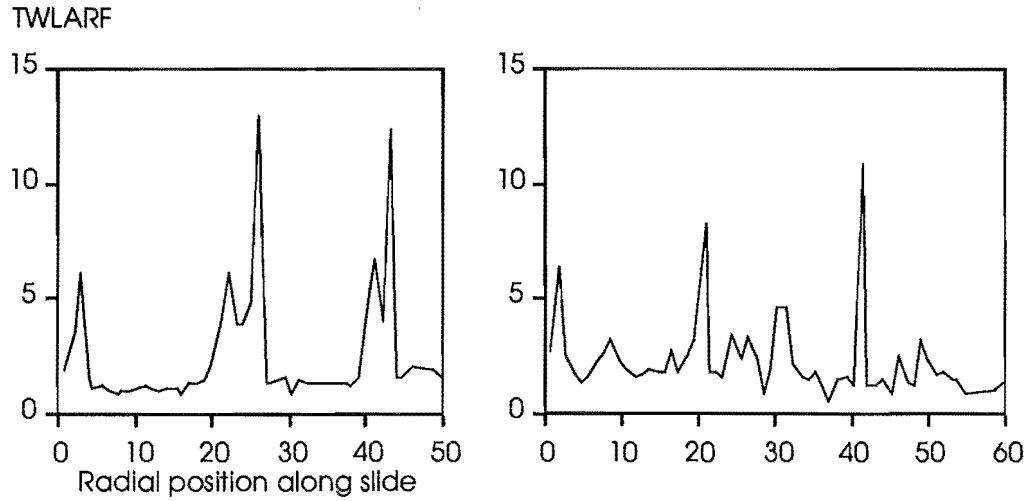

Figure 3.21 Radial variation of TWLARF values of *Eucalyptus regnans* showing the difference between the collapse region (RHS) and the non-collapsed region (LHS). The higher proportion of latewood fibres in the non-collapsed region (LHS) provides greater resistance to drying collapse (from Ilic and Hillis 1984).

Basic density increases with height in *Eucalyptus regnans* and *E. delegatensis* and is associated with a corresponding decrease in collapse with height (figure 3.22). The trend remains consistent in different trees, but its magnitude can vary greatly (Pankevicius 1961).

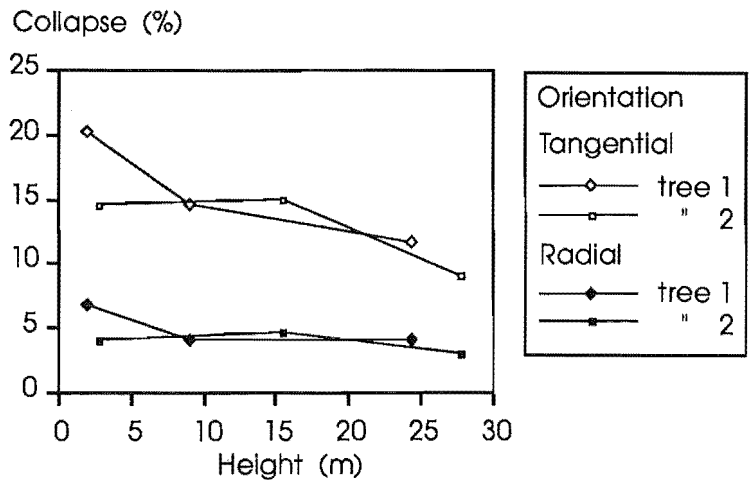

Figure 3.22 Decline in collapse with increasing height in two trees of *Eucalyptus delegatensis* (from Pankevicius 1961).

Radially, collapse increases from bark to pith in *Eucalyptus regnans* until the juvenile wood surrounding the pith is reached, whereupon it declines rapidly (figure 3.23). The trend is accentuated somewhat by the low level of collapse in the sapwood. Ignoring this, the increase in collapse better reflects the small decrease in basic density from bark to pith. The abrupt decline in collapse in the juvenile wood near the pith is attributed to an increase in permeability, brought about by compression failures in the cell walls of the brittle heart core (Chafe 1986).

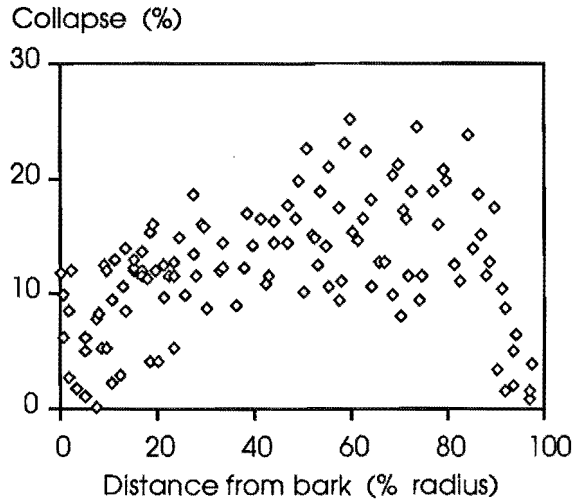

Figure 3.23 Radial variation in collapse from bark to pith in *Eucalyptus regnans* (from Chafe 1986).

3.1.6.2 Water saturation

Collapse susceptibility appears to be affected by the degree of cell saturation. Chafe (1985) found a positive correlation of collapse with the percent of the theoretical moisture content saturation in *Eucalyptus regnans*. The pattern of percent saturation change within trees of *E. regnans* parallels to some extent that of collapse. Percent saturation declines with height but remains constant from bark to pith, declining only near the pith due to the effects of cell wall compression failure in the brittle heart core of the juvenile wood. Within growth rings, latewood cells were found to be more highly water saturated than earlywood cells. Observations of similar levels of collapse in some late and earlywood cells suggests the higher saturation of latewood cells may offset some of the collapse resistance afforded by their greater density. The relationship between collapse and percent saturation was stronger in latewood than in earlywood. Water saturation it would seem is a more important

determinant of collapse susceptibility in latewood than in earlywood (Chafe 1986).

3.1.6.3 Cell wall composition and extractives

Collapse is negatively correlated to the polysaccharide cell wall component, and positively correlated to the lignin and polyphenol content, of the wood of *Eucalyptus delegatensis* (Bland 1971, Chafe 1987). Analysis of extracts revealed a strong negative correlation between collapse and holocellulose, and to a lesser extent between collapse and sodium hydroxide (NaOH) extractives (presumed high in hemicelluloses). The methanol-soluble ellagic acid component of the polyphenol extractives was found to be positively correlated with collapse (Chafe 1987).

3.1.6.4 Growth stress

Growth stresses affect the cell wall structure, and in their extreme form - tension wood - are responsible for severe and non-recoverable collapse. Considerable growth stress variation occurs between and within trees of *Eucalyptus* species. In *Eucalyptus regnans*, the average peripheral longitudinal stress varied from 4.9 to 16.3 MPa. Even straight, non-leaning trees were found to have significant longitudinal stress variation around their circumference (Nicholson 1973). The stresses arise from the differentiation of a range of different cell types as the trees re-orientate themselves in response to external influences such as competition. A relatively smooth and continuous change of cell types occurs with increasingly higher levels of growth stress. Tension wood fibres represent the upper limit, and low density thin-walled fibres the lower limit (Nicholson et al. 1975). These changes affect the wood's volumetric shrinkage, modulus of elasicity, basic density and lignin content as shown by the Klason lignin value. Volumetric shrinkage increases with increasing longitudinal stress in both sapwood and heartwood. The modulus of elasicity and basic density also increase, while the Klason lignin value declines with increasing longitudinal stress (Nicholson et al. 1972). No specific mention regarding collapse is made except for the

special case of tension wood, but it can be implied that the changes in cell wall structure associated with growth stress will have an effect on collapse susceptibility.

3.1.7 Summary of collapse review

3.1.7.1 Process of drying collapse

Liquid tension is the process primarily responsible for drying collapse in wood. The superposition of drying stresses, caused by differential shrinkage of the wood structure, influences the severity with which drying collapse occurs.

The size of the openings in the pit membranes and cell wall capillaries has generally been thought to limit the magnitude of liquid-tension exerted on the cell wall. In disputing this, Booker (1989) points to a lack of any correlation of wood permeability with collapse severity and suggests that the strength of the cell wall - sap adhesion is the main factor limiting liquid-tension collapse in wood. This is supported by experimental data which shows that the replacement of water with organic solvents of lower hydrogen bond strength with hydroxyl groups in the cell wall reduces the severity of collapse. It had previously been thought that the surface tension properties of the organic solvents were responsible. This, however, is disputed by the fact that the addition of surfactants to water, which effectively reduces the waters surface tension to that observed with organic solvents, does not alleviate the severity of collapse.

The expansion of pre-existing gas/vapour bubbles in cells has been found to alleviate collapse. Marked differences were found in the drying collapse of wood samples rehydrated with degased and air-saturated water. Artifical bubble nucleation, by supersaturation with dissolved gases and ultrasonics, has, however, proved ineffective in reducing collapse.

The use of anti-shrink chemicals to reduce drying stress has proved of limited use in preventing severe collapse.

3.1.7.2 Drying variables

The formation of collapse increases with temperature. The increase is proportional to the wood temperature, provided drying stress is low. Low relative humidities, however, increase drying stresses, producing high levels of compressive stress that introduce deviations from the linear relation between collapse and wood temperature.

Board orientation and geometry affects the pattern of drying collapse in wood. This results from differences in tangential and radial collapse, and the affects of cross-sectional geometry on the restraining action of tension set in the surface layers.

3.1.7.3 Wood variables

The collapse susceptibility of wood is affected by wood variables that are controlled by environmental and genetic factors. The effects are variations in the collapse susceptibility of wood from different sites, different trees within sites, and different heights and radial positions within trees.

Wood variables such as wood density, water saturation, cell wall composition, and the presence of extractives have all been shown to have an effect on collapse. It is the distribution of the wood density rather than the value of the mean density that appears to affect collapse susceptibility. Growth stresses also influence collapse, though indirectly, by determining the type and the composition of cells that make up the wood.

3.2 Experiment design

The experiment was designed to examine the variation of drying collapse in the wood of *Eucalyptus delegatensis* grown in New Zealand, and the effect of different drying temperatures and carbon dioxide gas treatments on drying collapse. The collapse susceptibility of the wood of *E. delegatensis* grown in Australia has been shown by Ilic and Hillis (1985) to vary significantly among sites, among trees within sites, and among height and radial positions within trees. The extent to which this occurs in New Zealand grown wood of *E. delegatensis*, and the proportions of the total variation of drying collapse that can be attributed to each of the levels of classification i.e. trees within sites, was assessed. The wood was dried at different temperatures to determine firstly what effect temperature had on the drying collapse in wood from different sites, trees within sites, and positions within trees, and secondly what effect temperature had on drying collapse in wood treated with carbon dioxide gas. The carbon dioxide gas treatments involved supersaturating the wood prior to drying with large quantities of dissolved carbon dioxide gas, at different solubilities, to generate gas bubbles within the cells of the wood. Boards of a size large enough to retain sufficient dissolved carbon dioxide gas during the period of drying collapse formation were used. This was considered a possible cause of why Kauman's (1964) experiment, in which 0.5 cm cubes of *Eucalyptus regnans* were supersaturated with dissolved carbon dioxide gas, showed no reduction in drying collapse. The initial mass flow and longitudinal diffusion of dissolved carbon dioxide gas, in wood samples of such short length, would be rapid and substantial giving a dissolved carbon dioxide gas residence time that may have been too short to have an effect on drying collapse. The variation of drying collapse and the significance of temperature and carbon dioxide gas treatment effects were assessed using measurements of volumetric, tangential and radial collapse, and an empirical measurement of board shape after drying. Volumetric, tangential and radial collapse measurements were taken in such a way that board end and edge effects on drying collapse could be assessed.

The variation of the basic density of *Eucalyptus delegatensis* wood among sites, among trees within sites, and within each tree was also assessed.

The design of the experiment was a mixed model nested analysis of variance (figure 3.24).

Figure 3.24 The structure of the nested analysis of variance design

Treatment	1.5 MPa, 1°C	1.5 MPa, 12°C		4.5 MPa, 17°C		Control	
Site	N	N	S	N	S	N	S
Tree	4	1 2 3 4 5	1 2 3 4 5	4 5	3 5	1 2 3 4 5	1 2 3 4 5

N = Nelson, S = Southland
The tree numbers represent the code for each tree, not the number of trees.

The highest level of classification involves fixed treatments (Model I), in this case different levels of carbon dioxide gas supersaturation, and controls. All subordinate levels of classification, nested within the fixed treatments, are randomly chosen (Model II, Sokal and Rohlf 1981). These subordinate levels of classification measure the magnitude of the variation of drying collapse within the wood used for the fixed carbon dioxide gas treatments. Knowing the magnitude of the variation of drying collapse, allows us to test the magnitude of the added component due to the fixed treatments, which determines whether or not the fixed carbon dioxide gas treatments do in fact have an effect on drying collapse.

The subordinate levels of classification consisted of five trees of *Eucalyptus delegatensis* selected from two sites (Nelson and Southland), with sample boards taken at various heights (0 - 5 m). For each board, two replicate sets of drying collapse measurements were made. According to Ilic and Hillis (1985), most of the variation of drying collapse in *Eucalyptus delegatensis* in Australia occurs between sites, with diminishing levels of variation between trees within sites, between heights within trees, and from pith to bark within trees, in that order. It was on this basis that the subordinate levels of classification were made.

The analysis was repeated for each of three low temperature kiln drying schedules. The schedules differ only in their initial dry bulb temperatures (30, 40 and 50 ° C), allowing an assessment of the effect of temperature on drying collapse and carbon dioxide gas treatment. The same moisture content / relative humidity reduction rate was used for each kiln drying schedule. High relative humidities were used to minimise the

contribution of drying stress to collapse formation. A low, constant fan speed was used for all three kiln schedules.

3.2.1 Carbon dioxide gas treatments

Three carbon dioxide gas treatments were used in the experiment, and a control (table 3.3).

Table 3.3 Carbon dioxide gas treatments and control

Treatments	Pressure MPa	Temperature ° C	Absorption time weeks	Allocation of boards
Carbon dioxide	1.5	1	8	6
" "	1.5	12	2	166
" "	4.5	17	2	16
Controls	-	-	-	166

The carbon dioxide gas treatments provided a range of gas solubilities in water within the wood. Equilibrium carbon dioxide gas solubility at 4.5 MPa and 17 ° C is approximately 5 g CO_2 / 100 g H_2O. At 1.5 MPa and 1 ° C it is approximately 4 g CO_2 / 100 g H_2O, and at 1.5 MPa and 12 ° C it is approximately 2.5 g CO_2 / 100 g H_2O. Because of the slow rate of dissolved carbon dioxide gas diffusion into the wood at 1 ° C, a long absorption period of 8 weeks was used. This period was reduced to two weeks for diffusion in boards at 12 and 17 ° C. The allocation of samples in table 3.3, was determined by the size constraints of the pressure cylinders used for carbon dioxide gas treatment. This constraint meant that only a subset of trees and sites were sampled in the low temperature (1 ° C and 1.5 MPa) and the high pressure (17 ° C and 4.5 MPa) treatments. For the low pressure treatment only boards from tree 4, Nelson were sampled. For the high pressure treatment only boards from trees 4 and 5, Nelson, and trees 3 and 5, Southland were sampled.

3.2.2 Wood - Sources

Five trees of *Eucalyptus delegatensis* were selected from each of two sites: Golden Downs Forest, Nelson, and Longwood Forest, Southland. The trees were selected on the basis of size, using tree diameter at breast height

over bark (d.b.h.o.b.) of 75 cm as a guide. The actual d.b.h.o.b. measurements for the selected trees are given in table 3.4. The stands in Nelson and Southland were of different ages, but the trees were of a similar size. The Nelson stand was planted in 1935 with stock of seed source - Tapanui district, Southland (Seedlot S35/16 - 232). The staff at the Forest Research Institute's Genetics and Tree Improvement section, were unable to source the final code 232, which it is assumed pinpoints the seed stand in Tapanui. The Southland stand was planted in 1954, with stock of what was almost certainly West Tapanui Forest ("Crookston" strain) seed source (D. Guild pers. comm.). This seed source was widely used in Southland until the late 1970's, and all early New Zealand Forest Service stands of *Eucalyptus delegatensis* , including Golden Downs Forest, Nelson, were planted with it. The Crookston strain is noted for a high frost tolerance, but is prone to drying collapse and internal checking.

Table 3.4 Diameter at breast height over bark of selected trees from Nelson and Southland

	d.b.h.o.b (cm)	
Tree	Nelson	Southland
1	76	72
2	77	76
3	77	74
4	93	72
5	72	73

3.2.3 Kiln schedules

The three low temperature kiln schedules used (table 3.5), were based on a British and three Australian kiln schedules for 25 mm thick *Eucalyptus delegatensis* (Boone et al. 1988, Campbell 1988). Each has a different initial dry bulb temperature (30, 40 and 50 °C), but the same moisture content / relative humidity reduction rate. The high initial relative humidities will reduce the contribution of drying stress to collapse formation, while similar rates of relative humidity reduction will help to ensure that the timing of maximum tensile and compressive stress occurs at the same moisture contents in all three kiln schedules. The fan speed was set as low as the equipment would allow, and reversed every 12 hours for the first three weeks, and 24 hours thereafter. An average fan speed of 3.3 m. s^{-1} (range 3.0 - 4.0 m s^{-1}) was measured through the stack, using a hot wire anemometer, Davimeter, Model 642 (Airflow Developments Limited, High Wycombe, England).

Table 3.5 *Eucalyptus delegatensis* kiln drying schedules

Moisture content %	Temperature dry bulb ° C	wet bulb ° C	Relative humidity %
Low temperature schedule			
Green	30.0	28.5	90
60	30.0	28.0	85
40	35.0	32.0	80
35	35.0	31.0	75
30	40.0	35.0	70
25	50.0	42.0	62
20	60.0	49.0	55
15 - 12	70.0	50.0	35
Medium temperature schedule			
Green	40.0	38.5	90
60	40.0	37.5	85
40	45.0	42.0	80
35	45.0	40.0	75
30	50.0	44.0	70
25	55.0	47.0	62
20	60.0	48.5	55
15 - 12	70.0	50.0	35
High temperature schedule			
Green	50.0	48.0	90
60	50.0	47.5	85
40	55.0	51.0	80
35	55.0	50.0	75
30	60.0	53.5	70
25	65.0	56.0	62
20	70.0	58.0	55
15 - 12	70.0	50.0	35

A load of 378 boards were dried with each kiln schedule, 354 of which were collapse measurements samples, and 24 for measurement of moisture content. The number of moisture content boards was based on the findings of a study by Fell and Hill (1980), on the precision of moisture content measurement in kiln loads of *Quercus rubra*. For the more critical stages of drying from 40 to 12 % moisture content, they found that 20 - 23 samples were required to provide estimates of moisture content within ± 2 % deviation from the mean. At moisture contents greater than 40 %, 10 - 12 samples were recommended, giving a deviation of ± 3 from the mean. For the three kiln loads dried in this experiment, moisture content was measured from green to 12 % with 24 boards.

3.3 Growth strain measurements prior to felling

Four longitudinal peripheral growth strain measurements were taken at equal intervals around the circumference of each tree at breast height (1.4 m). For two of the five trees in Southland, only two opposing measurements were taken due to time constraints. The method used was that of Nicholson (1971). The equipment was made available by the Forest Research Institute, Rotorua.

A selection of the cut wood segments, removed in the process of growth strain measurement, were microtomed and stained for the presence of tension wood. The staining procedure was that of Robards and Purvis (1964), and involved a double staining sequence with 1 % aqueous lignin pink, followed by 1 % chlorazol black E in methyl cellosolve to differentiate the gelatinous layer of the tension wood cells.

3.4 Log handling and sawing

A single 5 m log length was taken from the butt of 10 trees, 5 trees each from Longwood Forest, Southland and Golden Downs Forest, Nelson. From one tree at each site, 10 cm thick sectional disks were cut at heights 0, 5, and 13 m for density and shrinkage measurements. The ends of each log were spray painted a different colour so boards could be identified according to tree of origin and vertical position. The logs were transported to the respective sawmills, Alan Johnston Sawmilling Ltd, Tuatapere, Southland, and Donnelly Milling Co. Ltd, Richmond, Nelson, on the day of felling, and sawn the following day.

Log debarking presented no problems. The timing was early summer (November - early December) when the wood-to-bark bond is weakest. Most of the bark simply fell off during log handling on the way to the sawmill.

The logs were quarter-sawn according to Haslett's (1988b) traditional sizing carriage sawing pattern (TSC 5) (figure 3.25). 1T, 2T, and 3T correspond to the first, second, and third cuts. Each is located approximately two-thirds the distance from periphery to pith. The four flitches cut from each log

were resawn to 100 × 25 mm boards on a breast-bench according to the patterns in figure 3.25. The numbers correspond to successive saw cuts. Distortion caused by growth stress release did occur, but was minimised by cross-cutting the 5 m logs to 2.5 m lengths just prior to sawing. The only problem that occurred was some seizing of the breast-bench saw, this was overcome with the use of wedges.

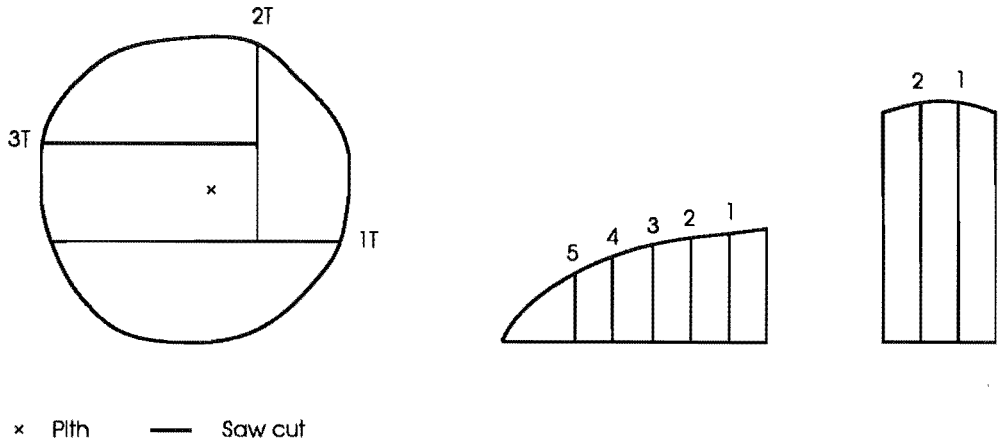

Figure 3.25 Quarter sawing patterns for log breakdown and resawing (Haslett 1988b).

The sawn boards were put through an anti-sapstain treatment, sealed in plastic and transported to Christchurch.

3.5 Sample Preparation

3.5.1 Prior to storage

Upon receipt, the boards were dressed to dimensions 100 × 25 mm, and samples (clears) of length 600 mm cut. The number of ring kinos in each sample was recorded, and the distance of each sample from the boards end was measured, allowing their height in each tree to be calculated. The samples were sealed in plastic, and stored at 1 ° C.

3.5.2 Prior to drying

The orientation of each sample and its distance from the pith was measured using the ring curvature procedure of Booker (1987). Thin sections of approximately 1 mm thickness were cut from the ends of each sample, for measurement of collapse-free shrinkage. The sample was then cut to a final length of 490 mm, with the offcuts from each end (figure 3.26) used to measure basic density, moisture content, and percent saturation. The green cross-sectional area and perimeter of the ends of each sample were measured using image processing. Caliper measurements of green width and thickness were taken at the ends and the centre of each sample.

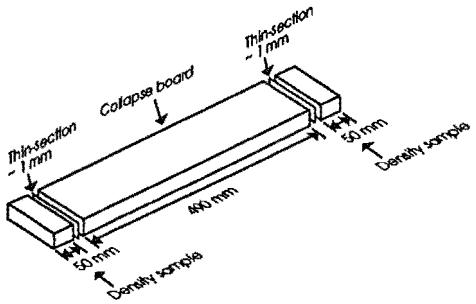

Figure 3.26 Samples taken from each end of the collapse board for measurement of collapse-free shrinkage, basic density, moisture content and percent saturation.

Devshield 235 epoxy resin was then applied to the ends of each sample and allowed to cure.

3.5.3 After drying and conditioning to 12 % moisture content

The epoxy resin was removed from the ends of each sample to re-expose the woods surface. The samples were then cut in half adjacent to the centre caliper measurements, and the exposed cross-section sanded to clearly define the external perimeter and the area and perimeter of internal checks. The cross-sectional area and perimeter of the ends of the two sections that now made up the original wood sample, were again measured using image processing. The caliper measurements were also repeated.

3.6 Measurement procedures

3.6.1 Sectional disks

The 10 cm thick sectional disks taken at heights 0, 5 and 13 m, were dressed and cut into two diametrically opposed sections. These were then subdivided into 50 mm cubes, in sequence from pith to bark (figure 3.27). The cubes were carefully air-dried at 18 ° C and 80 % relative humidity, to 12 % moisture content. Measurements included tangential, radial and volumetric shrinkage from green to 12 % moisture content, basic density, moisture content and percent saturation.

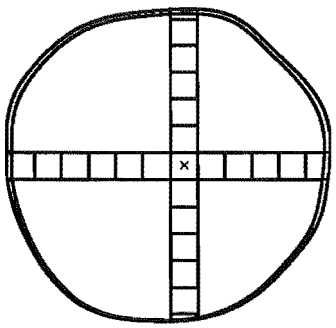

Figure 3.27 Sectional disk segmentation.

Tangential and radial shrinkage was measured at five equally spaced points from edge to edge with a digital caliper fitted with extension arms (figure 3.28). Volumetric shrinkage was measured using image processing measurements of cube cross-sectional area. The contribution of longitudinal shrinkage to volumetric shrinkage was considered negligible.

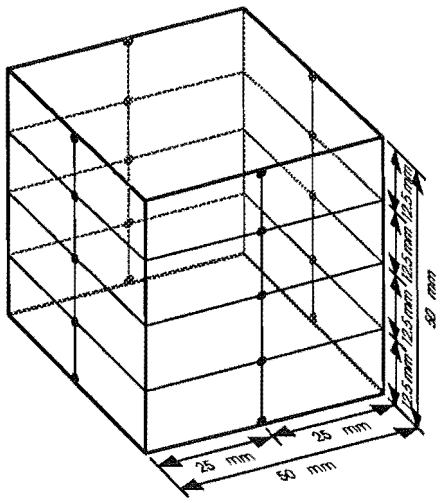

Figure 3.28 Cube caliper measurements. The spots represent the positions at which the radial and tangential measurements were taken.

3.6.2 Measurements on collapse sample boards and thin sections

3.6.2.1 Caliper measurements

Tangential and radial shrinkage was measured at five equally spaced points from edge to edge in thickness, and three equally spaced points from edge to edge in width, at the end faces A and B and in the middle face C of each sample (figure 3.29). Tangential and radial collapse free shrinkage was measured accordingly on end matched thin sections.

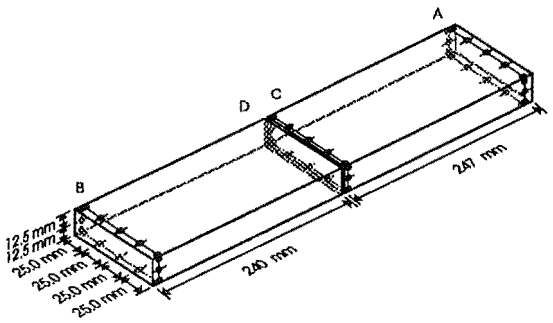

Figure 3.29 Collapse board caliper measurements. The spots represent the positions at which the radial and tangential measurements were taken in width and thickness. The letters A, B, C and D represent the cross-sectional faces at which the image processing measurements were taken. The board was cross-cut after drying to expose the cross-sectional faces C and D.

The caliper measurements provide not only average values of tangential and radial shrinkage, but also enable edge and end effects to be assessed. The edge and end effects will probably introduce a small bias into the average values of tangential and radial shrinkage, giving values that slightly underestimate the true level of shrinkage. The difference in the tangential and radial shrinkage of each end of the sample and the corresponding end matched thin sections was taken as a measure of tangential and radial collapse. The average collapse-free shrinkage of the two thin sections was used in calculating the tangential and radial collapse values for the middle section of the sample.

Time constraints on data preparation and analysis prevented an assessment of edge and end effects on drying collapse. The presentation is therefore confined to an analysis of the average values of tangential and radial collapse at the middle face C.

3.6.2.2 Image processing measurements

Volumetric collapse and collapse-free shrinkage was measured using image processing. Measurements of sample cross-sections included:

Cross-sectional	area	
	perimeter	
	internal checks	number
		area - total & individual
		perimeter - total & individual

Volumetric shrinkage was calculated from cross-sectional measurements at the end faces A and B, and the middle faces C and D using the equation:

$$VS = 1 - \frac{D}{G}$$

where VS = volumetric shrinkage,
D = area of dry cross-section (less the area occupied by internal checks),
G = area of green cross-section.

The green cross-sectional area of the middle sections was calculated from green caliper measurements.

Because longitudinal shrinkage is very low, its effect on volumetric shrinkage could be neglected and the change in the cross-sectional area before and after drying taken as equivalent to volumetric shrinkage.

Collapse-free volumetric shrinkage was measured in the same way on the end matched thin sections of end faces A and B.

Volumetric collapse was calculated from the difference in volumetric shrinkage between the wood samples and the end matched thin sections. The average volumetric collapse-free shrinkage of the two thin sections was used in calculating the volumetric collapse of the two middle cross-sections cut and exposed only after drying.

The volumetric collapse measurements at end faces A and B will provide an assessment of board end effects. Time constraints, however, confined the presentation to an analysis of the volumetric collapse measurements at middle faces C and D.

An empirical board shape factor - collapse factor (CF) - (Ilic and Hillis 1986), was used as a second method of quantifying drying collapse. The collapse factor was measured on the dried board cross-sectional faces C and D as

$$CF = \frac{(\text{the perimeter of the cross-section of the board})^2}{\text{cross-sectional area of the board}}$$

where perimeter includes the length of the outside boundary and that of any internal checks. The cross-sectional area was the total check-free area of the dried board cross-section. The collapse factor takes into account both internal checking and drying collapse.

3.7 Equipment

3.7.1 Pressure equipment

Four pressure cylinders were used for carbon dioxide gas treatment. The low pressure cylinders (1.5 MPa) were a small pulping cylinder (capacity 6 boards) and a large wood preservation cylinder (capacity 166 boards) normally used for impregnating wood with copper-chrome-arsenate (CCA). The pulping cylinder was housed in a refrigerated compartment maintained at 1 ° C, while the preservation cylinder was housed in a room with an ambient temperature of approximately 12 ° C. Two small high pressure cylinders were used for carbon dioxide gas treatment at 4.5 MPa. Their capacity was 8 boards each. They were both housed in an air-conditioned room with the temperature maintained at 17 ° C.

3.7.2 Kiln drying equipment

The wood was dried in an experimental high temperature drying kiln, capable of drying at temperatures of up to 180 ° C and air velocities of 10 m. s^{-1} (Winsor Engineering Limited, Johnsonville, Wellington, New Zealand). Heating and humidity were controlled with a DCP 511 Digital Control Programmer (Honeywell, Process Control Division, Pennsylvania, USA). A Yamatake-Honeywell chart recorder monitored wet and dry bulb temperatures. Fan speed was controlled with a Contrac Flow Economizer (ASEA-Parametrics, Connecticut, USA). The heating was provided by a bank of electrical heating coils, while humidity was provided by a steam coil contained in a trough of water.

3.7.3 Image processing equipment

The Vax Image Processing System (VIPS) was used for image processing measurements of cross-sectional area and perimeter. It was run using a Series 100 Real-Time Digital Image Processor (Imaging Technology Incorporated, Woburn, Massachusetts, USA) installed in a MicroVax II computer (Digital Equipment Corporation, Maynard, Massachusetts, USA). This included a frame grabber and a display board.

A FT-CCD monochrome solid state camera, Model P4312 (English Electric Valve Company Ltd) was used to take images of the wood samples and thin section cross-sections in the green state prior to drying. A JVC RGB colour video camera, Model BY10E (Victor Company of Japan, Tokyo, Japan) was used to take the cross-sectional images after drying at 12 % moisture content. A quartz halogen lamp was used to obliquely illuminate the dried wood sample cross-sections. All other measurements were made with the use of a tungsten filament lamp. The captured images were displayed on a PAL RGB colour monitor (640 × 512 pixels), Model no. MCM 14L (Matrox, Canada).

The captured images could be printed out on a Mitsubishi video copy processor, Model P60B (Mitsubishi Electric Corporation, Japan).

3.8 VIPS collapse program

The VIPS collapse program that calculated the area and perimeter of each sample cross-section, and the area and perimeter of internal checks, was written for this project by Nick Ward (Forest Research Institute, Rotorua). Minor changes were made to enable it to run on the Electrical and Electronic Engineering Departments Vax image processing system. The program was run using VIPS version 3.13. The program and an explanation of how it works is discussed next.

A brief explanation of the collapse program.

A grey scale (255 levels of grey from black to white) image from the camera is captured to the display hardware - the PAL RGB colour monitor. When using the colour video camera, only the red component was used. The VIPS software does not support colour.

A GET command transfers the image from the display to a VIPS image variable (a two-dimensional byte array of size 511 × 511 pixels). The image variable is than displayed on the monitor (figure 3.30a).

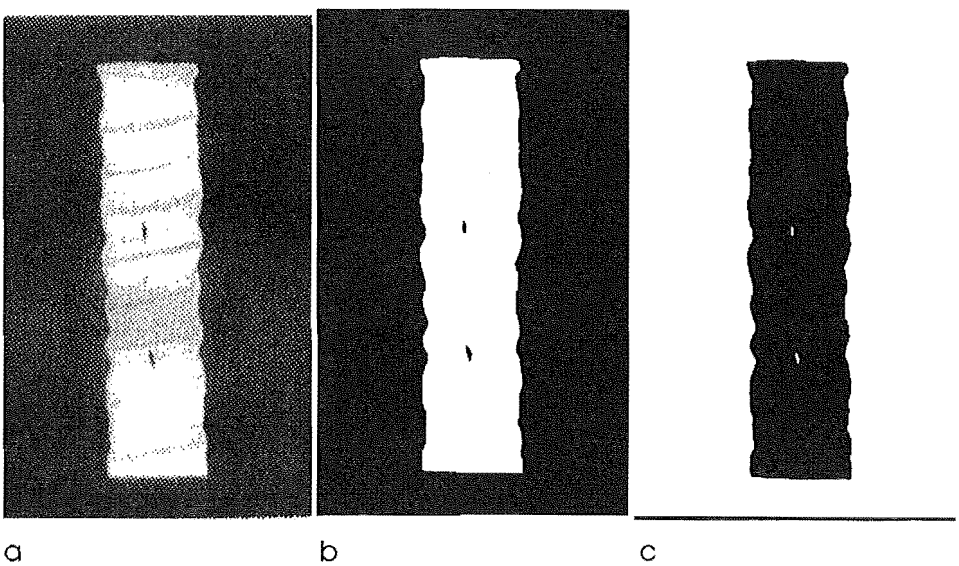

Figure 3.30 Image processing images.

A threshold value is prompted from the terminal and entered in via the keyboard. Every pixel in the image with a value less than the entered

threshold value is set to zero (black). Every pixel with a value greater than or equal to the threshold value is set to 255 (white). The result is a black and white binary image of the board cross-section. The threshold value is set such that the board cross-sectional area is white, with the background and internal checks black. The binary image is displayed to the monitor (figure 3.30b).

A camera aspect ratio is prompted for from the terminal. A value of 1.0 was entered to indicate that the image consisted of square pixels.

A chain code of the binary image is than obtained. The boundary between the black and white pixels is tracked and converted into a chain code. The tracking continues clockwise around the edge of the image until the original pixel is reached again. The result is a coded chain loop. If more than one chain loop is coded (if more than one white object is present in the image), the chain area (the number of pixels enclosed by the loop) and the chain perimeter (the perimeter of the loop in pixels) for each is calculated. The largest is assigned as the board cross-sectional area and perimeter. These are displayed to the terminal and written to file.

The binary image is then inverted. The black pixels become white and vice versa (figure 3.30c). The chain code is then obtained for each internal check, and the area and perimeter of each is calculated and summed. The results are displayed to the terminal and written to file.

```
PROGRAM
    ON CONTROLC /EXIT /COMMAND=DELETE C_*
    SET NOVERIFY
    SET NOOUTPUT

    OUT /L /L
    OUT "                                   COLLAPSE PROGRAM" /L
    OUT "                                         DEC -1988" /L  /L

!                                           DEFINE VARIABLES
!                                           ********************
DECLARE IMAGE (511, 511) c_mask1, c_mask2, c_mask3
DECLARE INTEGER c_camera, c_num, c_i, c_level
DECLARE INTEGER c_max_area
DECLARE REAL c_max_perim, c_p, c_total_perim, c_aspect, c_area, c_total_area
DECLARE STRING c_ans c_file c_id
DECLARE CHAIN c_chain, c_total_chain
INQUIRE "Enter the log file name:" /ENTITY c_file
```

```
FILE 'c_file' /APPEND
LET c_camera = 0
INQUIRE "Enter piece identification: " /ENTITY c_id
WRITE "Wood Sample" c_id /L

OUT "Place the timber shape under the camera with the lighting conditions" /L
OUT "you intend to use for this session. A dark, non reflective, background" /L
OUT "is strongly recommended also use side lighting to ensure checks are in" /L
OUT "shadow. Press any key when ready to capture the image." /L /L
CAPTURE
CONTINUE 0.5
GET c_mask1 (512, 0) (511, 511)
DISPLAY c_mask1

LET c_mask2 = c_mask1
REPEAT
    REPEAT
        LET vips_status = 0
        INQUIRE "Enter the intensity that distingushes the cross section from the checks:"
        c_level
        OUT /L
    UNTIL vips_status < 2
    THRESHOLD c_mask2 c_level
    DISPLAY c_mask2
    INQUIRE "Is this OK? (Y/N) : " /ENTITY c_ans
    IF c_ans = "Y"
    ELSE
        LET c_mask2 = c_mask1
    END
UNTIL c_ans = "Y"

REPEAT
    LET vips_status = 0
    INQUIRE "Enter the camera aspect ratio : " c_aspect
    OUT /L
UNTIL vips_status < 2
CHAIN CODE c_mask2 c_total_chain /REVERSE
CHAIN BRANCHES c_total_chain c_num
LET c_max_area = 0
LET c_max_perim = 0
FOR c_i = 1, c_num
    CHAIN EXTRACT c_total_chain c_i c_chain
    CHAIN AREA c_chain c_area
    CHAIN PERIMETER c_chain c_p c_aspect
    IF c_area > c_max_area
        LET c_max_area = c_area
        LET c_max_perim = c_p
    END
END
OUT /L
OUT /L
OUT "The cross section area is"
OUT c_max_area /L
WRITE "The cross section area is" c_max_area /L
OUT "The perimeter is"
OUT c_max_perim /L
WRITE "The perimeter is" c_max_perim /L
LET c_mask3 = c_mask2
```

```
INVERT c_mask3
CHAIN CODE c_mask3 c_total_chain /REVERSE
CHAIN BRANCHES c_total_chain c_num
LET c_total_area = 0.0
LET c_total_perim = 0.0
FOR c_i = 1, c_num
    CHAIN EXTRACT c_total_chain c_i c_chain
    CHAIN AREA c_chain c_area
    CHAIN PERIMETER c_chain c_p c_aspect
    IF c_area > 4
        OUT "Internal check"
        OUT c_i
        OUT " has an uncalibrated area of"
        OUT c_area /L
        OUT " and a perimeter of"
        OUT c_p /L
        WRITE "Internal check" c_i "has an uncalibrated area of" c_area
        WRITE " and a perimeter of" c_p /L
        LET c_total_area = c_total_area + c_area
        LET c_total_perim = c_total_perim + c_p
    END
END
DISPLAY c_mask3
OUT /L
OUT /L
OUT "The total internal check area is"
OUT c_total_area /L
OUT " with a total perimeter of"
OUT c_total_perim /L
WRITE "The total internal check area is" c_total_area " with a total perimeter of"
WRITE c_total_perim /L /L
FILE /CLOSE

DELETE c_*

END
```

3.9 Statistical analysis

3.9.1 Drying collapse

The statistical analysis follows a successional approach, in which the underlying variation of drying collapse in the wood is first analysed, followed by separate analysis for the effects of temperature and carbon dioxide gas treatments on drying collapse. The reason for this approach, is primarily for purposes of clarity of presentation. It allows the Model I and II levels of classification in the nested analysis of variance to be presented and explained separately.

3.9.1.1 Volumetric, tangential and radial collapse

The underlying variation of drying collapse in the wood sampled, and the temperature effects on drying collapse, were assessed using the control boards - boards not subject to carbon dioxide gas treatment. The structure of the nested analysis of variance is given in figure 3.31.

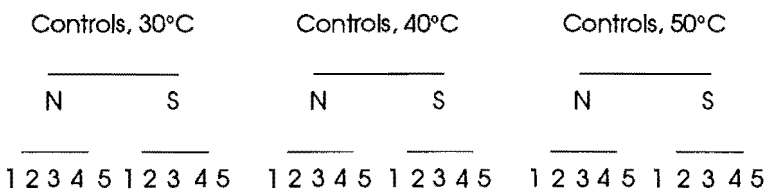

Figure 3.31 Structure of the analysis of variance of drying collapse - temperature effects, and the variation within the wood sampled.

The highest level of classification are the temperature treatments (Model I) of the three kiln runs (30, 40 and 50 ° C). The analysis of variance of temperature treatments will test for differences in drying collapse as a response to higher temperatures. Nested within the temperature treatments, are the levels of classification attributed to the random sample of wood (Model II). The analysis of variance will provide an estimate of the variance of drying collapse for each of the Model II levels of classification. This enables us to test for significant added variance in

drying collapse among the levels of classification, i.e. among trees within regions, and what percentage of the total variation in drying collapse can be attributed to each of the Model II levels of classification. The highest of these Model II levels of classification are the two regions, Nelson (N) and Southland (S), from which the wood came. These provide a measure of the variation in drying collapse that can be found among regions. Nested within the regions are the five trees that were sampled from each region. These provide a measure of the variation in drying collapse among trees within regions. Nested within the trees are a further three levels of classification not presented in the figure 3.31. The first of these are the four height classes nested within each tree: 0 - 1.30 m, 1.31 -2.60 m, 2.61 - 3.90 m, and 3.91 - 5.20 m. These provide a measure of the variation in drying collapse with height in each tree. The rationale behind the choice of height classes can be seen in the distribution of heights at which the collapse measurements were taken (figure 3.32).

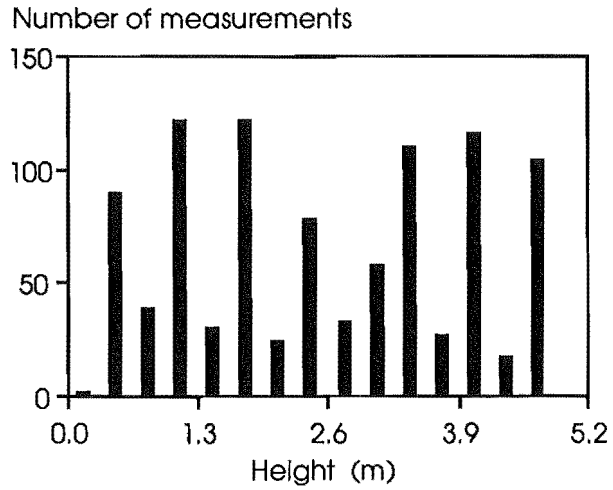

Figure 3.32 The height distribution of collapse measurements at cross-sectional faces C and D.

Nested within each height class are the boards, taken at a range of height, radial, and circumferential positions, outside the zone of juvenile wood surrounding the pith, within each height class. These provide a measure of the variation in drying collapse with position in each height class. Nested within each board are the collapse measurements. The analysis of variance for volumetric collapse is presented in the results section only for the board middle faces C and D (figure 3.29). With two collapse measurements per board, the lowest level of classification for volumetric collapse is the variation in drying collapse within boards. Tangential and radial drying collapse was measured at the middle face C. With only one collapse measurement per board the lowest level of classification for

tangential and radial collapse is the variation in drying collapse among boards within height classes.

The nested design of the statistical analysis determined the way in which the analysis of variance is performed. The hierarchical structure of the nested design means that each level in the design contains all the variation of the levels below it, in addition to the variance component of that particular level. This is defined formally in table 3.6.

Table 3.6 The expected mean squares

Source of variation	Expected *MS* for a Model II
Among groups	$\sigma^2 + n_o''\sigma^2_{C \supset B} + (nc)_o'\sigma^2_{B \supset A} + (ncb)_o\ \sigma^2_A$
Subgroups within groups	$\sigma^2 + n_o'\sigma^2_{C \supset B} + (nc)_o\ \sigma^2_{B \supset A}$
Subsubgroups within subgroups	$\sigma^2 + n_o\ \sigma^2_{C \supset B}$
Within subsubgroups	σ^2

From Sokal and Rohlf (1981)

The variance component of the lowest level in the classification (within subsubgroups) is σ^2, the variance component of the level above this is $\sigma^2_{C \supset B}$, the variance of C within B, and the variance component of the level above this $\sigma^2_{B \supset A}$, the variance of B within A. The variance component among groups is σ^2_A. The coefficients of the variance components are represented by n_o, $(nc)_o$, $(ncb)_o$, etc. For a mixed model analysis of variance, where the highest level of classification is differentiated by fixed treatment effects (Model I), i.e. temperature as in figure 3.31, the top line of the expected mean squares (MS_{groups}) should become

$$\sigma^2 + n_o''\sigma^2_{C \supset B} + (nc)_o'\sigma^2_{B \supset A} + (ncb)_o \frac{\Sigma\alpha^2}{\alpha - 1}$$

With fixed treatments we do not estimate a variance component, but simply test the significance of the added treatment effects. From the expected mean squares in table 3.6, it is apparent that in tests of significance, the F-ratio for each level of classification is calculated by dividing the mean square of each level with the mean square of the level below it, i.e. we test $MS_{subsubgr}/MS_{within}$ for the significance of $\sigma^2_{C \supset B}$, $MS_{subgr}/MS_{subsubgr}$ for the significance of $\sigma^2_{B \supset A}$, and MS_{group}/MS_{subgr} for

the existence of σ^2_A or $\Sigma\alpha^2/(\alpha - 1)$ the added component due to treatment effects. In the nested analysis of variance design of figure 3.31, we are in effect testing for a significant added component in drying collapse due to temperature treatments, in the collapse measurements from control boards at all heights within the five trees from each of the two regions. It may be, however, that there is not a significant added component due to temperature effects for all the collapse measurements from both regions, but there is for measurements from one region and not the other, or for some trees within one or both regions and not for others. Such tests are made by performing the analysis of variance on subsets of the data. The temperature effects of figure 3.31 could be tested using the collapse measurements from the Nelson region only, or for a particular tree from the Nelson region (figure 3.33a and b).

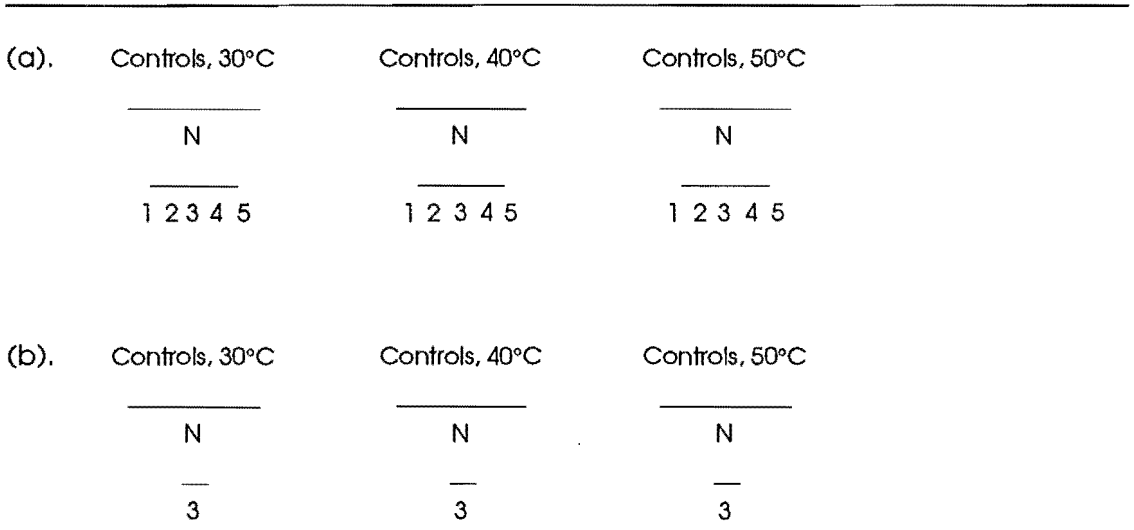

Figure 3.33 Structure of the analysis of variance of drying collapse for subsets of thedata in figure 3.31.

The nested design therefore determines the way in which the analysis of variance is performed, when analysing for treatment effects. The procedure outlined for the analysis of temperature treatments effects, also applies for the analysis of carbon dioxide gas treatment effects.

The significance of the added variance components of the Model II levels of classification, in the wood sampled for the treatment effects, are also tested in the mixed model analysis of variance in figures 3.31 and 3.33, i.e. the variance component of drying collapse among regions within

treatments, among trees within regions, etc. For the purposes of clarity of presentation, however, the analysis of variance of the Model II levels of classification were performed and presented separately from the treatment effects. Three separate Model II analysis of variance, of the form shown in table 3.6, were performed, one for each of the fixed temperature treatments (30, 40 and 50 ° C). With each analysis confined to one temperature, the highest level of classification in each was among regions.

The analysis of variance of the carbon dioxide gas treatment effects on drying collapse were also performed separately for each of the temperature treatments. For each temperature, the analysis of variance of the carbon dioxide gas treatments were performed on three data sets, the structure of which are shown in figure 3.34.

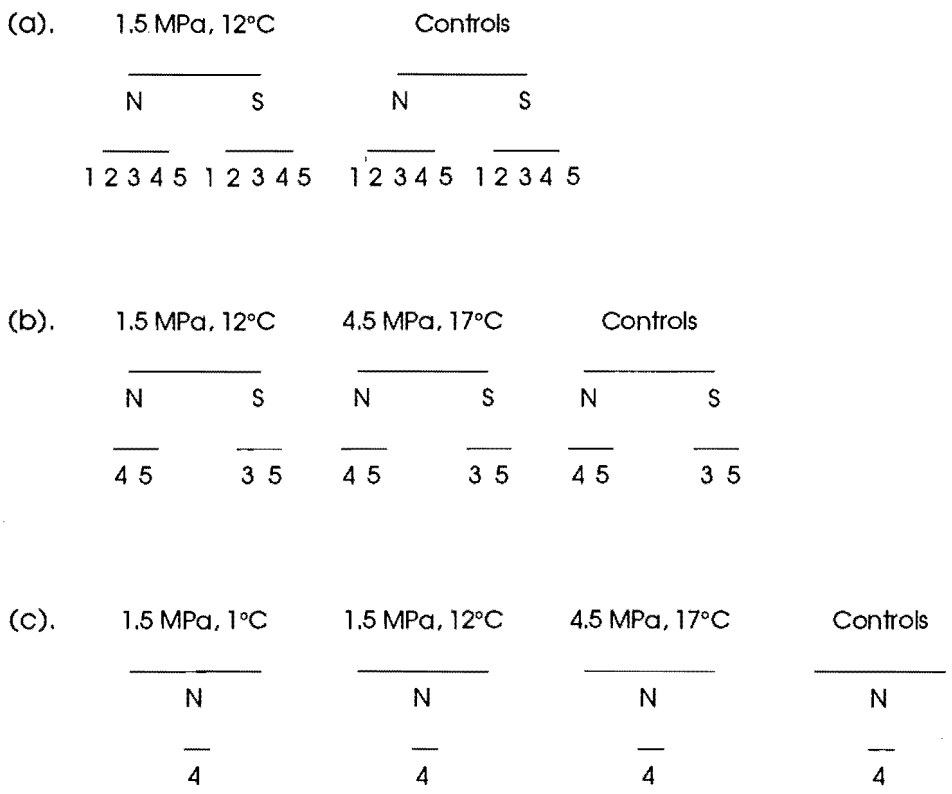

Figure 3.34 Structure of the analysis of variance of drying collapse for carbon dioxide gas effects.

The analysis of variance of the first data set (figure 3.34a) tests for the significance of an added component in drying collapse due to the low pressure carbon dioxide gas treatment at 1.5 MPa and 12 ° C. This

represents the low solubility treatment. Collapse measurements from the five trees from each of the two regions, Nelson and Southland, are used in the analysis.

The analysis of variance of the second data set (figure 3.34b) tests for the significance of an added component in drying collapse due to low and high pressure carbon dioxide gas treatments at 1.5 MPa and 12 ° C (low gas solubility), and 4.5 MPa and 17 ° C (high gas solubility) respectively. The analysis is restricted to collapse measurements from two trees each from regions Nelson and Southland. The low pressure carbon dioxide gas treatment and control collapse measurements are a subset of the data used for the analysis of figure 3.34a.

The analysis of variance of the third data set (figure 3.34c) tests for the significance of an added component in drying collapse due to three carbon dioxide gas treatments. Two low pressure gas treatments at 1.5 MPa and 12 ° C (low gas solubility) and 1 ° C (medium gas solubility), and one high pressure gas treatment at 4.5 MPa and 17 ° C (high gas solubility). The collapse measurements for this analysis were restricted to one tree from the Nelson region. The low pressure (12 ° C) and high pressure carbon dioxide gas treatment and control collapse measurements are a subset of the data used for the analysis of figure 3.34b.

3.9.1.2 Collapse factor

The same analysis of variance procedures used for the analysis of volumetric collapse, in the previous section, were also applied to the analysis of board shape after drying, using the measurement collapse factor.

3.9.2 Basic density

The variation of the basic density of the collapse boards was analysed using a nested Model II analysis of variance design. The highest level of classification was the variation among regions, Nelson and Southland. Nested within the regions were the five trees from each region. Nested

within each tree were three height classes: 0 - 1.75 m, 1.76 - 3.50 m, and 3.51 - 5.25 m. The difference in the height classes between drying collapse and basic density measurements, can be attributed to the sampling of basic density at the ends of each board. Nested within the height classes were the boards from which the basic density was sampled, one measurement from each end. The lowest level of classification was, therefore, the variation of basic density measurements within boards.

Initially it was decided to pool all the basic density measurements from the three kiln runs (three temperature treatments). However, it was found that the statistical computer package used was unable to handle such a large data set. The analysis of variance was, therefore, performed separately for the basic density data of boards used with each temperature treatment (kiln run).

The analysis of variance provides estimates of the variance of basic density for each level of classification. Knowing this, we can test for the significance of the added variance component of each level, and calculate the percentage contribution of each level to the total variation in basic density.

The statistical analysis were performed using the SAS/STAT statistical package, release 6.06 (SAS Institute Inc., Cary, North Carolina, USA), on a VAX minicomputer, Model 6000-340 (Digital Equipment Corporation, Maynard, Massachusetts, USA). Because of the unequal numbers of boards in each height class, the General Linear Model (GLM) procedure was used in performing the computations for the nested analysis of variance.

3.10 Results

3.10.1 Growth strain

The longitudinal perpherial growth strain measurements were calculated in units of microstrain (με). These are defined as the dimension change in micrometers per unit length in metres (1 με = 1 μm m^{-1}). Polar plots of growth strain for each tree are provided in figure 3.35, with microstrain values in table 3.7.

Table 3.7 Growth strain values for *Eucalyptus delegatensis* in microstrain (με)

Golden Downs Forest, Nelson					Average
Tree 1	720	2240	1900	1920	1695
" 2	540	1500	2800	600	1360
" 3	1300	860	1800	640	1150
" 4	700	1160	880	400	785
" 5	800	580	560	1300	810
Longwood Forest, Southland					
Tree 1	1200		2400		
" 2	4300		2000		
" 3	1520	1160	2800	1780	1815
" 4	680	580	1840	720	955
" 5	1040	1860	3240	1520	1915

Published values of growth strain for a number of *Eucalyptus* species including *Eucalyptus delegatensis* are given in table 3.8. Comparison of published values with the growth strain values of *E. delegatensis* from Nelson and Southland reveals that while they are above average for *E. delegatensis* in Australia (Jacobs 1939, 1945) they are within the upper range of growth strain values for *E. regnans* in Australia (Nicholson and Ditchburne 1973). The reason for such high levels of growth strain in the New Zealand trees could be explained by the amount of competition they have experienced. Competition between trees is responsible for an increase in growth strain. Trees generate growth strains in order to bend stems and branches into positions more favourable for growth. Growth strains should therefore be lower if trees have no reason to reorientate themselves. Ferrand (1982) found in *E. delegatensis* in Australia a significantly lower level of growth strain in trees grown at wide spacings, and on soils of high site index. For the New Zealand stands in Nelson and

Golden Downs Forest, Nelson

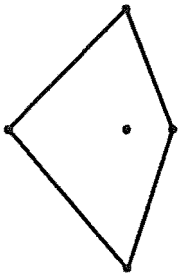

Tree 1

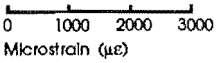

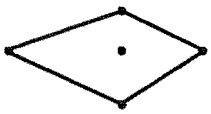

Tree 2

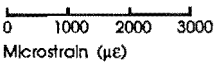

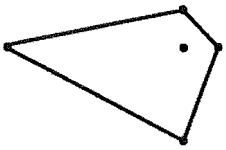

Tree 3

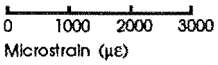

Tree 4

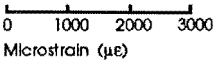

Tree 5

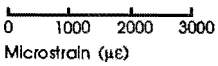

Longwood Forest, Southland

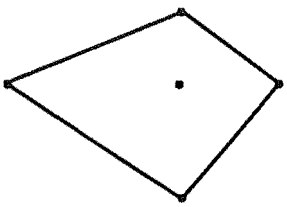

Tree 3

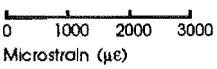

Direction of lean
Longwood only

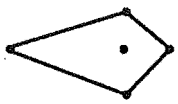

Tree 4

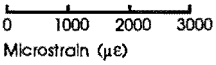

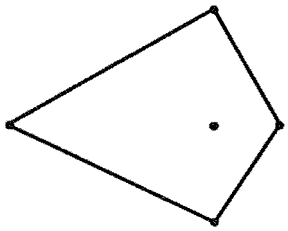

Tree 5

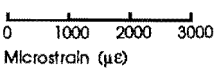

Figure 3.35 Polar plots of growth strain measurements in *Eucalyptus delegatensis*.

Table 3.8 Growth strain in *Eucalyptus* species

Species	Wood density 12 % mc kg. m^{-3}	Tree age years	Stem diameter cm	Number of trees per tree	Method	Growth strains (με) lowest single	lowest tree av.	mean	highest tree av.	highest single	
E. camaldulensis	960	-	-	-	D	-	520	1000	1500	-	Giordano & Curro 1972
E. delegatensis	680	-	0.3 - 71	≥ 200	D	-	-	770	-	-	Jacobs 1939, 1945
E. obliqua	680	75	40 - 70	12	N	-	530	730	1160	-	Nicholson & Ditchburne 1973
E. regnans	680	31	33 - 51	41	≥ 10	N	135	355	760	1185	3245	Nicholson 1973
E. viminalis	770	29	22	1	20?	K	290	-	668	-	1308	Sasaki, Okuyama & Kikata 1978

Methods of measurement

D = Diametral plank
K = Kikata's
N = Nicholson's

(from Kubler 1987).

Southland, the stockings were high with little or no thinning. This was particularly so for the Nelson stand, which was the older of the two stands. This and the fertility of the sites could certainly help to explain the high growth strains found.

The segments of wood removed in the process of growth strain measurement showed no incidence of tension wood when microtomed and stained for the presence of cell gelatenous layers. The reason for this probably lies in the fact that while growth strain values are high, they are not extreme.

3.10.2 Shrinkage and density distributions within trees - results from sectional disks

The within tree variation of basic density, moisture content, percent saturation, and volumetric, tangential and radial shrinkage to 12 % moisture content were measured from sectional disks taken at heights 0, 5 and 13 metres, from tree 2, Nelson, and tree 3, Southland (figures 3.36 and 3.37). Unpublished data from Harris (1975) allowed comparisons to be made with trees of *Eucalyptus delegatensis* from Kaingaroa Forest in the Bay of Plenty.

Basic density increased with height, and from pith to bark. The most marked increases were from 0 to 5 metres in height, and from juvenile to mature wood. The density of juvenile wood increased with height above 5 metres. The density of juvenile wood in tree 3, Southland, at a height of 13 metres, is however, far in excess of what would be expected. This can be explained by the location of the sectional disk, taken just below the point at which the main stem split into two main branches. Considerable growth stresses could be expected to occur, resulting in increased basic density.

Comparisons of basic density differences between regions needs to be treated with caution when only one tree is sampled per region, as was the case for Nelson and Southland. The basic densities of tree 2 from Nelson, and tree 3 from Southland, were found in later work to be representative

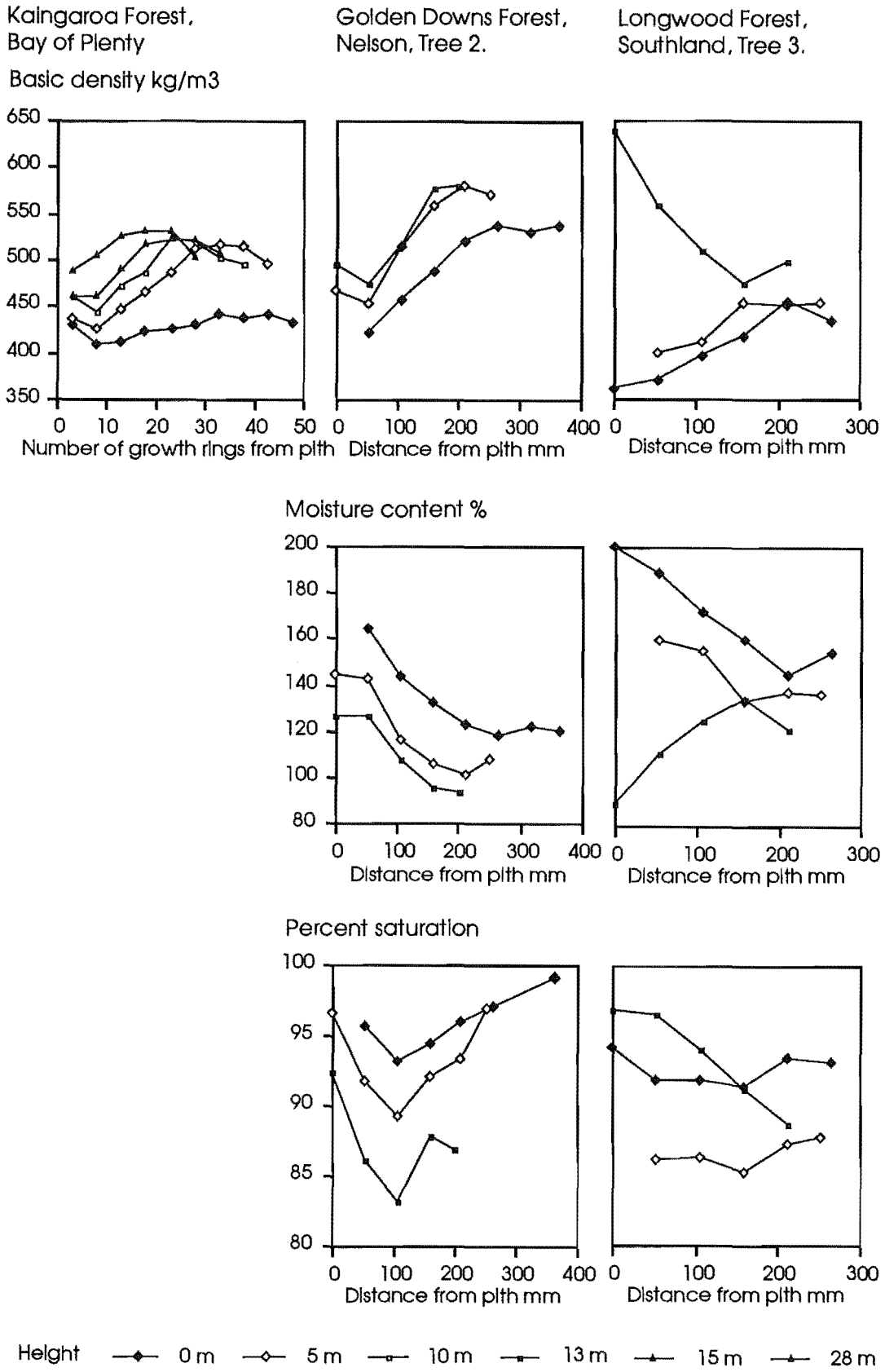

Figure 3.36 Sectional disk measurements of basic density, moisture content, and percent saturation, in trees of *Eucalyptus delegatensis* from different regions.

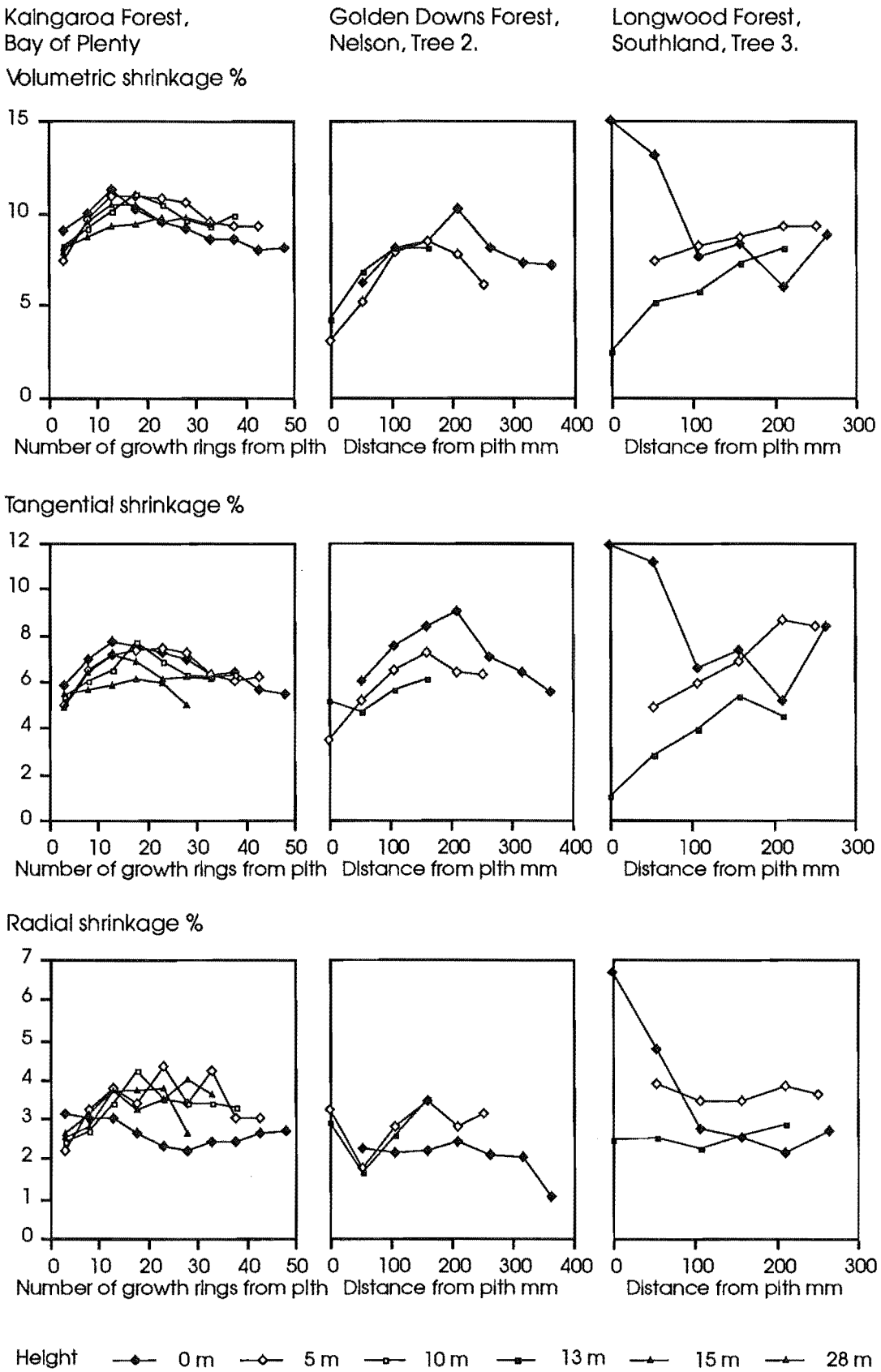

Figure 3.37 Sectional disk measurements of volumetric, tangential and radial shrinkage in trees of *Eucalyptus delegatensis* from different regions.

of the basic densities of the majority of the five trees sampled from Nelson and Southland. The data of Harris (1975) were assumed to be the averages of the five trees sampled from Kaingaroa Forest, Bay of Plenty. Given this, it does appear that differences in basic density do occur between regions. Trees from Golden Downs Forest, Nelson, appear to have higher basic densities than those from Kaingaroa Forest, Bay of Plenty, or Longwood Forest, Southland. The trees from Longwood Forest, Southland, appear to have particularly low basic densities. An interesting feature is the very high basic density of the mature wood of tree 2, Nelson, at a height of 0 metres. Its basic density is equivalent to that at heights of 5 to 28 metres in trees from Kaingaroa Forest, Bay of Plenty.

The inverse relationship between basic density and moisture content can be clearly seen in the moisture content measurements of the trees from Nelson and Southland. Moisture content declines with height, and from pith to bark. Moisture content is higher in trees from Southland than Nelson.

Percent saturation decreases with height in tree 2, Nelson. The pattern is disrupted in tree 3, Southland, by the very high percent saturation measurements at height 13 metres.

Volumetric, tangential and radial shrinkages to 12 % moisture content are very similar for all three regions. There is no consistent change in shrinkage with height, but there is a trend of increasing volumetric and tangential shrinkage from pith to bark, particularly in the Nelson and Southland trees. The large shrinkage values for tree 3, Southland, in the wood near the pith at a height of 0 metres can probably be attributed to drying collapse. The Nelson and Southland wood samples were not reconditioned after air drying. The wood samples from Kaingaroa Forest, Bay of Plenty, were reconditioned for 3 hours at 100 ° C (Harris 1975).

3.10.3 Ring kinos frequency in boards

Striking differences were observed in the incidence of ring kinos in trees of *Eucalyptus delegatensis* from Nelson and Southland. The measurement procedure involved recording the number of ring kinos in each board cut from the original 2.5 metre boards. The percentage distributions of ring kinos per board are plotted for each tree and log in figure 3.38.

Four of the five trees from Nelson, had a very low percentage of boards with ring kinos. The exception, tree 1, was unusual among the trees sampled. Its bark was permeated with kino that had exuded during the spring and early summer, hardening to form a dense brittle solid. This made bark removal very difficult during the process of growth strain measurement. The wood and bark, when cut during these measurements, emitted a very unpleasant turpentine odor, quite unlike anything observed in the other trees sampled.

By contrast, in four of the five trees from Southland over 50 % of the boards had ring kinos. The reason for the differences is thought to lie in insect attack by wood-boring *Platypus* beetles. Two species of *Platypus* beetle, *P. apicalis* and *P. gracilis*, are known to attack rapidly growing trees of *Eucalyptus delegatensis* (Milligan 1979). Though the attacks are repelled by the trees, damage to the cambium results in the formation of ring kinos. Kino filled *Platypus* tunnels were observed in the wood from Southland, but not from Nelson. The proximity of eucalypt stands to native vegetation, such as *Nothofagus*, has a large bearing on the incidence of attack. Other environmental conditions that can cause ring kino formation include branch shed, cambium damage by mechanical injury and fire, and fungal attack. Fire was not a factor at the Nelson and Southland sites.

The reason for the difference in ring kino occurence between tree 1, and other trees from Nelson, is not clear, but environmental factors are thought to be the main cause. Doran (1975) in a study of ring kino number and circumferential length in 26 open-pollinated families of *Eucalyptus regnans* at two sites, found no significant differences in ring kino occurence between families, and no significant correlation in family values between sites. Nicholls and Matheson (1980) found highly

Tree 1 - Nelson
Percentage of boards

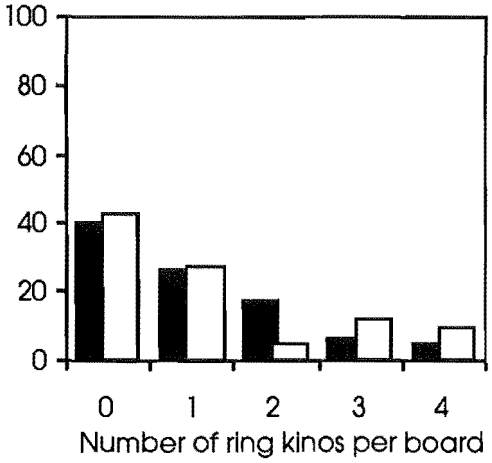

Tree 2 - Nelson
Percentage of boards

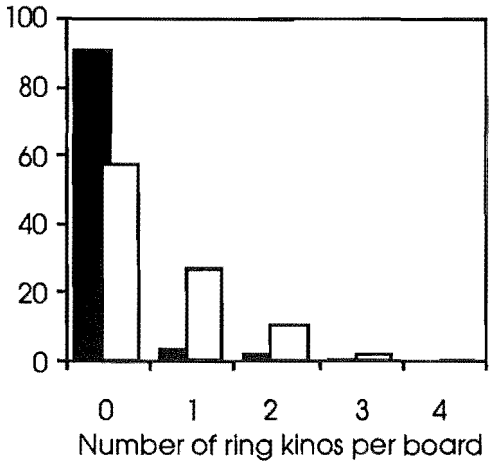

Tree 3 - Nelson
Percentage of boards

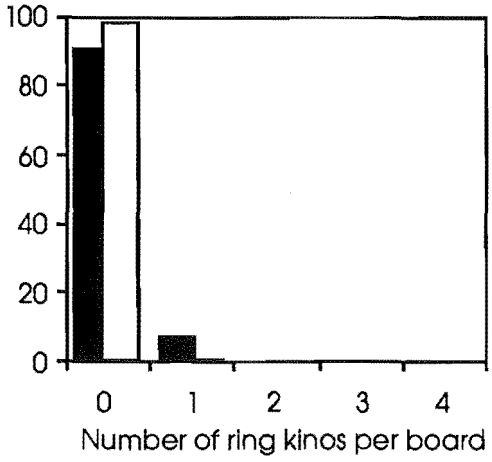

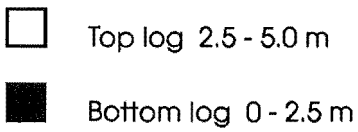

Tree 4 - Nelson
Percentage of boards

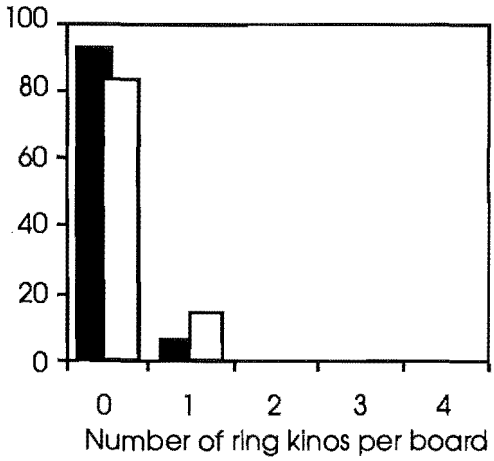

Tree 5 - Nelson
Percentage of boards

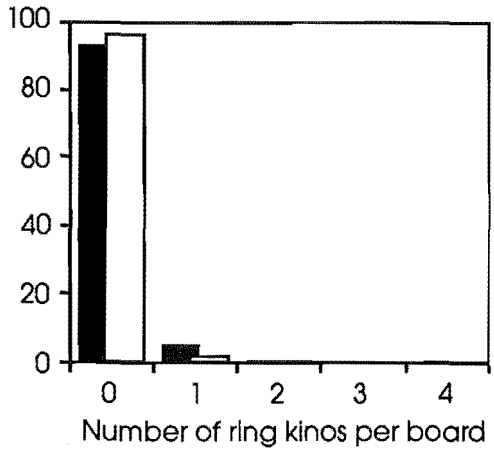

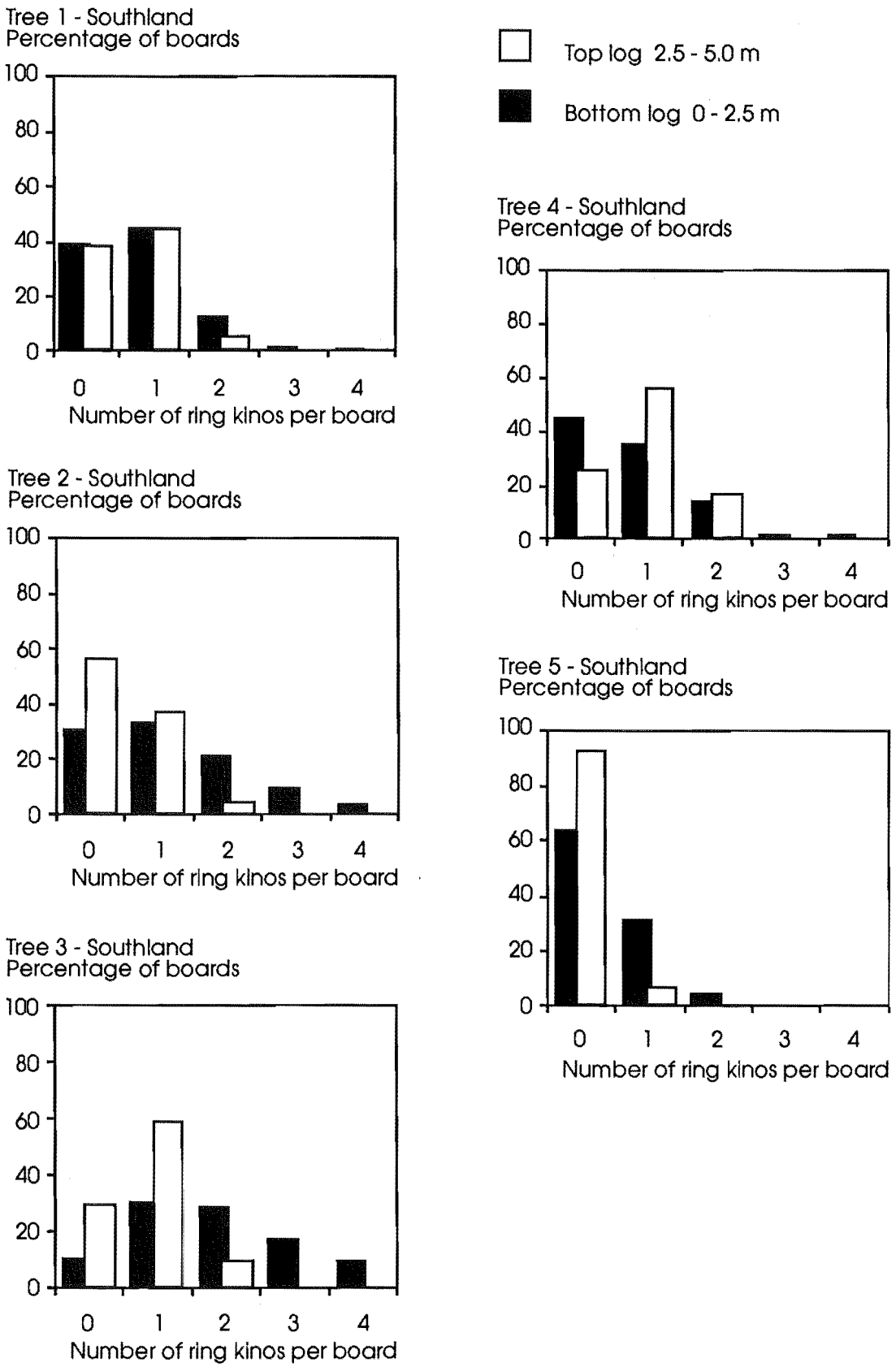

Figure 3.38 Percentages of collapse boards with ring kinos in trees of *Eucalyptus delegatensis* from Nelson and Southland.

significant differences in the ring kino occurence among provenances of *Eucalyptus obliqua*, but no significant differences among families within provenances. The variation in ring kino occurence (number of ring kinos per tree) among trees within provenances, such as for the Nelson stand, appears therefore, to be influenced more by environmental than genetic factors.

3.10.4 Kiln drying - carbon dioxide absorption and rate of drying

The amount of carbon dioxide gas absorbed into the green boards of *Eucalyptus delegatensis*, was measured for each of the three different carbon dioxide gas treatments (figure 3.39).

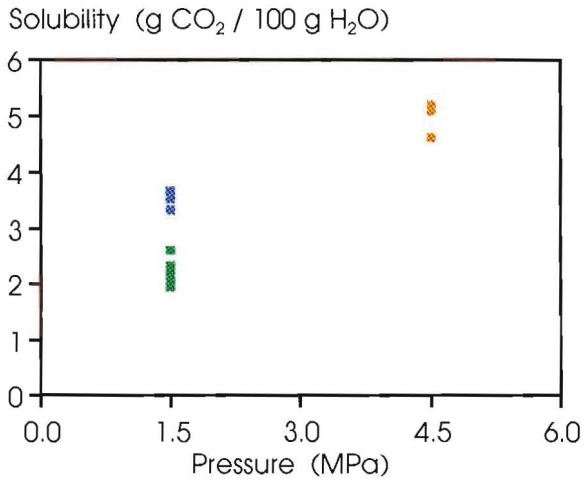

Figure 3.39 The solubility of carbon dioxide gas in treated boards of *Eucalyptus delegatensis* prior to kiln drying.

The range of carbon dioxide gas solubilities in water for the three gas treatments, extends from 2.0 to 5.2 g CO_2 / 100 g H_2O. For the gas treatment at 1.5 MPa and 12 ° C, the solubilities were 2.0 - 2.6 g CO_2 / 100 g H_2O. This conforms well with the literature value of 2.672 g CO_2 / 100 g H_2O at 12.4 ° C given by Wroblewski (1882). The figure of 12 ° C is however, only an approximate temperature. The ambient temperatures under which the carbon dioxide gas absorption took place, ranged from 10 - 15 ° C for this particular treatment. The range of solubilities for the gas treatment at 1.5 MPa and 1 ° C was 3.3 - 3.7 g CO_2 / 100 g H_2O. The only comparable literature value is 4.283 g CO_2 / 100 g H_2O at 0 ° C given by Haehnel (1920). An estimate, however, of 4.05 g CO_2 / 100 g H_2O at 1 ° C was obtained from the smoothed solubility curves of Dodds et al. (1956) that are based on the experimental data gathered prior to 1956. The solubilities in *Eucalyptus delegatensis* therefore appear to be a little low. This may have arisen from

problems of gas leakage from the pressure cylinder, which gave less control over gas pressure than would have been desired. The range of solubilities for the gas treatment at 4.5 MPa and 17 ° C was 4.6 - 5.2 g CO_2 / 100 g H_2O. The most relevant literature value is 5.023 g CO_2 / 100 g H_2O at 15 ° C given by Haehnel (1920). This fits in reasonably well with the range of solubilities obtained, although a couple of values do appear a bit high. These may have resulted from deviations from true values of basic density estimates used in calculating the amount of water present in the collapse boards. Basic density was measured using small wood samples obtained from the ends of each collapse board. The results do, however, indicate that the three carbon dioxide gas treatments were successful in producing three separate solubility classes, covering a wide range of gas solubilities.

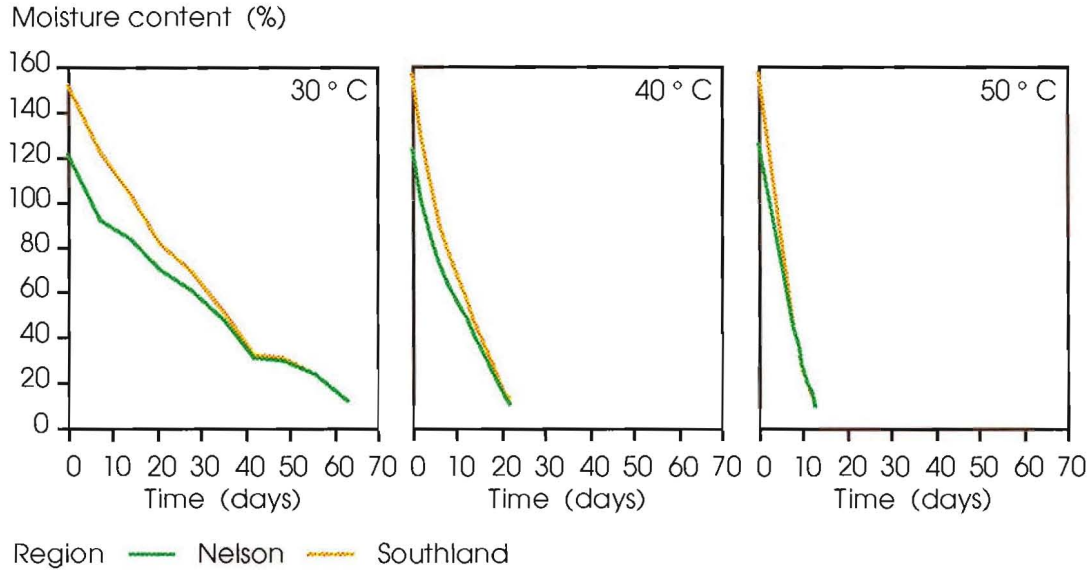

Figure 3.40 The rate of moisture content loss in boards of *Eucalyptus delegatensis* dried at each of the three initial dry bulb temperatures (30, 40, and 50 ° C).

Kiln drying rates differed markedly with increasing initial dry bulb temperature (figure 3.40). Eucalyptus delegatensis boards dried from 30 ° C took 63 days to reach 12 % moisture content, those dried from 40 ° C took 22 days, and those dried from 50 ° C took 13 days. The period of 63 days for kiln drying from 30 ° C reflects milder drying of the wood from 60 and 30 % moisture content than indicated in the kiln schedule of table 3.5. This is shown particularly by the leveling off of the drying rate between days 42 and 49 in figure 3.40. There were small differences in the relative humidity during the initial stages of drying for each of the three kiln runs.

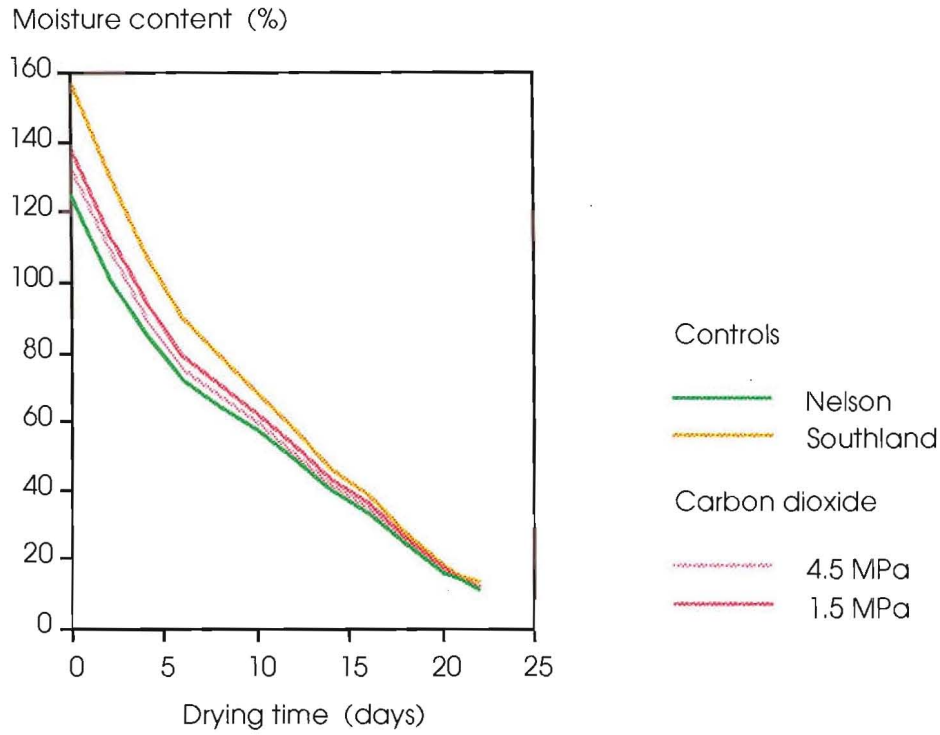

Figure 3.41 The mean drying rates of carbon dioxide gas treatment (4.5 MPa at 17 ° C and 1.5 MPa at 12 ° C) and control boards of *Eucalyptus delegatensis* from Nelson and Southland. The carbon dioxide gas treatments included boards from both Nelson and Southland. The initial dry bulb temperature of the kiln schedule was 40 ° C.

The relative humidity of the 30 ° C kiln run was a little above 90 %, that of the 50 ° C kiln run a little below 90 %, while that of the 40 ° C kiln run was 90 %. This merely reflects the limits to how closely the Digital Control Programmer could match the kiln conditions with that set by the given program.

Carbon dioxide gas treatment had no effect on the kiln drying rates of boards dried at an initial dry bulb temperature of 40 ° C (figure 3.41). The boards from both high and low solubility carbon dioxide gas treatments (4.5 MPa at 17 ° C and 1.5 MPa at 12 ° C respectively) had the same drying rates as controls from Nelson and Southland.

3.10.5 Drying collapse

3.10.5.1 Collapse variation in the wood sampled

Drying collapse in the wood sampled varied significantly among the Nelson and Southland regions, among the trees sampled within these regions, among the height classes within each tree, and among boards within each height class. The results are presented for the three separate sets of collapse measurements: volumetric, tangential, and radial collapse.

3.10.5.1.1 Volumetric collapse

The variation of volumetric collapse shows the same pattern for each of the three temperature treatments (kiln runs) at 30, 40 and 50 ° C (figures 3.42, 3.43 and 3.44). Anova tables 3.1, 3.2 and 3.3, show that there are significant added variance components of volumetric collapse among regions, among trees within regions, among heights classes within trees, and among boards within height classes. The percentage contributions of the variance components of each level of the classification, to the total variation of volumetric collapse in the wood sampled, are shown in table 3.9. The variance component among regions contributes 39.0 - 47.8 % of the total variation in volumetric collapse, the variance component among trees within regions 16.7 - 23.2 %, the variance component among height classes within trees 13.4 - 21.1 %, the variance component among boards within heights 9.5 - 16.0 %, and the variance component of collapse measurements within boards 0.3 - 12.7 %. The variation in volumetric collapse among regions therefore constitutes the largest source of variation of volumetric collapse in the wood sampled. This can be seen inthe very large differences in mean volumetric collapse values observed for the two regions, Nelson and Southland, with higher volumetric collapse occuring in the Southland wood (figures 3.42, 3.43 and 3.44). The variation in volumetric collapse among trees within regions, and among height classes within trees, while similar, constitutes only 28 - 60 % of the among regions contribution to the total variation in volumetric collapse. The large differences in mean volumetric collapse between trees, and the similar differences among height classes within trees (figures 3.42, 3.43 and

Table 3.9 Percentage contribution of variance components of volumetric collapse

Variance component	Percentage of total variation
30°C	
Among regions	47.8
Among trees within regions	16.7
Among heights within trees	13.4
Among boards within heights	9.5
Within boards	12.7
40°C	
Among regions	39.0
Among trees within regions	23.2
Among heights within trees	21.1
Among boards within heights	16.0
Within boards	0.6
50°C	
Among regions	44.5
Among trees within regions	22.6
Among heights within trees	19.1
Among boards within heights	13.4
Within boards	0.3

3.44), reflects the similar sizes of their respective variance components. The variation in volumetric collapse among boards within height classes, while a little smaller, constituting only 20 - 41 % of the among regions contribution to total variation in volumetric collapse, does indicate that areasonable amount of variation in volumetric collapse occurs as a result of small differences in height, radial and circumferential position. The variation of volumetric collapse measurements within boards was very small for two of the three temperature treatments (kiln runs). Why the within boards variance component of the 30 ° C temperature treatment is somewhat larger is not clear. It would appear for the other two temperature treatments, 40 and 50 ° C, however, that the collapse measurements within each board did not differ much.

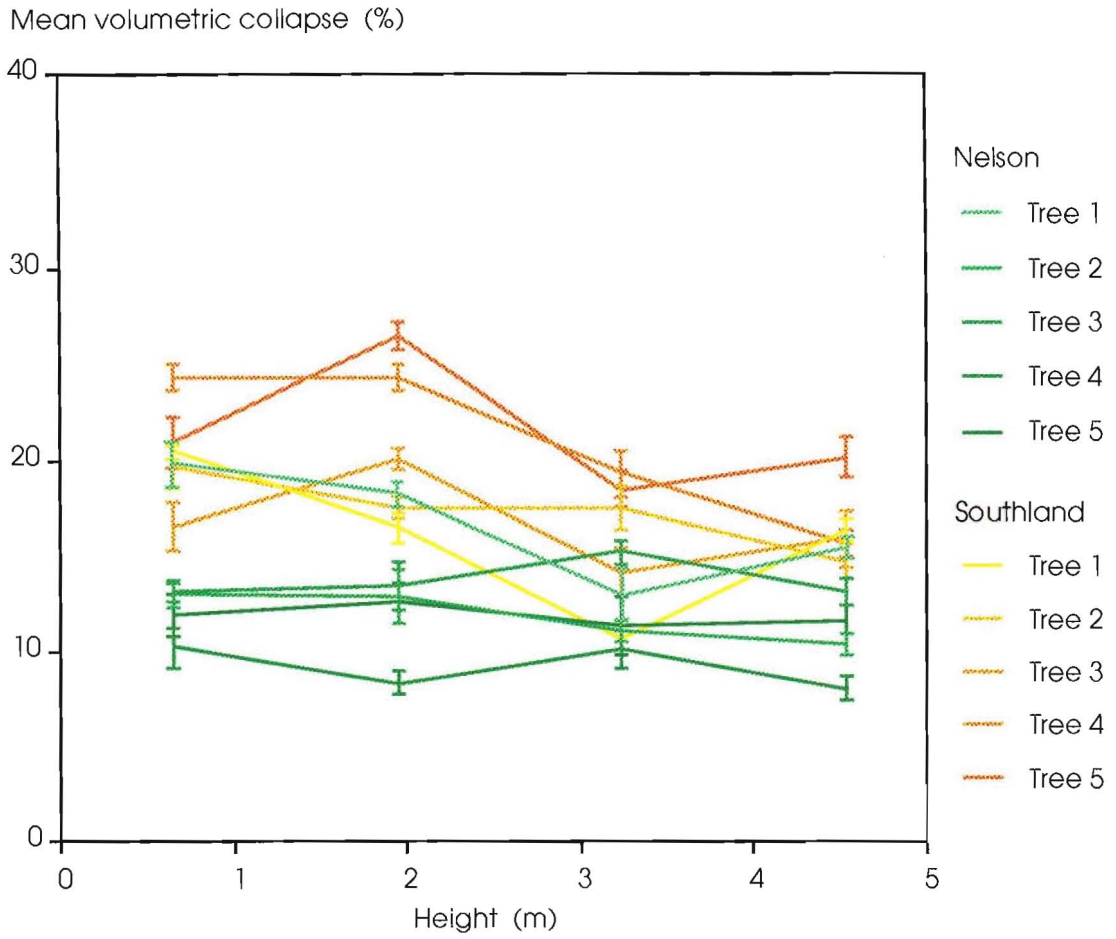

Figure 3.42 Mean volumetric collapse at 30 ° C in control boards at various heights within trees of *Eucalyptus delegatensis* from Nelson and Southland. The error bars are standard errors of the means.

Anova table 3.1: Analysis of variance of volumetric collapse in wood dried at 30 ° C

Source of variation	df	SS	MS	F_S	
Among regions	1	2572.19	2572.19	12.22	**
Among trees within regions	8	1683.53	210.44	4.97	**
Among heights within trees	30	1271.66	42.39	4.18	**
Among boards within heights	115	1166.50	10.14	2.50	**
Within boards	155	630.05	4.06		
Total	309	8032.27			

** = P < 0.01 * = P < 0.05 ns = not statistically significant

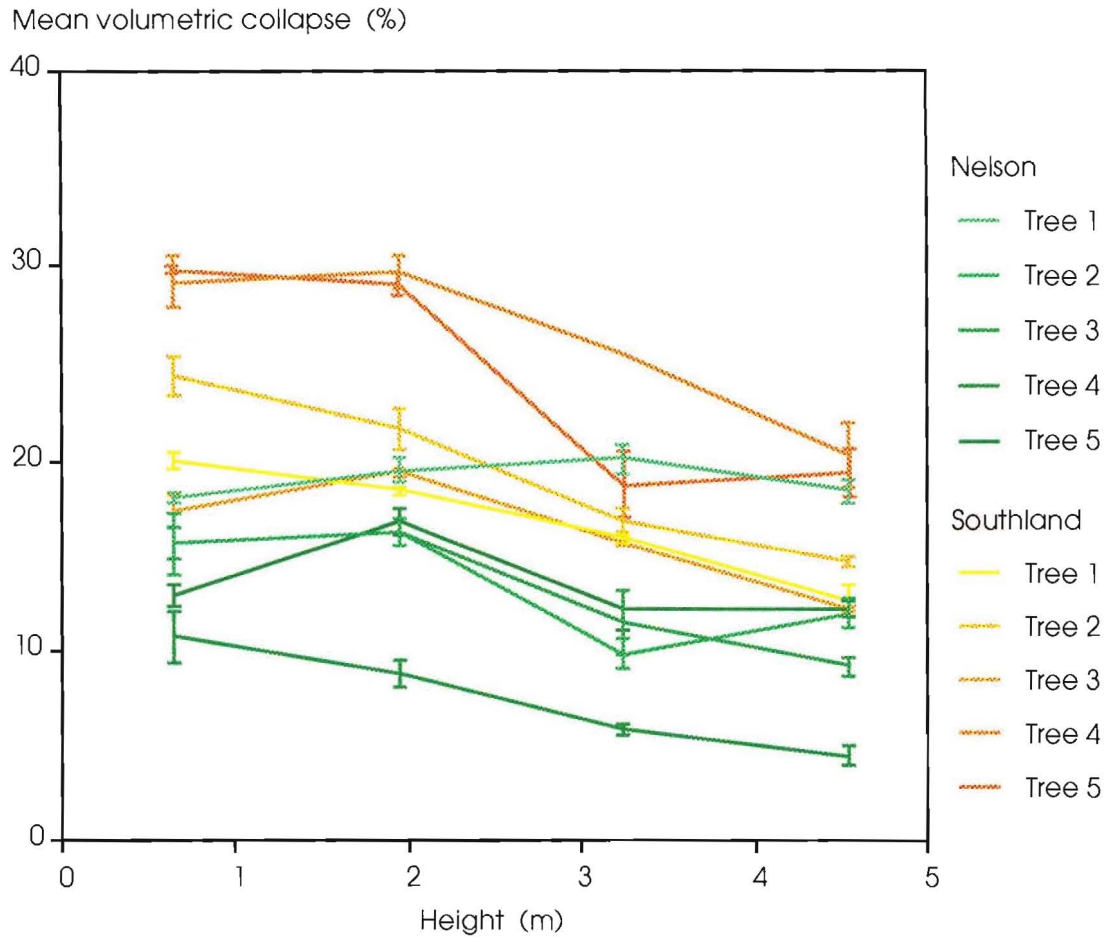

Figure 3.43 Mean volumetric collapse at 40 ° C in control boards at various heights within trees of *Eucalyptus delegatensis* from Nelson and Southland. The error bars are standard errors of the means.

Anova table 3.2: Analysis of variance of volumetric collapse in wood dried at 40 ° C

Source of variation	df	SS	MS	F_S	
Among regions	1	3316.32	3316.32	7.47	*
Among trees within regions	8	3551.95	443.99	4.88	**
Among heights within trees	30	2728.40	90.95	5.33	**
Among boards within heights	101	1722.99	17.06	53.81	**
Within boards	141	44.70	0.32		
Total	281	13119.14			

** = P < 0.01 * = P < 0.05 ns = not statistically significant

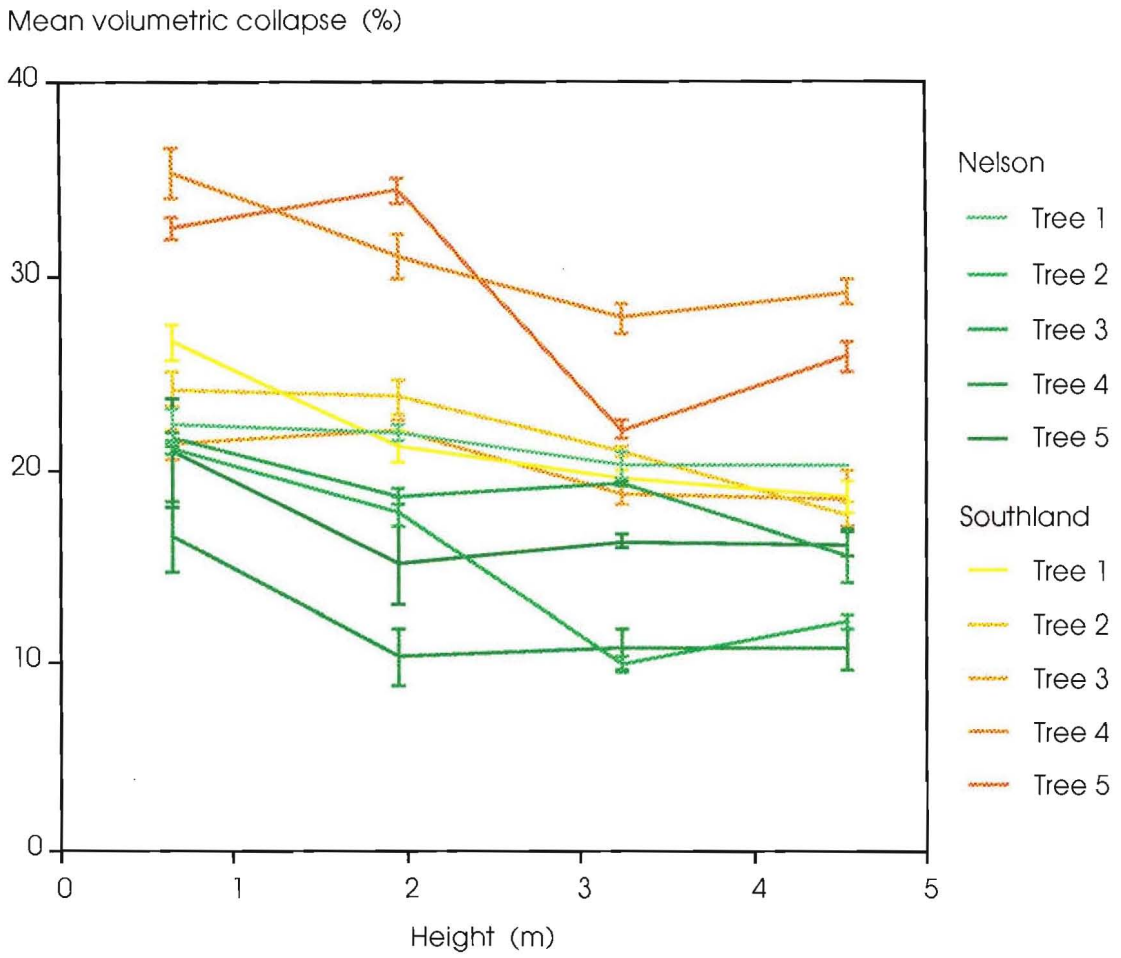

Figure 3.44 Mean volumetric collapse at 50 ° C in control boards at various heights within trees of *Eucalyptus delegatensis* from Nelson and Southland. The error bars are standard errors of the means.

Anova table 3.3: Analysis of variance of volumetric collapse in wood dried at 50 ° C

Source of variation	*df*	*SS*	*MS*	F_S	
Among regions	1	4549.69	4549.69	8.83	*
Among trees within regions	8	4123.53	515.44	5.21	**
Among heights within trees	30	2970.77	99.03	6.44	**
Among boards within heights	119	1829.24	15.37	81.06	**
Within boards	159	30.15	0.19		
Total	317	15165.24			

** = P < 0.01 * = P < 0.05 ns = not statistically significant

3.10.5.1.2 Tangential and radial collapse

The variation of tangential and radial collapse in the wood sampled, shows the same pattern as that for volumetric collapse (figures 3.45 - 3.50). The magnitude of tangential collapse was approximately double that of radial collapse for each of the three temperature treatments, 30, 40 and 50 ° C. Anova tables 3.4 - 3.9, show that for both tangential and radial collapse, there is significant added variance among regions, among trees within regions, and among height classes within trees.

3.10.5.2 Effect of temperature treatments

The figures 3.42 - 3.50 of the previous section suggest a marked increase in collapse with drying temperature, particularly for wood from the Southland region. Analysis of variance did indicate significant differences in collapse between temperature treatments, but the differences in response among regions, among trees within regions, and among heights within trees, coupled with the variation of collapse in the wood, produced statistical results that were less convincing than might have been expected.

3.10.5.2.1 Volumetric collapse

The analysis of variance of temperature treatments (30, 40 and 50 ° C), for all control boards - boards not subject to carbon dioxide gas treatment - showed no significant added temperature treatment effect for volumetric collapse (Anova table 3.10). It was felt, however, that the response to temperature might be different for the wood of each of the two regions. Separate analysis of variance using the subsets of the data, for each region, also failed, however, to show a significant added temperature effect. The F-values for temperature treatment effects in Nelson and Southland were 1.94 and 3.26 respectively, with 2 and 12 degrees of freedom.

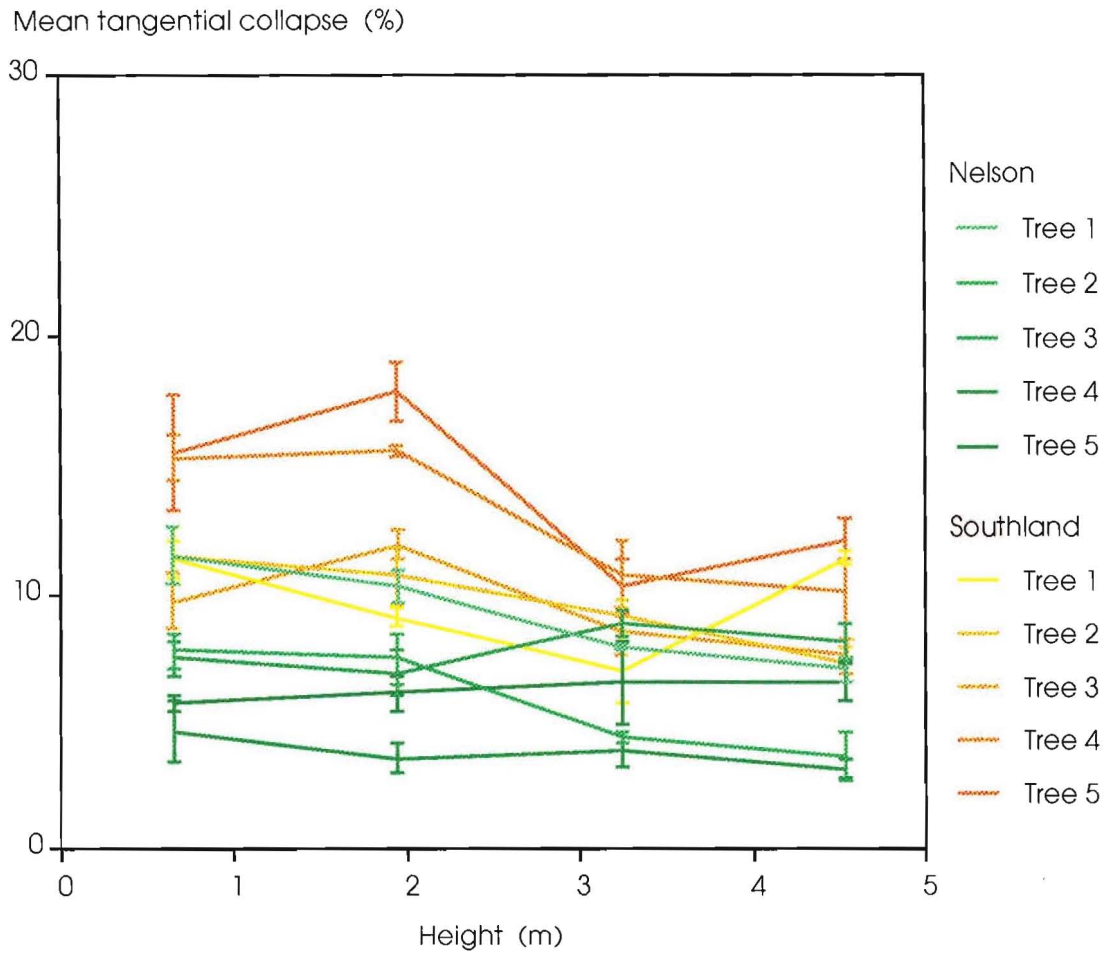

Figure 3.45 Mean tangential collapse at 30 ° C in control boards at various heights within trees of *Eucalyptus delegatensis* from Nelson and Southland. The error bars are standard errors of the means.

Anova table 3.4: Analysis of variance of tangential collapse in wood dried at 30 ° C

Source of variation	*df*	*SS*	*MS*	F_S	
Among regions	1	785.97	785.97	11.90	**
Among trees within regions	8	528.41	66.05	4.75	**
Among heights within trees	30	416.80	13.89	4.76	**
Among boards within heights	115	335.51	2.92		
Total	154	2253.25			

** = P < 0.01 * = P < 0.05 ns = not statistically significant

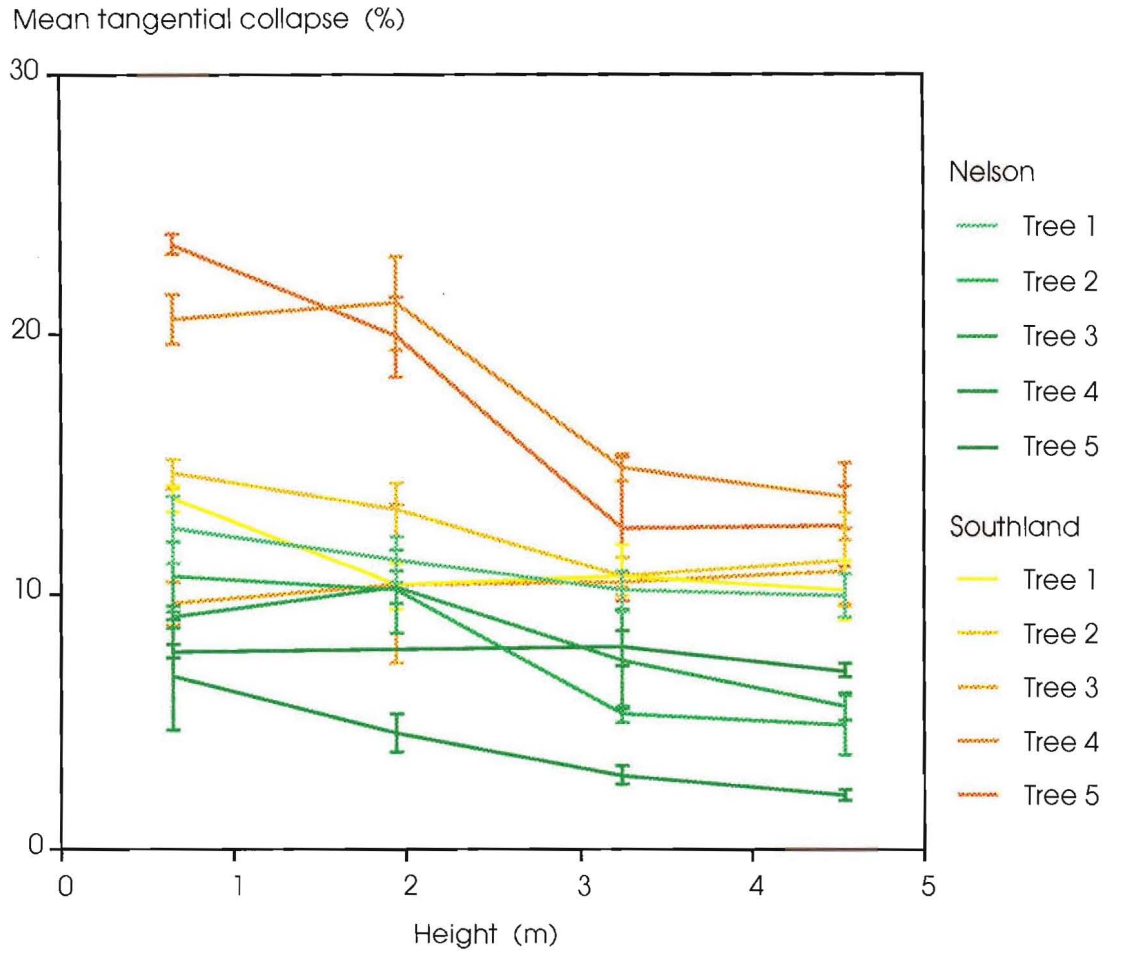

Figure 3.46 Mean tangential collapse at 40 ° C in control boards at various heights within trees of *Eucalyptus delegatensis* from Nelson and Southland. The error bars are standard errors of the means.

Anova table 3.5: Analysis of variance of tangential collapse in wood dried at 40 ° C

Source of variation	df	SS	MS	F_S	
Among regions	1	1325.47	1325.47	9.68	*
Among trees within regions	8	1094.99	136.87	4.63	**
Among heights within trees	30	886.86	29.56	5.15	**
Among boards within heights	126	724.02	5.75		
Total	165	4514.07			

** = P < 0.01 * = P < 0.05 ns = not statistically significant

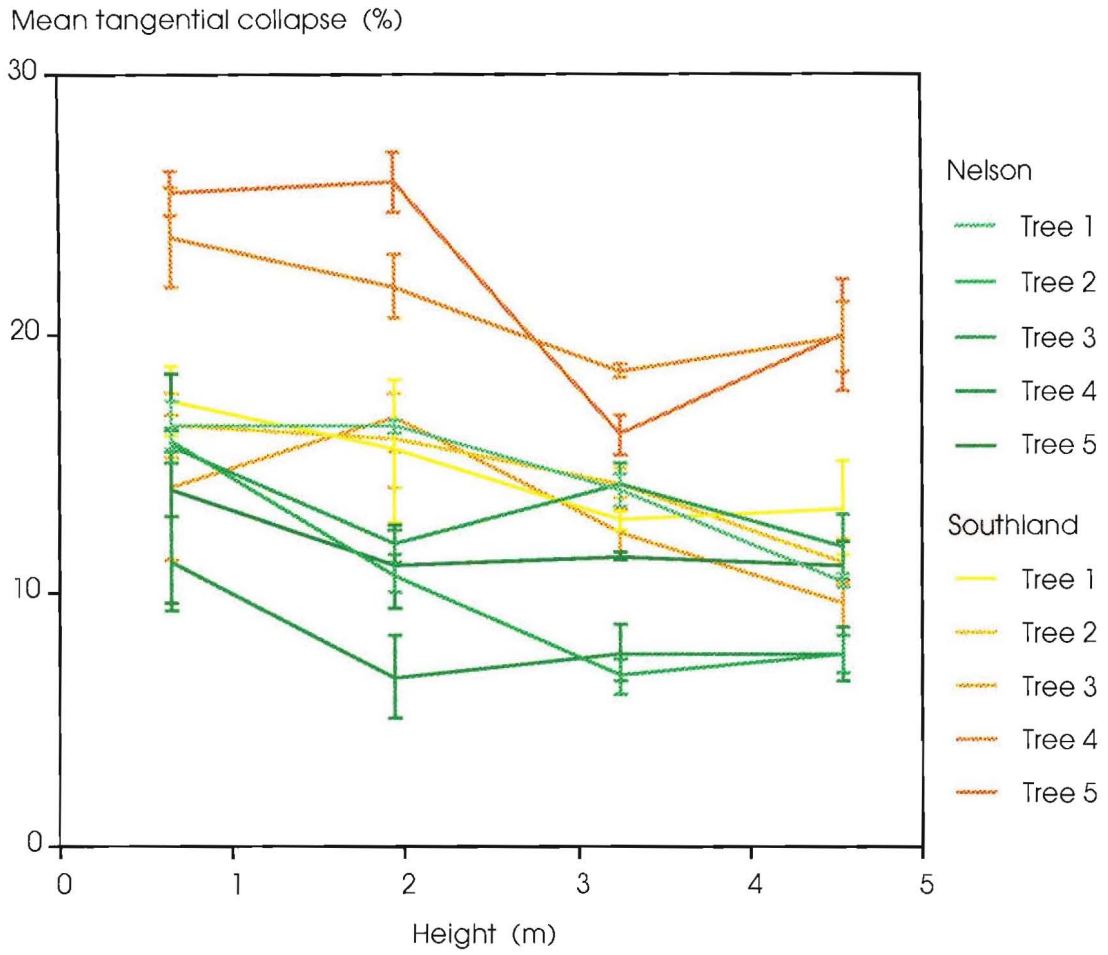

Figure 3.47 Mean tangential collapse at 50 ° C in control boards at various heights within trees of *Eucalyptus delegatensis* from Nelson and Southland. The error bars are standard errors of the means.

Anova table 3.6: Analysis of variance of tangential collapse in wood dried at 50 ° C

Source of variation	*df*	*SS*	*MS*	F_S	
Among regions	1	1176.19	1176.19	6.53	*
Among trees within regions	8	1440.59	180.07	5.39	**
Among heights within trees	30	1001.71	33.39	4.67	**
Among boards within heights	126	901.27	7.15		
Total	165	4993.91			

** = P < 0.01 * = P < 0.05 ns = not statistically significant

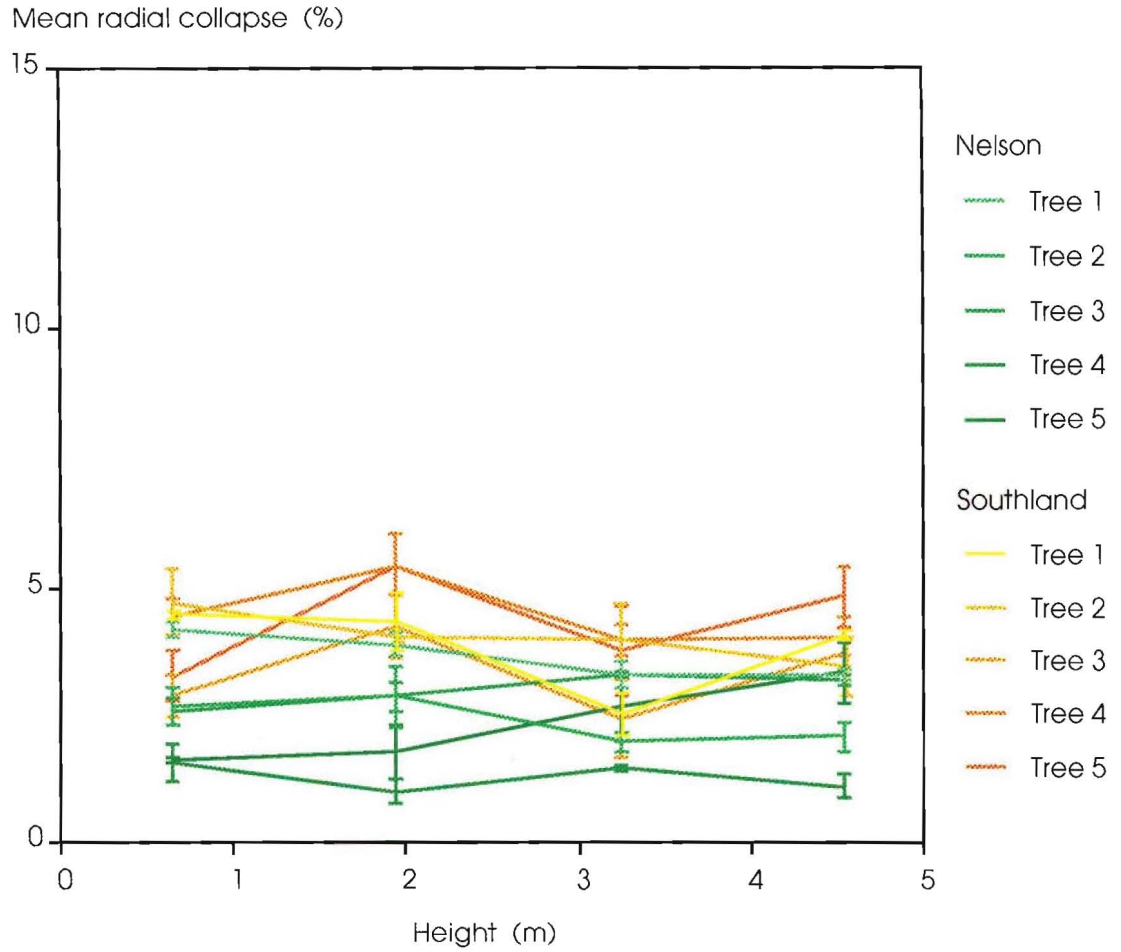

Figure 3.48 Mean radial collapse at 30 ° C in control boards at various heights within trees of *Eucalyptus delegatensis* from Nelson and Southland. The error bars are standard errors of the means.

Anova table 3.7: Analysis of variance of radial collapse in wood dried at 30 ° C

Source of variation	*df*	*SS*	*MS*	F_S	
Among regions	1	80.34	80.34	10.28	*
Among trees within regions	8	62.55	7.82	5.36	**
Among heights within trees	30	43.77	1.46	1.90	**
Among boards within heights	115	88.29	0.77		
Total	154	300.14			

** = P < 0.01 * = P < 0.05 ns = not statistically significant

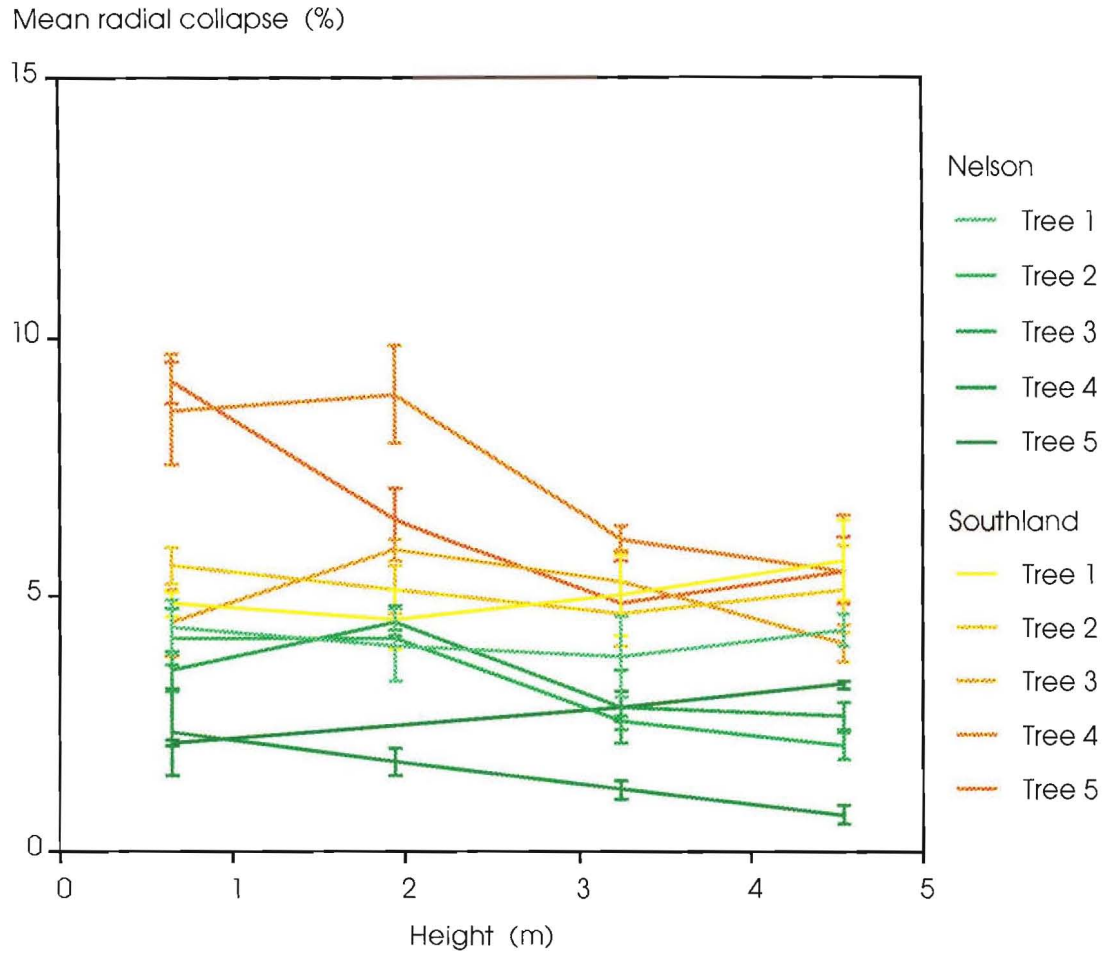

Figure 3.49 Mean radial collapse at 40 ° C in control boards at various heights within trees of *Eucalyptus delegatensis* from Nelson and Southland. The error bars are standard errors of the means.

Anova table 3.8: Analysis of variance of radial collapse in wood dried at 40 ° C

Source of variation	*df*	*SS*	*MS*	F_S	
Among regions	1	267.88	267.88	16.15	**
Among trees within regions	8	132.73	16.59	4.37	**
Among heights within trees	30	113.92	3.80	1.87	**
Among boards within heights	126	182.56	1.45		
Total	165	755.35			

** = P < 0.01 * = P < 0.05 ns = not statistically significant

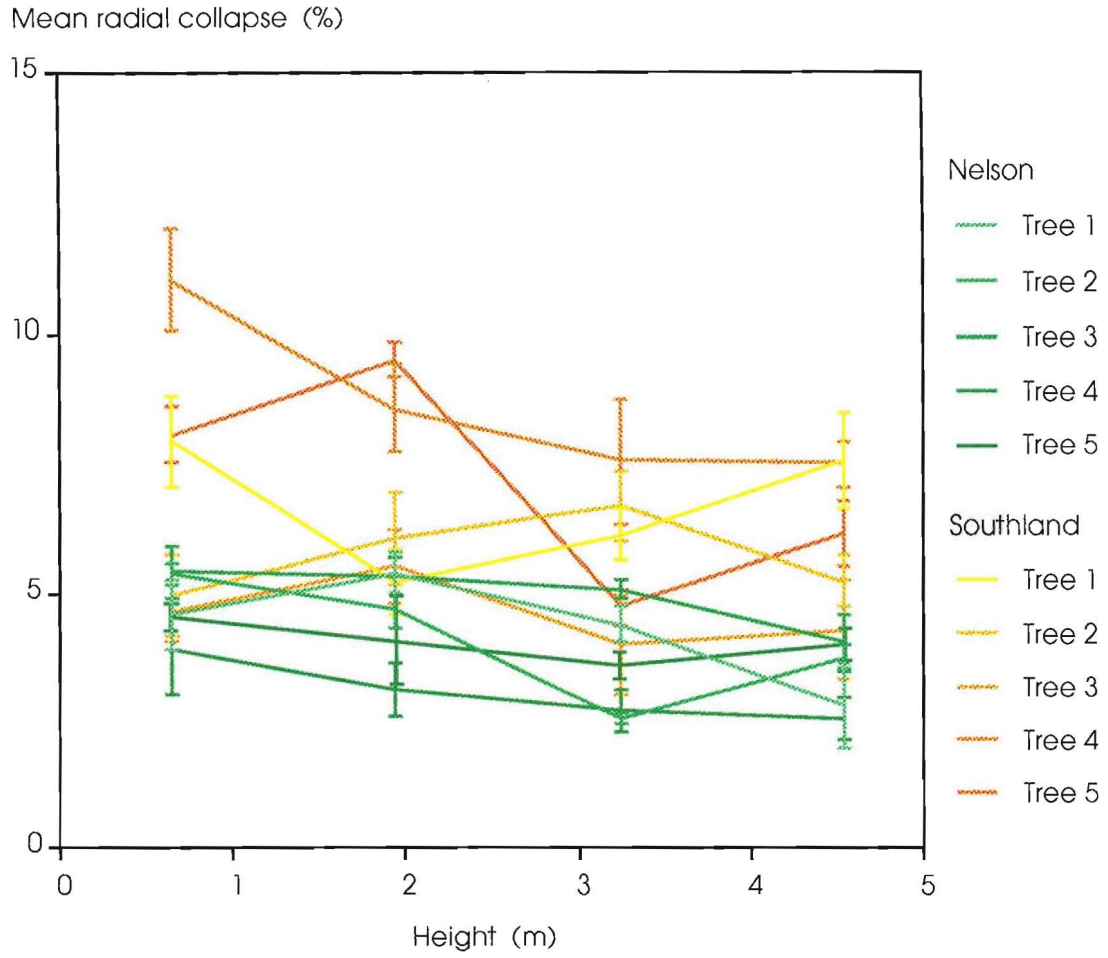

Figure 3.50 Mean radial collapse at 50 ° C in control boards at various heights within trees of *Eucalyptus delegatensis* from Nelson and Southland. The error bars are standard errors of the means.

Anova table 3.9: Analysis of variance of radial collapse in wood dried at 50 ° C

Source of variation	*df*	*SS*	*MS*	F_S	
Among regions	1	235.11	235.11	12.02	**
Among trees within regions	8	156.54	19.57	3.44	**
Among heights within trees	30	170.74	5.69	3.43	**
Among boards within heights	126	208.88	1.66		
Total	165	827.24			

** = P < 0.01 * = P < 0.05 ns = not statistically significant

Anova table 3.10: Temperature treatments at 30, 40 and 50 ° C, for all control boards from Nelson and Southland.

Source of variation	df	SS	MS	F_s	
Among treatments	2	3990.61	1995.30	0.57	ns
Among regions within treatments	3	10438.20	3479.40	8.92	**
Among trees within regions	24	9359.02	389.96	5.03	**
Among heights within trees	90	6970.83	77.45	5.50	**
Among boards within heights	335	4718.73	14.09	9.09	**
Within boards	455	704.91	1.55		
Total	909	41264.65			

** = P < 0.01 * = P < 0.05 ns = not statistically significant

When a further set of analysis of variance were performed using the subset of data for each tree, significant added temperature effects were found, but only in some trees (table 3.10). The effect of temperature on volumetric collapse, while apparent visually in figures 3.42 - 3.44, is not readily detected by statistical analysis due to the variability of the response of volumetric collapse in wood to drying temperature. Even at the tree level of classification, the effect of temperature on volumetric collapse, appears to be obscured in some trees by the variation, in the wood, of volumetric collapse among height classes (figure 3.51).

Table 3.10 F-values for the significance of temperature treatment effects on volumetric collapse in the wood of trees from Nelson and Southland, with 2 and 9 degrees of freedom.

Region	Tree 1	2	3	4	5
Nelson	6.14 *	0.84 ns	5.14 *	3.59 ns	11.06 **
Southland	2.60 ns	1.63 ns	3.74 ns	6.14 *	2.08 ns

** = P < 0.01 * = P < 0.05 ns = not statistically significant

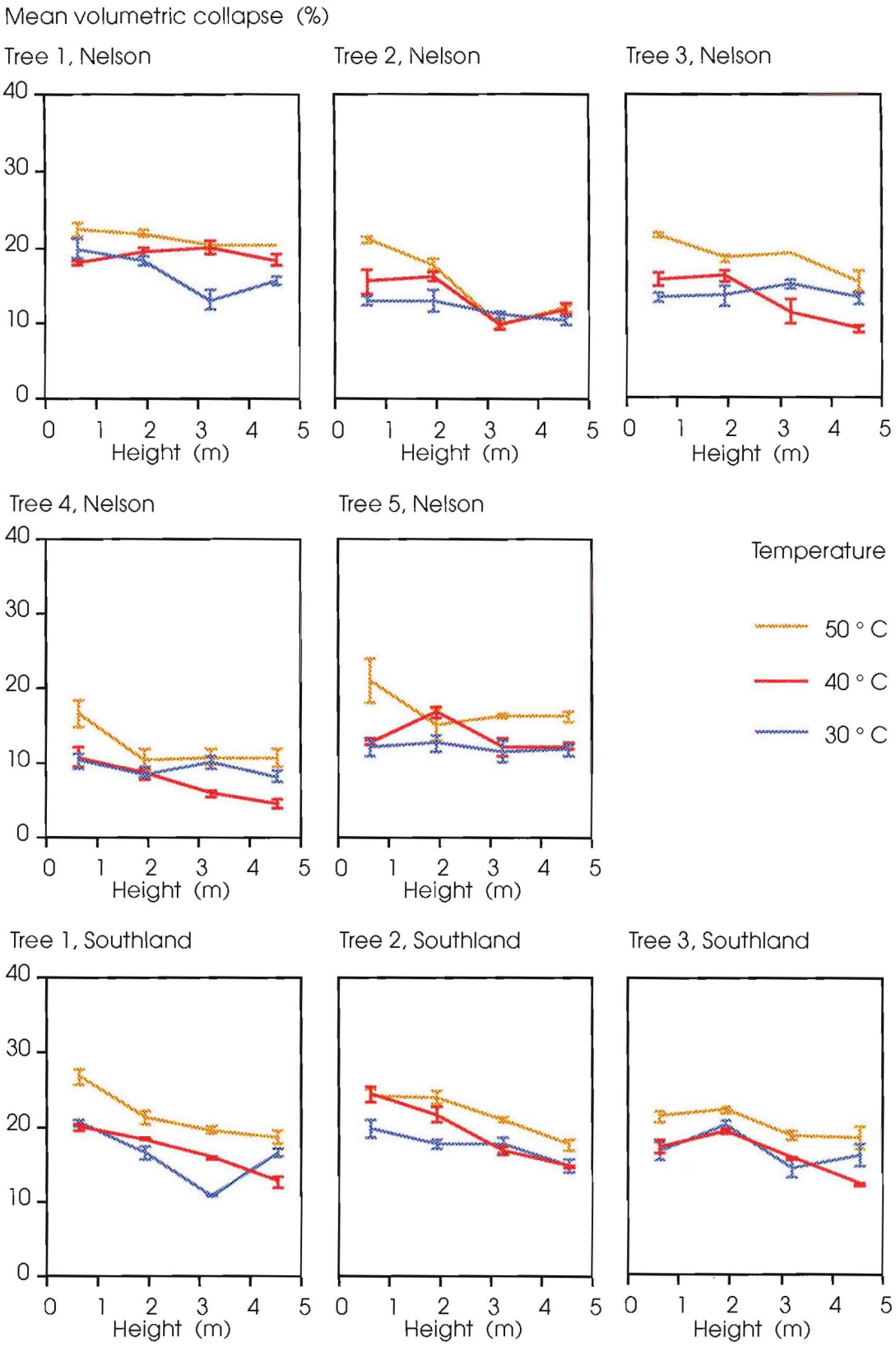
Mean volumetric collapse (%)
Tree 1, Nelson
Tree 2, Nelson
Tree 3, Nelson
Tree 4, Nelson
Tree 5, Nelson
Tree 1, Southland
Tree 2, Southland
Tree 3, Southland
0
10
20
30
40
0 1 2 3 4 5
Height (m)
Temperature
50 ° C
40 ° C
30 ° C

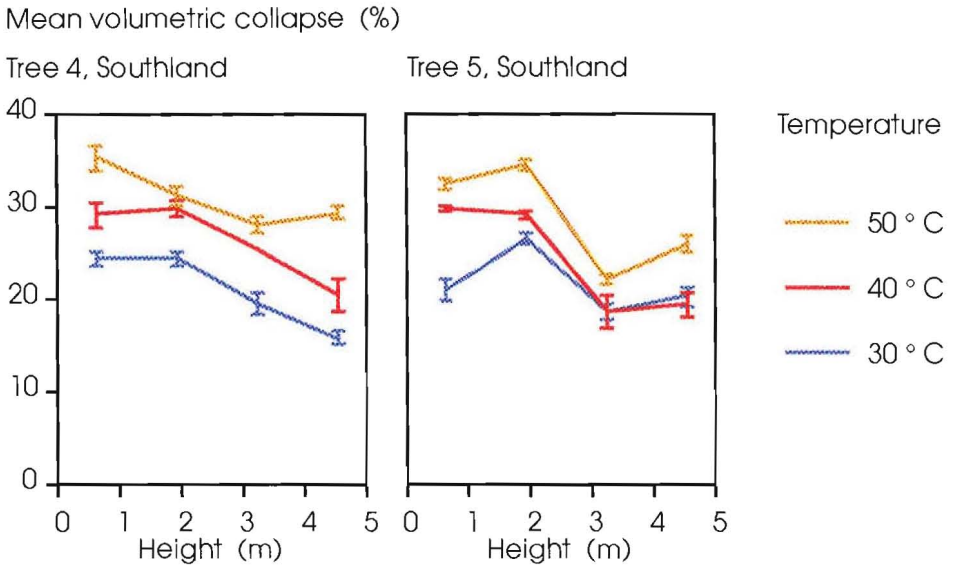

Figure 3.51 Temperature treatment effects on volumetric collapse in the wood of trees of *Eucalyptus delegatensis* from Nelson and Southland.

3.10.5.2.2 Tangential and radial collapse

The effect of temperature treatments were also non-significant for tangential and radial collapse, when all control boards from both Nelson and Southland were included in the analysis of variance. When the analysis of variance was repeated using the subsets of the data, for each region, the effects of temperature treatments were found to be significant for tangential collapse in the wood from Nelson, and for radial shrinkage in the wood from Nelson and Southland (table 3.11).

Table 3.11 F-values for the significance of temperature treatment effects on tangential and radial collapse in wood from Nelson and Southland, with 2 and 12 degrees of freedom.

Region	Tangential collapse	Radial collapse
Nelson	5.72 *	3.88 *
Southland	3.86 ns	7.15 * *

** = P < 0.01 * = P < 0.05 ns = not statistically significant

3.10.5.3 Effect of carbon dioxide gas treatments

Carbon dioxide gas treatments were found to have no effect on volumetric, tangential or radial collapse in the wood sampled. The results are presented for volumetric collapse only. The analysis of variance are grouped for each of the three combinations of carbon dioxide gas treatments and controls used in the analysis (figure 3.34). The groupings were necessitated by equipment constraints, restricting sampling of two of the three carbon dioxide gas treatments to subsets of the trees and regions.

3.10.5.3.1 Low pressure carbon dioxide gas treatment at 1.5 MPa and 12 ° C, and controls.

The effect of low carbon dioxide gas solubilities in wood, prior to decompression, on volumetric collapse were examined in this analysis of variance. The gas solubilities achieved were 2.0 - 2.6 g CO_2 / 100 g H_2O. The gas treatment was applied to boards from all trees of both the Nelson and Southland regions. The analysis of variance were performed separately for each of the temperatures (30, 40 and 50 ° C) at which the carbon dioxide gas treatment and control boards were dried. There was no significant difference in volumetric collapse between the controls and the carbon dioxide gas treatment when the data for both regions was used in the analysis of variance. The F-values for the treatment effects were 0.03, 0.002 and 0.04, with 1 and 2 degrees of freedom, for the drying temperatures 30, 40 and 50 ° C respectively. When the data for each region was analysed separately, again no significant difference for the carbon dioxide gas treatment was observed (Anova tables 3.11 - 3.16). The figures 3.52 - 3.57 illustrate quite clearly that there is no reduction in volumetric collapse associated with carbon dioxide gas treatment. Even when we examine the figures at a tree level there are very few instances of a consistent and large reduction in volumetric collapse associated with gas treatment. This is confirmed by analysis of variance of the data for each tree. Table 3.12 shows that there is only one instance for each of three trees of a significant difference in volumetric collapse between controls and the gas treatment. These are not repeated for each of the three drying temperatures, which suggests that they were produced by chance, as a result of the variation of volumetric collapse in the wood, rather than by

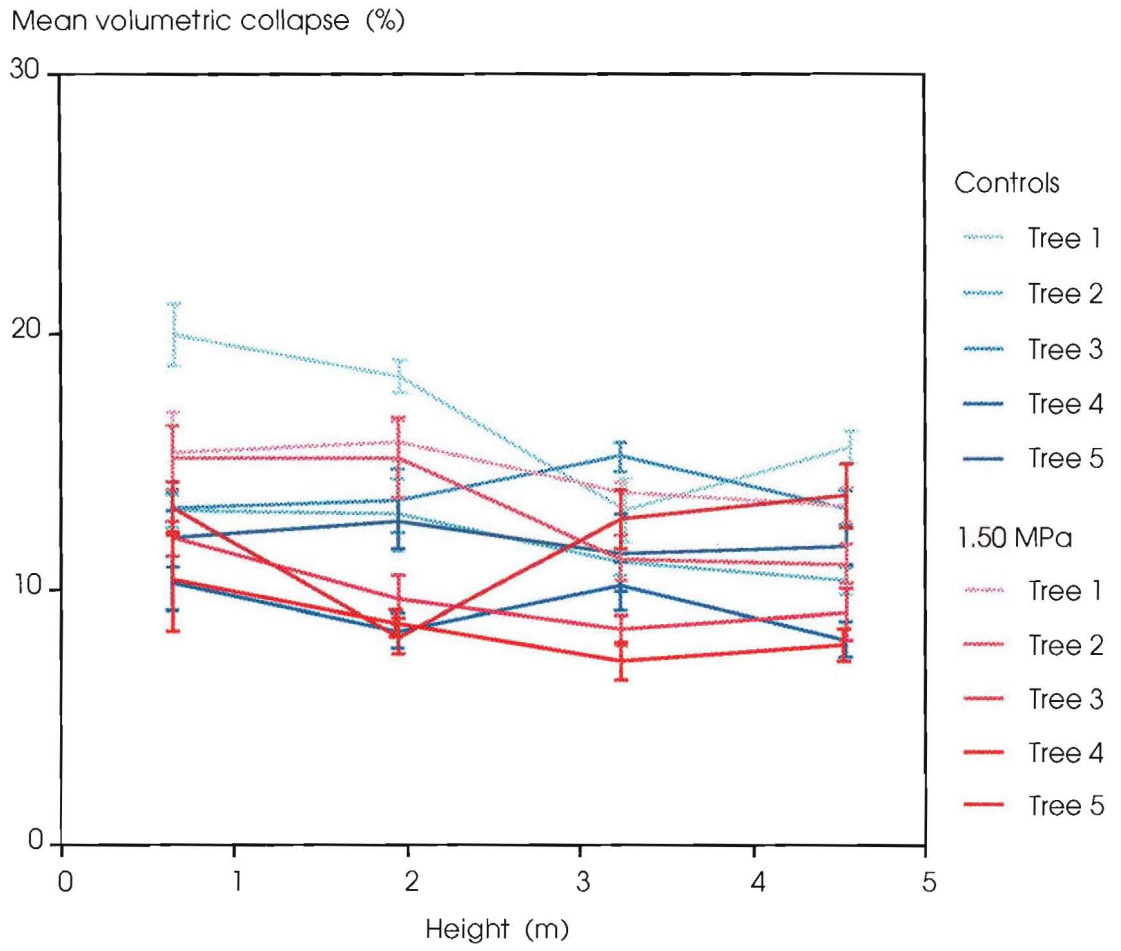

Figure 3.52 Mean volumetric collapse at 30 ° C in 1.5 MPa carbon dioxide gas treatment (12 ° C) and control boards at various heights within trees of *Eucalyptus delegatensis* from Nelson. The error bars are standard errors of the means.

Anova table 3.11: Low pressure (1.5 MPa) carbon dioxide gas treatment at 12 ° C, and controls for volumetric collapse in wood dried at 30 ° C. All trees from Nelson.

Source of variation	df	SS	MS	F_S	
Among treatments	1	85.99	85.99	0.39	ns
Among trees within treatments	8	1770.49	221.31	10.54	**
Among heights within trees	30	630.01	21.00	2.07	**
Among boards within heights	118	1194.98	10.13	2.41	**
Within boards	158	664.13	4.20		
Total	315	4570.38			

** = P < 0.01 * = P < 0.05 ns = not statistically significant

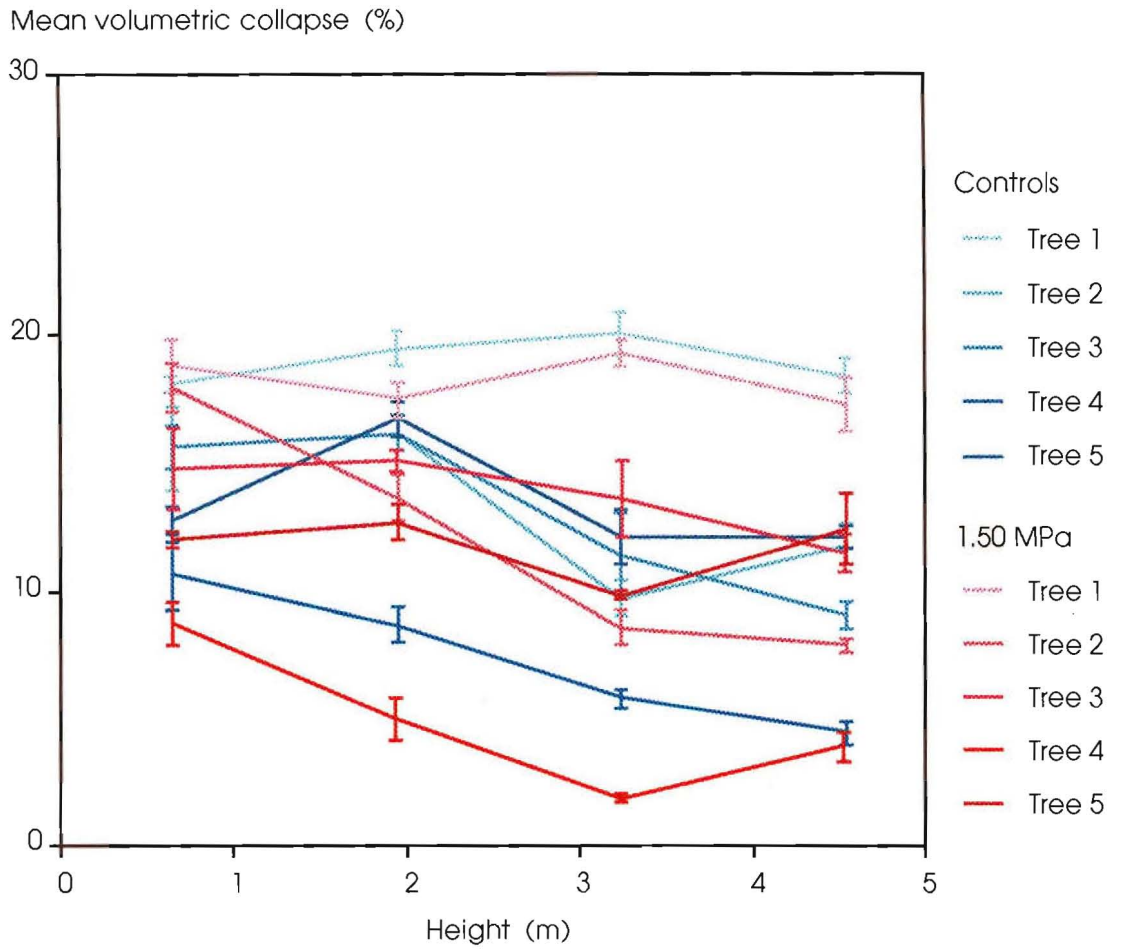

Figure 3.53 Mean volumetric collapse at 40 ° C in 1.5 MPa carbon dioxide gas treatment (12 ° C) and control boards at various heights within trees of *Eucalyptus delegatensis* from Nelson. The error bars are standard errors of the means.

Anova table 3.12: Low pressure (1.5 MPa) carbon dioxide gas treatment at 12 ° C, and controls for volumetric collapse in wood dried at 40 ° C. All trees from Nelson.

Source of variation	*df*	*SS*	*MS*	F_S	
Among treatments	1	27.95	29.95	0.06	ns
Among trees within treatments	8	3978.69	497.34	10.62	**
Among heights within trees	30	1404.75	46.83	3.13	**
Among boards within heights	113	1690.43	14.96	45.47	**
Within boards	153	50.35	0.33		
Total	305	7214.59			

** = P < 0.01 * = P < 0.05 ns = not statistically significant

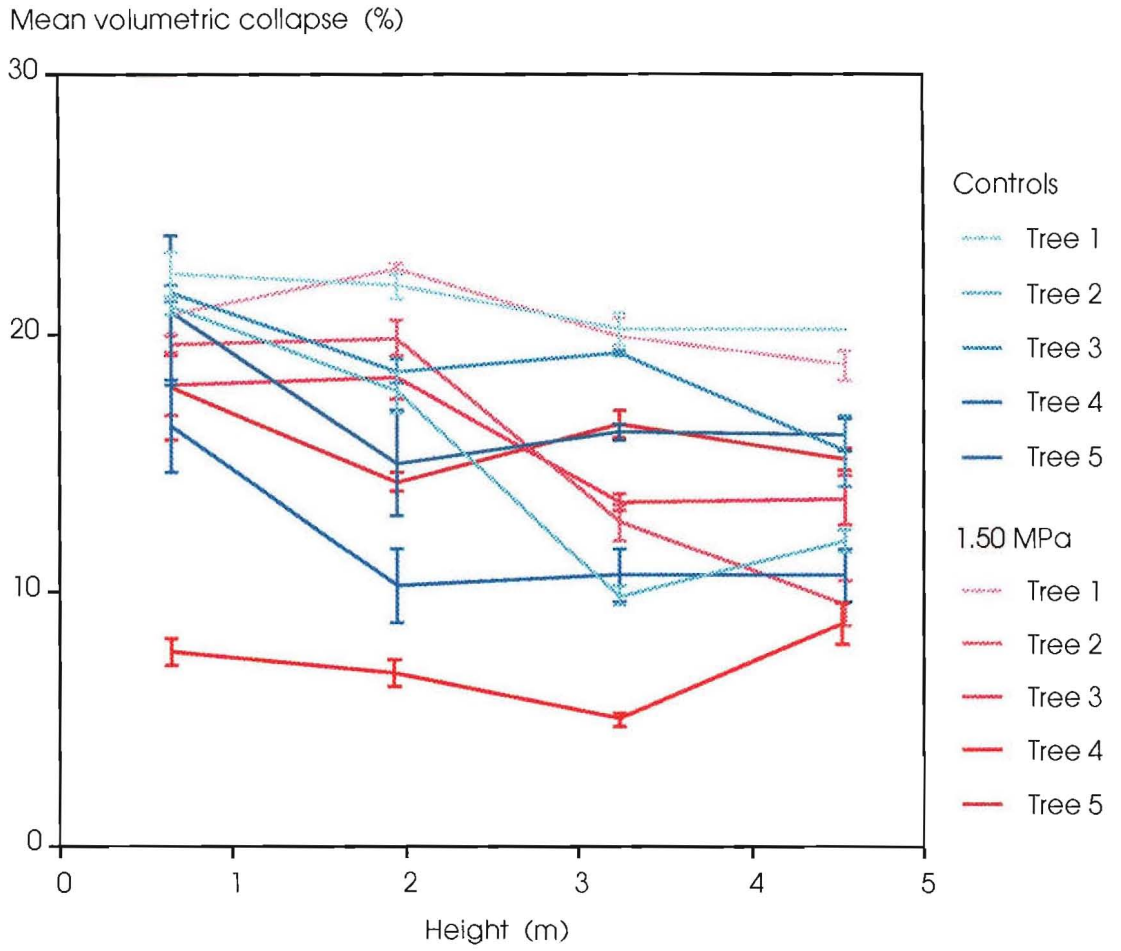

Figure 3.54 Mean volumetric collapse at 50 ° C in 1.5 MPa carbon dioxide gas treatment (12 ° C) and control boards at various heights within trees of *Eucalyptus delegatensis* from Nelson. The error bars are standard errors of the means.

Anova table 3.13: Low pressure (1.5 MPa) carbon dioxide gas treatment at 12 ° C, and controls for volumetric collapse in wood dried at 50 ° C. All trees from Nelson.

Source of variation	*df*	*SS*	*MS*	F_S	
Among treatments	1	221.20	221.20	0.40	ns
Among trees within treatments	8	4395.31	549.41	7.79	**
Among heights within trees	30	2115.39	70.51	4.87	**
Among boards within heights	119	1722.69	14.48	61.60	**
Within boards	159	37.29	0.23		
Total	317	8793.11			

** = P < 0.01 * = P < 0.05 ns = not statistically significant

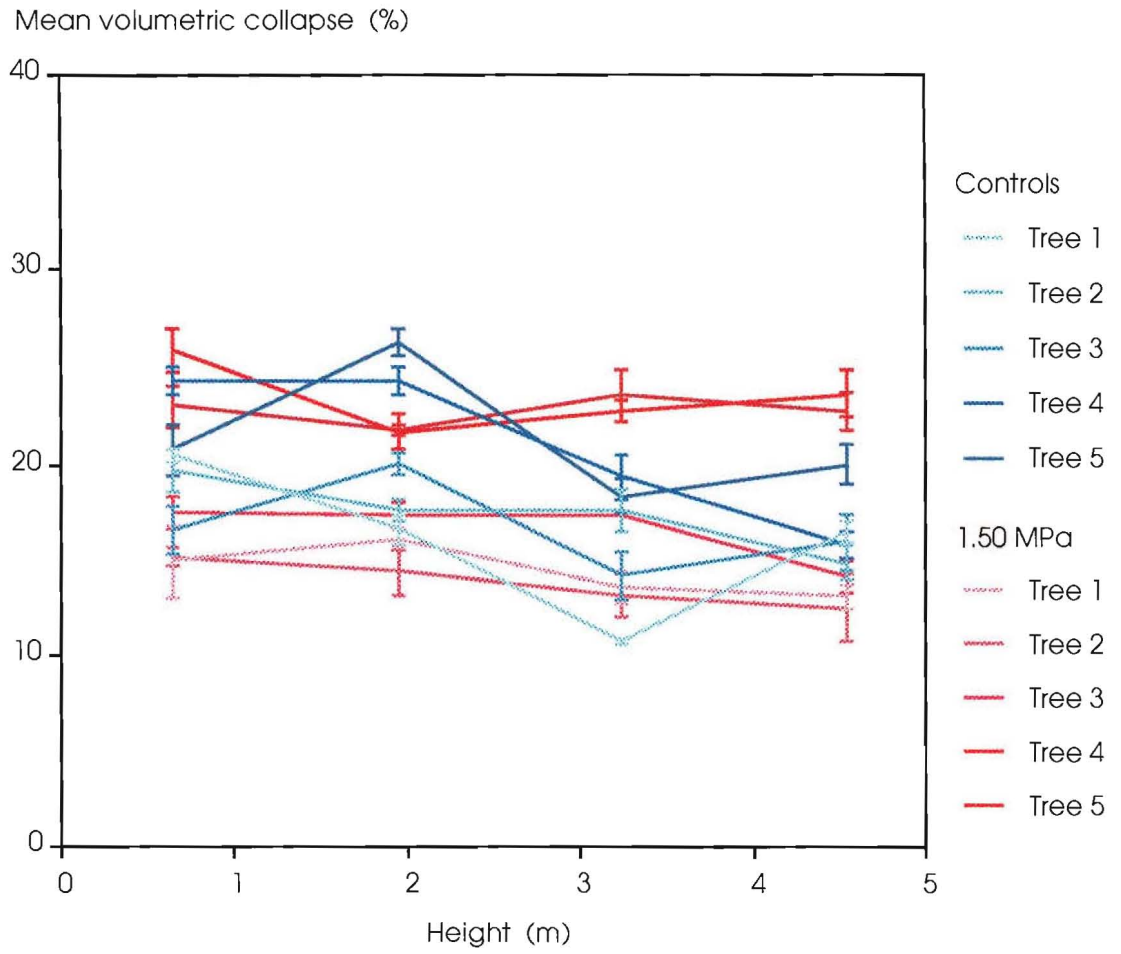

Figure 3.55 Mean volumetric collapse at 30 ° C in 1.5 MPa carbon dioxide gas treatment (12 ° C) and control boards at various heights within trees of *Eucalyptus delegatensis* from Southland. The error bars are standard errors of the means.

Anova table 3.14: Low pressure (1.5 MPa) carbon dioxide gas treatment at 12 ° C, and controls for volumetric collapse in wood dried at 30 ° C. All trees from Southland.

Source of variation	df	SS	MS	F_S	
Among treatments	1	12.83	12.83	0.03	ns
Among trees within treatments	8	2934.04	366.75	9.29	**
Among heights within trees	30	1184.64	39.49	2.97	**
Among boards within heights	102	1357.37	13.31	3.94	**
Within boards	142	480.06	3.38		
Total	283	6366.34			

** = P < 0.01 * = P < 0.05 ns = not statistically significant

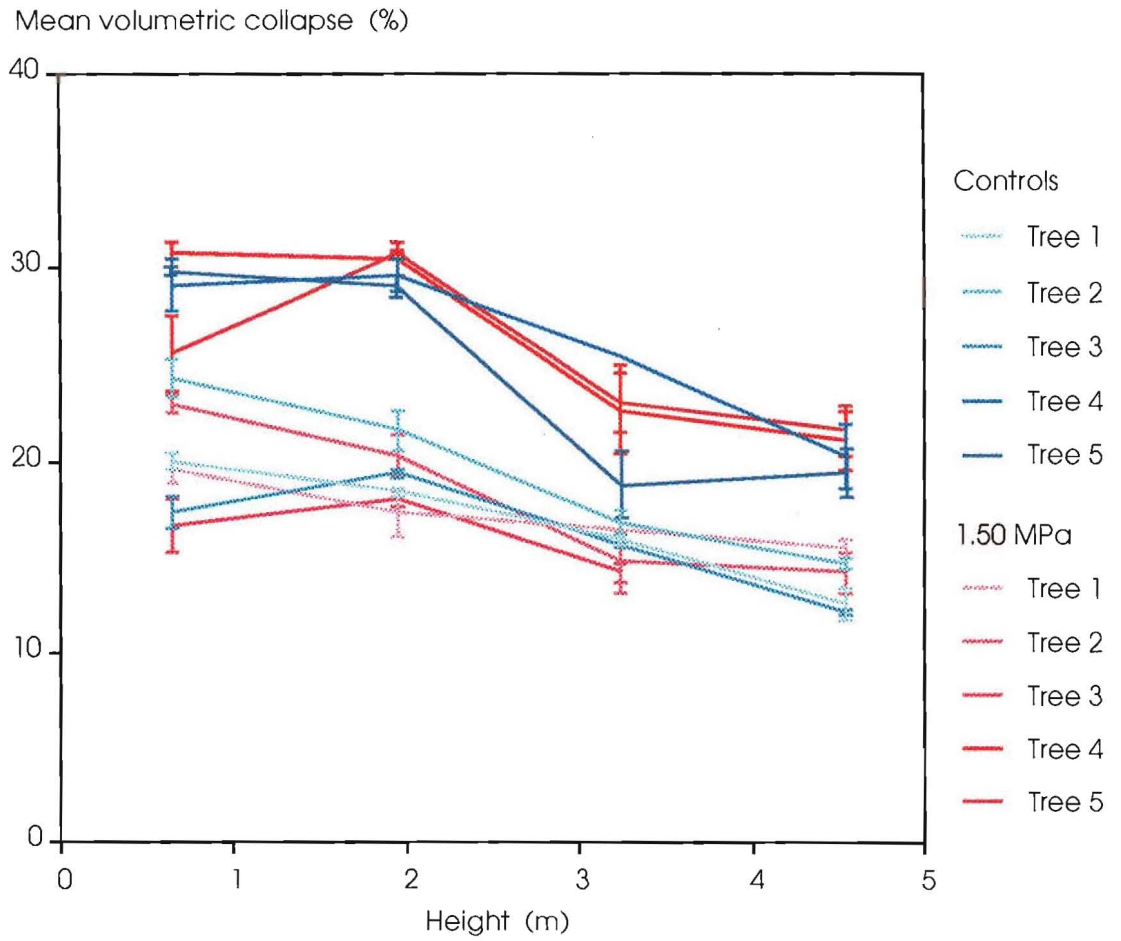

Figure 3.56 Mean volumetric collapse at 40 ° C in 1.5 MPa carbon dioxide gas treatment (12 ° C) and control boards at various heights within trees of *Eucalyptus delegatensis* from Southland. The error bars are standard errors of the means.

Anova table 3.15: Low pressure (1.5 MPa) carbon dioxide gas treatment at 12 ° C, and controls for volumetric collapse in wood dried at 40 ° C. All trees from Southland.

Source of variation	df	SS	MS	F_S	
Among treatments	1	2.08	2.08	0.01	ns
Among trees within treatments	8	3271.55	408.94	3.76	**
Among heights within trees	28	3047.65	108.85	5.17	**
Among boards within heights	86	1809.57	21.04	68.54	**
Within boards	124	38.13	0.31		
Total	247	8299.89			

** = P < 0.01 * = P < 0.05 ns = not statistically significant

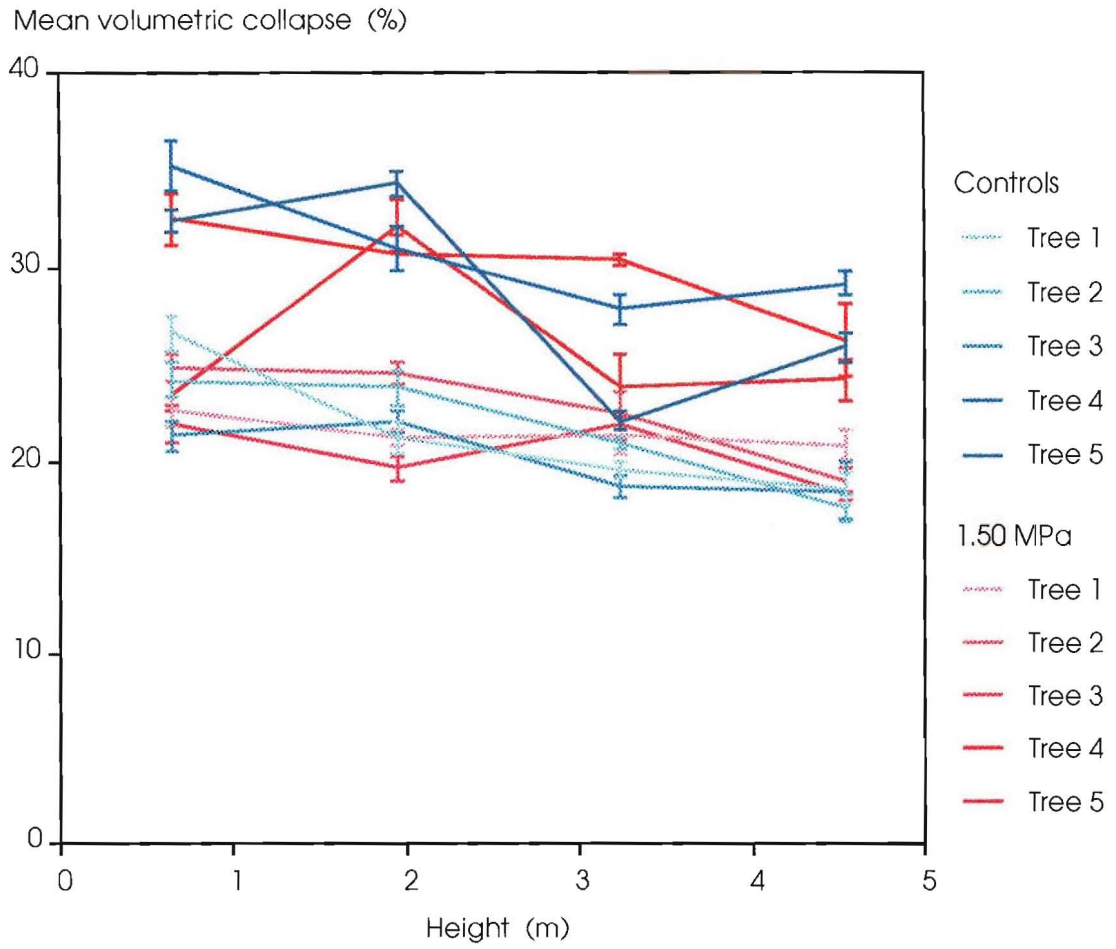

Figure 3.57 Mean volumetric collapse at 50 ° C in 1.5 MPa carbon dioxide gas treatment (12 ° C) and control boards at various heights within trees of *Eucalyptus delegatensis* from Southland. The error bars are standard errors of the means.

Anova table 3.16: Low pressure (1.5 MPa) carbon dioxide gas treatment at 12 ° C, and controls for volumetric collapse in wood dried at 50 ° C. All trees from Southland.

Source of variation	*df*	*SS*	*MS*	F_S	
Among treatments	1	20.53	20.53	0.04	ns
Among trees within treatments	8	4383.25	547.91	5.89	**
Among heights within trees	30	2790.33	93.01	5.87	**
Among boards within heights	124	1965.71	15.85	70.15	**
Within boards	164	37.05	0.23		
Total	327	9639.49			

** = P < 0.01 * = P < 0.05 ns = not statistically significant

Table 3.12 F-values for the significance of low pressure carbon dioxide gas treatment effects on volumetric collapse in the wood of trees from Nelson and Southland, with 1 and 6 degrees of freedom.

Region	Tree 1	2	3	4	5
30°C					
Nelson	1.79 ns	0.98 ns	18.12 **	0.76 ns	0.01 ns
Southland	0.98 ns	7.87 *	0.05 ns	1.25 ns	0.41 ns
40°C					
Nelson	1.37 ns	0.32 ns	0.12 ns	0.02 ns	1.75 ns
Southland	0.12 ns	0.15 ns	0.00 ns	0.01 ns	0.07 ns
50°C					
Nelson	0.46 ns	0.01 ns	2.31 ns	8.69 *	0.41 ns
Southland	0.02 ns	0.26 ns	0.02 ns	0.16 ns	0.62 ns

** = P < 0.01 * = P < 0.05 ns = not statistically significant

a carbon dioxide gas treatment effect.

3.10.5.3.2 Low pressure carbon dioxide gas treatment at 1.5 MPa and 12 ° C, and high pressure carbon dioxide gas treatment at 4.5 MPa and 17 ° C, and controls.

The effect of low and high carbon dioxide gas solubilities in wood, prior to decompression, on volumetric collapse were examined in this analysis of variance. The gas solubilities achieved were 2.0 - 2.6 and 4.6 - 5.2 g CO_2 / 100 g H_2O for low and high pressure carbon dioxide gas treatments respectively. The high pressure carbon dioxide gas treatment was applied only to boards of trees 4 and 5, Nelson, and trees 3 and 5, Southland. The low pressure carbon dioxide gas treatment and control data used in the analysis were a subset of the data used in the previous section. The analysis of variance was performed separately for each of the three drying temperatures (30, 40 and 50 ° C). Again there was no significant difference in volumetric collapse between the controls and carbon dioxide gas treatments when the data for both the Nelson and Southland regions were

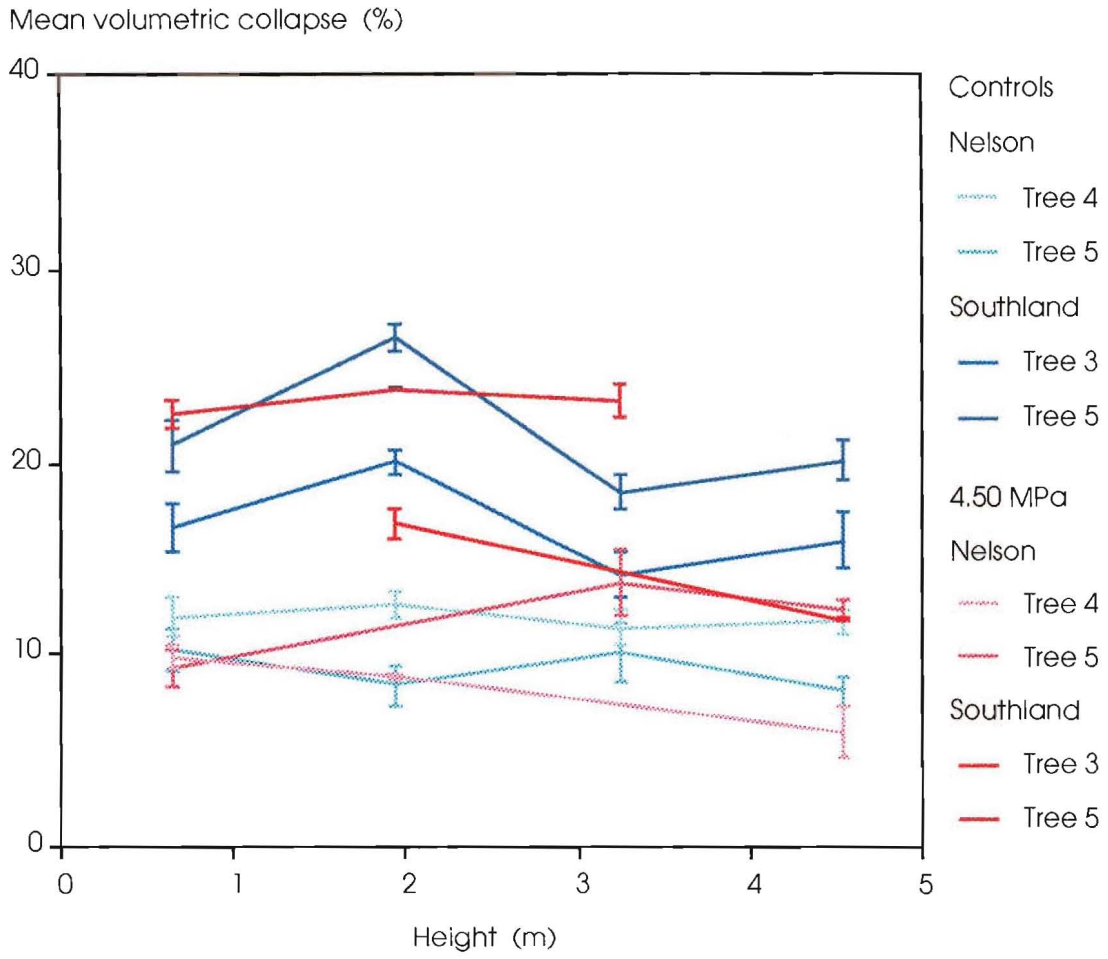

Figure 3.58 Mean volumetric collapse at 30 ° C in 4.5 MPa carbon dioxide gas treatment (17 ° C) and control boards at various heights within trees of *Eucalyptus delegatensis* from Nelson and Southland. The error bars are standard errors of the means.

Anova table 3.17: Low and high pressure (1.5 and 4.5 MPa) carbon dioxide gas treatments at 12 and 17 ° C respectively, and controls for volumetric collapse in wood dried at 30 ° C. Trees 4 and 5, Nelson, and trees 3 and 5, Southland.

Source of variation	*df*	*SS*	*MS*	F_S	
Among treatments	2	5.27	2.63	0.002	ns
Among regions within treatments	3	5396.66	1798.89	7.26	*
Among trees within regions	6	1485.85	247.64	10.76	**
Among heights within trees	31	713.53	23.02	1.73	*
Among boards within heights	94	1251.04	13.31	3.57	**
Within boards	137	510.86	3.73		
Total	273	10129.14			

** = P < 0.01 * = P < 0.05 ns = not statistically significant

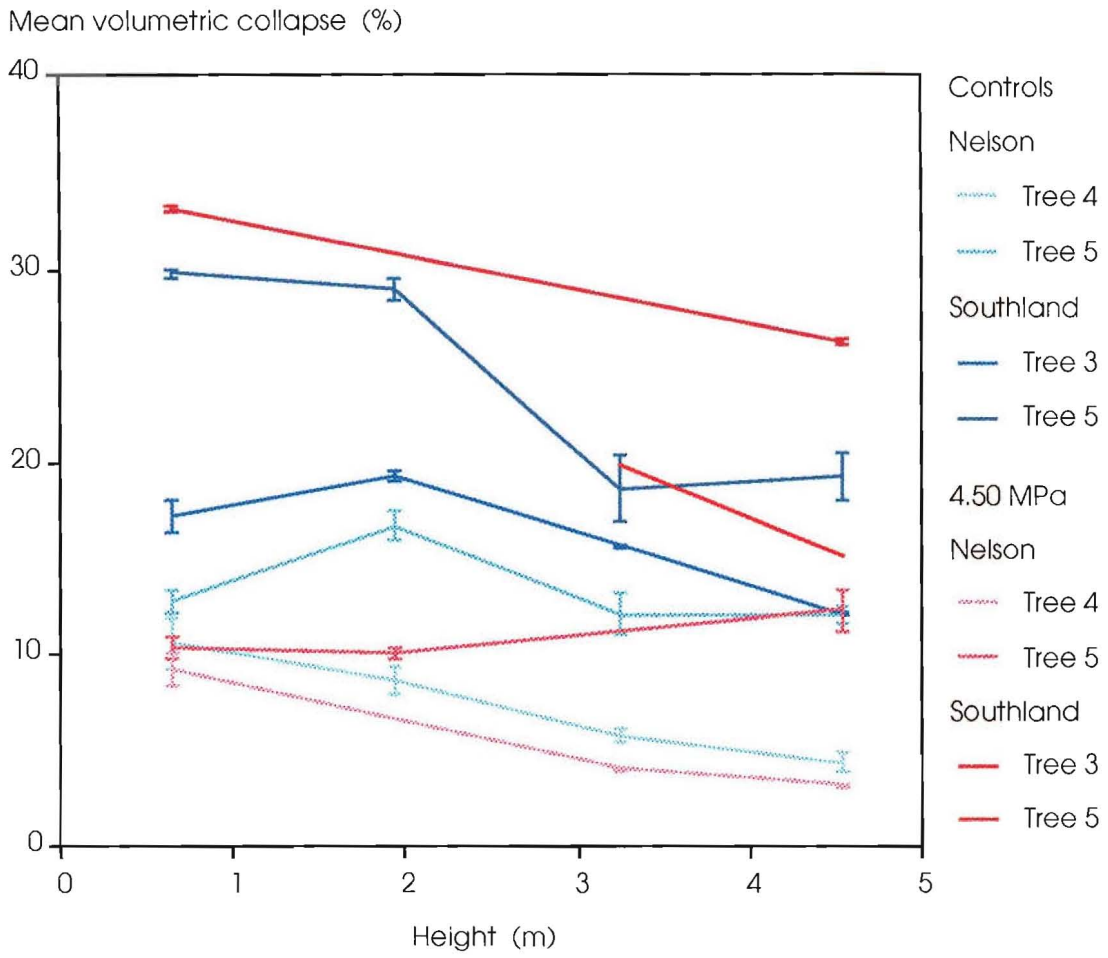

Figure 3.59 Mean volumetric collapse at 40 ° C in 4.5 MPa carbon dioxide gas treatment (17 ° C) and control boards at various heights within trees of *Eucalyptus delegatensis* from Nelson and Southland. The error bars are standard errors of the means.

Anova table 3.18: Low and high pressure (1.5 and 4.5 MPa) carbon dioxide gas treatments at 12 and 17 ° C respectively, and controls for volumetric collapse in wood dried at 40 ° C. Trees 4 and 5, Nelson, and trees 3 and 5, Southland.

Source of variation	*df*	*SS*	*MS*	F_S	
Among treatments	2	7.30	3.65	0.002	ns
Among regions within treatments	3	6066.35	2022.12	5.50	*
Among trees within regions	6	2204.78	367.46	7.32	**
Among heights within trees	29	1455.38	50.19	2.56	**
Among boards within heights	73	1431.96	19.62	77.53	**
Within boards	114	28.80	0.25		
Total	227	13199.11			

** = P < 0.01 * = P < 0.05 ns = not statistically significant

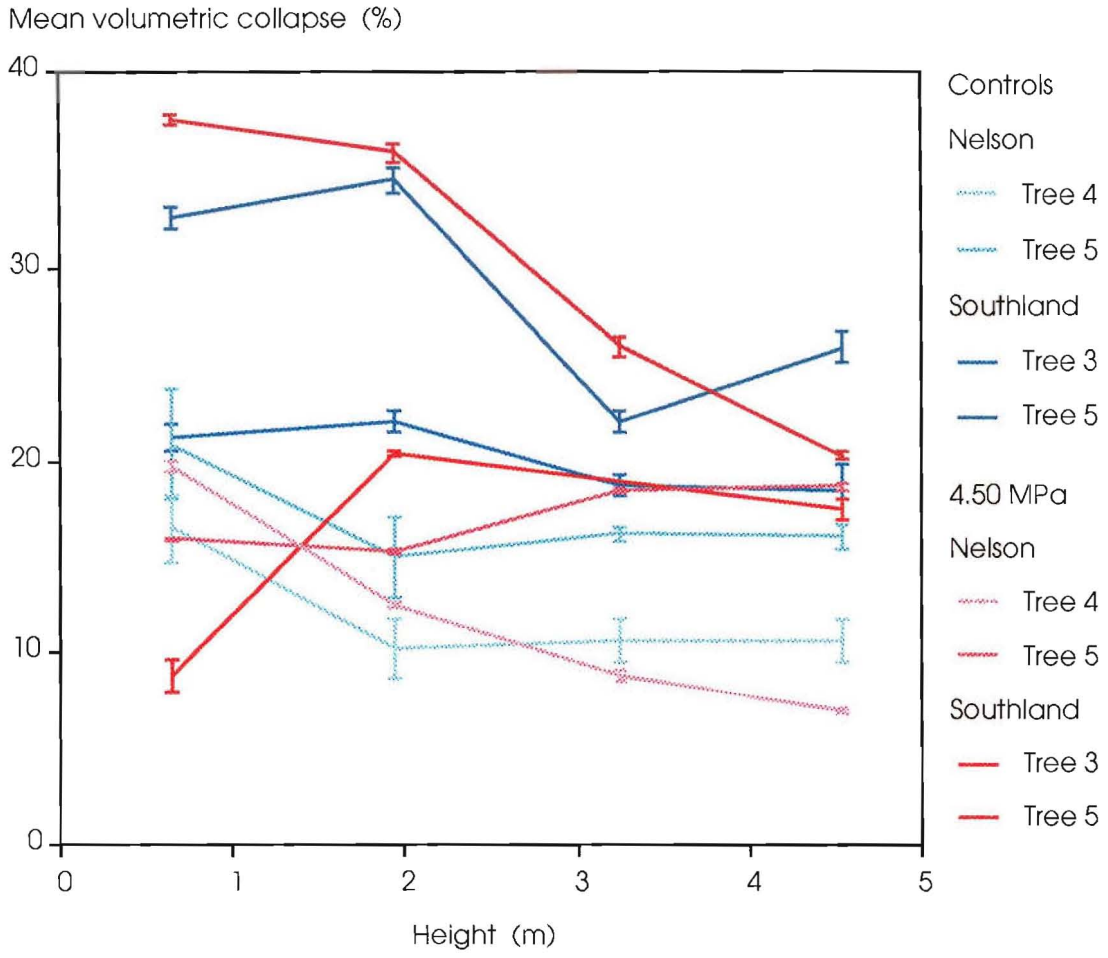

Figure 3.60 Mean volumetric collapse at 50 ° C in 4.5 MPa carbon dioxide gas treatment (17 ° C) and control boards at various heights within trees of *Eucalyptus delegatensis* from Nelson and Southland. The error bars are standard errors of the means.

Anova table 3.19: Low and high pressure (1.5 and 4.5 MPa) carbon dioxide gas treatments at 12 and 17 ° C respectively, and controls for volumetric collapse in wood dried at 50 ° C. Trees 4 and 5, Nelson, and trees 3 and 5, Southland.

Source of variation	*df*	*SS*	*MS*	F_S	
Among treatments	2	253.12	126.51	0.05	ns
Among regions within treatments	3	7236.44	2412.15	3.78	ns
Among trees within regions	6	3830.38	638.40	8.09	**
Among heights within trees	35	2760.56	78.87	3.95	**
Among boards within heights	93	1858.22	19.98	87.64	**
Within boards	140	31.85	0.23		
Total	279	19561.11			

** = P < 0.01 * = P < 0.05 ns = not statistically significant

used in the analysis of variance (Anova tables 3.17 - 3.19). Figures 3.58 - 3.60 show quite clearly the absence of a reduction in volumetric collapse with high pressure carbon dioxide gas treatment. Even on a regional or individual tree basis there is no sign of any reduction of volumetric collapse. Statistical analysis of regional and individual tree data confirmed this, tables 3.13 and 3.14. There were no instances of significant differences among the treatments and controls.

Table 3.13 F-values for the significance of low and high pressure carbon dioxide gas treatment effects on volumetric collapse in the wood from Nelson and Southland, with 2 and 3 degrees of freedom.

Temperature	Region	F-value	Region	F-value
30°C	Nelson	0.03 ns	Southland	0.01 ns
40°C	Nelson	0.07 ns	Southland	0.08 ns
50°C	Nelson	0.26 ns	Southland	0.04 ns

** = P < 0.01 * = P < 0.05 ns = not statistically significant

Table 3.14 F-values for the significance of low and high pressure carbon dioxide gas treatment effects on volumetric collapse in the wood of trees from Nelson and Southland, with 2 and 8 or 9 degrees of freedom.

Region	Tree 4	5	Region	Tree 3	5
30°C					
Nelson	0.56 ns	0.04 ns	Southland	0.37 ns	0.37 ns
40°C					
Nelson	0.17 ns	1.65 ns	Southland	0.11 ns	0.45 ns
50°C					
Nelson	4.25 ns	0.33 ns	Southland	2.10 ns	0.47 ns

** = P < 0.01 * = P < 0.05 ns = not statistically significant

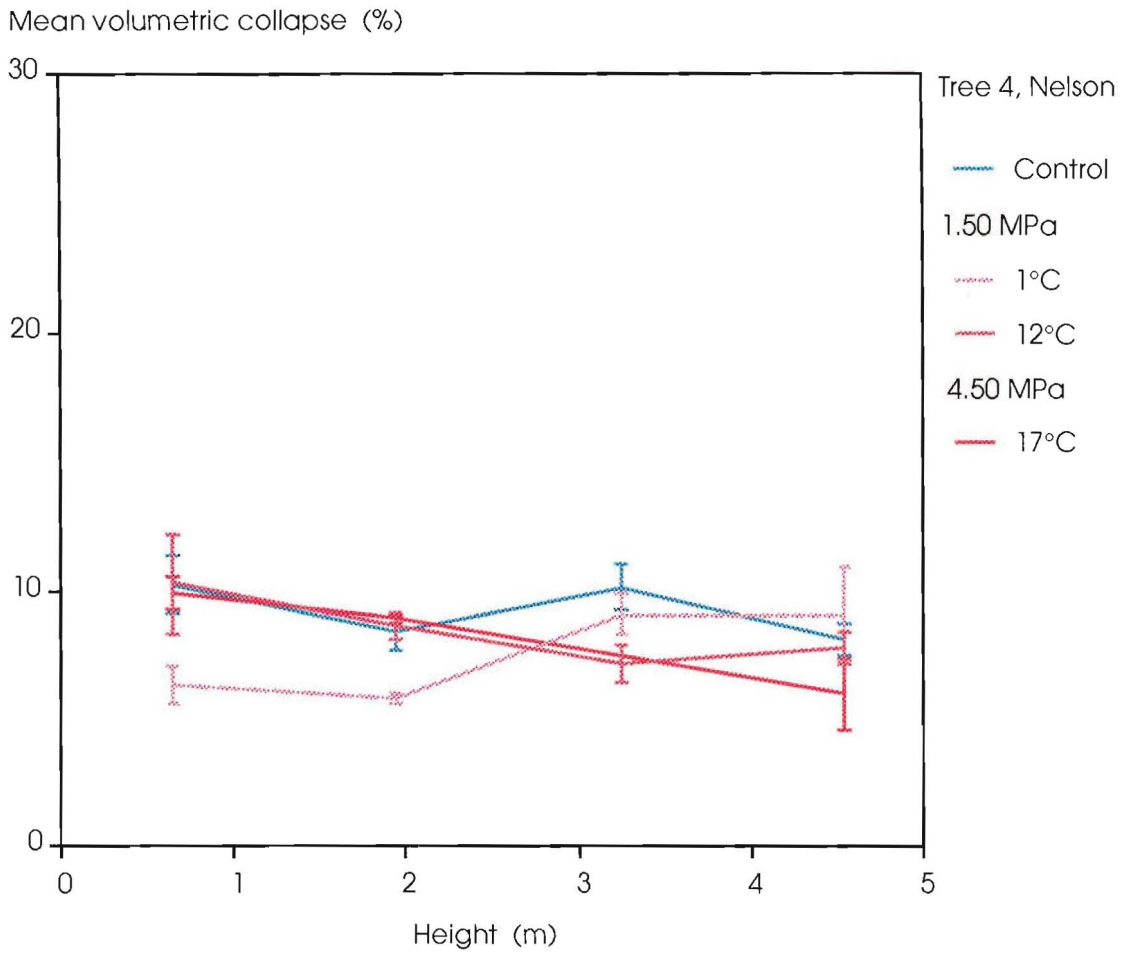

Figure 3.61 Mean volumetric collapse at 30 ° C in 1.5 and 4.5 MPa carbon dioxide gas treatment (1 and 12, and 17 ° C respectively) and control boards at various heights within trees of *Eucalyptus delegatensis* from Nelson and Southland. The error bars are standard errors of the means.

Anova table 3.20: Low pressure carbon dioxide gas treatments at 1.5 MPa and 1 and 12 ° C, and high pressure carbon dioxide gas treatment at 4.5 MPa and 17 ° C, and controls for volumetric collapse in wood dried at 30 ° C. Tree 4, Nelson.

Source of variation	*df*	*SS*	*MS*	F_S	
Among treatments	3	27.40	9.13	0.79	ns
Among heights within treatments	11	127.29	11.57	1.20	ns
Among boards within heights	31	298.02	9.61	2.41	**
Within boards	46	183.44	3.99		
Total	91	636.11			

** = P < 0.01 * = P < 0.05 ns = not statistically significant

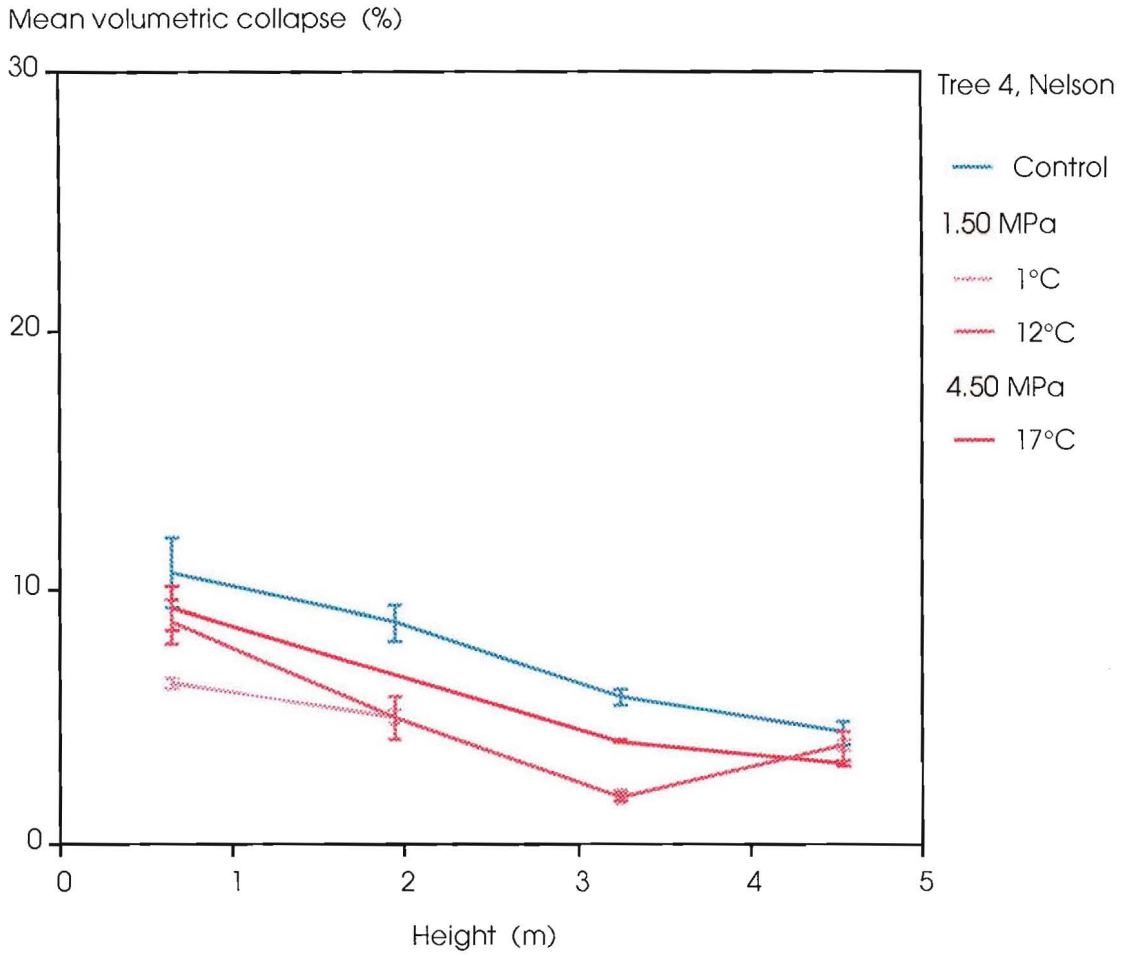

Figure 3.62 Mean volumetric collapse at 40 ° C in 1.5 and 4.5 MPa carbon dioxide gas treatment (1 and 12, and 17 ° C respectively) and control boards at various heights within trees of *Eucalyptus delegatensis* from Nelson and Southland. The error bars are standard errors of the means.

Anova table 3.21: Low pressure (1.5 MPa) carbon dioxide gas treatments at 1 and 12 ° C, and high pressure (4.5 MPa) carbon dioxide gas treatment at 17 ° C, and controls for volumetric collapse in wood dried at 40 ° C. Tree 4, Nelson.

Source of variation	*df*	*SS*	*MS*	F_S	
Among treatments	3	95.73	31.91	1.00	ns
Among heights within treatments	11	351.77	31.98	3.38	**
Among boards within heights	31	293.69	9.47	53.53	**
Within boards	46	8.13	0.18		
Total	91	741.36			

** = P < 0.01 * = P < 0.05 ns = not statistically significant

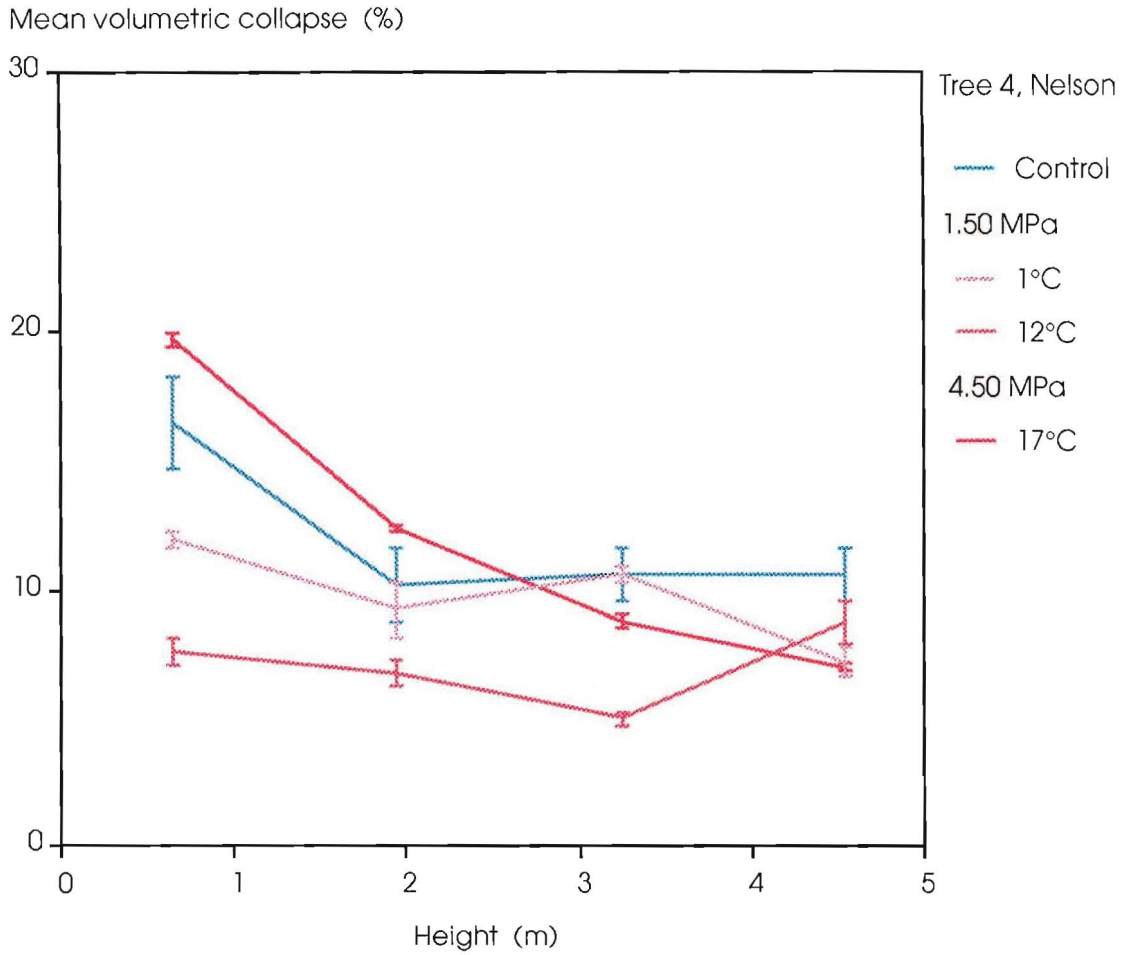

Figure 3.63 Mean volumetric collapse at 50 ° C in 1.5 and 4.5 MPa carbon dioxide gas treatment (1 and 12, and 17 ° C respectively) and control boards at various heights within trees of *Eucalyptus delegatensis* from Nelson and Southland. The error bars are standard errors of the means.

Anova table 3.22: Low pressure (1.5 MPa) carbon dioxide gas treatments at 1 and 12 ° C, and high pressure (4.5 MPa) carbon dioxide gas treatment at 17 ° C, and controls for volumetric collapse in wood dried at 50 ° C. Tree 4, Nelson.

Source of variation	*df*	*SS*	*MS*	F_S	
Among treatments	3	438.31	146.10	3.51	*
Among heights within treatments	12	499.31	41.61	1.79	ns
Among boards within heights	30	697.13	23.24	94.08	**
Within boards	46	11.34	0.25		
Total	91	1594.54			

** = P < 0.01 * = P < 0.05 ns = not statistically significant

3.10.5.3.3 Low pressure carbon dioxide gas treatments at 1.5 MPa and 1 and 12 ° C, and high pressure carbon dioxide gas treatment at 4.5 MPa and 17 ° C, and controls.

The effect of low, medium, and high carbon dioxide gas solubilities, prior to decompression, on volumetric collapse were examined in this analysis of variance. The carbon dioxide gas solubilities were 2.0 - 2.6, 3.3 - 3.7, and 4.6 - 5.2 g CO_2 / 100 g H_2O, for low pressure gas treatment at 12 and 1 ° C, and high pressure gas treatment respectively. The low pressure, low temperature gas treatment was applied only to boards from tree 4, Nelson. The analysis of variance was performed separately for each drying temperature (30, 40 and 50 ° C). There were no significant differences among treatments and controls at 30 and 40 ° C (Anova tables 3.20 and 3.21), but at 50 ° C significant differences did occur (Anova table 3.22). Figure 3.63 reveals, however, that while the differences in volumetric collapse of treatments and controls at 50 ° C may be sufficiently large to be statistically significant the ranking of treatments and control shows no evidence of a reduction of volumetric collapse with carbon dioxide gas treatment.

3.10.5.4 Shape variation in boards after drying

The collapse factor (CF) was used to analyse the variation of board shape after drying. Separate analysis of variance was performed for the collapse factor measurements of control boards at each drying temperature. Significant added variance of collapse factor was found among regions, among trees within regions, among height classes within trees, and among boards within height classes (Anova tables 3.23 - 3.25). The percentage contributions of the variance components of each level of the classification to the total variation of collapse factor in the wood sampled differed, however, from that found for volumetric collapse (table 3.15). The variance component among regions contributes 39.3 - 57.3 % of the total variation in collapse factor, the variance component among trees within regions 4.7 - 8.2 %, the variance component among height classes within trees 14.0 - 16.4 %, the variance component among boards within heights 15.7 - 34.3 %, and the variance component of collapse measurements within boards 1.9 - 8.3 %. The contribution of the variance

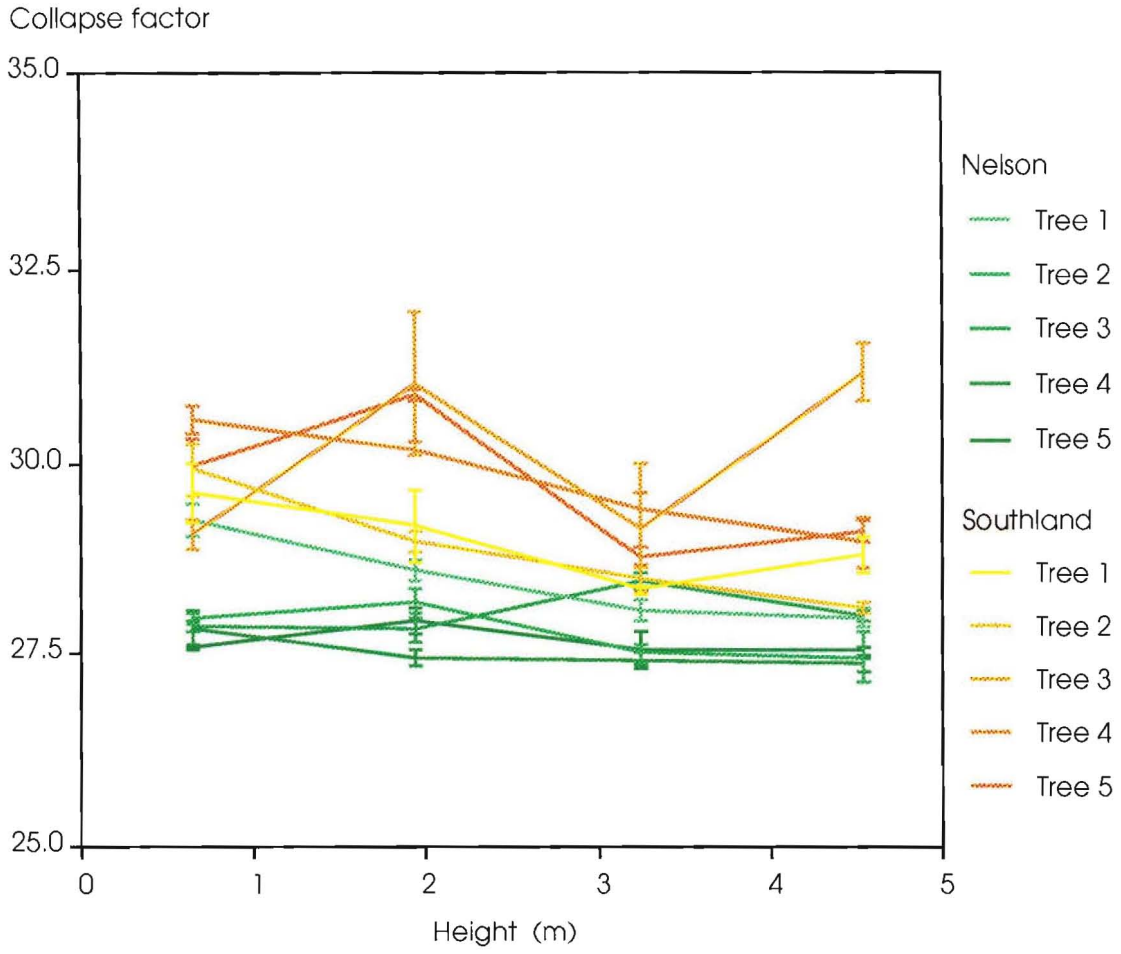

Figure 3.64 Mean collapse factor at 30 ° C in control boards at various heights within trees of *Eucalyptus delegatensis* from Nelson and Southland. The error bars are standard errors of the means.

Anova table 3.23: Analysis of variance of collapse factor in control boards dried at 30 ° C

Source of variation	df	SS	MS	F_S	
Among regions	1	186.23	186.23	30.47	**
Among trees within regions	8	48.90	6.11	2.07	ns
Among heights within trees	30	88.49	2.95	3.66	**
Among boards within heights	115	92.81	0.81	4.79	**
Within boards	155	26.13	0.17		
Total	309	455.49			

** = P < 0.01 * = P < 0.05 ns = not statistically significant

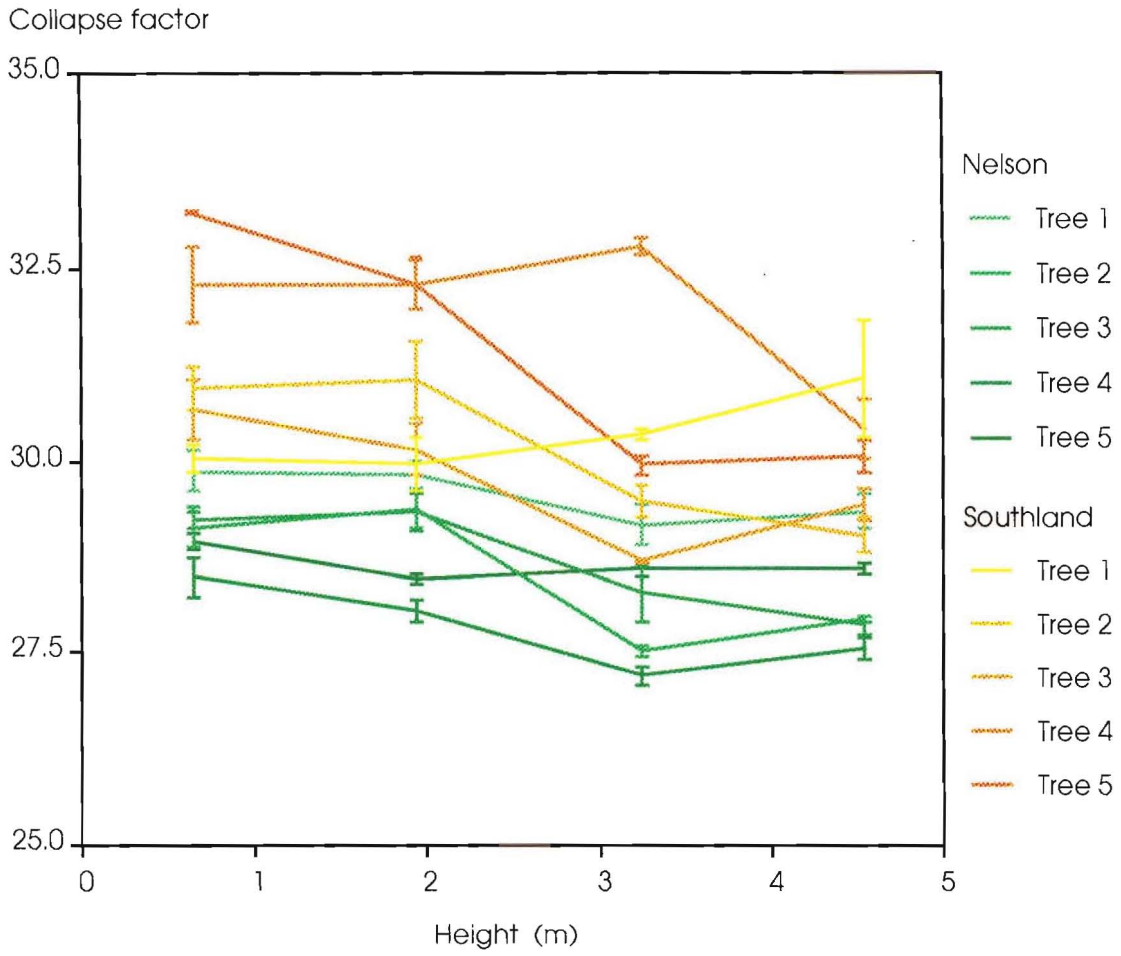

Figure 3.65 Mean collapse factor at 40 ° C in control boards at various heights within trees of *Eucalyptus delegatensis* from Nelson and Southland. The error bars are standard errors of the means.

Anova table 3.24: Analysis of variance of collapse factor in control boards dried at 40 ° C

Source of variation	df	SS	MS	F_S	
Among regions	1	255.55	255.55	19.71	**
Among trees within regions	8	103.73	12.97	2.67	*
Among heights within trees	30	145.68	4.86	3.68	**
Among boards within heights	101	133.30	1.32	23.70	**
Within boards	141	7.85	0.06		
Total	281	703.96			

** = P < 0.01 * = P < 0.05 ns = not statistically significant

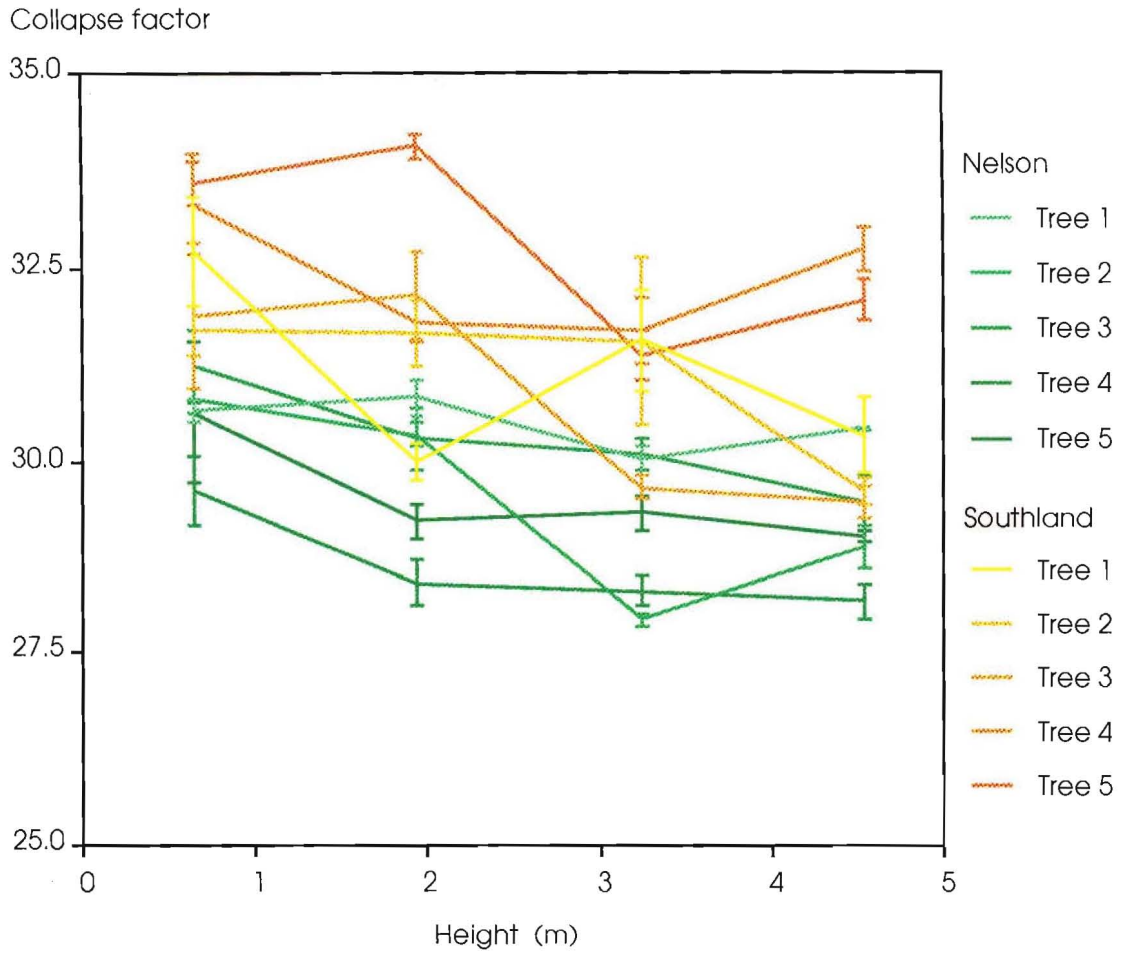

Figure 3.66 Mean collapse factor at 50 ° C in control boards at various heights within trees of *Eucalyptus delegatensis* from Nelson and Southland. The error bars are standard errors of the means.

Anova table 3.25: Analysis of variance of collapse factor in control boards dried at 50 ° C

Source of variation	df	SS	MS	F_S	
Among regions	1	295.11	295.11	15.07	**
Among trees within regions	8	156.61	19.58	2.43	*
Among heights within trees	30	241.38	8.05	2.50	**
Among boards within heights	119	382.61	3.22	17.04	**
Within boards	159	29.99	0.19		
Total	317	1209.36			

** = P < 0.01 * = P < 0.05 ns = not statistically significant

component among regions is similar to that observed for volumetric collapse, and constitutes the largest source of variation of collapse factor in the wood sampled. The contribution of the variance component among trees within regions is, however, much smaller than that for volumetric collapse. For drying at 30 ° C, the differences in collapse factor between trees, particularly for the Nelson region (figure 3.64), were such that nosignificant difference was detected between them (Anova table 23). The variance component for collapse factor among trees within regions at 30 ° C is only 4.7 % of the total variation (table 3.15).

Table 3.15 Percentage contribution of variance components of collapse factor

Variance component	Percentage of total variation
30°C	
Among regions	57.3
Among trees within regions	4.7
Among heights within trees	14.0
Among boards within heights	15.7
Within boards	8.3
40°C	
Among regions	53.9
Among trees within regions	8.2
Among heights within trees	16.4
Among boards within heights	19.6
Within boards	1.9
50°C	
Among regions	39.3
Among trees within regions	7.8
Among heights within trees	14.3
Among boards within heights	34.3
Within boards	4.3

The contribution of the variance component among height classes within trees is similar to that for volumetric collapse, but the contribution of the

variance component for boards within height classes is higher, tending to increase with temperature and increasing sharply at 50 ° C. Possibly differences in radial and circumferential position become more important at higher drying temperatures.

3.10.5.4.1 Effect of temperature treatments

The collapse factor (CF) measurements of control boards were analysed for differences among temperature treatments (30, 40 and 50 ° C). No significant differences were detected when the data from both regions was used in the analysis of variance, F-value = 1.14 with 2 and 3 degrees of freedom, but when the data was analysed separately for each region, highly significant differences among temperature treatments were found (Anova tables 3.26 and 3.27). For boards from Nelson there was a marked but gradual increase in collapse factor from 30 to 50 ° C, with larger differences in board shape occuring between trees at 40 and 50 ° C. For boards from Southland, there was a very substantial increase in collapse factor with an increase in drying temperature from 30 to 40 ° C, the increase being much larger for the boards from some trees than others.

Anova table 3.26: Temperature treatments at 30, 40 and 50 ° C, for the collapse factor of control boards from Nelson.

Source of variation	df	SS	MS	F_S	
Among treatments	2	232.66	116.33	11.01	**
Among trees within treatments	12	126.84	10.57	3.35	**
Among heights within trees	45	142.10	3.16	4.02	**
Among boards within heights	179	140.45	0.79	9.02	**
Within boards	239	20.66	0.09		
Total	477	670.40			

** = P < 0.01 * = P < 0.05 ns = not statistically significant

Anova table 3.27: Temperature treatments at 30, 40 and 50 ° C, for the collapse factor of control boards from Southland.

Source of variation	df	SS	MS	F_S	
Among treatments	2	330.02	165.01	10.86	**
Among trees within treatments	12	182.40	15.20	2.05	*
Among heights within trees	45	333.45	7.41	2.47	**
Among boards within heights	156	468.26	3.00	14.94	**
Within boards	216	43.31	0.20		
Total	431	1428.24			

** = P < 0.01 * = P < 0.05 ns = not statistically significant

3.10.5.4.2 Effect of carbon dioxide gas treatments

Analysis of variance were performed for the effects of carbon dioxide gas treatments on collapse factor, but no significant differences were found. The similarity of the results, to those obtained for volumetric collapse meant that no presentation was necessary.

3.10.6 Internal checking

Marked differences occured in the incidence of internal checking in boards from Nelson and Southland. The percentage of boards with internal checks increased with temperature for the Nelson region, from 3.3 % at 30 ° C to 14.6 % at 50 ° C (figure 3.67, and table 3.16). For the Southland region, there was a small decline with temperature in the percentage of boards with internal checks, from 35.2 % at 30 ° C to 27.3 % at 50 ° C. However, this reflects the increase in the severity of drying collapse with increasing temperature. With very severe collapse the incidence of internal checking declines. This can be seen in the large range of values for the percentage of boards with internal checks among trees from the Southland region (table 3.16). Trees 4 and 5 have the lowest incidence of boards with internal

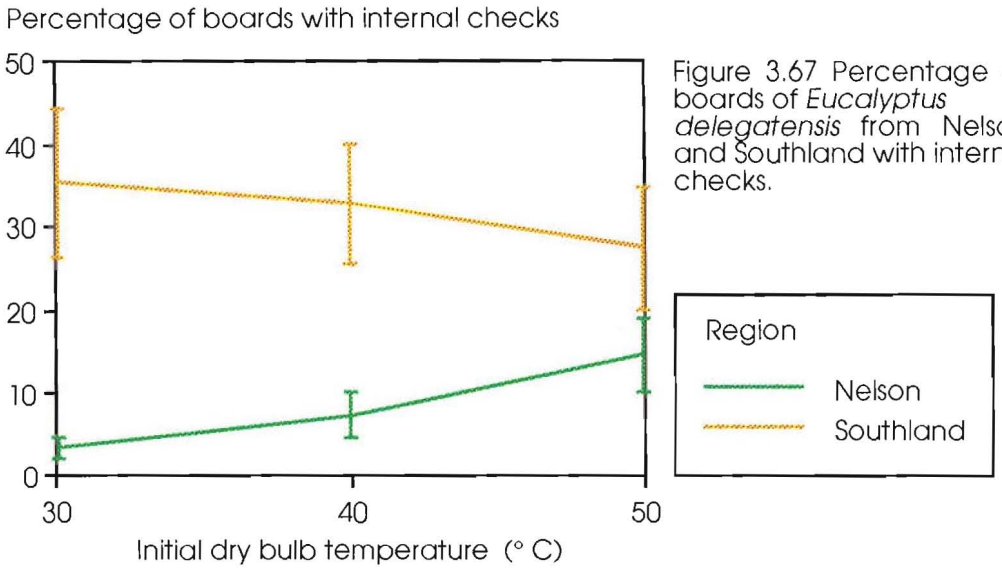

Figure 3.67 Percentage of boards of *Eucalyptus delegatensis* from Nelson and Southland with internal checks.

Table 3.16 Internal drying checks in boards of *Eucalyptus delegatensis* from Nelson and Southland

Region	Percentage of boards with internal drying checks Initial dry bulb temperature (° C) 30	40	50
Nelson			
Tree 1	0.0	9.7	18.7
" 2	6.4	11.1	13.9
" 3	0.0	14.7	26.5
" 4	6.2	2.1	12.5
" 5	2.8	0.0	0.0
Average	3.3	7.3	14.6
Southland			
Tree 1	56.2	43.2	44.4
" 2	33.3	27.5	22.5
" 3	57.6	56.7	46.7
" 4	23.3	19.2	15.4
" 5	11.9	20.4	11.4
Average	35.2	32.7	27.3

checks, but correspondingly, very high levels of drying collapse (figures 3.42 - 3.44).

Differences are also apparent between the two regions, when boards with internal checks are classified according to the number of internal checks per board (figure 3.68). A very large majority of the boards from Nelson with internal checks have only one internal check. A small percentage of

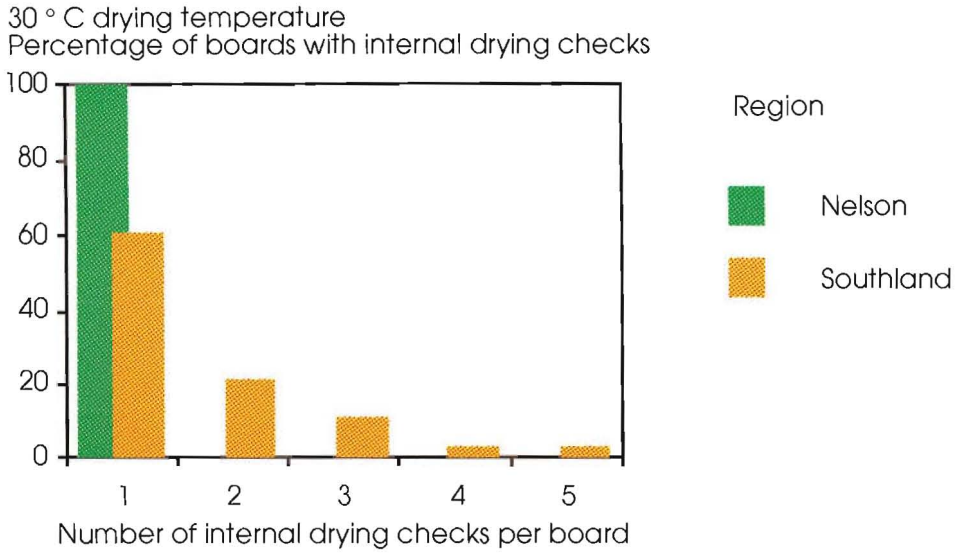

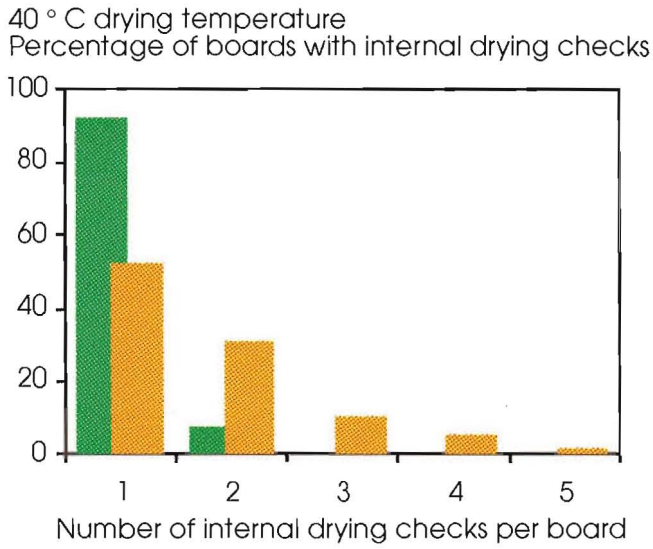

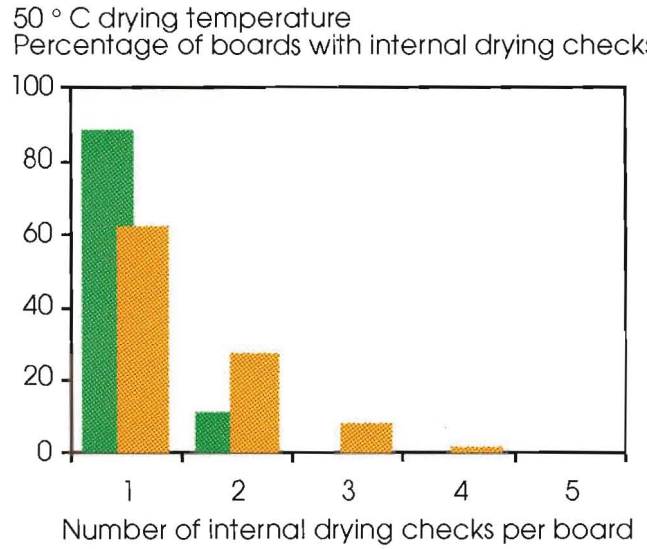

Figure 3.68 Percentages of boards of *Eucalyptus delegatensis* from Nelson and Southland with different numbers of internal checks.

the boards dried at 40 and 50 ° C have two checks. The majority of boards from Southland with internal checks have also only one internal check, but more than 20 % of the boards have two checks, and smaller percentages of boards have three, four and even five internal checks per board. Internal checking, therefore, is much more severe in boards from Southland than Nelson.

3.10.7 Variation of basic density in the wood sampled

There are significant added variance components of basic density among regions, among trees within regions, among heights classes within trees, and among boards within height classes (Anova table 3.28). The percentage contributions of the variance components of each level of the classification, to the total variation of basic density in the wood sampled, are shown in table 3.17, for the boards dried at 30 ° C. Similar results were obtained for the variation of basic density in boards dried at 40 and 50 ° C. The variance component among regions contributes 46.6 % of the total variation in basic density, the variance component among trees within regions 35.9 %, the variance component among height classes within trees 3.1 %, the variance component among boards within heights 11.7 %, and the variance component of collapse measurements within boards 2.7 %. The variation of basic density among regions is the largest source of variation of basic density in the wood sampled. The variation of basic density among trees within regions is also large. The impact of this can be seen in figure 3.69. Large differences in basic density occur among trees, particularly for the Nelson region where basic densities are generally very much higher than those of Southland. Two trees, one from each region, however, show very large departures in basic density from that of other trees in their region. Tree 5 from Nelson has basic densities that are equivalent to those found in the majority of trees from Southland, while tree 4 from Southland has basic densities in the lower end of the range of basic densities found in the majority of Nelson trees. The low level of basic density variation found among height classes within trees is reflected in the small increase in basic density for each tree, from 0 to 5 metres height. The somewhat higher variation of basic density within height classes can probably be largely attributed to differences in radial and circumferential position. The variation of basic density within boards is

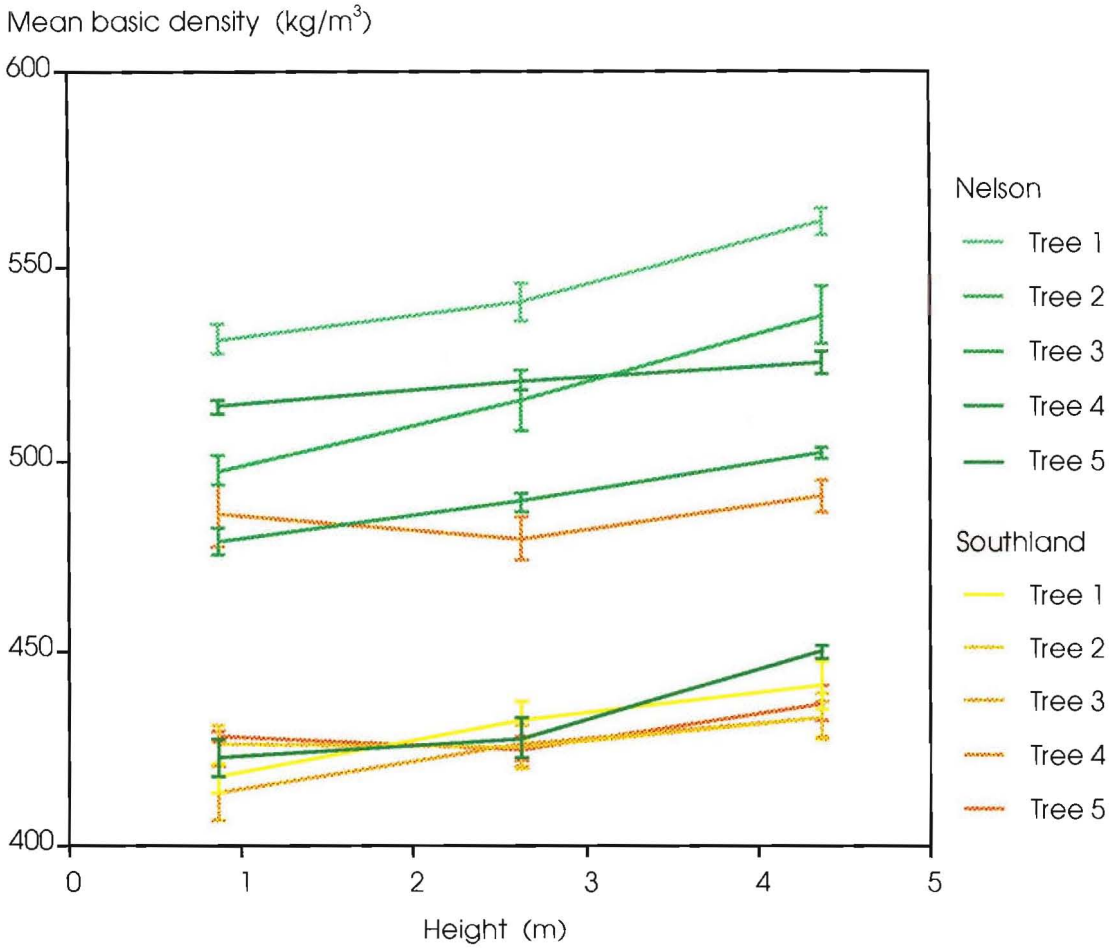

Figure 3.69 Mean basic density in boards at various heights within trees of *Eucalyptus delegatensis* from Nelson and Southland, dried at 30 ° C. The error bars are standard errors of the means.

Anova table 3.28: Basic density of the wood of collapse boards dried at 30 ° C

Source of variation	df	SS	MS	F_S	
Among regions	1	503214.71	503214.71	7.28	*
Among trees within regions	8	552847.78	69105.97	26.79	**
Among heights within trees	20	51581.21	2579.06	4.19	**
Among boards within heights	373	229489.09	615.25	7.73	**
Within boards	222	17675.79	79.62		
Total	624	1580288.53			

** = P < 0.01 * = P < 0.05 ns = not statistically significant

Table 3.17 Percentage contribution of variance components of basic density

Variance component	Percentage of total variation
Wood dried at 30 ° C	
Among regions	46.6
Among trees within regions	35.9
Among heights within trees	3.1
Among boards within heights	11.7
Within boards	2.7

small, which indicates that over the length of the boards (0.5 m between basic density measurements at each end), basic density does not differ much.

3.10.8 Correlation between drying collapse and basic density

The product-moment correlation coefficient was used to measure the intensity of association between volumetric collapse and basic density. A correlation coefficient of -0.41 was found between volumetric collapse at 50 ° C and basic density (figure 3.70). The *t*-test of the significance of the correlation coefficient, which is based on 690 observations, gives a critical value, for 500 degrees of freedom, of ± 0.115 at the 1 % level of significance. The observed correlation coefficient is larger than the critical value, which indicates that the association between volumetric collapse and basic density is greater than could be expected by chance.

The small size of the correlation coefficient, and the large spread of points in figure 3.70, indicates that mean basic density, provides a poor measurement of the structural features responsible for drying collapse in wood.

3.10.9 Inter- and intra-incremental variation in basic density

Radial variation in basic density within and between growth rings was measured using sequences of very thin radial sections taken from collapse boards. Marked differences in the pattern of radial density variation were

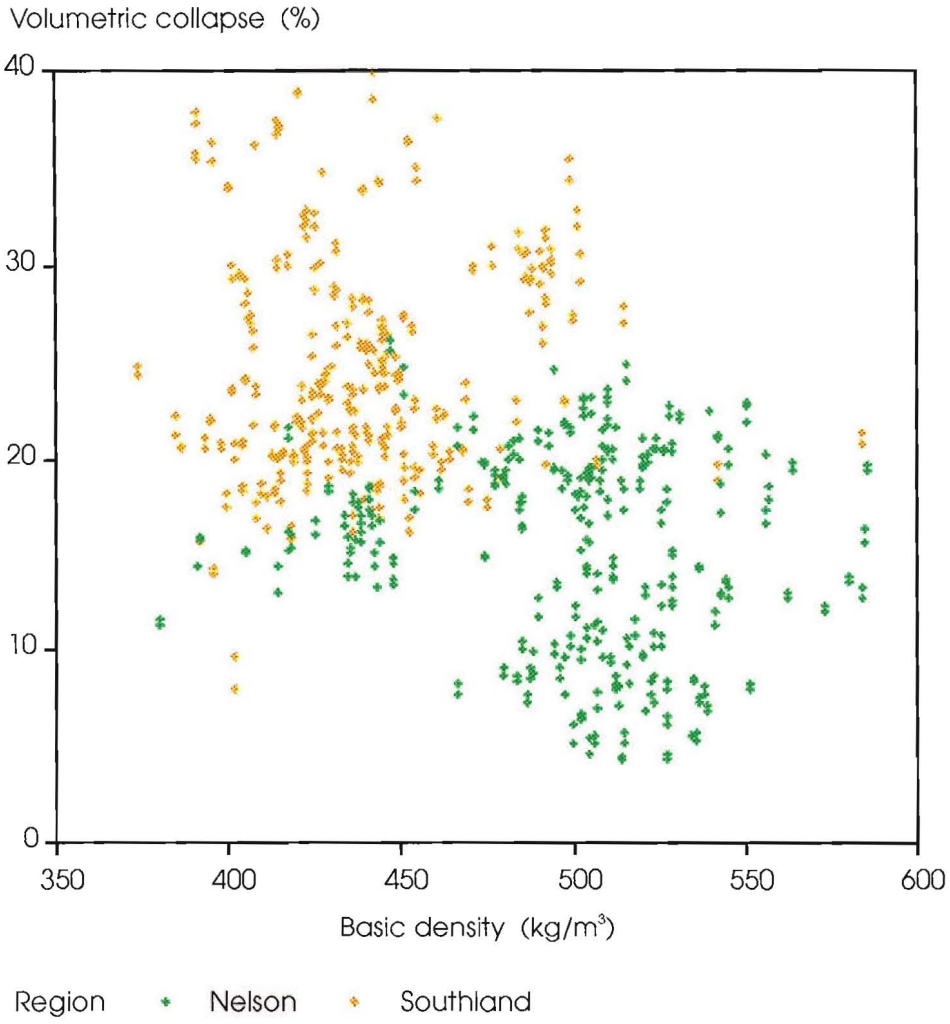

Figure 3.70 Correlation between volumetric collapse at 50 ° C and basic density.

observed among trees, particularly for those from Southland (figure 3.71). The pattern of earlywood and latewood was well defined and regular in form, in the wood from Nelson. The high mean basic densities of the wood of most trees (figure 3.69) could be attributed to the large proportion of high density latewood within each growth ring. The pattern of earlywood and latewood was far more variable in the wood from Southland. Tree 1, Southland, had a regular pattern of clearly defined latewood, similar to that found in Nelson trees, but only a low proportion of latewood within each growth ring resulting in low mean basic densities (figure 3.69). Other trees, such as trees 3 and 4, Southland, had far more irregular and gradual transitions from earlywood to latewood within growth rings. There were large variations in latewood basic densities, such as for tree 4, Southland, that resulted for most trees, in low mean basic densities.

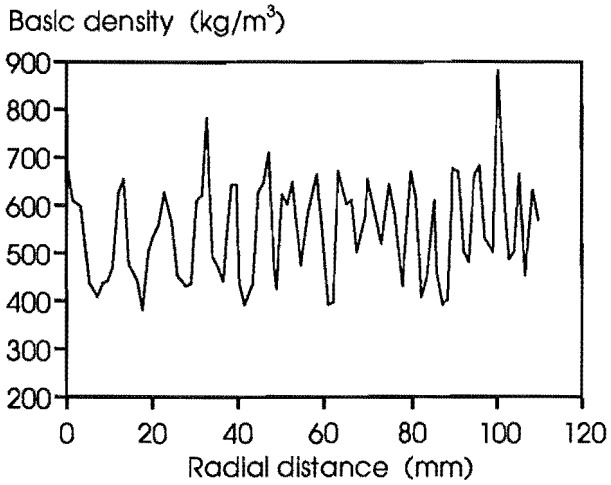

Tree 1, Nelson

Height 4.58 m

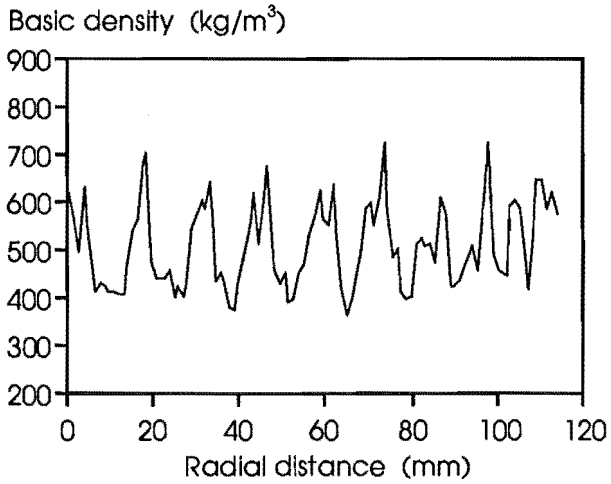

Tree 2, Nelson

Height 0.38 m

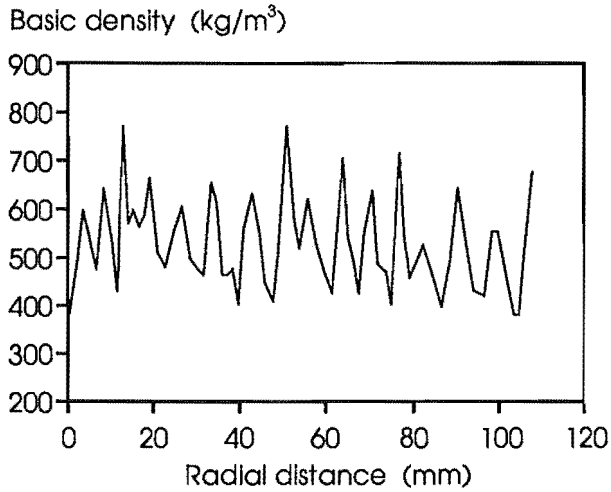

Tree 4, Nelson

Height 2.58 m

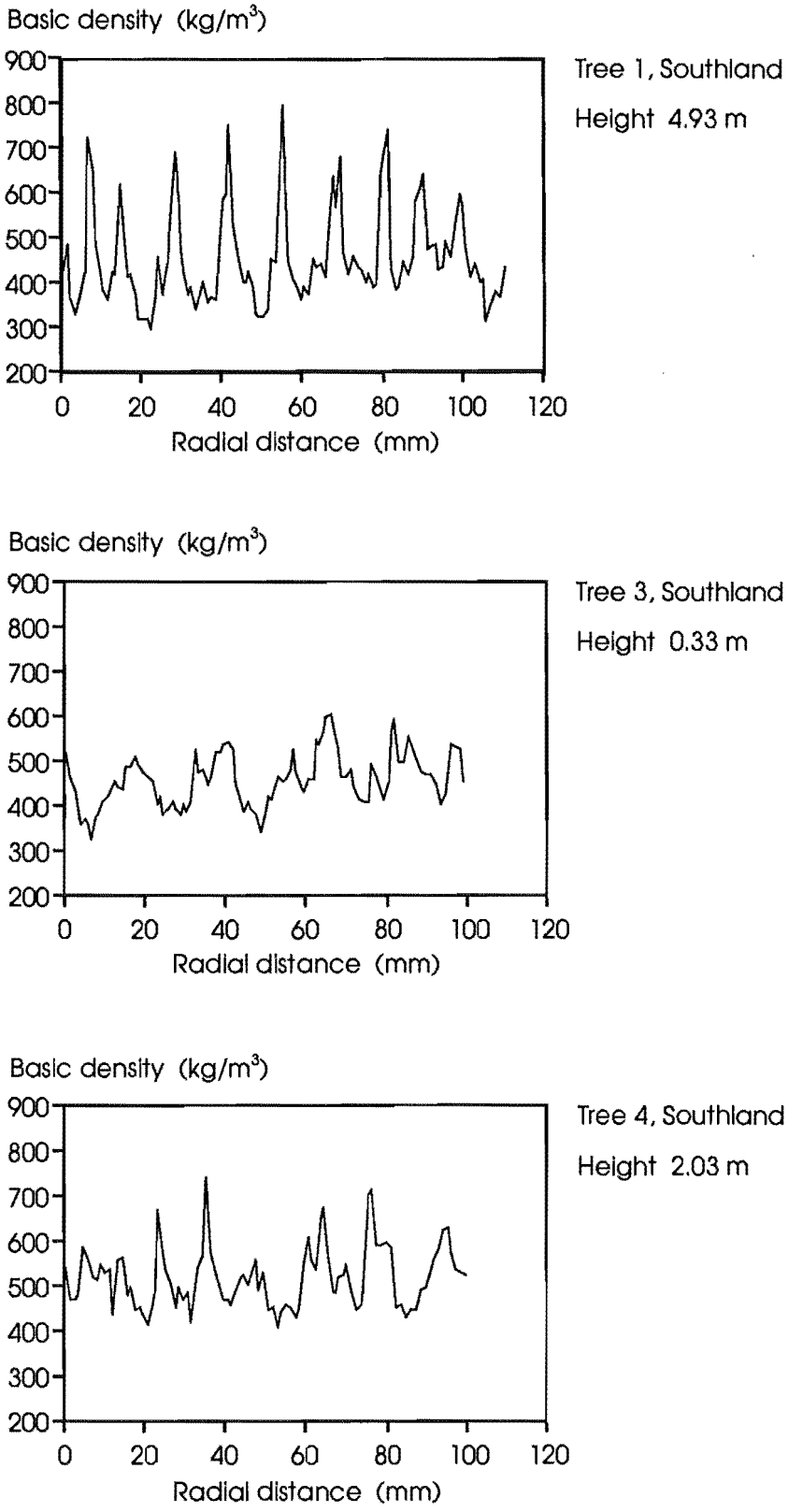

Figure 3.71 Inter- and intra-incremental variation in basic density of radial sections of collapse boards from Nelson and Southland.

3.11 Discussion

The wood properties of *Eucalyptus*, when grown as exotics, are affected by the environment into which they are introduced, and the strength of the genetic control imposed by the seed source. Little is known of the variation in wood properties of *Eucalyptus delegatensis* when grown as an exotic, but, generally, *Eucalyptus* have shown no major differences in wood properties when grown as an exotic in differing environments (Zobel and van Buijtenen 1989). Differences in the wood properties of *Eucalyptus* grown from different provenances within a species have been observed in exotic plantations, but the effects have usually been small. The major source of seed related variation has been that occuring among individual trees within a stand (Zobel and van Buijtenen 1989).

The variation of collapse susceptibility in *Eucalyptus delegatensis* has, however, been studied in natural regrowth stands, within its indigenous range in Australia, by Ilic and Hillis (1985). Very significant differences were found between five geographic sources of *E. delegatensis*, and between trees within each source. Significant differences were also found within trees, changing with height and radial position. The geographic variation of collapse susceptibility in natural stands can be caused by both environmental and genetic factors. The relative importance of each in controlling the variation in collapse susceptibility is unknown. The significant differences between trees within each geographic source indicates strong genetic control of collapse susceptibility among individual trees growing within each environment.

It is believed that the trees of *Eucalyptus delegatensis* from Nelson and Southland, used in this study of drying collapse, are both from the West Tapanui Forest ("Crookston" strain) seed source. This was used in plantings of *E. delegatensis* in both Southland (Longwood Forest), and in Golden Downs Forest, Nelson (Wilcox 1980). The West Tapanui Forest seed source is of mainland (New South Wales or Victoria) origin, judging from seedling morphology and bark characteristics, and is of probably a very restricted genetic base (Wilcox 1980). This would suggest that the significant differences in drying collapse and basic density observed between the two regions are caused by environmental rather than genetic factors. It indicates that there is strong environmental control over the

average drying collapse and basic density of the population of trees within each region. The significant differences in drying collapse and basic density among trees within each region indicates that there is strong genetic control of these two wood properties among individual trees within each environment. Given that wood properties are generally strongly inherited (Zobel and van Buijtenen 1989), the large variation in drying collapse and basic density among trees within each region suggests that there is potential for individual tree selection on the basis of these wood properties. Heritabilities for basic density in *Eucalyptus* species are strong, a narrow sense heritability of 0.61 was obtained by Otegbeye and Kellison (1980) for young trees of *E. viminalis* grown in Georgia, USA, and a broad sense heritiability of 0.54 was obtained by Malan (1988) for nine year old trees of *E. grandis* grown in South Africa.

The response of drying collapse to temperature was not as great statistically as might have been expected from visual assessment of figures 3.42 - 3.50. This was attributed to the very uneven response to temperature among trees, and among height classes within trees, figure 3.51. The way in which drying collapse affected board cross-sectional shape did, however, appear to be more consistent with temperature. Board collapse factor, a measurement quantifying the cross-sectional shape of dried boards, showed a very significant response to temperature. The dried boards of each tree, and each region, showed a very consistent and distinctive visual pattern of collapse, in terms of cross-sectional profiles or washboarding. It was the severity rather than the pattern of collapse that appeared to change with temperature. The cross-sectional profiles or washboarding that characteristed the wood of each tree, and region, became more accentuated with increasing temperature. These changes in board shape, reflected in the increasing ratio of the square of the cross-sectional perimeter to cross-sectional area, that makes up the collapse factor measurement provide a more consistent and sensitive measurement of the effect of temperature on wood than drying collapse.

The introduction of carbon dioxide gas to the wood, prior to drying, at solubilities of up to 5.2 g CO_2 / 100 g H_2O, had no effect on drying collapse or board shape. Though gas loss from the wood is rapid after decompression, particularly at higher temperatures, the residence time of the gas in the wood is thought to be sufficient given the development of

collapse during the initial stages of drying. Collapse at 40 ° C was observed to be essentially complete within four days of the start of drying. The question then arises as to whether the nucleation of gas bubbles does take place from a supersaturated state within the cells. Without nucleation sites the gas may remain in solution in the cell, with subsequent loss through the cell walls via dissolved gas diffusion. The ability to form bubbles within cells may be more difficult than previously thought. Booker (1989) found no effect on collapse of attempts to create vapour bubbles within cells by cavitation, through impact hammering a stack of wood during drying.

Microdensity variations were mentioned by Ilic and Hillis (1986) as a feature affecting drying collapse. Given the poor correlation between mean basic density and drying collapse (figure 3.70) it was thought that the inter- and intra-incremental variation of basic density within boards might provide some explanation for the differences in drying collapse and board shape observed among trees, and among regions. The boards from Nelson, generally had a large proportion of high basic density latewood within each growth ring, that were clearly demarcated from the earlywood in terms of density (figure 3.71). These latewood bands effectively resisted drying collapse, restricting collapse to the earlywood, and reducing changes in board shape by restraining the depth of earlywood washboarding. Severe collapse in Southland boards, by contrast, was unrestrained by the latewood, with collapse occuring across entire growth rings. The variable basic density of the latewood, the generally lower proportion of latewood within each growth ring, and the sometimes, gradual transitions in basic density between earlywood and latewood were factors that probably contributed to the difference. These differences in inter- and intra-incremental density variation don't, however, explain why the earlywood of some trees, such as trees 4 and 5, from Nelson, showed such little collapse and change in board shape, or why the collapse was so severe in trees 4 and 5, from Southland. It really only provides an explanation of why the differences in drying collapse and board shape between the two regions were so large. Factors other than density, it appears, are responsible for the differences in drying collapse between trees.

3.12 Summary

Eucalyptus delegatensis wood grown in Nelson and Southland, New Zealand, shows significant differences in drying collapse, board shape, and basic density among the two regions, among trees within the regions, and among height classes within the trees. The largest source of variation in drying collapse, board shape, and basic density occurs among the two regions. This is attributed to the strong environmental control of these wood properties. The smaller, but significant, source of variation among trees within regions suggests that there is strong genetic control of these wood properties among trees within each environment.

Drying temperature had a significant effect on drying collapse and board shape, but carbon dioxide gas treatment had no effect on either. The response of drying collapse to temperature varied greatly among regions, among trees within regions, and among height classes within trees. Board shape showed a more consistent response with temperature than other measurements of drying collapse.

The differences in drying collapse and board shape among the regions can be attributed to regional differences in the pattern of inter- and intra-incremental basic density variation. The differences in drying collapse and board shape that occured among trees within the regions were, it appears, caused by factors other than density.

Subsequent analysis of the data will assess the board edge and end effects on volumetric, tangential and radial drying collapse. Further assessment of the patterns of inter- and intra-incremental basic density variation could also be made. While the variation of drying collapse and board shape among the regions, Nelson and Southland, has been linked to differences in the pattern of inter- and intra-incremental basic density variation, the technique used provided only a broad-based view of the picture. The application of x-ray densitometry would provide a more comprehensive assessment of the micro-density patterns of inter- and intra-incremental basic density variation.

The genetic control of drying collapse variation among trees within regions could be applied in tree breeding programs of *Eucalyptus*

delegatensis. Further information from progeny trials, such as heritabilities and phenotypic and genotypic correlations with other wood properties, would, however, be required to ascertain what genetic changes were possible and how rapidly these changes could be achieved.

References

Babbitt, J. D., 1942, On the adsorption of water vapour by cellulose, *Canadian Journal of Research*, A-20, 143 - 172.

Bamber, R. K., 1976, Heartwood, its function and formation, *Wood Science and Technology*, 10(1), 1 - 8.

Bland, D. E., 1971, The relation of lignin and polyphenol content of Tasmanian Alpine Ash (*Eucalyptus delegatensis*) to shrinkage and recovery, *Wood Science and Technology*, 5(1), 17 - 26.

Booker, R. E., 1987, A method for recording annual ring orientation in boards, *Forest Products Journal*, 37(6), 31 - 33.

Booker, R. E., 1989, Direction of future research on the prevention of collapse, *Second Pacific Regional Wood Anatomy Conference, Laguna, Philippines*, 1 - 8.

Boone, R. S., Kozlik, C. J., Bois, P. J. and Wengert, E. M., 1988, Dry kiln schedules for commercial woods - temperate and tropical, United States Forest Service, Forest Products Laboratory General Technical Report, No. 57, 158 pp.

Bosshard, H. H., 1968, On the formation of facultatively colored heartwood in *Beilschmiedia tawa*, *Wood Science and Technology*, 2(1), 1 - 12.

Briggs, L. J., 1950, Limiting negative pressure of water, *Journal of Applied Physics*, 21(7), 721 - 722.

Campbell, G. S., 1980, Index of kiln drying schedules for timbers dried in Australia, *Division of Building Research, CSIRO, Australia*, 25 pp.

Chafe, S. C., 1985, The distribution and interrelationship of collapse, volumetric shrinkage, moisture content and density in trees

of *Eucalyptus regnans, Wood Science and Technology,* 19(4), 329 - 345.

Chafe, S. C., 1986, Radial variation of collapse, volumetric shrinkage, moisture content and density in *Eucalyptus regnans, Wood Science and Technology,* 20(3), 253 - 262.

Chafe, S. C., 1987, Collapse, volumetric shrinkage, specific gravity and extractives in *Eucalyptus* and other species. Part 2: The influence of wood extractives, *Wood Science and Technology,* 21(1), 27 - 41.

Craver, J. K., 1970, A classification of hydrogen-bonding solvents by sonic velocity measurements, *Journal of Applied Polymer Science,* 14, 1755 - 1765.

CSIRO, 1964, Timber seasoning: Collapse and recovery. (i) Factors affecting collapse. (ii) The theory of collapse, *Report of the Division of Forest Products, CSIRO, Australia,* 39 - 40.

Dodds, W. S., Stutzman, L. F. and Sollami, B. J., 1956, Carbon dioxide solubility in water, *Industrial and Engineering Chemistry: Chemical and Engineering Data Series,* 1(1), 92 - 95.

Doran, J. C., 1975, Occurrence of kino veins in two provenance trials of *Eucalyptus regnans, Australian Forest Research,* 7(1), 21 - 27.

Ellwood, E. L., Ecklund, B. A. and Zavarin, E., 1960, Collapse in wood ... exploratory experiments in its prevention, *Forest Products Journal,* 10(1), 8 - 21.

Fell, J. D. and Hill, J. L., 1980, Sampling levels for hardwood kiln-drying control, *Forest Products Journal,* 30(3), 32 - 36.

Ferrand, J. Ch., 1982, Growth stresses and silviculture of eucalypts, *Australian Forest Research,* 13(1), 75 - 81.

Gordy, W., 1939, Spectroscopic comparison of the proton-attracting properties of liquids, *Journal of Chemical Physics*, 7(2), 93 - 99.

Haehnel, O., 1920, The strength of carbonic acid at higher pressures, *Zentralblatt fur Mineralogie, Geologie und Palaontologie*, 25 - 32.

Harris, J. M., 1975, Physical properties of New Zealand grown eucalypts 1. *Eucalyptus delegatensis* grown in Kaingaroa Forest, *Forest Products Division Wood Quality Report, Forest Research Institute, New Zealand*, No. 4, 9 pp. (Unpublished).

Haslett, A. N., 1988a, Properties and utilisation of exotic speciality timbers grown in New Zealand. Part V: Ash eucalypts and *Eucalyptus nitens, Forest Research Institute Bulletin, New Zealand*, No. 119, 20 pp.

Haslett, A. N., 1988b, Handling and grade-sawing plantation-grown eucalypts, *Forest Research Institute Bulletin, New Zealand*, No. 142, 72 pp.

Hawley, L. F., 1931, Wood-liquid relations, *United States Department of Agriculture Technical Bulletin*, No. 248, 33 pp.

Ilic, J. and Hillis, W. E., 1984, Association of wood anatomy with collapse in ash-type eucalypts, *Pacific Regional Wood Anatomy Conference, Tsukuba, Japan*, 19 - 21.

Ilic, J. and Hillis, W. E., 1985, Variation in collapse in the dried wood of regrowth ash-type eucalypts, *Symposium on Forest Products Research, International achievements and the future, Pretoria, South Africa*, Vol. 3, Paper No. 8-4, 10 pp.

Ilic, J. and Hillis, W. E., 1986, Prediction of collapse in dried eucalypt wood, *Holzforschung*, 40(2), 109 - 112.

Jacobs, M. R., 1939, Further studies on fibre tension, *Bulletin, Commonwealth Forestry Bureau, Australia*, No. 24, 36 pp.

Jacobs, M. R., 1945, The growth of woody stems, *Bulletin, Commonwealth Forestry Bureau, Australia*, No. 28, 67 pp.

Kajita, H., Mukudai, J. and Yata, S., 1979, The interaction of wood with organic solvents, *Mokuzai Gakkaishi - Journal of the Japan Wood Research Society*, 25(2), 95 - 102.

Kauman, W. G., 1958, The influence of drying stresses and anisotropy on collapse in *Eucalyptus regnans, Division of Forest Products Technological Paper, CSIRO, Australia*, No. 3, 16 pp.

Kauman, W. G., 1960a, Collapse in some eucalypts after treatment in inorganic salt solutions, *Forest Products Journal*, 10(9), 463 - 467.

Kauman, W. G., 1960b, Contributions to the theory of cell collapse in wood: Investigations with *Eucalyptus regnans, Australian Journal of Applied Science*, 11(1), 122 - 145.

Kauman, W. G., 1964, Cell collapse in wood, *Division of Forest Products Reprint, CSIRO, Australia*, No. 566, 65 pp.

Kubler, H., 1987, Growth stresses in trees and related wood properties, *Forest Products Abstracts*, 10(3), 61 - 119.

McMillen, J. M., 1955a, Drying stresses in red oak, *Forest Products Journal*, 5(1), 71 - 76.

McMillen, J. M., 1955b, Drying stresses in red oak: Effect of temperature, *Forest Products Journal*, 5(4), 230 - 241.

Malan, F. S., 1988, Genetic variation in some growth and wood properties among 18 full-sib families of South African grown *Eucalyptus grandis*: A preliminary investigation, *South African Forestry Journal*, No. 146, 38 - 43.

Milligan, R. H., 1979, The native pinhole borers, *Forest and Timber Insects in New Zealand, Forest Research Institute, New Zealand*, No. 37, 15 pp.

Nayer, A. N. and Hossfeld, R. L., 1949, Hydrogen bonding and the swelling of wood in various organic liquids, *Journal of the American Chemical Society*, 71(8), 2852 - 2855.

Nicholls, J. W. P. and Matheson, A. C., 1980, Variation in wood characteristics in thinnings from a field trial of *Eucalyptus obliqua*, *Australian Forest Research*, 10(3), 239 - 247.

Nicholson, J. E., 1971, A rapid method for estimating longitudinal growth stresses in logs, *Wood Science and Technology*, 5(1), 40 - 48.

Nicholson, J. E., 1973, Growth stress differences in eucalypts, *Forest Science*, 19(3), 169 - 174.

Nicholson, J. E., Campbell, G. S. and Bland, D. E., 1972, Association between wood characteristics and growth stress level: A preliminary study, *Wood Science*, 5(2), 109 - 112.

Nicholson, J. E. and Ditchburne, N., 1973, Shrinkage prediction based on analysis of three wood properties, *Wood Science*, 6(2), 188 - 189.

Nicholson, J. E., Hillis, W. E. and Ditchburne, N., 1975, Some tree growth - wood property relationships of eucalypts, *Canadian Journal of Forest Research*, 5(3), 424 - 432.

Otegbeye, G. O. and Kellison, R. C., 1980, Genetics of wood and bark characteristics of *Eucalyptus viminalis*, *Silvae Genetica*, 29(1), 27 - 31.

Pankevicius, E. R., 1961, Influence of position in tree on recoverable collapse in wood, *Forest Products Journal*, 11(3), 131 - 132.

Raczkowski, J., 1963, The swelling heat of wood, *Fifth FAO Conference on Wood Technology, Forest Products Laboratory, Madison, USA*, 4 pp.

Rees, W. H., 1960, Heat of absorption. In: Hearle, J. W. S. and Peters, R. H. (eds) Moisture in textiles, Wiley Interscience, New York, 33 - 58.

Robards, A. W. and Purvis, M., 1964, Chlorazol black E as a stain for tension wood, *Stain Technology*, 39(5), 309 - 315.

Rudman, P., 1966, Studies in wood preservation. III The penetration of the fine structure of wood by inorganic solutions, including wood preservatives, *Holzforschung*, 20(2), 60 - 67.

Skaar, C., 1988, Wood-water relations, Springer-Verlag, New York, 283 pp.

Sedgewick, S. A. and Trevena, D. H., 1976, An estimate of the ultimate tensile strength of water, *Journal of Applied Physics*, 9, L203 - L205.

Sokal, R. R. and Rohlf, F. J., 1981, Biometry, Second edition, W. H. Freeman and Company, New York, 859 pp.

Stamm, A. J., 1964, Wood and cellulose science, The Ronald Press Company, New York, 549 pp.

Stamm, A. J. and Arganbright, D. G., 1970, Surface tension of the sap of several species of wood, *Wood and Fiber*, 2(1), 65 - 66.

Wilcox, M. D., 1980, Genetic improvement of eucalypts in New Zealand, *New Zealand Journal of Forestry Science*, 10(2), 343 - 359.

Wroblewski, S., 1882, *Comptes Rendues*, 94, 1335.

Zimmermann, M. H., 1983, Xylem structure and the ascent of sap, Springer-Verlag, New York, 142 pp.

Zobel, B. J. and van Buijtenen, J. P., 1989, Wood variation, its causes and control, Springer-Verlag, New York, 363 pp.

Chapter 4

Supercritical fluid extraction of *Pinus radiata* bark

4.1 Introduction

Supercritical fluids - fluids pushed by heat and pressure to the point where they effectively combine the properties of liquids and gases - offer an alternative to organic solvents in the extraction of chemicals from bark. Their densities are compariable with those of liquids, with viscosities and diffusivities intermediate between liquids and gases (table 4.1). Solubilities are therefore good, with mass transfer coefficients approaching those of gases.

Table 4.1 Comparison of critical-fluid properties

	Liquid	Supercritical	Gas
Density (g. cm^3)	1.0	0.2 - 0.7	0.001
Viscosity ($\times 10^{-3}$ N. s. m^2)	0.5 - 1.0	0.05 - 0.10	0.01
Diffusivity (cm^2. s^{-1})	10^{-5}	10^{-4} - 10^{-3}	10^{-1}

from de Filippi 1982

Supercritical fluids are confined to temperatures and pressures in excess of the critical point CP as seen in the PT diagram for carbon dioxide (figure 4.1). The critical temperatures and pressures of solvents are important parameters in determining their suitability as supercritical fluid extractants. A listing of potential solvents is given in table 4.2.

Table 4.2 Critical temperatures and pressures of various solvents

	T_c ° C	P_c MPa
Carbon dioxide	31.0	7.38
Ethanol	240.7	6.14
Ethylene	9.1	5.04
Methanol	239.4	8.09
Nitrous oxide	36.4	7.24
Propane	96.6	4.25

Carbon dioxide is the most commonly used supercritical fluid. Its advantages include non-toxic and non-flammable properties, environmental acceptability, cheapness, and lack of residues. Its low critical temperature (31 ° C) allows extractions to be accomplished with minimal thermal degradation of heat labile chemicals, while pressures are moderate.

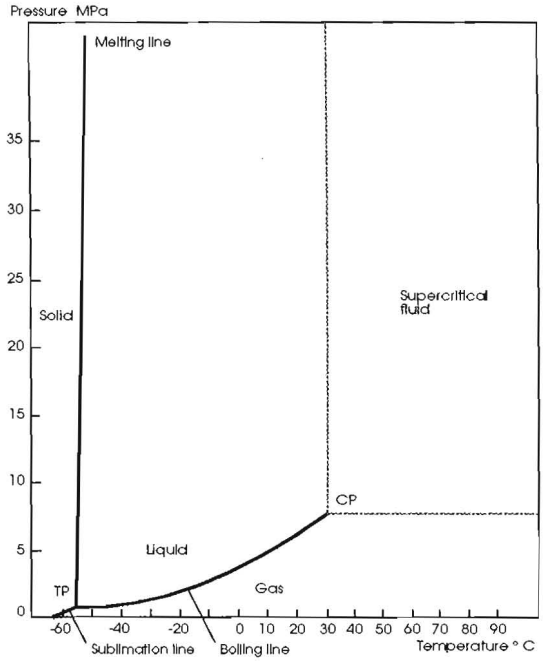

Figure 4.1 PT diagram of carbon dioxide

The solvent power of supercritical carbon dioxide is dependent on the density and temperature of the fluid. The solubility of naphthalene in supercritical carbon dioxide (figure 4.2)

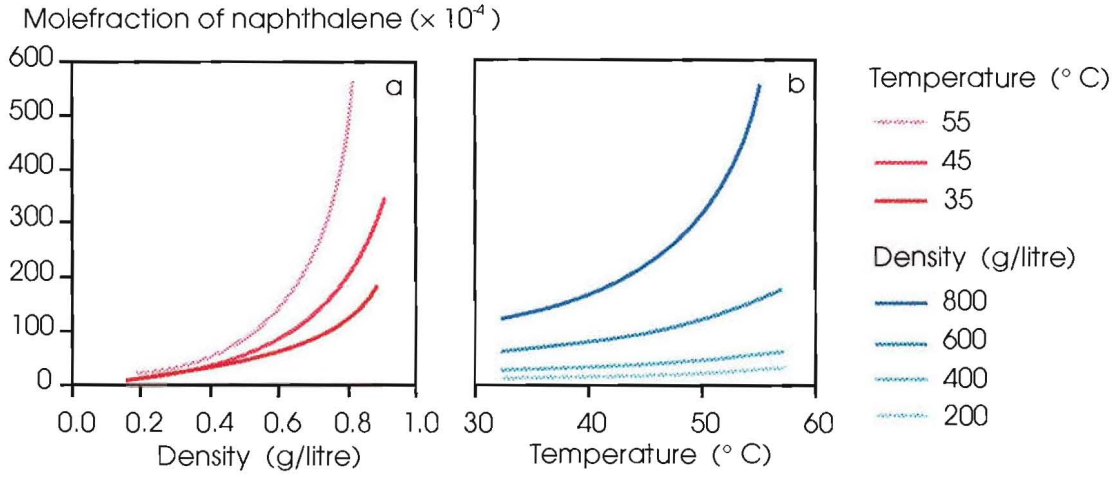

Figure 4.2 Solubility of naphthalene in carbon dioxide as a function of density at constant temperatures and as a function of temperature at constant densities (from Brogle 1982).

illustrates the general rules regarding the use of supercritical fluids:

- solvent power of a supercritical fluid increases with density at a given temperature;

- solvent power of a supercritical fluid increases with temperature at a given density.

There are large gradations of density within the supercritical fluid region (figure 4.3). These pass through into the liquid and gas states due to the absence of phase transitions. Densities increase from the gas state through the supercritical fluid into the liquid state. This produces very steep density gradients in the region of the critical point as the lines of equal density reverse round from the gas side to the liquid side of the boiling line. Small changes of temperature and pressure in the critical point region can produce large changes in density, a feature of interest in process development.

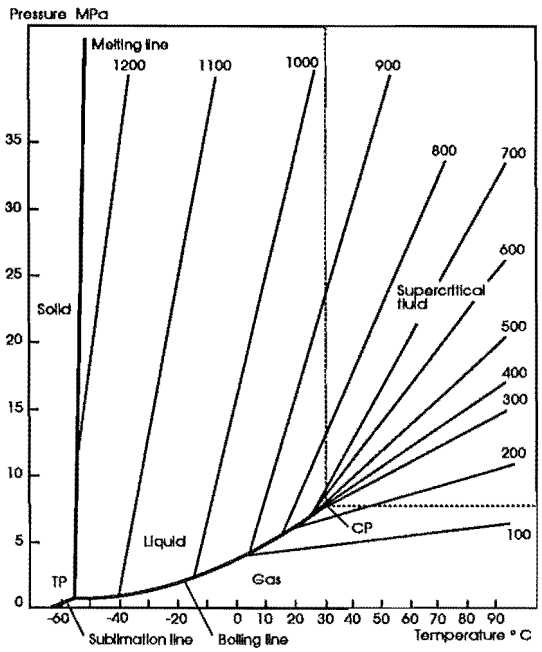

Figure 4.3 PT diagram of carbon dioxide with density (g/litre) as the third dimension (from Brogle 1982).

Product recovery can be achieved with a minimum of energy loss, avoiding the energy wasteful liquid-to-gas-to-liquid phase changes associated with the recycling of organic solvents.

4.2 Chemical selectivity

Any increase in solvent power increases not only the solubility of a given solute, but also the number of compounds soluble in measurable quantities. That is, a solvent will dissolve more compounds of a given mixture at high solvent power than at low solvent power. The chemical selectivity of the solvent is high at low solvent power, and low at high solvent power (Brogle 1982). In the case of supercritical carbon dioxide, at low solvent power only the more volatile compounds such as essential oils can be extracted. As the solvent power increases with increased temperature and pressure, compounds of reduced volatility and greater

molecular weight such as heavier terpenes, fatty oils, waxes and resins can also be extracted (Brogle 1982).

Carbon dioxide is a non-polar solvent and the more physically and chemically similar the solvent and the solute, the higher the solubility. Lipophilic organic compounds of low polarity such as hydrocarbons are easily extracted with supercritical carbon dioxide at pressures of 7 - 10 MPa. When strongly polar functional groups such as hydroxyl and carboxyl groups are added, these compounds become increasingly difficult to extract. Aromatic compounds with up to three hydroxyl groups or one carboxyl and two hydroxyl groups can still just be extracted, but the presence of one further hydroxyl group prevents extraction. More strongly polar compounds such as sugars and amino acids cannot be extracted at pressures up to 50 MPa. Even at pressures of 250 MPa, only very small quantities of sugars and amino acids can be extracted (Stahl 1980).

Supercritical carbon dioxide shows little if any solvent selectivity to polar compounds. This is because the forces of attraction between solute and carbon dioxide molecules are almost entirely non-specific van der Waals forces. The contribution of dipole/induced-dipole interactions of polar solutes with carbon dioxide molecules amounts to only one one hundredth of that of non-specific van der Waals forces. (van Alsten and Eckert 1985). This can be attributed to the very low polarizability of carbon dioxide (26.5×10^{-25} cm^3), which is less than that of all the hydrocarbons except methane (Dobbs et al. 1987). The polar selectivity of supercritical carbon dioxide can, however, be very substantially improved if low concentrations (1 - 5 %) of co-solvents containing polar functional groups are added. The dipole/dipole interactions between polar solute and polar co-solvent molecules can produce large solubility enhancements, superimposing a polarity effect on the density effect of supercritical carbon dioxide noted earlier. The result is an increase in the solubility of polar compounds, with virtually no increase in the solubility of non-polar compounds. In addition, the solubility enhancement for polar compounds increases with the polarity of the compound. Solubility increases of over 500 % have been observed (van Alsten and Eckert 1985).

4.3 Supercritical fluid extraction of wood and bark

4.3.1 Cellulose and phenolic compounds

Lignin extraction using supercritical fluids has been a focus of alternative procedures for α-cellulose, and chemical and liquid fuel production. A number of different supercritical fluids have been proposed, many of which are mixtures of solvents with very high critical temperatures.

Methylamine/water (83 / 17 wt. %) at 180 ° C and 11.0 MPa, has been proposed as an alternative to chemical pulping for the extraction of lignin from spruce wood as part of the process of α-cellulose production (Beer and Peter 1985). Ethanol/water (20 - 50 % water) at 250 - 280 ° C and 10.0 MPa has been used with birch wood (Koll et al. 1979).

t-butanol was used at 185 - 275 ° C and 4.17 - 6.76 MPa to extract lignin derivatives, particularly phenolics, from white fir (*Abies concolor*) sapwood. The high critical temperature of t-butanol 235 ° C, also caused partial pyrolysis of cellulose making the process unsuitable for α-cellulose production (Reyes et al. 1989).

Acetone, tetrahydrofuran, dioxane and toluene at 250 - 340 ° C and 8.0 - 9.0 MPa have been used as an alternative to pyrolysis for the extraction of phenolic compounds from spruce wood. Such compounds, it is thought, could form part of the feed stock for the petrochemicals industry. Yields of between 14 and 24% soluble material were obtained. This was generally greater than that obtained by pyrolysis, with less thermal degradation (Calimli and Olcay 1978). Acetone and methanol were used at 260 - 350 ° C and 10.0 - 28.0 MPa to convert the phenolic and carbohydrate components of Western red cedar (*Thuja plicata*) to liquid fuels. Liquid yields of between 20 and 74% were obtained, 5% of which were identified as substituted guaiacols and levoglucosan (McDonald et al. 1983).

4.3.2 Resin acids, fatty acids, and neutral components

Supercritical fluid extraction of resin acids and fatty acids has centred largely on their removal from wood prior to pulping. They contribute to a

number of pulping problems including: consumption of pulping chemicals, decreased penetration of pulping liquors, increased organic loading on recovery furnaces and evaporators, and reduced fibre to fibre bonding causing a reduction in paper strength (Ritter and Campbell 1991). In addition, resin acid and fatty acid yields, obtained from the by-product raw tall oil, are reduced by thermal degradation during the pulping process. Their usage is mainly as modified chemical derivatives in a number of industrial products such as emulsifiers, adhesives, inks, and protective coatings. Prior extraction would not only help to alleviate pulping problems, but would also improve resin acid and fatty acid recoveries.

An alternative approach has been to use supercritical fluids as a preliminary means of separating the resin acid, fatty acid, and neutral components of the recovered tall oil.

Southern pine and *Pinus ponderosa* wood and bark have been used to assess the extract composition and yields from various supercritical fluids, and the ways in which these are affected by process variables.

McDonald et al. (1983) extracted southern pine wood with supercritical propane, nitrous oxide, ethylene and carbon dioxide at 21 and 62 MPa and various temperatures (table 4.3). They attributed the higher yields from propane and nitrous oxide to their dipole moments, producing dipole/dipole interactions with the polar functional groups of the resin acids and fatty acids. The composition of the extracts was similar regardless of pressure or solvent. Successional analysis of the extracts over time revealed that initially over 90% of the extract was resin acids and fatty acids. As the extraction proceeded, both the amount and the content of resin acids and fatty acids in the fractions declined. The last fractions contained 30 - 50% resin acids and fatty acids. A typical extract comprised 31% abietic, 26% levopimaric and palustric, 14% neoabietic, 8.3% isopimaric, 4.9% dehydroabietic, 4.0% pimaric, 1.1% sandaracopimaric, 0.22% linoleic, and 0.14% oleic and linolenic acid. The composition reflects the resin acid rich nature of southern pine wood. Saponification of extracts gave no change to the composition of fatty acids, revealing an absence of triglycerides, which suggests that only free fatty acids were extracted.

Table 4.3 Supercritical fluid extract yields from southern pine wood

Pressure MPa	Extract yield, percent weight of dry wood Propane 105 ° C	Nitrous oxide 45 ° C	Ethylene 15 ° C	Carbon dioxide 40 ° C
21	18.8	6.8	2.3	2.1
62	-	14.2	6.9	5.6

from McDonald et al. 1983

Ritter and Campbell (1991) used southern pine and *Pinus ponderosa* wood to investigate the effect of process variables on the supercritical carbon dioxide extraction of resin acids and fatty acids. Yields were dependent on temperature, pressure, particle size and fluid-to-wood ratio. Moisture content was found to have no effect on yield.

The effects of temperature were influenced by the relative composition of resin acids and fatty acids in the wood. Southern pine wood, which is rich in resin acids, gave increased yields of extracts for temperature was raised from 30 to 180 ° C at 27.6 MPa. *Pinus ponderosa* wood, which is rich in fatty acids, showed a slight decline in extract yields as the temperature was raised from 30 to 160 ° C at 20.7 MPa. Resin acid solubility appears to increase with temperature while fatty acid solubility declines. The difference is thought to be due to the higher vapour pressure of resin acids at elevated temperatures.

Extract yields from southern pine and *Pinus ponderosa* wood increased with pressure from 6.8 - 34.2 MPa at 40 ° C. The resin acid composition of extracts was found however to decline with pressure at 13.8 - 27.6 MPa and 40 ° C. The suggestion is that resin acid solubility may controlled to a greater degree by vapour pressure than by solvent density.

Particle size affected extract yields for a given fluid-to-wood ratio. Yields increased with declining particle size from > 8 to < 40 mesh size. The smallest size fraction 40 - 60 mesh size was the most effective.

Extract yields per gram of carbon dioxide decreased with fluid-to-wood ratios of 18 - 110 : 1. The rate at which extracts are removed declines as the particle surfaces become progressively depleted. For southern pine wood, total extract yields levelled off at a fluid-to-wood ratio of 60 : 1.

Harvala et al. (1987) avoided the complication of extraction from solid wood by using recovered tall oil from sulphate pulping. Multi-stage supercritical carbon dioxide extraction was used to separate the resin acids, fatty acids, and neutral components in the recovered tall oil and in subsequent extracts. The recovered tall oil was extracted at 25 MPa and 47 ° C, followed by extraction of the extract at 20 MPa, and extraction of the second extract at 15 MPa. Most of the resin acids were retained in the recovered tall oil and the 25 MPa extract. Only small amounts were extracted at 20 and 15 MPa. Fatty acids were fairly evenly distributed in all three extracts 25, 20 and 15 MPa, no fatty acids were retained in the recovered tall oil. Neutral components (hydrocarbons, alcohols, waxes and sterols) were concentrated in the 15 MPa extract, with lesser amounts retained in the earlier 25 and 20 MPa extracts and recovered tall oil.

McDonald et al. (1983) also extracted a pale yellow wax from Douglas fir (*Pseudotsuga menziesii*) bark using supercritical propane, nitrous oxide, carbon dioxide and ethylene at 21 and 62 MPa and various temperatures (table 4.4). Again yields were highest for propane and nitrous oxide, as observed for southern pine wood. Gas chromatography and mass spectrometry tentatively identified four compounds in the nitrous oxide extract as 1-octadecanol, triacontanoic acid, 2-methyl-1-hexadecanol and tetracosanoic acid.

Table 4.4 Supercritical fluid wax yields from Douglas fir bark

Pressure MPa	Wax yield, percent weight of dry wood Propane 105 ° C	Nitrous oxide 45 ° C	Ethylene 15 ° C	Carbon dioxide 40 ° C
21	5.5	2.2	0.54	1.1
62	-	2.7	0.82	1.8

from McDonald et al. 1983

Jennings et al. (1991) extracted taxol from the bark of *Taxus brevifolia* using supercritical carbon dioxide and carbon dioxide/ethanol at 18.1 - 25.7 MPa and 45 ° C. Carbon dioxide/ethanol was more effective in removing taxol, extracting approximately 50% of the total amount present, while carbon dioxide only extracted 25%. The proportion of taxol in carbon dioxide/ethanol extracts was higher than that of carbon dioxide, indicating a greater level of selectivity. Supercritical carbon

dioxide/ethanol was also more selective than liquid extraction using ethanol.

4.4 *Pinus radiata* bark extractives

Pinus radiata bark contains a large number of extractive compounds, most of which occur in very small quantities. These can be classified into three groups: (1) aliphatic compounds (mainly fats and waxes); (2) terpenes and terpenoids; and (3) phenolic compounds (Sjostrom 1981).

4.4.1 Aliphatic compounds

	% benzene soluble neutrals
Hydrocarbons	
n-alkanes C_{13} - C_{34}	12.5
isoalkanes C_{15} - C_{19}	1.7
Waxes	1.9
Alcohols	
Docosanol	4.0
Tetracosanol	9.3

(Weston 1973)

Fatty acids		Weight %
Lauric	12 : 0	trace
Myristic	14 : 0	0.2
Palmitic	16 : 0	1.9
Palmitoleic	16 : 1	0.8
Stearic	18 : 0	5.1
Oleic	18 : 1	3.6
Linoleic	18 : 2	0.5
Linolenic	18 : 3	0.3
Arachidic	20 : 0	11.8
Behenic	22 : 0	37.6
Lignoceric	24 : 0	28.6

Shorthand notation - acids listed by number of carbon atoms : number of double bonds.

(Hartman and Weenink 1967)

The waxes consist of esters of alcohols. When saponified, the wax component gave an alcohol mixture of 12 : 1 : 1 docosanol, tetracosanol and triacontanol respectively, with a smaller amount of eicosanol. In their free form, docosanol and tetracosanol are the two major alcohols present (Weston 1973).

The saturated fatty acids stearic, arachidic, behenic and lignoceric acid make up 83% of the total bark fatty acids. This contrasts sharply with the fatty acid composition of *Pinus radiata* wood, where the unsaturated fatty acids oleic and linoleic acid make up 76% of the total fatty acids, while stearic and arachidic acid make up just 3%, and behenic and lignoceric acid occur as only trace amounts (Hansen 1966).

The fatty acids in bark occur mostly as esters, the most important of which are glycerol esters in the form of triglycerides. The composition of the free and combined forms of fatty acids can be listed as follows:

Acetone extract		% free acids *	% combined acids †
Palmitic	16 : 0	2.3	-
Palmitoleic	16 : 1	0.2	-
Stearic	18 : 0	2.8	3.3
Oleic	18 : 1	0.8	-
Linoleic	18 : 2	1.5	-
Arachidic	20 : 0	6.5	16.8
Behenic	22 : 0	15.7	44.0
Lignoceric	24 : 0	13.3	35.9

* expressed as % of the fatty acid and resin acid components;
† calculated from the increase in the proportion of these components after saponification of the bark extract, on the assumption that resin acids are not combined as esters. Saponification of the four combined fatty acids (stearic, arachidic, behenic and lignoceric acid) increased the weight of free fatty acids by 49%.

(Porter 1969)

4.4.2 Terpenes and terpenoids

Terpenes can be further classified into monoterpenes ($C_{10}H_{16}$), oxygenated terpenes and sesquiterpenes ($C_{15}H_{24}$).

% Composition of bark oil	mean	range
Monoterpenes		
α-Pinene	27.0	61.8 - 10.5
Camphene	0.2	0.5 - 0.1
β-Pinene	54.6	70.9 - 28.8
3-Carene	0.3	1.9 - 0.0
Sabinene	1.7	11.1 - 0.2
α-Phellandrene*	t	
Myrcene	1.1	1.8 - 0.5
Limonene	4.4	10.0 - 0.5
β-Phellandrene	2.6	12.3 - 0.7
γ-Terpinene	0.1	2.1 - 0.0
cis-β-Ocimene	0.2	1.2 - 0.0
Terpinolene	0.9	12.2 - 0.0
p-Cymene	t	
α,p-Dimethylstyrene	t	
Oxygenated terpenes		
Fenchone	0.02	0.04 - 0.00
Citronellal	0.97	1.86 - 0.07
{Camphor* Pinocamphone*}	0.02	0.04 - 0.00
Isopinocamphone	0.03	0.10 - 0.00
Lanalool	0.58	1.49 - 0.05
trans-Dihydro-α-terpineol*	0.12	0.49 - 0.08
Isopulegol	0.19	0.36 - 0.06
α-Fenchol	0.05	0.10 - 0.02
Bornyl acetate	0.04	0.08 - 0.01
{Thymyl methyl ether Terpinen-4-ol}	0.24	2.08 - 0.04
Myrtenal	0.02	0.07 - 0.01
Pulegone	0.01	0.02 - 0.00
trans-Pinocarveol	0.18	0.48 - 0.02
{α-Terpineol Borneol}	1.01	1.87 - 0.27
Piperitone	0.34	1.10 - 0.02
Citronellol	0.85	1.85 - 0.16
Myrtenol	0.03	0.07 - 0.01
Anethole*	0.03	0.07 - 0.01
p-Cymen-8-ol	0.04	0.19 - 0.01
Geranlol	0.01	0.04 - 0.00
δ-Cadinol*	0.09	0.23 - 0.01
α-Cadinol	0.09	0.42 - 0.00
Thymol	0.02	0.06 - 0.01

13-Epimanool	0.24	2.45 - 0.00
Sesquiterpenes		
α-Copaene	0.02	
β-Elemene	0.03	
Caryophyllene	0.05	
trans-α-Bergamotene	0.13	
Aromadendrene	0.04	
γ-Muurolene	0.04	
β-Selinene	t	
α-Muurolene	0.25	
γ-Cadinene	0.09	
Calamenene	t	
δ-Cadinene	0.25	

* tentative
t = trace

(Simpson and McQuilkin 1976)

The composition of bark oil is 93% monoterpenes, 6% oxygenated terpenes and 1% sesquiterpenes.

Acetone extract	% of resin acids and fatty acids
Resin acids	
Pimaric	2.8
Sandaracopimaric	2.1
Palustric	3.6
Dehydroabietic	1.0
Abietic	42.3
Neoabietic	2.5

(Porter 1969)

	% benzene soluble neutrals
Sterols	
Stigmast-4-en-3-one	0.3
β-Sitosterol	9.4
Campesterol	1.4

(Weston 1973)

Terpenes, resin acids and sterols are located in the resin canals, cork cells and the pathological exudate (oleoresin) of wounded bark. Oleoresin in pine wood consists of 70 - 80% resin acids (Sjostrom 1981).

4.4.3 Phenolic compounds

Flavonoids

The flavonoid groups of *Pinus radiata* bark comprise monomeric flavans, flavonols, flavanonols, stilbenes; oligomeric procyanidins; and polymeric condensed tannins.

Monomeric

flavans:	catechin, gallocatechin;
flavonols:	quercetin, myricetin;
flavanonols:	dihydroquercetin;
stilbenes:	pinosylvin;

Oligomeric

procyanidins:	B-1, B-3, B-6, C-2;

Polymeric

condensed tannins of the procyanidin and prodelphinidin type.

	%weight of bark	
Catechin	0.06	(air-dry weight)
Quercetin	0.2	(oven-dry weight)
Dihydroquercetin	2.0	"
Procyanidins	1.0	"
Condensed tannins	20	"

(Markham and Porter 1973, Porter 1974)

Dihydroquercetin is the main monomeric flavonoid compound in *Pinus radiata* bark. Quercetin, myricetin and pinosylvin are minor compounds. Catechin and gallocatechin in their unpolymerised form, occur in very small quantities.

4.5 Experiment design

A two stage supercritical extraction process was proposed for *Pinus radiata* bark (Lomax pers. comm.). The bark was first extracted with supercritical carbon dioxide to remove resin acids, fatty acids, terpenes, waxes and sterols. Then re-extracted with carbon dioxide/methanol to remove what it was hoped would be monomeric flavonoid compounds.

Extraction with carbon dioxide was performed at 50.0 ° C and at pressures of 10, 15, 20, 25 and 30 MPa. Extraction with carbon dioxide/methanol was performed only at 30 MPa. Bark re-extraction with carbon dioxide/methanol took place only for samples previously extracted with carbon dioxide at 30 MPa. A once through flow of supercritical fluid was used. Extracts were collected for gravimetric measurement and chemical analysis. High performance liquid chromatography (HPLC) was used to detect and quantify the resin acid abietic acid, unsaturated fatty acids palmitoleic, linoleic and linolenic acid, sterols β-sitosterol and campesterol, and the flavonoid compound dihydroquercetin contained in the extracts.

Extraction of *Pinus radiata* bark was also performed with diethyl ether to determine the total quantity of each compound in the bark.

4.6 The supercritical fluid system

The apparatus used was designed and built by Pat Jordan and David Pearce of the Chemical and Process Engineering Department, University of Canterbury. It has a maximum design pressure of 68 MPa, but the actual cell used for extraction had a maximum design pressure of only 40 MPa. The configuration is shown in figure 4.4. Its components include:

Newport Scientific Inc. (Jessup, Maryland, USA) model 46-13411-2 motor driven single ended diaphram compressor, capable of generating pressures of up to 68 MPa with a maximum compression ratio of 14 : 1;

Tescom (Elk River, Minnesota, USA) model 26-1722-24 back pressure regulator, rated from 0.35 - 41.5 MPa;

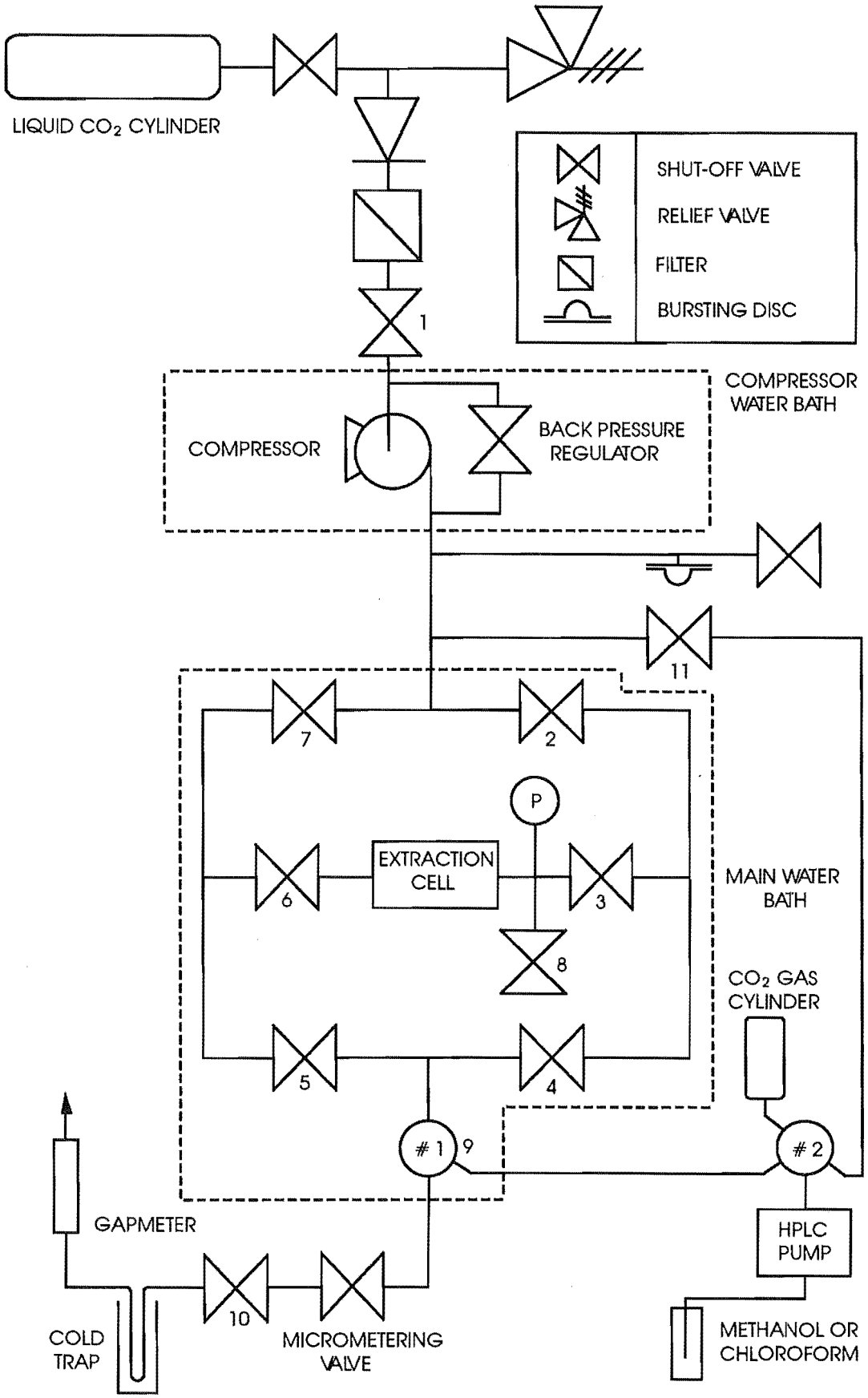

Figure 4.4 Supercritical fluid extraction apparatus.

3D Instruments Inc. (Huntington Beach, California, USA) pressure gauge, type 25504-39B11- ISOD, 0 - 100 MPa graduated in 0.5 MPa;

Swagelok (Solon, Ohio, USA) 4R3A1 relief valve;

Rheodyne (Cotati, California, USA) model 7000 six-port valves;

Autoclave Engineers' Inc. (Erie, Pennsylvania, USA) model 10VRMM micrometering valve;

G. A. Platon Ltd (Croydon, Surrey, England) Gapmeter flow measuring device fitted with a C6 tube and a hollow Duralumin float (100 - 2000 $cm^3.min^{-1}$ air at NTP);

Waters (Milford, Massachusetts, USA) model 510 HPLC pump;

John Fluke MFG Co. Inc. (Everett, Washington, USA) Fluke 52 K/J Thermometer for monitoring both the water bath and micrometering valve temperatures;

Autoclave Engineers' Inc. (Erie, Pennsylvania, USA) 1/8 " valves, fittings and tubing were used throughout the system. The size was chosen to keep the non-cell volume small;

A cold trap consisting of a long pyrex dip tube in a thermos flask containing a dry ice/acetone mixture (temperature -77 ° C).

The compressor head and the main unit are housed in separate water baths (figure 4.5). These are linked by a Levco (Auckland, New Zealand) "Comet 2" magnetically driven pump. Water is drawn from the bottom of the main water bath and recirculated through the compressor head water bath.

The main water bath is heated with steam and two coils of BICC Ltd (Hebburn-on-Tyne, England) "Pyrotenax" HCHHIL2000 heating cable. The steam is used to quickly heat the water to the operating temperature. The heating cable maintains the operating temperature during run time. An on-off controller monitors and adjusts the load to one of the coils, while a

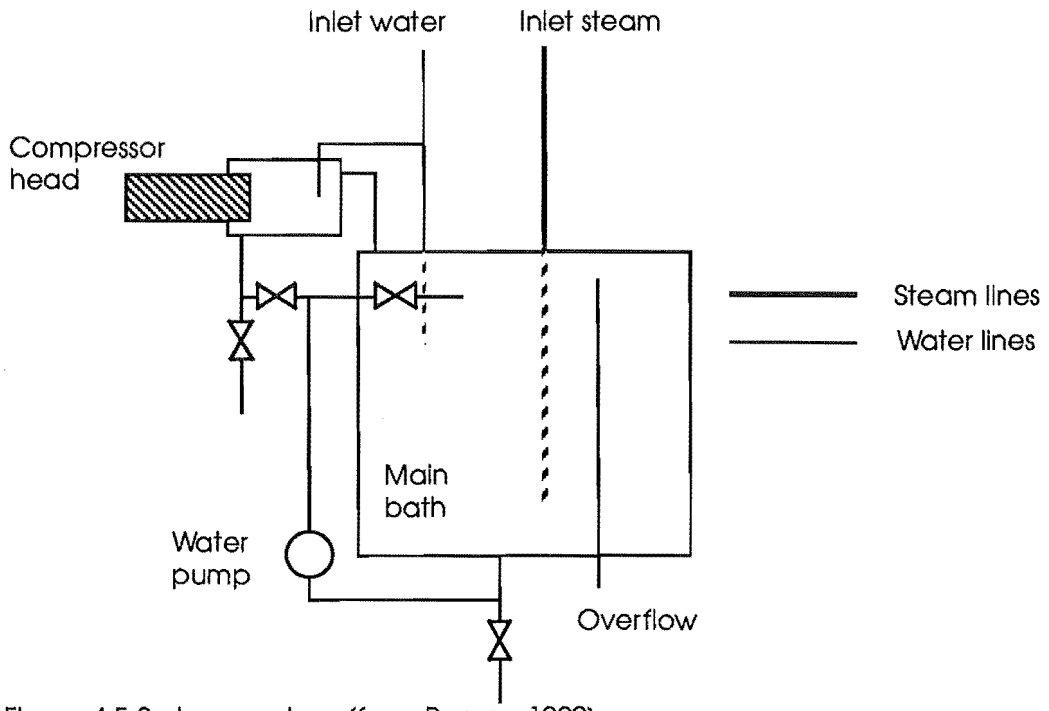

Figure 4.5 System services (from Pearce 1990).

variable voltage transformer controls the base load setting to the other. A marine impeller attached to a ASEA Class F motor maintained a uniform temperature distribution within the main water bath.

The micrometering valve is heated with 1 m of Isopad Ltd (Stirling Way, Borehamwood, Hertfordshire, England) "Unitrace IUR-30" heating tape.

The bark sample was held in a solid sample holder within the extraction cell. The extraction cell consisted of a 6" length of 0.5" nominal ID hex nipple tubing (Cajon SS-8-HLN-6.00), connected at one end to two Swagelok Full flow Quick Connects (SS-QF8-S-8PF Female NPT connected to a SS-QF8-B-8PF Female NPT). This made it easy to open and close the extraction cell when the solid sample holder needed to be inserted and removed during each run. The solid sample holder is a thin walled stainless steel tube of length 13.6 cm, ID 1.0 cm, and volume 10.68 cm^3, into each end of which is screwed an encased 7 μm frit (figure 4.6). The frits give a good initial distribution of supercritical fluid, and

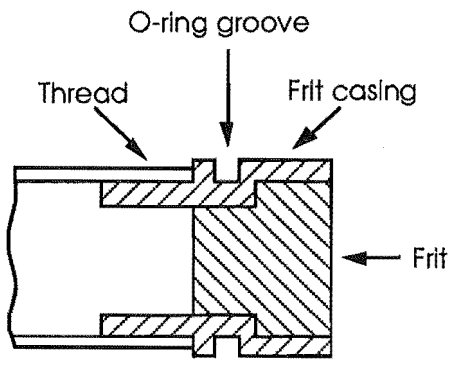

Figure 4.6 Sectional view of the frit and the casing into which it was welded.

help to prevent entrainment of the bark in the outlet stream. Both frit casings had o-ring grooves cut into them. The o-rings sealed against the sides of the cell, preventing the supercritical fluid from by-passing the bark held in the sample holder.

4.7 The HPLC system

A modular HPLC system was used for chemical analysis. The configuration is shown in figure 4.7, along with details of the various components.

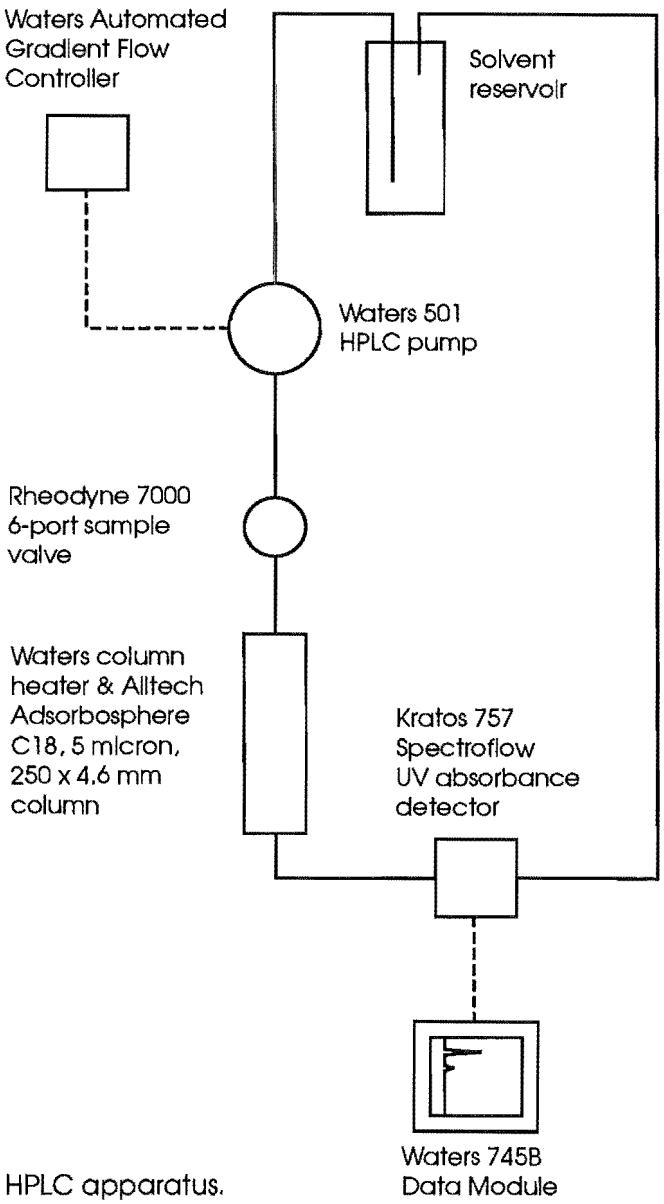

Figure 4.7 The HPLC apparatus.

4.8 Bark - source and preparation

Pinus radiata bark was collected in late January from the logs of 15 trees, aged 25 years. The logs were sourced from Ashley Forest, North Canterbury.

The bark was washed and dried for two weeks at 20 ° C, before being ground using a Wiley Laboratory Mill, model 4 (Arthur H. Thomas Co., Philadelphia, Pennsylvania, USA). The ground bark was then sieved using a Fritsch ®analysette 3 vibratory sieve shaker. The fraction collected between sieve sizes 425 μm and 250 μm (40 and 60 mesh sizes) was used for all extractions.

The sieved bark was stored at 0 ° C. All extractions were completed within two months of the bark collection date.

4.9 Experimental procedures

4.9.1 Supercritical fluid extraction

The procedure used was an adaption of that of Vannort (1991).

Loading the extraction cell

The solid sample holder was packed with alternating layers of glass beads and bark, with glass wool packing at each end. The weight of the solid sample holder and that of the bark was measured. The glass wool facilitated easy removal of the bark from the sample holder after extraction. The o-rings were smeared with a thin film of silicon lubricant (Arandee Chemicals Silicone Paste A4). This prevented binding of the o-rings with the cell walls. The sample holder was then pushed into the cell until the bottom of the holder made contact with the base of the cell.

Getting to temperature and pressure

The compressor head water bath was filled and the main water bath filled to a height just below the extraction cell with cold water. The valves open/closed status was then checked prior to pressurisation. Valves 1, 8, 10 and 11 (figure 4.4) were closed, and valves 2, 3, 4, 5, 6 and 7 opened. If either of valves 2 and 7 are closed, the flow of carbon dioxide at pressurisation will result in rapid displacement of the solid sample holder in the cell, leading to possible damage to both. The system was pressurised to 5.5 MPa (bottle pressure) by slowly opening valve 1. A check was made for audible leaks before completely filling the main water bath. After checking again for leaks, the compressor was started and system taken to 10.0 MPa, a little above the critical pressure of carbon dioxide (7.4 MPa). The compressor was turned off, the electrical systems turned on (the micrometering valve heating tape, the water circulation pump, the stirrer motor and the heating cables), and live steam introduced to the main water bath to accelerate heating. The water from the main water bath was circulated through the compressor head water bath, and in this way the compressor head was brought up to the operating pressure along with the rest of the system.

The cold trap was then set up above the main water bath, and connected to the tubing from valve 10 and the Gapmeter.

When the main water bath had reached 50.0 ° C, the steam was turned off, and the electrical heating controller set point adjusted as necessary, to ensure the temperature deviation was no more than ± 0.1 ° C. Fifteen minutes was allowed for the system to reach thermal equilibrium before the compressor was turned on, and the system pressurised to the operating pressure by adjusting the setting on the back pressure regulator.

Running

The micrometering valve was checked to ensure it was almost fully closed, and valve 10 slowly opened. The micrometering valve was then adjusted until the desired flow rate of 1034 cm^3. min^{-1} at STP was attained. Valves 2 and 5 were then closed, forcing the supercritical fluid

through the bark in the extraction cell. Deposition of the extract in the micrometering valve caused the carbon dioxide flow rate to drop off slowly during the course of the run. This required periodic adjustments to the micrometering valve to maintain the desired flow rate. Occasional adjustments to the back pressure regulator were also necessary. Adiabatic expansion of carbon dioxide in the micrometering valve caused a 10 ° C drop in the micrometering valve temperature during the run time. Provided the micrometering valve temperature was maintained at greater than 90 ° C, problems with carbon dioxide freezing were avoided.

The length of the run time was determined by the time required to put 10 cell volumes of supercritical carbon dioxide through the cell at a constant flow rate of 1034 cm^3. min^{-1} at STP. Run times are given in table 4.5.

Table 4.5 Length of run times for each pressure

Pressure MPa	Run time minutes
10.0	21
15.0	37
20.0	42
25.0	44
30.0	46

Depressurisation

At the end of the run time, the compressor was turned off and the liquid carbon dioxide supply cylinder valve and valve 1 were closed. Valves 2 and 5 were opened and the water released from the main and compressor head water baths. Depressurisation took place at a carbon dioxide flow rate of approximately 1034 cm^3. min^{-1} at STP. When ambient pressure was reached, the top of the extraction cell was opened by disconnecting the Full flow Quick Connects. The cell was then left for 2 hours while the swollen o-rings of the solid sample holder shrank with carbon dioxide loss.

Flushing extract from the system

The cold trap was removed and the micrometering valve, valve 10 and the tubing leading to the cold trap flushed with chloroform and methanol after depressurisation to remove deposited extracts. Most of the extract was found to be deposited in the micrometering valve and tubing rather than in the cold trap. The six-port valve 1 was switched to its second position, and six-port valve 2 to its first position (figure 4.8), and

chloroform and methanol pumped through in succession with the HPLC pump. The six-port valve 2 was then switched to its second position (figure 4.9) and the methanol remaining in the tubing flushed out with high purity carbon dioxide gas.

Once the cold trap dip tube had thawed, it too was flushed with chloroform and methanol.

The organic solvent was evaporated under vacuum to a small volume in a rotary evaporator, placed in a glass vial and evaporated further with a small amount of heating under a stream of dry nitrogen gas. Final drying took place in a vacuum oven at ambient temperature (approximately 20 ° C) until constant weight was reached.

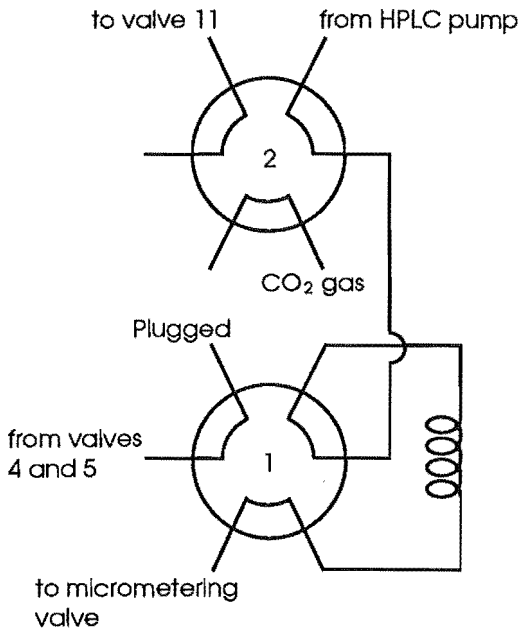

Figure 4.8 Flushing the micrometering valve with chloroform and methanol from the HPLC pump.

The solid sample holder was removed after two hours and the weight loss recorded. The bark was removed from the holder and the empty holder was then placed back in the extraction cell. A blank supercritical carbon dioxide run was then undertaken to flush any remaining extract in the system. This was to ensure there was no carry over of extract from one extraction to the next. The procedure followed that outlined for bark

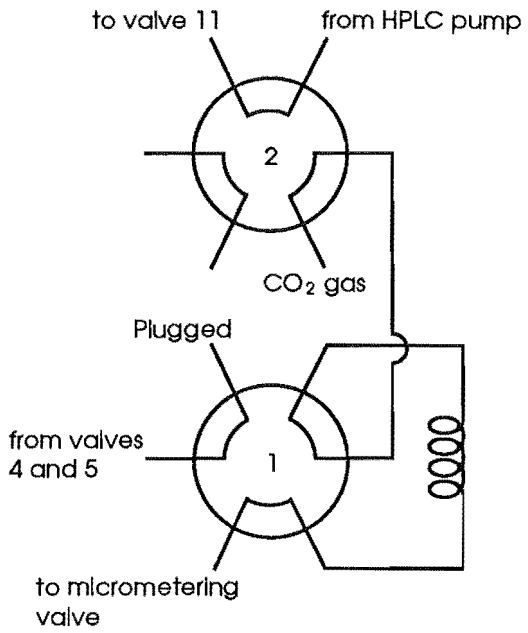

Figure 4.9 Flushing methanol from the micro-metering valve with carbon dioxide gas.

extraction on the previous pages. A pressure of 30.0 MPa was used for all blank runs, irrespective of the preceding extraction run pressure. Twenty cell volumes of supercritical carbon dioxide were passed through the system with a run time of 92 minutes. The micrometering valve, valve 10, tubing to the cold trap and the cold trap were again flushed with chloroform and methanol and the evaporated extract added to that of the preceding extraction.

Extraction and re-extraction with carbon dioxide/methanol

The procedure was the same as that for carbon dioxide, except that methanol was added to the carbon dioxide once the desired flow rate had been attained. Before valves 2 and 5 were closed, and the flow of carbon dioxide was forced through the extraction cell, the six-port valve 2 was switched to its second position (figure 4.10) and methanol pumped through to valve 11 with the HPLC pump. With valve 11 closed, back pressure built up in the tubing. As the pressure approached 4500 psi, the HPLC pump flow rate was set to 0.1 $cm^3.\ min^{-1}$. At 4500 psi valve 11 was opened, the pressure of the HPLC pump equilibrated with that of the

compressor, and methanol entered into the carbon dioxide flow. The methanol flow rate of 0.1 cm^3. min^{-1} gave a methanol/carbon dioxide concentration of 4.3 % by mass.

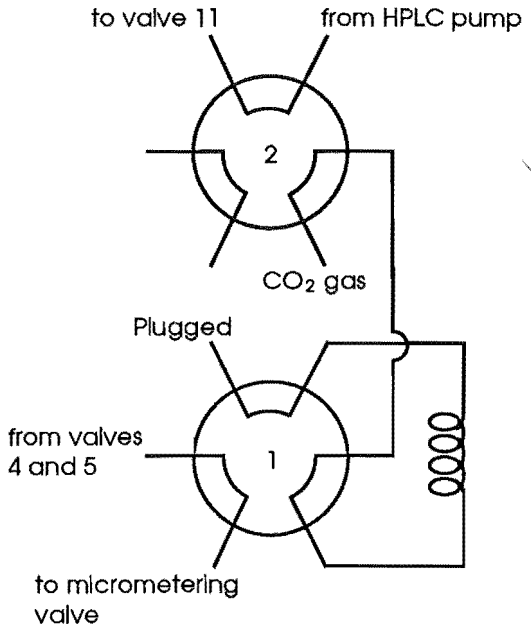

Figure 4.10 Addition of methanol co-solvent to the supercritical carbon dioxide.

At the end of the run time, valve 11 was closed and the HPLC pump quickly stopped to avoid excessive back pressure build up. The pressure in the tubing was then released by switching the HPLC pump to waste. The depressurisation procedure was then followed.

The blank flushing run following carbon dioxide/methanol extraction also utilised carbon dioxide/methanol. While 20 cell volumes of carbon dioxide were put through the system with a run time of 92 minutes, methanol was added only for the first 52 minutes. The last 40 minutes with just carbon dioxide, ensured that all methanol was flushed from the system prior to the next extraction.

4.9.2 Diethyl ether extraction

Pinus radiata bark was extracted with diethyl ether to determine the total quantity of each of the compounds under study in the bark. The ASTM

Standard D1108 was used. The procedure involved exhaustive extraction of 2 grams of air-dried ground bark with diethyl ether for 8 hours in a Soxhlet extraction apparatus. The diethyl ether was finally evaporated from the extraction flask using a rotary evaporator. The only variation from the standard was that extracts were dried in a vacuum oven at ambient temperature (approximately 20 ° C) rather than at 100 - 105 ° C.

4.10 HPLC procedures

4.10.1 Resin and fatty acids

The procedure used was an adaption of Aveldano's et al. (1983) procedures for the analysis of underivatised free fatty acids. This involved customising the mobile phase and the flow rate for the separation of the particular mix of resin acid and fatty acids in extracts with the type of HPLC column used. McDonald et al. (1983) had found that only free fatty acids were extracted from southern pine wood using supercritical carbon dioxide, and the assumption was made that this might also apply to *Pinus radiata* bark.

The use of ultraviolet absorption as the means of detection, limited the analysis of fatty acids to unsaturated compounds. The presence of a conjugated double bond gives them a high level of ultraviolet absorption. Saturated fatty acids lack this and any other strongly ultraviolet absorbing chemical structure. Their absorption peaks are accordingly small, and this together with obstruction from the peaks of other compounds prevented any assessment of their presence in the extracts.

The resin acid abietic acid and the unsaturated fatty acids palmitoleic, linoleic and linolenic were the subject of the analysis.

An Alltech Associates Inc. (Deerfield, Illinois, USA) Adsorbosphere C18, 5 micron, 250 × 4.6 mm, reverse phase column was used in conjunction with a column heater at 35.0 ° C. The mobile phase was acetonitrile - water (82 : 18 v/v) with 0.05% orthophosphoric acid added to maintain peak symmetry. The flow rate was 1.0 cm^3. min^{-1} with a back pressure of

710 - 870 psi. The ultraviolet absorbance detector was set to a wavelength of 205 nm, with the range set at 0.5 AUFS.

The supercritical bark extracts were dissolved in 1.0 cm^3 of tetrahydrofuran - methanol (4 : 1 v/v) and filtered prior to injection. A 10 µl sample loop was used for injection. Its calibrated volume was 14.5 µl (Pearce 1990).

Column depletion problems caused by the acidity of the mobile phase (pH 2.7) meant that replication was kept to a minimum. Generally absorption peak areas were very consistent, with some increase in variability at higher concentrations.

4.10.2 Sterols

β-Sitosterol and campesterol are the two main sterols in *Pinus radiata* bark. Both were included in the analysis.

An Alltech Associates Inc. (Deerfield, Illinois, USA) Adsorbosphere C18, 5 micron, 250 × 4.6 mm, reverse phase column was used in conjunction with a column heater at 35.0 ° C. The mobile phase was acetonitrile with 0.05 % orthophosphoric acid added to maintain peak symmetry. The flow rate was 1.0 cm^3. min^{-1} with a back pressure of 560 - 630 psi. The ultraviolet absorbance detector was set to a wavelength of 205 nm, with the range set at 0.5 AUFS.

The dissolved extracts were those used for resin and fatty acid analysis. The same 10 µl sample loop was used for injection.

4.10.3 Flavonoids

The procedure of Wulf & Nagel (1976) was used for the analysis of dihydroquercetin (taxifolin) in the extracts.

An Alltech Associates Inc. (Deerfield, Illinois, USA) Adsorbosphere C18, 5 micron, 250 × 4.6 mm, reverse phase column was used at ambient

temperature 22 - 26 ° C. The mobile phase was methanol - acetic acid - water (30 : 5 : 65 v/v). The flow rate was 1.5 cm^3. min^{-1} with a back pressure of 3500 - 3700 psi. The ultraviolet absorbance detector was set to a wavelength of 254 nm, with the range set at 0.5 AUFS.

The supercritical bark extracts were dissolved in 1.0 cm^3 of acetonitrile - water (4 : 1 v/v) and filtered prior to injection. The 10 µl sample loop was again used for injection.

4.11 Sources of chemicals

The liquid carbon dioxide was obtained from New Zealand Industrial Gases (Christchurch, NZ) and was of "Food Grade" (99.9%).

The HPLC solvents were obtained from BDH (Poole, England). The grade was HiPerSolv and the product codes were:

Methanol	15250
Chloroform	15283
Acetonitrile 'Far UV'	15251 6Q
Tetrahydrofuran	15247
Orthophosphoric acid	15315
Acetic acid	15310

High purity water for HPLC was obtained from the Chemistry Department, University of Canterbury.

The HPLC solvents were filtered prior to use with 0.45 µm HV type filters (Millipore Corp., Bedford, Massachusetts, USA).

The chemical standards used for HPLC calibration were obtained from the Sigma Chemical Co. (St Louis, Missouri, USA). The purity and product codes were:

Abietic acid	A 9494	Approx.	85%
Palmitoleic acid	P 0875	"	99%
Linoleic acid	L 1376	"	99%
Linolenic acid	L 2376	"	98%
β-Sitosterol	S 5753	"	60%
Dihydroquercetin (Taxifolin)	T 4512		

The β-Sitosterol standard also contained campesterol and dihydrobrassicasterol.

The standards and the supercritical bark extracts were filtered prior to injection with single use Anotec syringe filters, type Anotop 25, 0.2 μm (Whatman, Maidstone, England) and single use syringes, B-D 10 cm^3 syringes, Luer Lok (Becton Dickinson & Co., Rutherford, New Jersey, USA).

4.12 Results

Supercritical carbon dioxide extract yields from bark, generally increase with pressure (10 - 30 MPa) at 50.0 ° C (figure 4.11). The addition of methanol (4.3 % by mass) as a co-solvent gave no increase in extract yields.

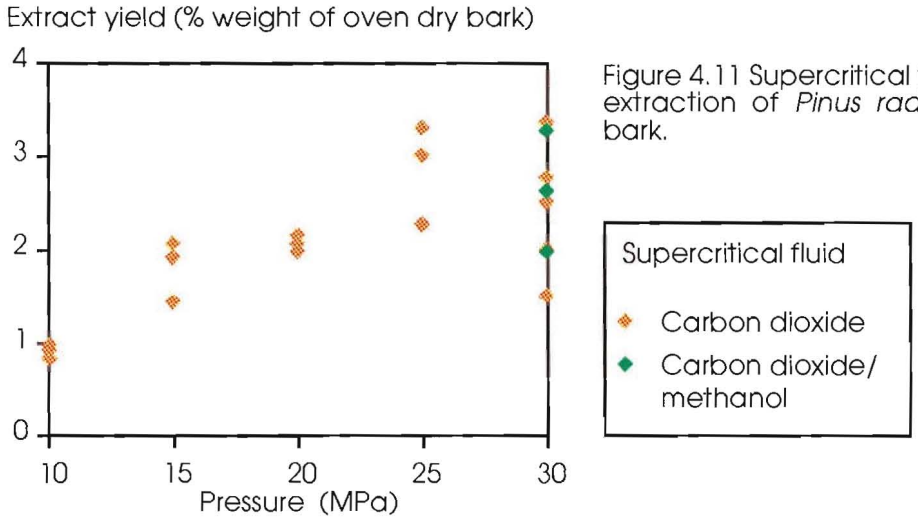

Figure 4.11 Supercritical fluid extraction of *Pinus radiata* bark.

Re-extraction of carbon dioxide extracted bark with carbon dioxide/methanol gave a further 40 - 50 % increase in extract yields (table 4.6).

Table 4.6 Bark extraction and re-extraction extract yields at 30 MPa

Run no.	Percent weight of oven dry bark	
	First extraction carbon dioxide	Second extraction carbon dioxide/ methanol
1	1.49	0.73
2	2.01	0.97
3	2.49	0.93

Supercritical carbon dioxide extract yields at 30 MPa, were less than 50 % of diethyl ether extracts (table 4.7).

Table 4.7 Extract yields for carbon dioxide at 30 MPa and diethyl ether

Percent weight of oven dry bark

Run no.	Carbon dioxide	Run no.	Diethyl ether
1	1.49	1	5.80
2	2.01	2	5.88
3	2.49	3	5.99
4	2.77	4	7.37
5	3.36		

HPLC analysis of extracts identified the resin acid abietic acid, the free fatty acids palmitoleic, linoleic and linolenic acid, and the sterols β-sitosterol and campesterol (figures 4.12 and 4.13). The flavonoid dihydroquercetin was not found in carbon dioxide/methanol extracts.

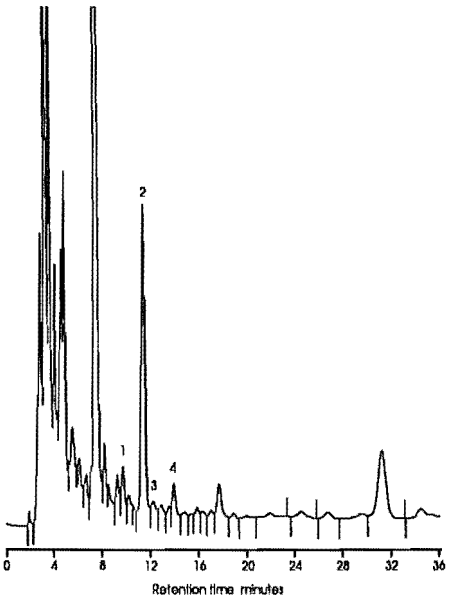

Figure 4.12 Separation of resin acid and fatty acids: 1 = Linolenic acid, 2 = Abietic acid, 3 = Palmitoleic acid, 4 = Linoleic acid.

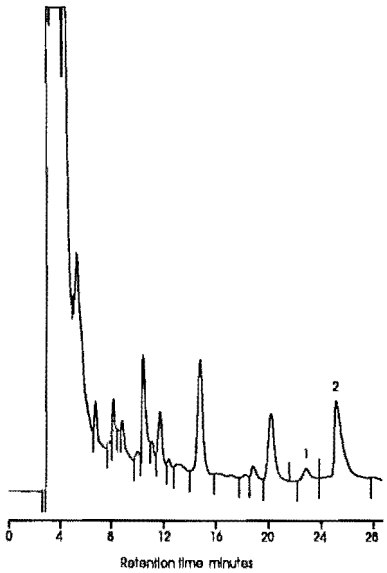

Figure 4.13 Separation of sterols: 1 = Campesterol, 2 = β-Sitosterol.

No differences were found in the relative proportions of these compounds in the carbon dioxide and carbon dioxide/methanol extracts (figure 4.14). For carbon dioxide extracts, increased amounts of abietic acid and β-sitosterol were extracted with increasing pressure. No pattern of change with pressure was apparent for the fatty acids linoleic, linolenic and palmitoleic acid, and the sterol campesterol. The broad spread of

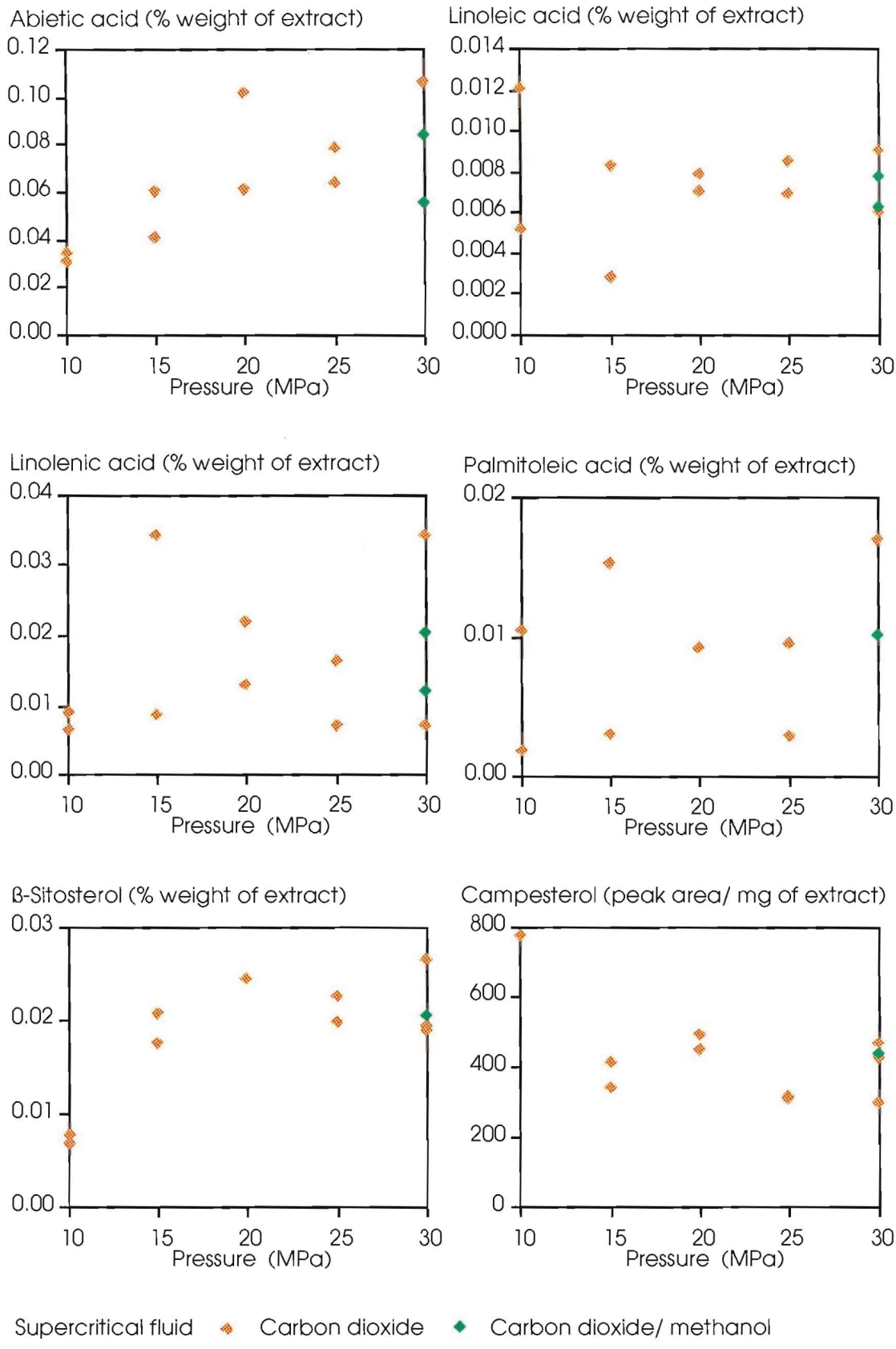

Figure 4.14 The percent weight of resin acid, fatty acids, and sterols in supercritical fluid extracts at different pressures.

points for the fatty acids palmitoleic and linolenic acid, can be attributed to the effects of tailing by large proceeding peaks.

The amount of abietic acid extracted increases with pressure, from 2.4 - 3.1 mg/kg of oven dry bark at 10 MPa to 13.8 - 29.4 mg at 30 MPa (figure 4.15). This is as much as 60 % of that extracted with diethyl ether.

Linoleic acid shows a small increase in the amount extracted with pressure, from 0.4 - 1.1 mg/kg of oven dry bark at 10 MPa to 1.7 - 2.2 mg at 30 MPa. This is 30 % of that extracted with diethyl ether. For linolenic and palmitoleic acid the broad spread of points tends to obscure any trends. However, if we take the minimum values as indicative, there is the suggestion of a small increase in the amount extracted with pressure. The presence of a carbon dioxide extraction value for linolenic acid in excess of the diethyl ether value, supports the idea that the larger carbon dioxide and carbon dioxide/methanol extraction values for linolenic and palmitoleic acid are too high. Overall the quantities of free fatty acids extracted are minor and similar to one another. This is in accordance with the analysis of *Pinus radiata* bark fatty acids given by Hartman and Weenink (1967) and Porter (1969).

The amount of β-sitosterol extracted increases with pressure, from 0.6 - 0.7 mg/kg of oven dry bark at 10 MPa to 6.3 - 7.4 mg at 30 MPa. This is 80 - 85 % of the diethyl ether extractable β-sitosterol. Campesterol shows only a small increase with pressure. The quantities extracted are not available due to the lack of calibration. The relative HPLC peak areas for this compound do however indicate that 50 % of the diethyl ether extractable campesterol was extracted.

The percent weight of abietic acid, linoleic and palmitoleic acid, and β-sitosterol in re-extracted bark extracts shows a marked decline (table 4.8). For abietic acid the percent weight in re-extracted bark extracts is 29 % of that in the first extract. Similarly for linoleic and palmitoleic acid the percent weights in re-extracted bark extracts were 31 and 32 % of the first extract percent weight respectively. β-Sitosterol shows an even greater reduction to only 16 % of the first extract percent weight. This ties in well with the very high level of β-sitosterol removal in the first extraction.

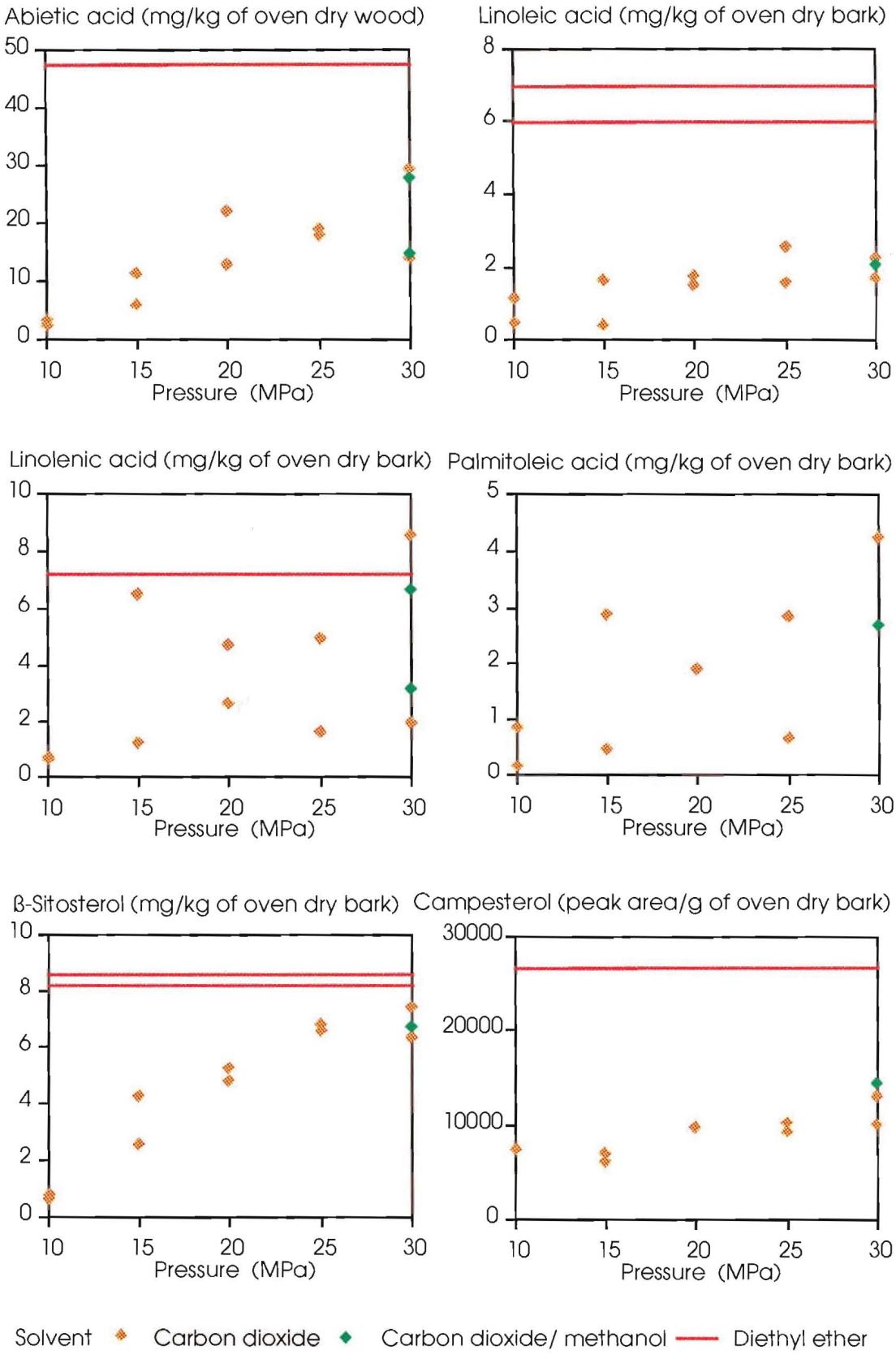

Figure 4.15 Amounts of resin acid, fatty acids, and sterols extracted with supercritical fluids at different pressures.

Table 4.8 Changes in the yields of resin acid, fatty acid, and sterol compounds with bark re-extraction at 30 MPa

Compound	Percent weight of extract	
	First extraction carbon dioxide	Second extraction carbon dioxide/ methanol
Abietic acid	0.056	0.016
Linoleic acid	0.017	0.005
Palmitoleic acid	0.009	0.003
ß-Sitosterol	0.019	0.003

4.13 Discussion

The increase in solubility with pressure is common for large molecules in supercritical carbon dioxide. This was observed for the compounds in this study, and by Jennings et al. (1991) for the extraction of taxol from *Taxus brevifolia* bark.

The considerable variability in supercritical extract yields (figure 4.11 and table 4.7) was put down to localised differences in the bark samples. The range of particle sizes within the ground bark, from which the samples were drawn, was quite large, extending from 425 to 250 µm. Changes in the chemical composition of the bark over time was minimised by storage in an air-tight container, maintained at 0 ° C.

A large number of preliminary runs were devoted to refining the extraction procedures, to ensure that these weren't contributing to the variation in extract yields. Thorough flushing between extraction runs was found to be necessary to prevent carry over of extract from one extraction run to the next. All flushing runs were therefore performed at the maximum pressure used for extraction (30.0 MPa), irrespective of the pressure used for the proceeding extraction. Twenty cell volumes of supercritical fluid were past through the system during flushing, twice the amount that was used during bark extraction. Further flushing was found to produce only traces of extract.

The relative proportions of resin acids and fatty acids in extracts were unaffected by yield. This tends to suggest that the particle size distribution within the bark samples may have been a contributing factor to the

variation in extract yields. The variation in yields obtained by the exhaustive extraction of bark with diethyl ether (table 4.7), suggests that differences in the amount of extractives in the bark samples may also have contributed to the variation in extract yields.

The absence of any increase in extract yields and changes in composition with the addition of the polar co-solvent, methanol, is in contrast to the findings of Jennings et al. (1991) and Ritter and Campbell (1991), but in keeping with the findings of McDonald et al (1983). Jennings et al. found the addition of the polar co-solvent ethanol to supercritical carbon dioxide increased both the amount and the proportion of taxol in *Taxus brevifolia* extracts. Ritter and Campbell found the addition of ethanol to *Pinus ponderosa* bark, before extraction with supercritical carbon dioxide, doubled extract yields. This result should however be treated with caution, due to the unusual way in which ethanol was added. Co-solvents, such as ethanol, are usually added at low concentrations to the supercritical fluid prior to its contact with the substrate, as was the case with methanol in this study. The prior and separate addition of ethanol to the bark, could solubilise compounds that would not otherwise be extracted with ethanol added as a co-solvent at low concentrations to the supercritical fluid. Such procedural differences, as introduced by Ritter and Campbell, could well affect the results of supercritical fluid extraction. McDonald et al. found in supercritical fluid extraction of southern pine wood with propane, nitrous oxide, ethylene and carbon dioxide, that although yields were higher with supercritical fluids with dipole moments, the relative proportions of resin acids and fatty acids in extracts was similar, regardless of dipole moment. This suggests that supercritical fluids with dipole moments are able to extract additional sources of resin acids and fatty acids in southern pine wood, by the interaction of their dipole moments with the polar functional groups in the acids. It would appear in *Pinus radiata* bark, that the interaction of the dipole moments of the methanol molecules with the polar functional groups in the acids, does not increase the availability of resin acids and fatty acids. That these compounds remain unavailable, is shown clearly in the increased amounts of resin acids and fatty acids extractable with diethyl ether (figure 4.15).

The decline in the amount and the relative proportions of resin acids and fatty acids in supercritical fluid extracts from *Pinus radiata* bark with time (table 4.7), is similar to that observed by McDonald et al. (1983) for supercritical fluid extraction of southern pine wood. The relative amounts of resin acids and fatty acids in the final extracts also remained the same as in the initital extracts.

The commercial application of supercritical fluid extraction processes is expensive due to the high capital costs of compressors and high pressure vessels. Short term applications of supercritical fluid technology are limited to high value, stable priced products such as those in the specialised food and drug industry. In this regard, perhaps the most significant finding is the high proportion of β-sitosterol that is extracted from *Pinus radiata* bark with supercritical carbon dioxide. β-sitosterol can be used in the synthesis of steroid hormones and related pharmaceutical products such as cortisone derivatives (Sjostrom 1981).

4.14 Summary

In general, supercritical carbon dioxide extract yields from *Pinus radiata* bark increase with pressure (10 - 30 MPa) at 50 ° C. HPLC analysis identified the resin acid abietic acid, the fatty acids linoleic, linolenic and palmitoleic acid, and the sterols β-sitosterol and campesterol as present in the extracts. The amounts of each increased with pressure, the amounts being small for linoleic, linolenic and palmitoleic acid, and campesterol. The extract composition of abietic acid and β-sitosterol increased with pressure.

The addition of the polar co-solvent methanol (4.3 % by mass) at 30 MPa neither increased extract yields nor changed the extract composition of resin and fatty acids, and sterols.

The flavonoid dihydroquercetin was not extracted with supercritical carbon dioxide, even with the addition of the co-solvent methanol.

Short term commercial application of supercritical fluid technology is limited to high value products such as those of the specialised food and

drug industry. The extraction of β-sitosterol is therefore perhaps the most significant finding given that it can be used in the synthesis of steroid hormones and cortisone derivatives.

The resin acid, unsaturated fatty acids, and sterols that were identified and quantified in the supercritical fluid bark extracts, were all minor components. A major focus of further work is a more thorough analysis of the chemical composition of the supercritical fluid bark extracts. This could involve the use of such analytical techniques as mass spectroscopy and refractive index detection in addition to ultraviolet absorption.

References

Aveldano, M. I, van Rollins, M. and Horrocks, L. A., 1983, Separation and quantification of free fatty acids and fatty acid methyl esters by reverse phase high pressure liquid chromatography, *Journal of Lipid Research*, 24, 83 - 93.

Beer, R. and Peter, S., 1985, High pressure extraction of lignin from wood. In: Penninger, J. M. L., Radosz, M., McHugh, M. A. and Krukonis, V. J., Supercritical Fluid Technology, Process Technology Proceedings, 3, Elsevier, New York, Chapter 19, 385 - 396.

Brogle, H., 1982, CO_2 as a solvent: its properties and applications, *Chemistry and Industry*, 385 - 390.

Calimli, A. and Olcay, A., 1978, Supercritical-gas extraction of Spruce wood, *Holzforschung*, 32(1), 7 - 10.

de Filippi, R. P., 1982, CO_2 as a solvent: application to fats, oils and other materials, *Chemistry and Industry*, 390 - 394.

Dobbs, J. M., Wong, J. M., Lahiere, R. J. and Johnston, K. P., 1987, Modification of supercritical fluid phase behaviour using polar cosolvents, *Industrial and Engineering Chemistry Research*, 26(1), 56 - 65.

Hansen, R. P., 1966, A preliminary investigation of the fatty acid composition of the lipids of *Pinus radiata* and *Pinus nigra*, *New Zealand Journal of Science*, 9(4), 801 - 805.

Hartman, L. and Weenink, R. O., 1967, A note on the fatty acid composition of the lipids from the bark of *Pinus radiata*, *New Zealand Journal of Science*, 10(3), 636 - 638.

Harvala, T., Alkio, M. and Komppa, V., 1987, Extraction of tall oil with supercritical carbon dioxide, *The Institution of Chemical Engineers Symposium Series*, No. 103, 233 - 243.

Jennings, D. W., Deutsch, H. M., Zalkow, L. H. and Teja, A. S., 1991, Supercritical extraction of taxol from the bark of *Taxus Brevifolia, Second International Symposium on Supercritical Fluids, Boston,* Poster paper, 20 pp.

Koll, P., Bronstrup, B. and Metzger, J., 1979, Thermal degradation of birch wood with supercritical gases (organic solvents) in a high-pressure, high-temperature flow apparatus; the liquefaction of wood and further evidence for an alternative cellulose pulp technology, *Holzforschung,* 33(4), 112 - 116.

McDonald, E. C., Howard, J. and Bennett, B., 1983, Chemicals from forest products by supercritical fluid extraction, *Fluid Phase Equilibria,* 10(2 and 3), 337 - 344.

Markham, K. R. and Porter, L. J., 1973, Extractives of *Pinus radiata* bark 1. Phenolic components, *New Zealand Journal of Science,* 16(4), 751 - 761.

Pearce, D. L., 1990, Solubility of triglycerides in supercritical carbon dioxide, Ph.D. Thesis, Chemical and Process Engineering, University of Canterbury.

Porter, L. J., 1969, The resin and fatty acid content of living *Pinus radiata* wood, *New Zealand Journal of Science,* 12(4), 687 - 693.

Porter, L. J., 1974, Extractives of *Pinus radiata* bark 2. Procyanidin constituents, *New Zealand Journal of Science,* 17(2), 213 - 218.

Reyes, T., Bandyopadhyay, S. S. and McCoy, B. J., 1989, Extraction of lignin from wood with supercritical alcohols, *The Journal of Supercritical Fluids,* 2(2 and 3), 80 - 84.

Ritter, D. C. and Campbell, A. G., 1991, Supercritical carbon dioxide extraction of southern pine and ponderosa pine, *Wood and Fiber Science,* 23(1), 98 - 113.

Simpson, R. F. and McQuilkin, R. M., 1976, Terpenes of the bark oil of *Pinus radiata*, *Phytochemistry*, 15(2), 328 - 329.

Sjostrom, E., 1981, Wood chemistry: fundamentals and applications, Academic Press, New York, 223 pp.

Stahl, E., 1980, Extraction of natural products with the means of supercritical gases, *Revista Latinoamericana Quimica*, 11, 1 - 7.

van Alsten, J. G. and Eckert, C. A., 1985, Mixed supercritical solvents for selective solubility enhancement, *Division of Fuel Chemistry - ACS*, 30(3), 13 - 15.

Vannoort, R., 1991, Supercritical fluid extraction of wool, Unpublished report.

Weston, R. J., 1973, Neutral extractives from *Pinus radiata* bark, *Australian Journal of Chemistry*, 26(12), 2729 - 2734.

Wulf, L. W. and Nagel, C. W., 1976, Analysis of phenolic acids and flavonoids by high pressure liquid chromatography, *Journal of Chromatography*, 116(2), 271 - 279.

Appendix one

HPLC calibrations

The ultraviolet absorbance detector was calibrated with standard solutions of abietic acid, linoleic, linolenic and palmitoleic acid, and β-sitosterol. These were weighed into vials and a known mass of tetrahydrofuran and methanol (4 : 1 v/v) was added. The detector settings and mobile phases were the same as those used for extract samples.

The masses were measured using a Mettler AE200 electronic balance.

The calibration data are presented in figure 1. The linear regression equations are given below. The equations were determined using the plotting package Cricket Graph (Cricket Software Inc., Malvern, Pennsylvania, USA).

Abietic acid	y = -1.2830e-3 + 7.1096e-8x	R^2 = 0.996
Linoleic acid	y = 1.9317e-4 + 6.1656e-8x	R^2 = 0.993
Linolenic acid	y = 6.5666e-4 + 7.8482e-8x	R^2 = 0.997
Palmitoleic acid	y = -3.9898e-4 + 1.1166e-7x	R^2 = 1.000
β-Sitosterol	y = 7.7425e-5 + 6.5109e-8x	R^2 = 0.996

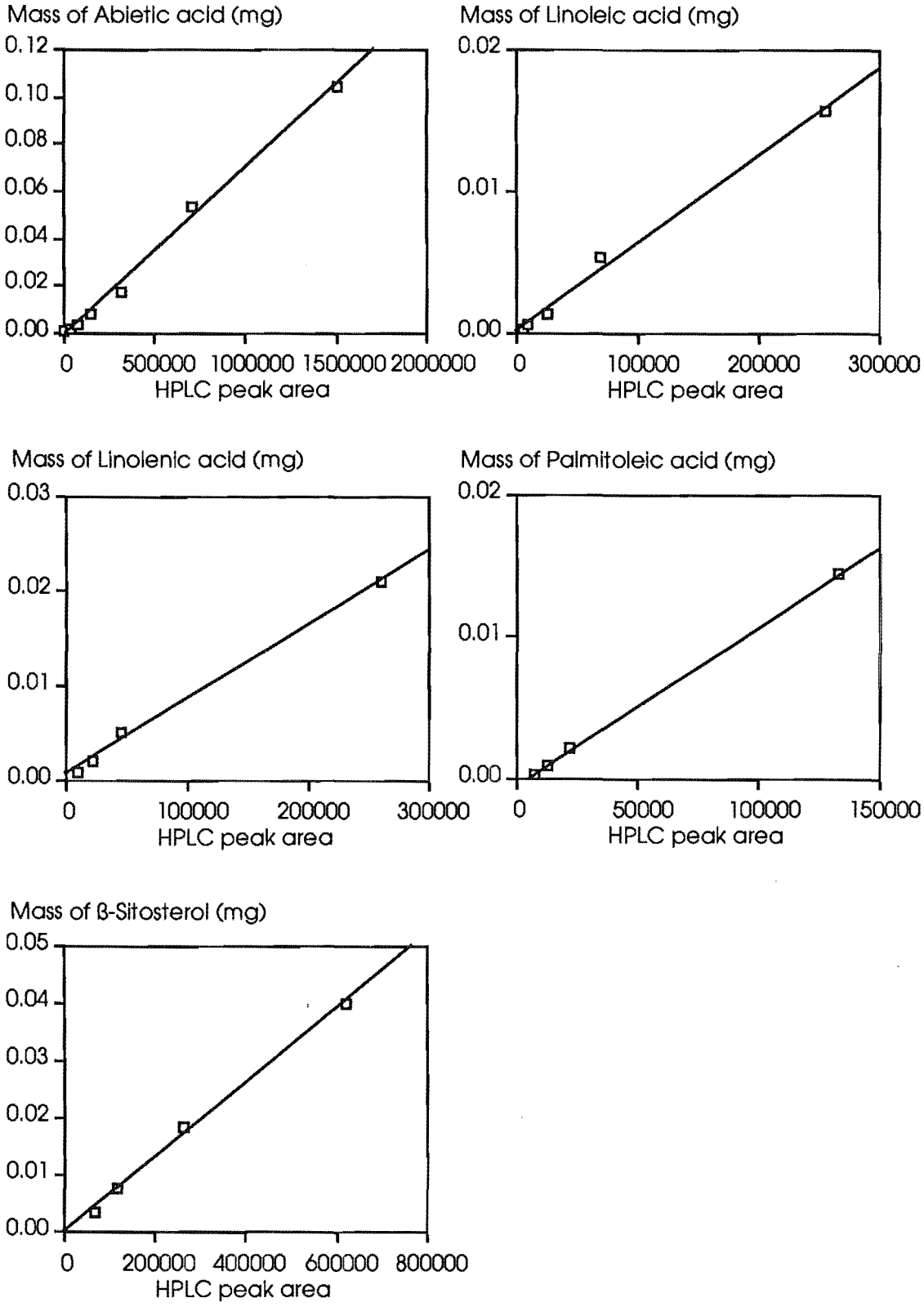

Figure 1. HPLC calibration plots

Chapter 5

Conclusions and suggestions for future work

5.1 Dissolved carbon dioxide gas diffusion in green *Nothofagus fusca* heartwood

The activation energy for dissolved carbon dioxide gas diffusion in green *Nothofagus fusca* heartwood is higher than the activation energy for dissolved carbon dioxide gas diffusion in water. The presence of a reaction mechanism between the dissolved carbon dioxide gas molecules and the cell wall constituents could account for the high activation energy value.

The solubilities of carbon dioxide gas in the water of *N. fusca* heartwood are similar to those published for carbon dioxide gas in pure water.

The initial carbon dioxide gas loss from *N. fusca* heartwood occurs largely through mass flow of carbon dioxide gas bubbles from surface vessels and longitudinal diffusion. In wood of large longitudinal length, the majority of carbon dioxide gas is lost by transverse diffusion.

Future work could involve the development of a bimodal diffusion equation to model the longitudinal and transverse diffusion of dissolved carbon dioxide gas in green wood. Account would need to be taken of the contribution of mass flow, and the affect of the wood's dimensions on each component of carbon dioxide gas absorption and desorption.

5.2 Decompression drying of *Pinus radiata* sapwood chips

Bubble nucleation in green *Pinus radiata* sapwood chips supersaturated with dissolved carbon dioxide gas can result in the removal of a significant

proportion of the water present. Water loss increases with the supersaturation of dissolved carbon dioxide gas in water, as exemplified by increased gas pressure and gas absorption time. Large differences in water loss occur at low carbon dioxide gas supersaturations over temperature intervals as small as five degrees Celsius, with no consistent pattern with regard to carbon dioxide gas solubilities in water.

Water loss is significantly greater with repeated cycles of decompression drying at high carbon dioxide gas supersaturations than for one cycle of equivalent gas absorption time.

The energy efficiency of decompression drying is far lower than for compression drying with hydraulically driven platens.

Future work could assess the unexpected effect of temperature on water loss at low carbon dioxide gas supersaturations. Of particular interest are the temperature effects on the large differences in water loss at 1.50 and 4.89 MPa. An extension of the current study, that would be of interest, is an assessment of the effect on water loss of the interaction of temperature and gas pressure at gas pressures between 1.50 and 4.89 MPa. The work on repeated cycles of decompression drying could also be taken further with an evaluation of other/more gas pressures and gas absorption time combinations with a view to optimising water loss and energy efficiencies.

5.3 Drying collapse in *Eucalyptus delegatensis* heartwood

Carbon dioxide gas supersaturation in the sap of green *Eucalyptus delegatensis* heartwood has no effect on drying collapse. There is, however, significant variation in drying collapse among the different sources of wood from Nelson and Southland, New Zealand. Significant differences in drying collapse occurred among regions, among trees within regions, and among height classes within trees. The differences among regions could be attributed to environmental control of inter- and intra-incremental basic density variation, affecting the resistance of latewood increments to the drying collapse in earlywood. The differences among trees within regions could be attributed to variation in the collapse susceptibility of earlywood. The variation in drying collapse among trees

within regions may be in part due to genetic differences between trees. It may, therefore, be possible to breed for reduced collapse susceptibility in the earlywood of *E. delegatensis*. Future work would involve progeny testing of selected trees to provide estimates of the variance components and heritability of drying collapse in *E. delegatensis*, genetic correlations with other wood properties, and an estimate of the genotype × environment interaction. The information would give some idea of the genetic gains that could be made, and the way and speed with which they could be achieved.

5.4 Supercritical fluid extraction of *Pinus radiata* bark

Supercritical carbon dioxide extract yields from *Pinus radiata* bark increase with pressure from 10 to 30 MPa at 50 ° C. The addition of 4.3 % methanol as a co-solvent at 30 MPa gave no increase in extract yields. Provided extraction is exhaustive, supercritical carbon dioxide and carbon dioxide/methanol can extract a large proportion of the diethyl ether soluble extractives in *P. radiata* bark.

The resin acid abietic acid, the fatty acids linoleic, linolenic, and palmitoleic acid, and the sterols ß-sitosterol and campesterol were identified as present in the supercritical fluid extracts. The amount of all the compounds extracted increased with increasing pressure, but of greater interest is the increase in the proportions of abietic acid and ß-sitosterol in the extracts with increased pressure. The extract composition of resin acid, fatty acids, and sterols remained unchanged with the addition of the co-solvent methanol. The flavonoid dihydroquercetin was not found in the carbon dioxide/methanol extracts.

Future work could extend the analysis of the chemical composition of the supercritical fluid extracts. Analytical techniques such as refractive index detection and mass spectroscopy could be used to identify and quantify chemical groupings such as the saturated long-chain fatty acids that make up a large proportion of the fatty acid compounds in *P. radiata* bark.